DOE INDIRECT COAL LIQUEFACTION - HURDLES AND OPPORTUNITIES FOR ITS EARLY COMMERCIALIZATION. **John Shen and Edward Schmetz, U.S. Department of Energy, Germantown, MD 20874, Gary Stiegel and Richard Tischer, U.S. Department of Energy, P.O. Box 10940, Pittsburgh, PA 15236**

Keywords: Fischer-Tropsch, Slurry phase reactor, Co-production

INTRODUCTION

Coal is the most abundant domestic energy resource in the United States. The Fossil Energy organization within the U.S. Department of Energy (DOE) has been supporting a coal liquefaction program to develop improved technologies for converting coal to clean and cost-effective liquid fuels and/or chemicals to complement the dwindling supply of domestic petroleum crude. The goal of this program is to produce coal liquids that are competitive with crude at $25 per barrel. Indirect and direct liquefaction routes are the two technologies being pursued under the DOE coal liquefaction program. In indirect liquefaction, the emphasis is on the development of improved liquid phase reactor technology to convert "lean syngas" (low hydrogen to carbon monoxide ratio) produced from advanced coal gasifiers. In this paper, the terms of "liquid phase reactor" and "slurry phase reactor " are considered interchangeable.

An overview of the DOE indirect liquefaction program, including the development highlights of the Liquid Phase Methanol technology which is undergoing commercial demonstration at the Eastman Chemicals plant in Kingsport, Tennessee within the DOE Clean Coal Program, can be found elsewhere (Shen, et al. 1996). This paper will update the status of DOE indirect liquefaction program, and briefly review the recent development in the commercial liquid phase reactor design. It also will discuss the hurdles and opportunities for the early commercialization of this technology.

UPDATED STATUS OF DOE INDIRECT LIQUEFACTION PROGRAM

Slurry Phase Fischer-Tropsch Three slurry phase Fischer-Tropsch runs have been made at the proof-of-concept (POC) unit at LaPorte, Texas between 1992 and 1996, with costs shared by industrial consortiums headed by Air Products and Chemicals (APCI). The first two runs used iron catalysts and the third one a cobalt catalyst. Highlights of the first two runs have been reported earlier (Shen, et al. 1996). More detailed review of the first run data also has been published (Bhatt, et al. 1995)..These results indicate that, with the system to convert lean syngas over iron catalysts, more work is needed to improve the correlations between the autoclave and POC slurry phase reactor data. Also, efforts should be directed to explore the advantages of iron over cobalt catalysts to produce a more versatile product slate including olefins. Finally, more fundamental study is needed to gain a better understanding of the iron catalyst behavior in a slurry phase F-T reactor. Data workup for the third run with a cobalt catalyst is now underway

Liquid Phase Dimethyl Ether (DME) The feasibility of liquid phase DME technology was first demonstrated by APCI at the LaPorte POC unit in 1991. Since then, there have been considerable industrial interests in this one-step syngas to DME technology, which could reduce the DME cost as a fuel or a precursor to chemicals. Recent work at bench scale unit has been aimed to further reduce the deactivation rate for the physical mixture of methanol synthesis and methanol dehydration catalysts present in a liquid phase reactor. Results obtained with APCI's improved proprietary dehydration catalyst appear encouraging (Parris, et al. 1996). The commercial demonstration of liquid phase DME technology at the Liquid Phase Methanol project site at Kingsport is tentatively scheduled for year 2000.

Synthesis Gas to Oxygenates and Chemicals Novel catalyst R&D has been underway to convert synthesis gas to oxygenates and chemicals under cost-shared contracts. The products include mixed alcohols including isobutanol (Xu, et al. 1996), vinyl acetate monomer (Tustin, et al. 1996), methyl methacrylate (Spivey, et al. 1996), and dimethyl carbonate (Hagen, 1996). The industrial participants in this program include APCI, Eastman Chemicals, RTI, Bechtel, and Amoco.

Commercial Liquid Phase Reactor Development

A recent media release indicates that Sasol has placed orders for seven SAS (Sasol Advanced Synthol) gas phase reactors with diameters up to 10.7 meters (Sasol 1996). It seems reasonable to assume that the same size reactor also can be used for slurry phase reactor applications. In an earlier DOE supported study, Bechtel has designed a commercial slurry phase reactor with a diameter of 4.8 meters (Fox, et al. 1990). At that time considerable considerations have been given to the reactor physical constraints including the weight of tube sheets holding the internal tube exchanger. It seems prudent that, in view of the Sasol announcement, the commercial slurry phase reactor design should be revisited to evaluate the various impacts of a larger reactor size.

Hurdles and Opportunities for the Early Commercialization of Indirect Liquefaction Technology

Due to the federal budget constraints, DOE has been exploring the use of "financial incentives" rather than "cost-sharing" to promote the commercial demonstration of slurry phase F-T technology. Preliminary results from this scoping study, conducted by Mitretek with DOE support, will be reported in a separate paper at this meeting (Gray, et al. 1997). Under this proposal, an industrial consortium would be formed to lead the effort, with DOE to cost-share the Phase Zero project feasibility study and to serve as an advocate for the use of incentives. Use of incentives is deemed necessary to mitigate the high risks associated with these projects. It is also consistent with our precedents to offer "limited" incentives to introduce a new domestic resource based transportation fuel because of its vital importance to the economic well-being of our country.

IGCC (integrated gasification combined cycle) system, which is an integrated part of the indirect liquefaction technology, has recently received more commercial interests, partly in response to the emerging trend in tighter environmental regulations (Rhodes 1996; Aalund, 1996). In these applications and others under considerations, a variety of carbonaceous feedstock are used to address the local need to dispose the environmentally disadvantageous materials. With more and more these IGCC systems in place, the opportunity to co-produce power, premium quality transportation fuels and/or chemicals could offer the best prospect for the early commercial deployment of the slurry phase F-T technology. With the learning experience gained from these operations, a transition to coal based IGCC/slurry phase F-T could be underway between 2010 and 2015 when coal liquid is projected to be competitive with crude (Gray, et al. 1996).

CONCLUSIONS

We have presented an updated summary of the work performed under DOE indirect liquefaction program since 1994. In the slurry phase F-T area, we also have identified areas for future R&D work. A "financial incentives" based approach, to be led by an industrial consortium, has been proposed to promote the commercial demonstration of slurry phase F-T technology. The early commercial deployment of this technology could be in the IGCC based power plants to co-produce power, premium quality transportation fuels, and/or chemicals. The DOE supported slurry phase F-T technology is tailored for co-production applications with enhanced system efficiency.

REFERENCES

Aalund, L.R., "Italian Refinery Gasification Project to Make Electricity, Steam, and Hydrogen from Tar", Oil & Gas Journal, P. 33, October 21, 1996

Bhatt, B.L., R. Frame, A. Hoek, K. Kinnari, V.U.S. Rao, and F.L. Tungate 1995 "Catalyst Processing Scale-up for Fischer-Tropsch Synthesis", Topics in Catalysis 2 (1995) 235-257.

Fox, J.M., B.D. Degen, G. Cady, F.D. Deslate, and R.L. Summers 1990 "Slurry Reactor Design Studies: Slurry vs. Fixed-Bed Reactors for Fischer-Tropsch and Methanol", Final Report, DOE/PC/89867/T2, June 1990

Gray, D., and G. Tomlinson 1996 "Incentives for the Commercialization of Liquefaction Technologies", Paper Presented at the First Joint Power & Fuel Systems Contractors Conference, Pittsburgh, PA, July 9-11, 1996

Gray, D., and G. Tomlinson 1997 "Opportunities for Early Commercial Deployment of Indirect Liquefaction", Paper to be Presented at the American Chemical Society Meeting, San Francisco, CA, 4/13-4/17, 1997

Hagen, G.P. 1996 "Synthesis of Oxygenate Products for High Volume Fuels Applications", Paper Presented at the First Joint Power & Fuel Systems Contractors Conference, Pittsburgh, PA, July 9-11, 1996

Parris, G.E., X.D. Peng, and B.A. Toseland 1996 "Some Advances in Catalysis for Alternate Fuels", Paper Presented at the First Joint Power & Fuel Systems Contractors Conference, Pittsburgh, PA, July 9-11, 1996

Rhodes, A.K., "Kansas Refinery Starts Up Coke Gasification Unit", Oil & Gas Journal, P. 31, August 5, 1996

Sasol 1996 Media Release: "Sasol Awards Contract to the Consortium of Hitachi Zosen and Marubeni for Seven Advanced Synthol Reactors", October 22, 1996

Shen, J., G. Stiegel, and A. Bose 1996 "DOE Indirect Coal Liquefaction Program - An Overview", Fuel Sciences & Technology Int'l, 14(4), 559-576 (1996)

Spivey, J.J., M.R. Gogate, J.R. Zoeller, R.D. Colberg, G.N. Choi, and S.S. Tam 1996 "Synthesis of Methyl Methacrylate from Coal-Derived Syngas", Paper Presented at the First Joint Power & Fuel Systems Contractors Conference, Pittsburgh, PA, July 9-11, 1996

Tustin, G.C., J.R. Zoeller, and L. DePew 1996 "Synthesis of Vinyl Acetate Monomer from Synthesis Gas", Paper Presented at the First Joint Power & Fuel Systems Contractors Conference, Pittsburgh, PA, July 9-11, 1996

Xu, M., B.L. Stephens, M.J.L. Gines, and E. Iglesia 1996 "Reaction Pathways and Catalyst Requirements in the synthesis of Isobutanol from CO and Hydrogen", Paper Presented at the First Joint Power & Fuel Systems Contractors Conference, Pittsburgh, PA, July 9-11, 1996

AN EVALUATION OF PROPERTIES FOR CALIFORNIA REFORMULATED GASOLINE

Analisa R. Bevan, Tony R. Brasil, and James J. Guthrie
California Air Resources Board
2020 L Street
Sacramento, California 95814

Keywords: California, Reformulated, Gasoline

ABSTRACT
California began using a cleaner-burning reformulated gasoline in March 1996. The California reformulated gasoline regulations limit eight specific properties, with flexibility given to refiners to average properties, or to use a predictive model to blend gasolines having equivalent emission benefits. Data were collected from refiners, compliance fuel sample monitoring, and the California Energy Commission. These data are used to compile a picture of California reformulated gasoline's average properties and the range of properties. The properties evaluated include sulfur, aromatic hydrocarbon, benzene, olefin, and oxygen content, distillation temperatures at 50 and 90 percent volume, and Reid vapor pressure. Additionally, data have been collected pertaining to the energy density which affects the fuel economy of this cleaner-burning gasoline. This evaluation confirms the Air Resources Board's pre-regulation analysis on emission performance and fuel economy.

INTRODUCTION

Presented is an evaluation of data which illustrates the present composition of gasoline in California. California introduced a cleaner-burning reformulated gasoline (CaRFG) in 1996 as part of its comprehensive program to reduce air pollution. Since CaRFG's introduction, the Air Resources Board (ARB) has monitored the composition of gasoline sold in California through several mechanisms. An evaluation of this data was performed to verify that estimated emission benefits are being met. The ARB also calculated the energy difference of CaRFG on a subset of available data using oxygen content, specific gravity, distillation temperatures at 10, 50 and 90 percent volume (T10, T50 and T90), and aromatic hydrocarbon content.

BACKGROUND

Air Quality Compared to California Phase 1 gasoline (Post-1992), CaRFG reduces emissions of volatile organic compounds (VOC), oxides of nitrogen (NOX), and carbon monoxide (CO), as well as the risk from exposure to toxic air contaminants. Table 1 shows the emission reductions attributable to CaRFG.

CaRFG Regulation The CaRFG regulations set specifications for eight properties with several compliance options available to gasoline producers. Compliance options which provide refiners flexibility in meeting the regulation include; (1) compliance with regulation flat limits, (2) the use of averaging based on the regulation averaging limits; (3) the use of a predictive model; or (4) the use of an alternative formulation certified to have equivalent emission performance. Since the implementation of the CaRFG regulation, no fuel producers have used the alternative formulation method of compliance.

The CaRFG regulation sets cap limits for each of the eight regulated properties. The cap limits ensure that compliance can be demonstrated at all points of the distribution and marketing system. These limits are listed in Table 2.

Regulation Flat limits The regulation flat limits, listed in Table 2, are fixed for each regulated property and cannot be exceeded

when complying by this method. Refiners are not required to report batch properties to the ARB when using this method of compliance.

Averaging Limits The averaging limits are listed in Table 2. Gasoline producers using the averaging limits to comply with the CaRFG must demonstrate that volume weighted gasoline production averages meet each specification limit by the end of the averaging period without exceeding the cap limit. As shown in Table 2, the averaging limits are lower than the flat limits. Under this compliance option refiners must report the measured properties and volumes of each batch of fuel produced to the ARB.

Predictive Model The Predictive Model provides fuel producers with flexibility to optimize the gasoline properties of fuel produced to match the capabilities of their facilities. The predictive model allows fuel producers to designate alternative flat limits and averaging limits while maintaining the emission benefits of the CaRFG regulation. The majority of producers have chosen to use this method of compliance. The compliance reporting requirements are similar to the compliance options described above. However, the specifications of the eight regulated properties must be reported to the ARB.

DATA COLLECTED

Regulation Flat Limits Since no reporting by fuel producers to the ARB is required for this option, it was assumed that fuel producers using this option produced fuel with properties at the regulation flat limits. The gasoline production volume was obtained from the California Energy Commission (CEC) from weekly production data.

Regulation or Predictive Model Averaging Limits Under this option, gasoline producers must report the properties and volume of each batch produced to the ARB; thus, the average properties were calculated directly from their compliance reports.

Predictive Model Flat Limits Many gasoline producers used several predictive model formulations in a given month. Since the volume of gasoline produced under each formulation was not reported, a typical formulation reported from each producer in a given month was used. The production volume for each producer was again estimated with CEC weekly gasoline production data.

Compliance Sample Data ARB compliance sampling data were used to evaluate energy density changes associated with CaRFG. A total of 103 samples comprised this subset of CaRFG data.

Presented Data

Table 3 lists the approximate volume weighted average properties of the gasoline being produced in California from March 1996 through September 1996.

Table 4 summarizes the properties found in samples of summertime CaRFG sold in 1996. The table also summarizes and provides a comparison to summertime California gasoline sold in 1990 and 1991.

DATA ANALYSIS

Evaluation CaRFG Regulatory Compliance Table 3 shows that the average CaRFG properties of fuel sold in California are very similar to the regulation flat limits. Of the eight properties, only the T90 specification is higher. It is higher because many fuel producers have been able to increase the T90 when meeting the predictive model flat limits.

Evaluation of Emissions Effects The predictive model provides the basis for the emissions characteristics of the formulations

presented here. The predictive model predicts the relative change in emissions compared to the regulation flat limits or averaging limits. Although changes in emissions compared to changes in properties are not always linear, they can be estimated linearly for the range of properties allowed in the regulation. Because of this, the average emissions of each batch are expected to be similar to the emissions of the average properties of all batches.

The in-use California average gasoline properties have the same emissions benefits as anticipated by the ARB. Since the averaging limits are more stringent than the flat limits, the average properties of the in-use gasolines meeting averaging limit specifications were evaluated separately from those meeting flat limit specifications. Table 3 lists the average gasoline properties from March to September 1996 for gasoline meeting the flat limits, averaging limits, and the overall average gasoline properties.

Evaluation of Fuel Economy Effects All of the eight CaRFG property limits may have some impact on volumetric energy content (Btu/gal) and vehicle fuel economy (mpg). Vehicle fuel economy has been shown to correlate well with gasoline energy content as estimated by ASTM D 3338, modified by considering oxygenated contents separately (Hochhauser, et al, 1993). The most significant of the regulated properties to this procedure are oxygen content, aromatic hydrocarbon content, T50 and T90. The sulfur content has an insignificant impact at the levels found in CaRFG, and is not considered in our estimation of the energy contents of CaRFG.

The oxygen content requirement decreases energy content, because the oxygenated compounds have reduced lower heating values (Btu/lbm) than gasoline. Gasoline with 2 percent by weight oxygen has about a 2 percent lower volumetric energy content than non-oxygenated gasoline. The specific gravity is second only to the oxygen content in its significance to the energy content of CaRFG. Specific gravity is not a regulated property; however, all of the eight regulated properties may have some impact on the specific gravity. The reduction of Reid vapor pressure required of summertime CaRFG may be the only property regulation which tends to increase specific gravity and, consequently, energy content and fuel economy. Aromatic hydrocarbon content, T50 and T90 limits tend to decrease specific gravity, energy content, and fuel economy. The difference in the mean energy contents of CaRFG and Pre-CaRFG is shown in Table 4 to be -3.5 percent.

Consider a vehicle and engine operating at steady speed and load at a given excess-air factor (air-to-fuel ratio relative to theoretical). Ignore changes in thermal efficiency due to small changes in air, fuel, and exhaust flow, which are required to maintain the fixed conditions. Then, a small relative change in fuel energy content should result in an equivalent relative change in vehicle fuel economy (Blackmore and Thomas, 1977). Compared to a fuel with 3 percent greater energy content, under the same conditions the vehicle will travel a 3 percent shorter distance burning the same volume of lower energy fuel. Under the assumptions, a decrease in specific gravity and increase in oxygen content, such as from CaRFG regulations, do not change this relationship. However, under transient operation of the vehicle and engine, or with carburetion designed to maintain a fixed air-to-fuel ratio, the CaRFG regulations should result in reduced fuel mass flow and enleanment (excess-air factor increase) (API, 1988). A slight increase in fuel volume flow should have a negative effect on vehicle fuel economy. Enleanment could increase or decrease engine thermal efficiency; the decrease occurring only with enleanment beyond an excess-air factor of about 1.1 (Adler, 1986).

The change in thermal efficiency should have a corresponding effect on vehicle fuel economy. This theory suggests that, the relative change in vehicle fuel economy is proportional and roughly equivalent to the relative change in gasoline energy content under normal operation of most vehicles. Laboratory dynamometer testing of vehicles operated over the Federal Test Procedure cycle confirms this theory and suggests that the constant proportionality is less than one (Hochhauser, et al, 1993). We conclude that the percent change in average fuel economy of California's gasoline-fueled vehicles, due to the introduction of CaRFG, is less than the percent change in the average energy content of gasoline.

CONCLUSIONS

Our evaluation of CaRFG data shows that fuel producers have met the regulation property limits and that they have made use of available regulation flexibility by implementing various compliance options. Based on analysis performed on the average properties presented, it appears that emission benefits predicted for the regulation are being realized. Additionally, based on sample data and energy density calculations, the effect on fuel economy is relatively small. The overall evaluation of the data confirms pre-regulation analysis of emissions and fuel economy effects.

TABLE 1
Predicted Emission Benefits of California Reformulated Gasoline

Market Segment Reductions	VOC	NOx	CO
On-Road	17%	11%	11%
Off-Road	10%	--	--
Marketing Operations	7%	--	--
Total	**15%**	**11%**	**11%**

Note: Emission benefits of CaRFG for off-road and marketing operations are not separated from on-road categories.

TABLE 2
California Reformulated Gasoline Specification Limits

Property	Flat Limits	Averaging Limits	Cap Limits
Aromatic Hydrocarbon, vol%	25	22	30
Benzene, vol%	1.0	0.80	1.2
T50, F	210	200	220
T90, F	300	290	330
Olefins, vol%	6.0	4.0	10.0
RVP, psi	7.0	--	7.0
Sulfur, ppmw	40	30	80
Oxygen, vol%	1.8 to 2.2	--	1.8 to 2.7

TABLE 3
California Average Gasoline Properties
(March to September 1996)

Property	Flat Limits	Averaging Limits	Overall
Aromatic Hydrocarbon, vol%	24.5	23.9	24.2
Benzene, vol%	0.87	0.55	0.73
T50, F	204	200	202
T90, F	313	298	306
Olefins, vol%	6.6	3.6	5.2
RVP, psi	7.0	7.0	7.0
Sulfur, ppmw	41	14	29
Oxygen, vol%	2.0	1.8	1.9

TABLE 4
Evaluation of Fuel Economy Effects of CaRFG

	Oxygen (%wt)	AroHC (%vol)	RVP (psia)	T10 (F)	T50 (F)	T90 (F)	Sp.Grav. @ 60F	ASTM D 3338 (Btu/gal)
CaRFG (103 Samples)								
Minimum	1.30	9.5	5.96	139	162	276	0.7241	110,200
Maximum	2.90	31.6	7.19	158	229	339	0.7522	113,000
Median	2.17	22.9	6.73	144	201	308	0.7407	111,800
Mean	2.18	22.4	6.71	145	201	309	0.7400	111,700
Pre-CaRFG (90-91) (441 Samples)	Not Known, But Small							
Minimum		4.5	6.9	98	170	281	0.706	109,900
Maximum		60.8	9.3	156	251	362	0.795	120,300
Median		35.8	8.5	130	222	331	0.757	115,800
Mean		36.1	8.4	131	221	329	0.758	115,800
Difference of Means	+2	-13.7	-1.7	+14	-20	-20	-2.4%	-3.5%

REFERENCES

California Air Resources Board, Stationary Source Division, 1991. Proposed Regulations for California Reformulated Gasoline. Vol. 1. California Reformulated Gasoline Specifications. Staff Report. Sacramento, California.

California Air Resources Board, Stationary Source Division, 1994. Proposed Amendments to the California Phase 2 Reformulated Gasoline Regulations, Including Amendments Providing for the Use of a Predictive Model. Sacramento, California.

California Air Resources Board, 1994. Memorandum, "Phase 2 Reformulated Gasoline Emission Benefits." Peter D. Venturini to K.D. Drachand and Terry McGuire.

Adler, U, Editor-in-Chief, 1986. Automotive Handbook, Robert Bosch Gmbh, Stuttgart.

API, 1988. Alcohols and Ethers. A Technical Assessment of Their Application as Fuels and Fuel Components, API Publication 4261, American Petroleum Institute, Washington, D.C.

ASTM, 1992. "Standard Test Method for Estimation of Net Heat of Combustion of Aviation Fuels," ASTM D 3338-92, American Society for Testing and Materials, Philadelphia.

Blackmore and Thomas, editors, 1977. Fuel Economy of the Gasoline Engine: Fuel, Lubricant and Other Effects, John Wiley & Sons, New York.

Hochhauser, Benson, Burns, Gorse, Koehl, Painter, Reuter, and Rutherford, 1993. "Fuel Composition Effects on Automotive Fuel Economy--Auto/Oil Air Quality Improvement Research Program," SAE 930138, Society of Automotive Engineers, Inc, Warrendale, Pennsylvania.

ACKNOWLEDGMENTS

Staff of the Air Resources Board and California Energy Commission were valuable to the collection of data presented. Contributions from the following staff were appreciated: C. Beddow, D. Lum, and F. Schmidt (ARB Compliance Division); A. Hebert and J. Cohan (ARB Monitoring and Lab Division); D. Simeroth, J. Courtis, K. Macias, R. Vincent and N. Chan (ARB Stationary Source Division); G. Shremp (California Energy Commission).

DEVELOPMENT OF A CERAMIC MEMBRANE FOR UPGRADING METHANE TO HIGH-VALUE-ADDED CLEAN FUELS

U. Balachandran, J. T. Dusek, J. J. Picciolo, P. S. Maiya,
B. Ma, and R. L. Mieville
Argonne National Laboratory, Argonne, IL 60439

M. S. Kleefisch and C. A. Udovich
Amoco Exploration and Production, Naperville, IL 60566

Keywords: Mixed conductor, dense ceramic membrane, methane conversion

INTRODUCTION

The upgrading of natural gas (which consists mostly of methane) to high-value-added clean-burning fuels such as dimethyl ether, alcohols, and pollution-fighting fuel additives is driven by the abundance of natural gas discovered in remote areas. Recently, extensive efforts have focused on both direct and indirect conversion of methane to these value-added products [1,2]. The direct-conversion route is the most difficult approach because the products are more reactive than the starting reactant, methane [3]. Indirect routes require the partial oxidation of methane to synthesis gas (syngas, CO + H_2) in a first stage. The syngas is then converted to upgraded products in a second stage. The most significant cost associated with partial oxidation of methane to syngas is that of the oxygen plant. In this paper, we offer a technology that is based on dense ceramic membranes and that uses air as the oxidant for methane-conversion reactions, thus eliminating the need for the costly oxygen plant. Certain ceramic materials exhibit both electronic and oxide-ionic conductivities. These mixed-conductor materials transport not only oxygen ions (functioning as selective oxygen separators), but also electrons. No external electrodes are required and such a system will operate without an externally applied potential. Oxygen is transported across the ceramic material in the form of oxygen anions, not oxygen molecules.

Recent reports in the literature suggest that ceramic membranes made of these mixed conductors can successfully separate oxygen from air at flux rates that could be considered commercially feasible. Thus, they have potential applications for improving the economics of methane conversion [4-6].

Teraoka et al. [4] showed that oxides in the La-Sr-Fe-Co-O system exhibit mixed conductivity and appreciable oxygen permeability. However, we have found that these oxides are unstable when exposed to methane at elevated temperatures and are therefore unsuitable for syngas conversion. We have developed a novel ceramic composition, namely $SrFeCo_{0.5}O_x$, that is stable in methane and that has oxygen permeation suitable for the partial oxidation of methane [7,8].

EXPERIMENTAL

Ceramic powders of composition $SrFeCo_{0.5}O_x$ were made by solid-state reaction of the constituent cation salts. Appropriate amounts of $SrCO_3$, $Co(NO_3)_2{\cdot}6H_2O$, and Fe_2O_3 were mixed and milled in isopropanol with ZrO_2 media for ≈15 h. When dry, the mixtures were calcined in air at ≈850°C for ≈16 h, with intermittent grinding. After final calcination, we ground the powder with an agate mortar and pestle to an average particle size of ≈7 μm. The resulting powders were characterized by X-ray diffraction (XRD), scanning electron microscopy (SEM), and thermal analysis and were also analyzed for particle-size distribution.

The powder was made into a slip containing a solvent, dispersant, binder, and plasticizer. Membrane tubes were fabricated by extrusion of the slip to an outside diameter of ≈6.5 mm, lengths up to ≈30 cm, and wall thicknesses of 0.25-1.20 mm. The tubes were sintered at ≈1200°C, then characterized by SEM and XRD, and finally used in our methane partial-oxidation studies.

The tubes were evaluated for performance in a quartz reactor system, as shown in Fig. 1. The quartz reactor supports the ceramic membrane tube with hot Pyrex seals. An Rh-based reforming catalyst was loaded adjacent to the tube, and a gold wire mesh was wrapped around the tube to prevent solid-state reactions between the catalyst and the ceramic tube. Both the feed gas (generally 80% CH_4 and 20% Ar) and the effluents were analyzed with a gas chromatograph. Inside the membrane tube, air was the source of oxygen.

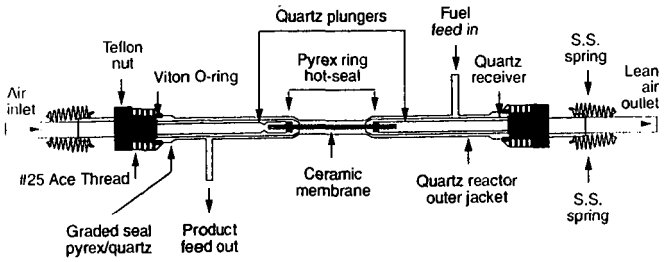

Fig. 1. Schematic diagram of ceramic membrane reactor.

Electrical conductivity was determined by a four-probe method that used a blocking electrode of yttria-stabilized zirconia (YSZ) for oxygen ion conduction [9], while the oxygen diffusion coefficient was measured by a time relaxation method. The sample was subjected to a sudden increase in oxygen partial pressure, and ionic conductivity was monitored as a function of time and temperature [10].

RESULTS AND DISCUSSION

The XRD pattern of an $SrFeCo_{0.5}O_x$ sample recorded at 850°C in an Ar-O_2 gas mixture is shown in Fig. 2. The material exhibited remarkable structural stability at high temperature, and no phase transition was observed as oxygen partial pressure was changed. This structural stability of $SrFeCo_{0.5}Ox$, when compared with that of other mixed conducting oxides of similar type, is reflected in its physical and mechanical properties, as shown in our earlier publications [7,11].

The measured electronic and ionic conductivities of $SrFeCo_{0.5}O_x$ and other materials of the same family are shown in Table 1. It is clear that this material is unique in that its ratio of ionic to electronic conductivity is close to unity. The chemical diffusion coefficient, as determined by the conductivity relaxation method [9], is shown in Fig. 3. The diffusion coefficient increases exponentially with temperature, and at 900°C, is $\approx 9 \times 10^{-7}$ cm^2/s. Activation energy associated with oxygen diffusion is ≈0.9 eV, which indicates that oxide ions can move more easily in the $SrFeCo_{0.5}O_x$ sample than in other mixed-conducting oxides.

Figure 4 shows conversion data obtained with an $SrFeCo_{0.5}O_x$ membrane tube operated at 850°C for ≈70 h in the reactor setup shown in Fig. 1. As seen in Fig. 4, methane conversion efficiency is >98% and CO selectivity is ≈90%. Measured H_2 yield is about twice that of CO, as expected.

Observations by Liu et al. [12] indicate that not only the conductivity of the membrane material, but also the catalytic activity of the surface or interfaces, has a significant effect on the rate of oxygen permeation. Conductivity (ionic and electronic) determines the mass and charge transport rates through the membrane, while catalytic activity controls the rate of interfacial electrochemical reactions. To decouple the role of the catalyst in oxygen transport across the membrane, an $SrFeCo_{0.5}O_x$ tube was tested without the reforming catalyst. The results from a run of ≈350 h are shown in Fig. 5. The feed gases are the same as earlier (80% CH_4 and 20% Ar). In the absence of a catalyst, the oxygen that was transported through the membrane reacted with CH_4 to form CO_2 and H_2O. As seen in Fig. 5, methane conversion efficiency was ≈35% and CO_2 selectivity was ≈90%.

Further confirmation of the stability and high performance of this membrane tube is shown in Fig. 6, which illustrates reactor results over a period of 1000 h. The feed during this period was a typical mixture expected in a commercial recycling feed, namely CH_4, CO, CO_2, and H_2. Throughout the run, methane conversion was high. A small decline in oxygen permeation was observed. The high oxygen flux is consistent with the high diffusion coefficient of 9×10^{-7} cm^2 s^{-1} that was measured by the time-relaxation method [9].

Table 1. Electronic and ionic conductivities of various mixed oxides

Sample	Electronic σ_{el} ($S \cdot cm^{-1}$)	Ionic σ_i ($S \cdot cm^{-1}$)	Method for Measuring σ_i
$SrFeCo_{0.5}O_x$	10	7	4-terminal, YSZ electron block
$SrFe_{0.8}Co_{0.2}O_x$	76	4	4-terminal, YSZ electron block
$La_{0.6}Sr_{0.4}Co_{0.2}Fe_{0.8}O_3$	300	0.01	4-terminal, YSZ electron block
$La_{0.6}Sr_{0.4}Co_{0.2}Fe_{0.8}O_3$	300	0.003	2-terminal, electron block
$La_{0.8}Sr_{0.2}Co_{0.8}Fe_{0.2}O_3$	600	15	4-terminal, YSZ electron block
$La_{0.8}Sr_{0.2}Co_{0.8}Fe_{0.2}O_3$	250	0.10	4-terminal, YSZ electron block
$La_{0.75}Sr_{0.25}FeO_3$	50	0.03	$^{18}O/^{16}O$ exchange

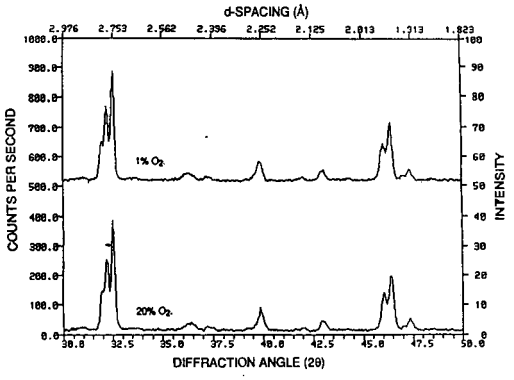

Fig. 2. XRD of $SrFeCo_{0.5}O_x$ at 850°C in 1% and 20% O_2 (balance is Ar) atmosphere.

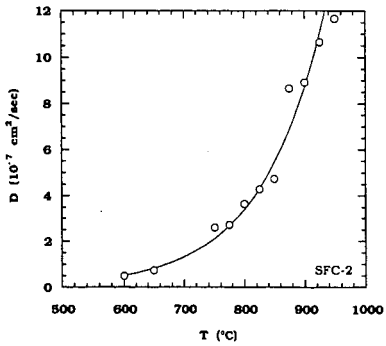

Fig. 3. Chemical diffusion coefficient in $SrFeCO_{0.5}O_x$ as a function of temperature.

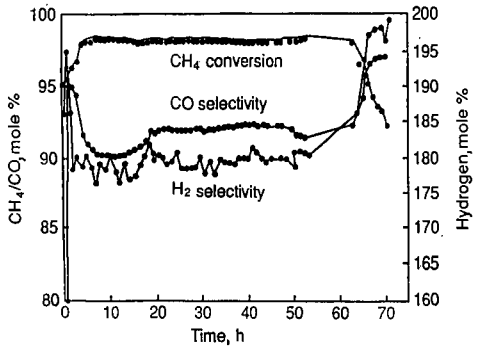

Fig. 4. Methane conversion and CO and H_2 selectivity in $SrFeCo_{0.5}O_x$ membrane reactor with reforming catalyst.

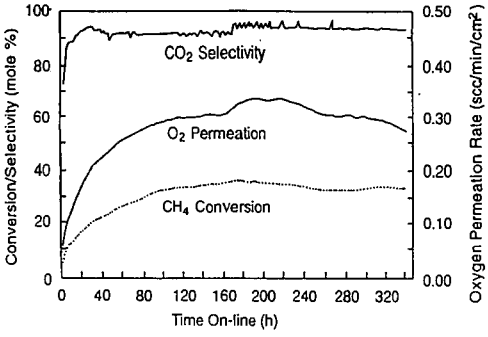

Fig. 5. Methane conversion, CO_2 selectivity, and O_2 permeation in $SrFeCo_{0.5}O_x$ membrane reactor without reforming catalyst.

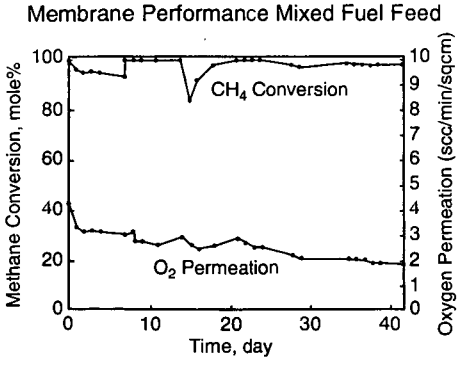

Fig. 6. Methane conversion and O_2 flux for a mixed feed in $SrFeCo_{0.5}O_x$ membrane reactor with reforming catalyst.

To use the $SrFeCo_{0.5}O_x$ membrane tube in converting methane to syngas, it appears critical to reduce the tube wall thickness. Once this is achieved, any oxygen lost from the lattice of the membrane material to the reaction stream can be replaced by the oxygen permeating from the air side at a faster rate. As a result, the material in contact with the reaction stream will not be lost by chemical decomposition. Meanwhile, the difference in oxygen content between the inside and outside surfaces of the tube becomes smaller and consequently, fracturing of the tube is less likely. Thus, a thin-wall membrane tube appears to be more promising for methane conversion in the future. A thin-wall tube will also maximize the surface-area-to-volume ratio and thereby reduce the reactor size. Several suggestions have been made for manifolded monolithic systems of the type reported by Hazbun [13]. In the area of solid-oxide fuel cells, several monolithic designs have been suggested and demonstrated [14-16]; these could be adapted for use in a monolithic reactor.

CONCLUSIONS

We have developed a mixed-conducting ceramic material of the composition $SrFeCo_{0.5}O_x$ that selectively separates oxygen from air. The separated oxygen is then utilized for partial oxidation of methane into syngas. Long tubes of $SrFeCo_{0.5}O_x$ membrane have been fabricated by plastic extrusion. Performance of the membranes has been evaluated in a methane conversion reactor, and excellent methane conversion efficiency (>98%) and good CO selectivity (≈90%) were obtained in reactors run for >1000 h at 900°C. These ceramic membranes operate without electrodes or external power supply.

ACKNOWLEDGMENT

Work at ANL is supported by the U.S. Department of Energy, Federal Energy Technology Center, under Contract W-31-109-Eng-38.

REFERENCES

1. H. D. Gesser and N. R. Hunter, Chem. Rev., 85 (1985) 235.
2. N. D. Spenser and C. J. Pereira, J. Catal., 116 (1989) 399.
3. Y. Amenomiya, V. I. Birss, M. Goledzinski, J. Galuszka, and A. R. Sanger, Catal. Rev., Sci. Eng., 32 (1990) 163.
4. Y. Teraoka, H. M. Zhang, S. Furukawa, and N. Yamozoe, Chem. Lett., 1743 (1985).
5. T. J. Mazanec, T. L. Cable, and J. G. Frye, Jr., Solid State Ionics, 111 (1992) 53.
6. A. C. Bose, G. J. Stiegel, and R. D. Srivastava, Proc. 208th American Chemical Society Meeting, Washington, DC, Aug. 20-25, 1994, Vol. 39, No. 4, p. 1006 (ed. by H. P. Stephens, D. C. Cronauer, K. S. Vorres, and J. C. Crelling, American Chemical Society).
7. U. Balachandran, J. T. Dusek, S. M. Sweeney, R. B. Poeppel, R. L. Mieville, P. S. Maiya, M. S. Kleefisch, S. Pei, T. P. Kobylinski, and A. C. Bose, Bull. Amer. Ceram. Soc. 74 (1995) 71.
8. U. Balachandran, M. S. Kleefisch, T. P. Kobylinski, S. L. Morissette, and S. Pei, U.S. Patent 5,580,497, Dec. 3, 1996.
9. B. Ma, U. Balachandran, J.-H. Park, and C. U. Segre, Solid State Ionics, 83 (1996) 65.
10. B. Ma, U. Balachandran, J.-H. Park, and C. U. Segre, J. Electrochem. Soc., 143 (1996) 1736.
11. U. Balachandran, J. T. Dusek, R. L. Mieville, R. B. Poeppel, M. S. Kleefisch, S. Pei, T. P. Kobylinski, C. A. Udovich, and A. C. Bose, Applied Catalysis A: General, 133 (1995) 19.
12. M. Liu, Y. Shen, J. Ludlow, A. Joshi, and K. Krist, Proc. Intl. Gas Research Conf. (ed. by H. A. Thompson, Government Institutes, Inc., Rockville, MD, 1992) 183.
13. E. A. Hazbun, U.S. Patent 4,791,079, Dec. 13, 1988.
14. J. P. Ackerman and J. E. Young, U.S. Patent 4,476,198, Oct. 9, 1984.
15. T. D. Claar, D. E. Busch, and J. J. Picciolo, U.S. Patent 4,883,497, Nov. 28, 1989.
16. R. B. Poeppel and J. T. Dusek, U.S. Patent 4,476,196, Oct. 9, 1984.

THE USE OF CERAMIC MEMBRANE REACTORS FOR THE PARTIAL OXIDATION OF METHANE TO SYNTHESIS GAS

M. Schwartz, J. H. White, M. G. Myers, S. Deych and A.F. Sammells
Eltron Research, Inc., 5660 Airport Blvd., Boulder, CO 80301

Keywords: Ceramic membrane reactor; partial oxidation; synthesis gas

INTRODUCTION

Materials exhibiting mixed ionic and electronic conductivity are of commercial interest due to their application in fields such as oxygen separation, membrane reactors for oxidation reactions and electrocatalysis. Much of this work has focused on metal oxides crystallizing in the perovskite structure. For example, early work[1-3] studied compounds selected from $La_{1-x}Sr_xCo_{1-y}Fe_yO_{3-\delta}$. In this work, electrical and ionic conductivities were measured on a range of compositions and it was found that oxygen ion conduction was controlled mainly through oxygen vacancies in the lattice, indicating the importance of this structural feature in achieving high oxygen permeability.

Vacancies in the perovskite lattice are formed either through doping of the lattice or through the loss of oxygen when the material is exposed to atmospheres of low oxygen partial pressures. However, both of these vacancy formation mechanisms present problems. For example, doping of cations into the lattice can cause association between the dopants and the resulting oxygen vacancies.[4] This leads to high activation energies for ionic conduction. Loss of oxygen by reaction with the atmosphere leads to increases in lattice parameters and eventual phase decomposition, limiting the usefulness of such materials in commercial applications.

To overcome such problems, Eltron has been studying ionic conductors[5] and mixed ionic and electronic conductors based on the brownmillerite structure. This structure has general composition $A_2B_2O_5$ and is attractive as an oxide ion conductor since it can support a large population of oxide ion vacancies, both ordered and disordered, as well as a variety of substituents in the A and B lattice sites. The structure consists of BO_6 octahedral layers sharing vertices with a layer of BO_4 tetrahedra (Figure 1a). This difference in coordination sphere of B metal ions lends itself to controlled substitution. Depending on the particular metal ions, some distortion may be present in the polyhedra. This structure may be compared to the perovskite structure (Figure 1b) where B metal atoms occupy only octahedral sites with no inherent oxide ion vacancies.

The rationale for selecting specific A and B lattice substituents within the $A_2B_2O_5$ brownmillerite structure has evolved in part from recent studies performed at Eltron[5-8] which have identified clear correlations between perovskite crystallographic and thermodynamic parameters relating to the activation energy for ionic transport. These parameters include: 1) the average metal-oxygen bond energy within the perovskite, 2) lattice free volumes, obtained by subtracting the ionic volumes of cations and O^{2-} in the unit cell from the overall crystallographic unit cell, 3) the parameter $r_{critical}$ (r_c) which corresponds to the radius of the opening between the two A site cations and one B site cation through which the mobile anion must pass, and 4) lattice polarizability towards ionic migration. Eltron is currently applying this rationale to the selection of new brownmillerite materials for use as mixed conducting membranes.

Of all the potential applications of mixed ionic electronic conducting materials, the partial oxidation of methane to synthesis gas (syngas) is one of the most exciting and commercially important. The partial oxidation reaction of methane and oxygen to yield syngas is:

$$CH_4 + 1/2O_2 \rightarrow CO + 2H_2 \qquad (1)$$

The syngas can then serve as a precursor for a variety of products such as methanol, higher alcohols or Fischer-Tropsch products. This process is currently performed industrially but requires oxygen on a large scale, which is expensive. By performing this reaction with a membrane reactor, the oxygen is separated directly from air. This allows air to be used as the oxidant, greatly reducing syngas production costs.

In addition to the partial oxidation reaction, Eltron has been studying the combined partial oxidation/steam reforming and partial oxidation/CO_2 reforming reactions, similar to industrial autothermal reforming. In these processes, steam or CO_2 is added to the methane feedstream. This serves two purposes. First, since the partial oxidation reaction is highly exothermic and the steam and CO_2 reforming reactions are highly endothermic, the heat generated from the partial oxidation reaction can be used to drive the reforming reactions. This will allow for better thermal control of the reactions within the membrane reactor. The second purpose for a mixed feedstream is that the composition of the syngas product can be varied. Specifically, the addition of steam in the feedstream will increase the H_2:CO ratio in the synthesis gas product stream while the addition of CO_2 will decrease the H_2:CO ratio. The specific composition desired will depend upon the eventual end use of the syngas product.

In order to promote the partial oxidation reaction utilizing a mixed conducting membrane,

the ceramic membrane material needs to be formed into an appropriate reactor shape such as a thin plate, tube or monolith. In practice, one side of this reactor is exposed to air. The membrane reactor then serves to separate oxygen from the air. This oxygen is then transported as oxide ions through the membrane where it goes on to react with the methane present on the second side of the membrane yielding syngas. A schematic illustration of this process is shown in Figure 2.

In addition to Eltron, several other research groups are studying the use of mixed conducting ceramic membrane reactors for the partial oxidation of methane to syngas. One group, Mazenec et al. at BP Chemicals, have been studying materials as partial oxidation membrane reactors.[9,10] For example, they fabricated a membrane of composition $La_{0.2}Sr_{0.8}Fe_{0.8}Cr_{0.2}O_x$ into a tube and operated it for >1000hr at 1100°C as a partial oxidation reactor.[10] A second group, consisting of a team from Amoco and Argonne,[11] has been studying materials derived from intergrowths of the perovskite structure. Specifically, materials of composition $SrCo_{0.5}FeO_x$ have been fabricated into tubular membrane reactors and used to convert methane to syngas at 900°C at rates of 2-3scc/min-cm^2. High methane conversion was achieved and reactors were operated for 40 days.

As a means to develop commercially viable ceramic membrane reactors for the partial oxidation of natural gas, Eltron has prepared novel mixed conducting brownmillerite materials and successfully fabricated them into sintered disks and tubes. These disks and tubes have been incorporated into membrane reactors for the partial oxidation of methane. These materials have shown complete chemical and mechanical stability under expected operating conditions, including a long-term performance testing of >3000hr.

EXPERIMENTAL

Mixed conducting membrane materials were prepared by standard ceramic processing techniques. Metal oxides and carbonates, serving as the starting materials, were thoroughly mixed and calcined at 1200-1300°C until the desired brownmillerite phase was formed. These powders were then reduced in particle size using an attrition mill after which they were mixed with a standard binder. Membrane shapes were formed by pressing: uniaxial pressing in the case of disks and isostatic pressing in the case of open-both ends and closed-one-end tubes. After forming, the green bodies were densified by sintering in air at 1200-1400°C.

Membrane materials were characterized by X-ray diffraction (XRD) using Cuk_α radiation and experimental densities of sintered disks and tubes were determined using Archimedes' method. All materials studied in membrane reactors were single-phased and >90% of theoretical density.

Membrane reactors for the partial oxidation of methane to syngas were fabricated using sintered disks and open-both-end and closed-one-end tubes. Sealing of the reactors was achieved using glass seals. In all reactor experiments, air was used as the oxidant. 80% methane in helium was used primarily as the feedstock. However, experiments in which CO_2 or steam were added to the methane were also performed. CO_2 was added by mixing gases prior to entry into the reactor. Steam was added by sparging the methane:helium feedstream into a water bubbler. The concentration of the steam with respect to the methane was varied by heating the water bubbler. The humidity of the incoming and effluent streams was measured with commercial humidity sensors. Gas chromatography was used to analyze the syngas product stream as well as any leakage of air across the membrane.

RESULTS AND DISCUSSION

One of the most important properties necessary for industrial use of this technology is long-term stability of the membrane materials under actual operating conditions. An example of the long-term stability of Eltron's brownmillerite-based membrane materials is shown in Figure 3. In this experiment, a closed-one-end tube, 3.5cm long, served as the membrane reactor. The tube had an inner diameter of 8.6mm and a 1.2mm wall thickness. The outside of the tube was coated with a partial oxidation catalyst consisting of Ni supported on a perovskite-type metal oxide. The inside of the tube was coated with $La_{0.8}Sr_{0.2}CoO_3$ which served as the oxygen reduction catalyst. The experiment was performed at atmospheric pressure and 900°C.

As shown in Figure 3, the reactor has been operating for >3000hr with a syngas production rate between 10-15ml/min-cm^2 with a H_2:CO ratio that varied from 1.8 to 2, close to the expected value of 2. At ~700hr, there was a complete loss of activity because the methane tank serving the reactor ran empty. When the methane tank was replaced and the methane concentration returned to the previous value in the feed, the reactor resumed syngas production at a slightly lower, but steady rate. The reason for the lower production rate after restarting the reactor is not known but may be due to some loss of activity due to catalyst deactivation. No change in the H_2:CO ratio was observed after restarting the reactor. In addition to the syngas production, the CO_2 formed in the product was also monitored and was never more than 1-2% of the CO production rate indicating that no deep oxidation was occurring. During the course of this experiment, no evidence for mechanical or chemical instability was observed. Additionally, no leakage into the tube, as measured by the N_2 concentration in the product stream, was observed.

Further evidence of chemical stability is shown by XRD experiments performed on membrane materials operated in syngas production reactors for extended time periods. For example, a reactor fabricated from a sintered disk was operated for >1000hr at 900°C with a feed of ~80% CH_4 in helium. The oxygen partial pressure of the gas on this side of the membrane was estimated to be $< 10^{-17}$atm. After the reactor was voluntarily stopped, XRD was performed on the membrane partial oxidation surface. Figure 4 shows a comparison of this membrane surface with fresh powder. The two patterns are identical which indicates that even after this extended period of syngas production, the membrane material is stable with respect to chemical decomposition under operating conditions. Additionally, the membrane disk maintained its mechanical integrity over the course of the experiment.

As discussed above, Eltron has also studied the combined partial oxidation/steam reforming reactions. In a typical example, an open-both-ends tube served as the membrane reactor. The tube had an effective length of 3.9cm, an inner diameter of 0.7cm and a wall thickness of 1.6mm. The outside of the tube was coated with a partial oxidation catalyst, specifically Ni (40wt%) supported on Al_2O_3. The inside of the tube was coated with $La_{0.8}Sr_{0.2}CoO_3$ which served as the oxygen reduction catalyst. Steam was added to the methane stream and the CH_4:H_2O ratio was varied and measured as discussed above. The experiment was performed at atmospheric pressure and 900°C.

Figure 5 summarizes the results obtained during this experiment. The amount of H_2 produced decreased initially and then increased as a function of increasing H_2O in the feedstream. Additionally, the H_2:CO ratio in the product stream increased as expected. Also important was the observation that typically greater than 90% of the H_2O in the feedstream was consumed in the combined reactions. This indicates that the premise of combining these two reactions within a ceramic membrane reactor is valid.

In a similar fashion, the combined partial oxidation/CO_2 reforming reactions have also been studied. As a typical example, a sintered disk served as the membrane reactor. The effective surface area was 0.5cm^2 and the membrane thickness was 1.4mm. One side of the disk was coated with a partial oxidation catalyst, specifically Rh (5wt%) supported on a metal oxide. The opposite side of the disk was coated with $La_{0.8}Sr_{0.2}CoO_3$ which served as the oxygen reduction catalyst. The feed gas consisted of 80% methane with CO_2 and helium making the balance. The experiment was performed at atmospheric pressure and 900°C.

Figure 6 summarizes the results of this experiment. The amount of syngas produced initially increased and then decreased with increasing CO_2 content in the feedstream. The H_2:CO ratio decreased as expected. These results validate the concept of promoting the combined CH_4 partial oxidation reaction with the CH_4/CO_2 reforming reactions within a brownmillerite-based membrane reactor.

CONCLUSION

Eltron has developed new mixed ionic and electronic conducting ceramic materials based on the brownmillerite structure. These materials have been fabricated into shapes and incorporated into membrane reactors. These membrane reactors have been used to promote the partial oxidation of methane to syngas. The long-term stability of these materials has been demonstrated by the continuous operation of a tubular partial oxidation reactor for >3000hr. Additionally, the membrane reactors have been used in an autothermal configuration using steam or CO_2 with the methane feed.

REFERENCES

1. Teraoka, Y.; Zhang, H.M.; Furukawa, S; Yamazoe, N. *Chem. Lett.* **1985**, 1743-1746.
2. Teraoka, Y.; Zhang, H.M.; Okamoto, K.; Yamazoe, N. *Mat. Res. Bull.* **1988**, *23*, 51-58.
3. Teraoka, Y.; Nobunaga, T.; Yamazoe, N. *Chem. Lett.* **1988**, 503-506.
4. Kilner, J.A.; Brook, R.J. *Solid State Ionics* **1982**, *6*, 237-252.
5. Schwartz, M; Link, B.F.; Sammells, A.F. *J. Electrochem. Soc.* **1993**, *140*, L62-63.
6. Sammells, A.F.; Cook, R.L.; White, J.H.; Osborne, J.J.; MacDuff, R.C. *Solid State Ionics* **1992**, *52*, 111-123.
7. Sammells, A.F.; Cook, R.L. *Solid State Ionics* **1991**, *45*, 311-321.
8. Cook, R.L.; MacDuff, R.C.; Sammells, A.F. *J. Electrochem. Soc.* **1990**, *137*, 3309-3310.
9. Mazenec, T.J.; Cable, T.L.; Frye, Jr., J.G.; Kliewer, W.R. U.S. Patent 5 306 411, 1994.
10. Mazenec, T.J Presented at the 188th Electrochemical Society Meeting, Chicago, IL, October 1995.
11. Balachandran, U.;, Dusek, J.T.; Mieville, R.L.; Poeppel, R.B.; Kleefisch, M.S.; Pei, S.; Kobylinski, T.P.; Udovich, C.A.; Bose, A.C. *Appl. Cat. A: Gen.* **1995**, *133*, 19-29.

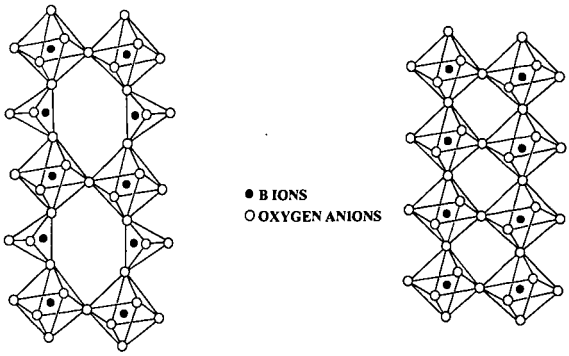

Figure 1. Comparison of brownmillerite (A) and perovskite (B) structures. A cations are omitted for clarity.

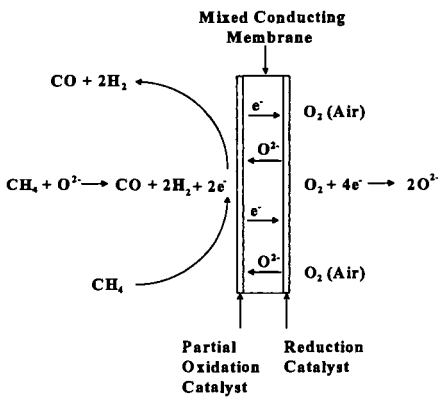

Figure 2. Schematic illustration of processes occurring during the partial oxidation of methane using a ceramic membrane reactor.

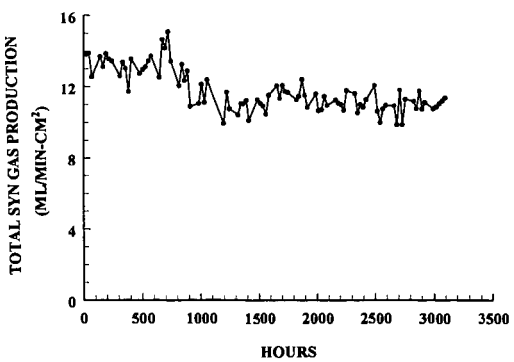

Figure 3. Plot of total synthesis gas production from the partial oxidation of methane using a tubular ceramic membrane reactor showing long-term stability.

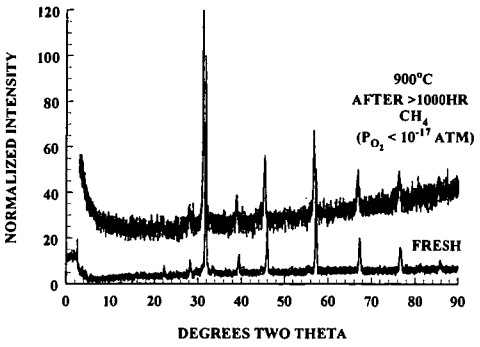

Figure 4. Comparison of XRD patterns for as-prepared membrane material and of the surface of the membrane exposed to methane during the partial oxidation reaction for >1000 hours at 900°C.

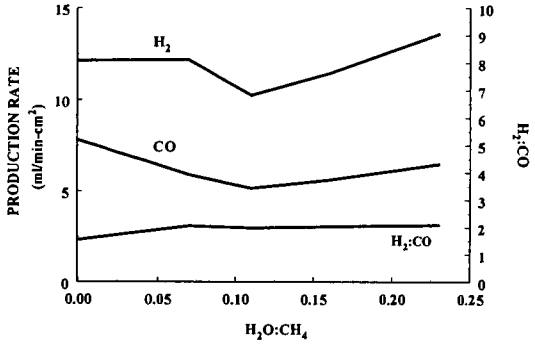

Figure 5. Plots of H_2 and CO production rates and H_2:CO ratio as a function of the H_2O:CH_4 ratio in the feedstream for the combined partial oxidation/steam reforming reactions mediated by a ceramic membrane reactor at 900°C.

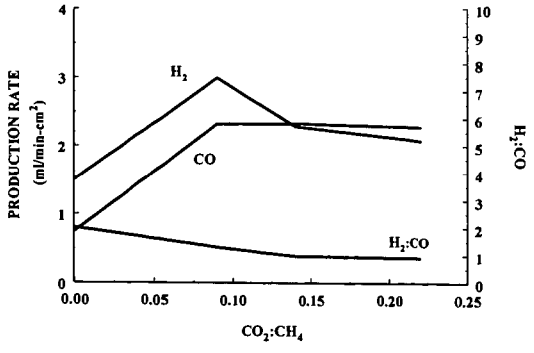

Figure 6. Plot of H_2 and CO production rates and H_2:CO ratio as a function of the CO_2:CH_4 ratio in the feedstream for the combined partial oxidation/CO_2 reforming reactions mediated by a ceramic membrane reactor at 900°C.

PARTIAL OXIDATION OF METHANE TO SYNGAS USING FAST FLOW MEMBRANE REACTORS

Michael W. Alibrando and Eduardo E. Wolf
Department of Chemical Engineering
University of Notre Dame
Notre Dame, IN 46637

Keywords: Methane, Syngas, Membranes

Previous studies have shown that high methane conversions and selectivities to syngas can be achieved while operating at very high space velocities and relatively low methane/oxygen feed ratios. This has been accomplished at relatively high temperatures (~1000°C) in a monolith reactor. (1, 2) The monolith reactor is characterized by an open pore structure which permits very fast gas flows and results not only in high syngas yields, but autothermal operation as well.

Achieving autothermal behavior is significant because a reactor which operates autothermally requires heat only during ignition. In the case of Schmidt and coworkers (1, 2), ignition occurs by passing an ammonia/air mixture over the monolith at around 300°C. Once ignited, the temperature increases rapidly to the steady state temperature, and the ammonia/air mixture is replaced by the methane/oxygen mixture. If industrial scale reactors could be operated autothermally, a significant amount of capital can be saved due to the fact that the reactor must be heated only during startup.

Although these results are very promising, this reactor configuration presents several problems. It requires operating at relatively high temperatures and the use of a different gas mixture during startup. In addition, at these high temperatures and low methane/oxygen feed ratios the potential for an explosion exists due to the possibility of flame flashback. As a result, this reactor configuration could never be implemented industrially due to safety concerns.

Therefore, we attempted to achieve high syngas yields and autothermal behavior while operating in a safer, industrially favorable environment. The intention was to operate at high space velocities, but at significantly lower temperatures. This was accomplished with the use of a highly active 3% Rh supported on TiO_2 catalyst. This catalyst was used in previous studies on the methane partial oxidation reaction in which the reactor was operated at lower space velocities and diluted gas feeds. (3)

In this case, a small amount of the 3% Rh catalyst (only 30 mg) was used in a fixed bed reactor which was operated at millisecond residence times and a methane/oxygen feed ratio of 2/1. The results are shown in Table 1. Despite the fact that the total feed rate was varied between 235 and 1500 cc/min there was very little change in conversion and selectivity. Methane conversion remained between 55 and 70% and CO selectivity remained around 90%. In addition, oxygen conversion was 100% in all cases.

However, under these conditions, relatively high conversions and selectivities were achieved at steady state temperatures in the range of 500-600°C. Although the yields are lower than Schmidt and coworkers, the reaction temperatures were significantly lower. In addition, the system was ignited under methane/oxygen mixtures at 320°C which is several hundred degrees lower than the ignition temperatures using the monolith, thus eliminating the need for the ammonia/air mixture. Another benefit of the Rh catalyst was that it was stable and did not deactivate for several days.

Despite the fact that the use of the 3% Rh catalyst in the fixed bed reactor allowed for safer operation than the monolith reactor, a difficulty still exists. Although the temperatures with the fixed bed were drastically lower than with the monolith and the possibility of explosion has been lowered, the potential for an explosive mixture still exists. An oxygen rich mixture still contacts a high temperature surface, and if the high flow reactor system is to be implemented in industry, the potential for explosion must be eliminated.

Therefore, a reactor scheme was conceived which would allow for high space velocities and overall low methane/oxygen feed ratios while separating the gas reactants until reaching the catalyst surface. The idea of using a separate oxygen feed for methane oxidation was based on previous work in our group on the distribution of oxygen during the methane oxidative coupling reaction. (4) The implementation of the new reactor scheme opens up the possibility of practical applications for the partial oxidation of methane to syngas and also the oxidative dehydrogenation of alkanes.

The membrane reactor consists of a highly porous membrane tube, with one end sealed, which is placed concentrically inside a quartz tube. The upper portion of the membrane tube is made impermeable using a ceramic glaze, leaving only a small length at the lower portion of the tube permeable. The catalyst is placed around the permeable portion of the membrane tube forming a ring in between the membrane tube and the outer quartz wall. Oxygen is fed to the membrane tube and flows exclusively inside the membrane tube until reaching the permeable portion at the bottom of the tube where it permeates to the shell side and immediately contacts the catalyst surface. Methane is fed to the shell side and flows in the annular space between the membrane wall and the quartz wall. In this scheme, the reactants mix only in the region where the catalyst is located, and because 100% oxygen conversion was achieved in every previous experiment, the possibility of oxygen rich mixtures developing is negligible. The membrane wall itself is highly permeable allowing for the use of fast flowrates in the range of millisecond residence times. Thus, the overall methane/oxygen feed ratio can remain low while operating at high space velocities in a reactor configuration which is both safe and economical.

The membrane reactor successfully achieved its goal of obtaining high conversions and selectivities while providing a safe operating environment. Table 2 shows the effect of feed rate on conversion and selectivity using 60 mg of catalyst and a methane/oxygen feed ratio of 2/1. The minimal amount of catalyst that can be used is 60 mg as this is the amount required to completely surround the permeable portion of the membrane tube.

The results are similar to those in the case of the fixed bed reactor in that for a significant change in feed rate (300 cc/min to 1080 cc/min) there is only a slight change in conversion and selectivity. Methane conversion remained primarily between 65 and 75%, CO selectivity remained around 90% and hydrogen selectivity remained primarily around 70%. Once again oxygen conversion was 100% in all cases.

Although methane conversion is slightly lower in the membrane reactor than in the fixed bed reactor, the membrane reactor is the preferred reactor due to the safety factor. Complete oxygen conversion is achieved indicating that the possibility of oxygen rich mixtures, and therefore the possibility of explosion, is negligible. Most industrial reactors are operated well below optimal yields for safety reasons, and a 5% drop in conversion is acceptable if a safe operating environment is assured.

Further experiments were conducted in the membrane reactor in an attempt to increase methane conversion. As soon as a safe reactor configuration had been developed, it was desired to determine if the yields could be improved within this system. The operational variable on which syngas production was most dependent was the methane/oxygen feed ratio. Because the methane and oxygen feeds are kept separate until contacting the catalyst, the partial oxidation reaction could be studied at lower methane/oxygen feed ratios. Table 3 shows the effect of the methane/oxygen feed ratio in the membrane reactor using 60 mg of catalyst.

Methane conversion varies from as high as 64% at the lower ratios to as low as 44% at the higher ratios. Hydrogen and CO selectivities vary from 22 and 67% at low ratios to 82 and 90% respectively at high ratios. However, even at low methane/oxygen ratios, oxygen conversion remains at 100%.

The important result obtained is that both CO and hydrogen selectivities were lower at the lower feed ratios, particularly when the ratio is less than 2/1. The hydrogen selectivity falls below 25%, and the CO selectivity falls below 70%. This is an indication that the partial oxidation reaction is no longer dominant, and the complete combustion reaction begins to occur. This effect can be explained by the fact that at the lower feed ratios, more oxygen is available to form carbon dioxide and water. At higher feed ratios, the concentration of oxygen is low and hence methane reacts to form CO instead of CO_2.

The decreasing of temperature would seem to justify the above conclusion. At lower feed ratios, the temperature is significantly greater than at the higher ratios. At feed ratios less than 2/1, the steady state temperature rises above 700°C, but at ratios greater than or equal to 2/1 the temperature is in the 500°C range. The higher temperature can be accounted for by the reaction of hydrogen and oxygen to form water and the occurrence of complete combustion which has a higher heat of reaction than partial oxidation. In addition, as methane conversion decreases the heat generated decreases and the temperature decreases.

The effect feed ratio has on methane conversion is interesting. Although 100% conversion of oxygen is achieved at low feed ratios, methane conversion levels off at 64%. This is not expected because as the concentration of oxygen increases higher methane conversions would be expected due to the fact that oxygen was the limiting reagent in all experiments. Additional oxygen should result in higher conversions, but instead results in more of the reacted methane being converted to CO_2 and water. At higher feed ratios, the reactor operates as expected as the methane conversion begins to decrease.

After it had been determined that the conversion could not be significantly increased by varying the operational parameters of the membrane reactor, an attempt was made to increase conversion by allowing the unreacted methane to participate in another reaction. For this purpose a new, double bed reactor was designed to allow for a second catalyst bed and a third reactant feed downstream from the first catalyst bed.

The double bed reactor is identical to the membrane reactor in the upper portion allowing for autothermal behavior of the partial oxidation reaction. The difference is that an additional quartz tube is placed concentrically inside the quartz reactor shell downstream from the first catalyst bed. At the top of the additional tube is a quartz cross which serves the purpose of supporting a second catalyst bed. The quartz tube is open at both ends allowing for an additional reactant to be fed over the second catalyst bed and downstream from the first catalyst bed.

The reaction chosen for the second bed was the dry reforming reaction. The hypothesis was that the unreacted methane from the partial oxidation reaction would react with carbon dioxide which would be added downstream and over the second catalyst bed. The dry reforming reaction is very endothermic, but an enormous amount of heat is evolved from the reaction in the first bed and the original hypothesis was that the heat from the first bed reaction could be used to drive the reaction in the second bed.

Initial results indicated that feeding carbon dioxide downstream would increase methane conversion, but only slightly. The reason was that the first catalyst bed did not provide enough heat to sustain the very endothermic dry reforming reaction over the second catalyst bed. It was observed that the temperature of the second catalyst bed decreased upon introduction of carbon dioxide to the reactor. This indicates that the dry reforming reaction does occur, but there is not enough heat available to sustain the reaction.

It was then decided to continue to feed carbon dioxide downstream from the first bed, but to increase the temperature of the second bed to provide enough heat for the dry reforming reaction. In this experiment, 60 mg of the Rh catalyst were used in both beds and the methane, oxygen and carbon dioxide feed rates were maintained at 500, 250 and 60 cc/min respectively as the second bed temperature was increased. Table 4 shows the effect of the second bed temperature on conversion and selectivity.

The results indicate that high methane conversions can be achieved while maintaining high CO and hydrogen selectivities. At a second bed temperature of 700°C, methane conversion reached 83% with CO and hydrogen selectivities of 85 and 64% respectively. These high syngas yields have been obtained in a reaction environment which is safe and could be modified for industrial use.

In addition, further studies with the double bed reactor indicate that both catalyst beds can be operated autothermally if oxygen is used as the downstream feed instead of carbon dioxide. In this case, the second bed temperature rapidly increases upon introduction of the downstream oxygen feed. This indicates that a second ignition occurs in the reactor and that both beds operate autothermally.

The double bed reactor served the purpose of increasing conversion, but there was still no explanation for the fact the operational parameters had little effect on conversion and selectivity in the fixed bed and membrane reactors. It was not until theoretical reactor simulations were conducted that the reason became clear.

The theoretical model is similar to the elementary step model proposed by Hickman and Schmidt (5), and is used to evaluate results from the fixed bed reactor. The mechanism consists of twenty-one elementary steps which are combined with the reactor mass balances. All of the kinetic parameters used in the model are taken from previous studies. The only modification is that the activation energy for CO desorption was lowered due to the fact that the CO surface concentration was significantly higher than the other species. Lowering the activation energy can be justified by previous studies that report the activation energy will decrease at higher surface concentrations. (5, 6) At this lower value of the activation energy for CO desorption, the model results adequately matched the experimental data.

After comparing the model results to the fixed bed experiments, a parametric sensitivity study was conducted. The study indicated that an increase in methane conversion requires and increase in the rate of methane adsorption and a decrease in oxygen adsorption. The sensitivity study also indicated that CO desorption is one of the rate determining steps and that the dry and steam reforming reactions have little effect on conversion and selectivity at these conditions.

The model also predicts that most of the reaction occurs in a very narrow region near the entrance of the bed, with the rest of the bed contribution being relatively small. In addition, all of the oxygen is consumed by the midpoint of the bed. This would explain the lack of sensitivity of the fixed bed experimental results to changes in operating variables.

Although the model results are for a fixed bed reactor, certain conclusions about the membrane reactor can be drawn. A reasonable assumption is that the profiles near the membrane tube wall are similar to the entrance of the fixed bed reactor. This would indicate that all of the oxygen is consumed near the membrane wall and most of the reaction occurs in this region. This would explain why varying the operating conditions would not result in an increase in methane conversion. All of the oxygen is consumed near the membrane wall and therefore any methane that flows near the outer portion of the reactor will not be converted. To further study the profiles and performance of the membrane reactor, a two dimensional reactor model is now under development.

In summary, very promising results have been achieved in this study. High conversions and selectivities to syngas have been achieved in the membrane reactor. In addition, the reaction is carried out in safe and economical environment without the explosive problems which exist in previous reports. Future possibilities involve the study of the oxidative dehydrogenation of alkanes, which is a very important reaction at the industrial level.

REFERENCES

1. D. A. Hickman and L. D. Schmidt. *J. Catal.* **138** 267 (1992).
2. P. M. Torniainen, X. Chu and L. D. Schmidt. *J. Catal.* **146** 1 (1994).
3. T. Shiraha. M. S. Thesis. University of Notre Dame (1995).
4. J. M. Santamaría, E. E. Miro and E. E. Wolf. *Ind. Eng. Chem. Res.* **30** 1157 (1991).
5. D. A. Hickman and L. D. Schmidt. *AIChE J.* **39** 1164 (1993).
6. V. Nehasil, I. Starva and V. Matolin. *Surf. Sci.* **331-333** 105 (1995).

Table 1. Effect of Total Feed Rate.					
Total Feed Rate (cc/min)	Temperature (°C)	Methane Conversion (%)	Oxygen Conversion (%)	CO Selectivity (%)	Hydrogen Selectivity (%)
235	401	54	100	76	34
525	558	58	100	88	77
750	564	70	100	89	70
1130	629	65	100	90	64
1500	641	68	100	90	50

Table 2. Effect of Total Feed Rate Using the Membrane Reactor.					
Total Feed Rate (cc/min)	Temperature (°C)	Methane Conversion (%)	Oxygen Conversion (%)	CO Selectivity (%)	Hydrogen Selectivity (%)
300	419	64	100	75	62
450	494	75	100	88	72
600	520	64	100	86	76
750	515	64	100	90	82
900	607	52	100	86	69
1080	680	35	100	81	90

Table 3. Effect of Methane/Oxygen Feed Ratio Using the Membrane Reactor.					
Methane/ Oxygen Feed Ratio	Temperature (°C)	Methane Conversion (%)	Oxygen Conversion (%)	CO Selectivity (%)	Hydrogen Selectivity (%)
1	710	64	100	67	22
1.33	757	64	100	81	35
1.5	702	63	100	85	45
2	515	64	100	90	82
2.6	510	52	100	90	82
3.3	410	44	100	84	80

Table 4. Effect of Second Bed Temperature Using the Double Bed Reactor.					
Second Bed Temperature (°C)	First Bed Temperature (°C)	Methane Conversion (%)	Oxygen Conversion (%)	CO Selectivity (%)	Hydrogen Selectivity (%)
300	516	73	100	87	83
400	596	74	100	77	60
500	627	75	100	78	61
600	682	78	100	81	64
700	759	83	100	85	64

GROUP (V) AND (VI) TRANSITION METAL CARBIDES AS NEW CATALYSTS FOR THE REFORMING OF METHANE TO SYNTHESIS GAS

Andrew P. E. York, John B. Claridge,[†] Carlos Márquez-Alvarez,[‡] Attila J. Brungs and Malcolm L. H. Green*

The Catalysis Centre, Inorganic Chemistry Laboratory, University of Oxford, South Parks Road, Oxford, OX1 3QR, U. K.

[†] Current address: Department of Chemistry and Biochemistry, University of South Carolina, Columbia, SC 29208, U.S.A.

[‡] On leave from: Instituto de Catálisis y Petroleoquímica, CSIC, Campus Cantoblanco, 28049 Madrid, Spain

Keywords: early transition metal carbides; methane dry reforming; methane partial oxidation.

ABSTRACT

High surface area group V and VI transition metal carbides, synthesised by temperature programmed reduction of the metal oxides with methane/hydrogen, have been tested as catalysts for the dry reforming of methane with carbon dioxide and partial oxidation of methane with air. Mo_2C and WC were stable and highly active catalysts for these reactions at elevated pressure, while they deactivated at ambient pressure. The product distribution obtained was close to that predicted by the thermodynamic equilibrium, except that no carbon formation was observed on the catalyst surface. The carbides of niobium and tantalum deactivated, even in the dry reforming reaction at elevated pressure, due to their greater tendency towards oxidation.

INTRODUCTION

Synthesis gas (carbon monoxide and hydrogen) is an extremely important intermediate in the production of many chemicals, for example Fischer-Tropsch synthesis of hydrocarbons (e.g. in the Shell middle distillate process or at SASOL) and alcohols [1-3], ammonia synthesis (Fe catalysts) [4], methanol synthesis ($Cu/ZnO/Al_2O_3$) [5,6], and hydroformylation (homogeneous Rh catalyst) [7], and is also used in the reduction of iron ore. Of these many products, methanol, and higher alcohols, are often discussed as environmentally friendly fuel alternatives [8], while the development of hydrogen for use as an altemative fuel or in fuel cells is currently receiving much attention [9].

At present, synthesis gas is produced in great quantities from methane, mainly by the highly endothermic steam reforming process *(1)*, and to a lesser extent by endothermic dry reforming with carbon dioxide *(2)*; an alternative route is *via* the exothermic partial oxidation reaction *(3)*.

$$CH_4 + H_2O \rightarrow CO + 3\,H_2 \qquad \Delta H^\circ_{298} = +206 \text{ kJ mol}^{-1} \qquad (1)$$

$$CH_4 + CO_2 \rightarrow 2\,CO + 2\,H_2 \qquad \Delta H^\circ_{298} = +247 \text{ kJ mol}^{-1} \qquad (2)$$

$$CH_4 + \tfrac{1}{2}O_2 \rightarrow CO + 2\,H_2 \qquad \Delta H^\circ_{298} = -38 \text{ kJ mol}^{-1} \qquad (3)$$

Currently, nickel catalysts are employed industrially for both the steam reforming and dry reforming reactions [10], while partial oxidation is carried out autothermally [11]. However, since nickel also catalyses the carbon deposition reactions, methane decomposition and CO disproportionation (Boudouard reaction), an excess of oxidants is needed in order to prevent catalyst deactivation and blockages in the reactor tubes; this results in the production of synthesis gas with product ratios that are not optimal for further conversion downstream [10,12]. Alternative catalysts are the supported noble metals [13-18], or sulphur passivated nickel [19], both of which have been shown to exhibit kinetic resistance to carbon formation at or near stoichiometric reactant ratios; however, their application has been limited by the unfavourable economics and scarcity of the former, and the low activity of the latter.

In the past two decades, it has been shown that some transition metal carbides and nitrides, particularly those of group VI, possess catalytic properties similar to the noble metals [20-22]. Since the group VI transition metals are abundant and relatively cheap, it has been suggested that they can replace the scarce and expensive noble metals for a number of catalytic applications. Initial problems centred on the synthesis of high specific surface area (S_g) materials suitable for use as catalysts. However, following the publication of a number of methods for the synthesis of metal carbides/nitrides with $S_g \leq 220$ m^2 g^{-1} [23-25], it was shown that these materials were active for a number of catalytic reactions, including alkane isomerization, ammonia synthesis, and Fischer-Tropsch synthesis, to name only a few [26].

In this paper we present the results of methane dry reforming and partial oxidation over the group V and VI transition metal carbides. We have found that the high surface area carbides of molybdenum and tungsten, under stoichiometric reactant feeds and elevated pressure, are

stable and highly active catalysts for these reactions; no carbon formation was observed over the carbide surface during the reactions.

EXPERIMENTAL

Catalyst Synthesis and Characterisation

The high surface area metal carbide materials were prepared using the temperature programmed reduction method pioneered by Boudart and co-workers [23]: briefly the low surface area metal oxide powder was heated in flowing 20% CH_4/H_2 mixture from room temperature to 1000-1223K, depending on the oxide (discussed later), at 1 K min^{-1}. Normally the catalysts were prepared *in situ* and tested immediately. The post-synthesis high surface area carbides are readily and exothermically oxidised by air at room temperature and, therefore, passivation in flowing 1% O_2/N_2 for 10 hours at room temperature was carried out before exposure to the atmosphere and characterization. Crystalline components of the materials were identified by X-ray diffraction (XRD) using a Philips PW1710 diffractometer with Cu-Kα radiation.

Catalyst Testing

The apparatus used in this work was a modified version of the commercial Labcon microreactor described previously [27]. The reactor was built using 1/8" and 1/16" o.d. 316 stainless steel tubing and 316 stainless steel Swagelok fittings throughout. The catalyst sample was placed between two quartz wool plugs in the centre of a 4 mm i.d. silica tube and inserted into a vertical Severn Science tube furnace, heated to the required reaction temperature and controlled from a Eurotherm 905 temperature controller. For safety reasons, in experiments carried out at elevated pressures the silica tube was placed inside a steel tube. Inlet gas flow rates were controlled using Brooks 5850TR mass flow controllers, and the exit gas stream from the reactor passed through a Tescom two stage back-pressure regulator to allow elevated pressure experiments to be carried out. All the pipework was heated to prevent condensation of the products.

Product analysis was carried out using a Hewlett-Packard 5890II gas chromatograph, fitted with both a thermal conductivity detector, and a methanator/flame ionization detector. Separation of the products was achieved using a 3m Porapak Q packed column, with argon carrier gas. In all cases stoichiometric gas mixtures were used and carbon balances were better than 97%.

RESULTS AND DISCUSSION

Synthesis and Characterisation

Synthesis of the metal carbides was carried out using temperature programmed reduction with CH_4/H_2, as mentioned above, and it was noticed, by monitoring the effluent gas by real-time mass spectrometry, that the final temperature needed for complete formation of the carbide varied from 1023K for molybdenum carbide to 1223K for tantalum carbide; this is due to the relative reducibility of the oxides.

Some of the characterising data obtained for the metal oxides and metal carbides studied are presented in Table 1. The metal carbide phase formed was determined by XRD of passivated samples; the structures were identified by comparison with the literature [28]. No metal oxide could be seen in any of the diffraction patterns, showing that the passivation method only results in the oxidation of the surface of the carbide samples, while the bulk remains unaffected. N_2 BET of passivated metal carbide samples confirmed that high surface area materials had been synthesised.

Methane Dry Reforming with Carbon Dioxide

The results obtained for the dry reforming of methane with carbon dioxide over bulk NbC_x, TaC_x, β-Mo_2C and α-WC, as well as over bulk SiC, are presented in Table 2. The silicon carbide (Norton Materials UK) used here had a low surface area ($\approx$1 m^2 g^{-1}), and had very low catalytic activity for the dry reforming reaction. Indeed, at 1223K, the methane and carbon dioxide conversions were only 13.3% and 3.4% respectively, while at 1373K the conversions were much higher, due to the important role of autothermal processes. Thus, it can be concluded that the autothermal contribution is minor at or below 1223K, i.e. in the temperature range used for the catalytic study of the carbides.

The results obtained for Mo_2C and WC, presented in Table 2, are extremely similar to those expected from thermodynamics, demonstrating that these materials are efficient catalysts for methane dry reforming; in contrast, NbC_x and TaC_x gave relatively low conversions and yields, except when the temperature was increased to 1373 K. This indicates that the carbides of niobium and tantalum are formed, but that they are only stable at very high temperatures (and probably higher pressures). Indeed, Figure 1 shows that Mo_2C is the most stable of the carbides tested, while NbC_x and TaC_x deactivated rapidly at 1223K; NbC_x was stabilised to some extent at 1373K, but the high H_2/CO ratio given in Table 2 indicated that carbon formation was occurring at this high temperature, probably *via* autothermal reactions. The stability of WC was found to be

extremely similar to that of Mo_2C under the conditions employed here (not shown), with no deactivation observed for > 72 h on stream at 8 bar and 1223 K. Further, Figure 1 shows that elevated pressures are required to stabilise the catalysts. Powder XRD of post-catalytic β-Mo_2C samples demonstrated that the deactivated sample contained a large amount of MoO_2, which has only a very low activity for methane dry reforming, while the stabilised catalyst had only peaks due to the starting carbide. The reason for the deactivation of the NbC_x and TaC_x samples is that these materials are less stable than the carbides of Mo and W, as borne out by the higher temperature needed to synthesise the carbide; this means that, under the equilibrium conditions existing during the reaction, oxidation of NbC_x or TaC_x proceeds more readily than recarbidation.

Since carbon formation is a well known problem in methane dry reforming, post-catalytic samples of β-Mo_2C and α-WC were studied by high resolution electron microscopy (not shown). No carbon deposits were observed on the catalyst surface, even under our stoichiometric reactant feeds; this compares favourably with the results published previously for commercial nickel catalysts [29].

Methane Partial Oxidation with Air

Table 3 shows the results obtained for the partial oxidation of methane with air, over β-Mo_2C and α-WC. Oxygen conversion was essentially 100% for all the experiments. As before, when the oxidation reactions were carried out at ambient pressure the catalyst deactivated by forming MO_2, although the deactivation occurred much more quickly in the presence of air than was the case with carbon dioxide, meaning that an initial activity could not be obtained. However, when the partial oxidation was carried out at elevated pressure the catalyst activity was stabilised, and no deactivation was observed for the duration of the experiments (> 72 h), as shown in Figure 2 for β-Mo_2C. Post-catalytic XRD of the samples showed that no phase changes had occurred, and that no MO_2 or MO_3 had been formed during the reaction. This is particularly important in the case of molybdenum, since the formation of MoO_3 at these high temperatures would lead to loss of catalyst by vaporisation, or movement of the catalyst along the reactor tube. HRTEM of the post-catalytic samples indicated that no carbon deposition had occurred on the catalyst surface during the reaction.

The effect of temperature and pressure on the product distribution was determined using a β-Mo_2C catalyst, at temperatures between 1073 K and 1223 K and at pressures varying from 3 to 12 bar; the results obtained are presented in Figures 3a and b. As the temperature was increased or the pressure decreased, the conversion of methane and selectivity to carbon monoxide increased; these trends can be predicted from thermodynamic calculations, and demonstrates that the carbides are efficient catalysts for this reaction.

CONCLUSIONS

We have found that high surface area molybdenum and tungsten carbides are stable catalysts for the stoichiometric carbon free reforming of methane with carbon dioxide and air at elevated pressure. These materials are much cheaper than the platinum group metals, e.g. MoO_3 is 2000 times cheaper than platinum [30], so they may be useful alternatives to conventional industrial catalysts for synthesis gas production. Methane dry reforming with niobium and tantalum carbides showed that these materials are less stable, although niobium carbide was stabilised when very high temperatures were used.

REFERENCES

1. G. Henrici-Olivé and S. Olivé, *Angew. Chem. Int. Ed. Engl.*, **15**, 136 (1976).
2. M. E. Dry, *J. Organomet. Chem.*, **372**, 117 (1989).
3. J. Eilers, S. A. Posthuma and S. T. Sie, *Catal. Lett.*, 7, 253 (1990).
4. M. V. Twigg (ed.), "Catalyst Handbook" 2nd Edn., 384 (Wolfe Publishing, London, 1989).
5. J. C. Bart and R. P. A. Sneeden, *Catal. Today*, **2**, 1 (1987).
6. G. Chichen, P. J. Denny, J. R. Jennings, M. S. Spencer and K. C. Waugh, *Appl. Catal.*, **36**, 1 (1988).
7. R. L. Pruett, *J. Chem. Ed.*, **63**, 196 (1986).
8. R. Sethuraman, H. W. Parker, T. T. Maxwell and J. C. Jones, *J. Energy Res. Tech. - Trans. ASME*, **116**, 155 (1994).
9. D. Knott, *Oil and Gas Journal*, **92**, 26 (1994).
10. J. R. Rostrup-Nielsen, in "Catalysis Science and Technology" (eds. J. R. Andersen and M. Boudart),Vol. 5, p.1. (Springer, Berlin. 1984).
11. S. T. Sie, M. M. G. Senden and H. M. H. Wechem, *Catal. Today*, **8**, 371 (1991).
12. J. M. Fox III, *Catal. Rev.-Sci. Eng.*, **35**, 169 (1993).
13. J. R. Rostrup-Nielsen, *J. Catal.*, **31**, 173 (1973).
14. A. T. Ashcroft, A. K. Cheetham, J. S. Foord, M. L. H. Green, C. P. Grey, A. J. Murrell and P. D. F. Vernon, *Nature*, **344**, 319 (1990).
15. P. D. F. Vernon, M. L. H. Green, A. K. Cheetham and A. T. Ashcroft, *Catal. Lett.*, **6**, 181 (1990).

16. A. T. Ashcroft, A. K. Cheetham, M. L. H. Green and P. D. F. Vernon, *Nature*, **352**, 225 (1991).
17. J. R. Rostrup-Nielsen and J.-H. Bak Hansen, *J. Catal.*, **144**, 38 (1993).
18. J. B. Claridge, M. L. H. Green, S. C. Tsang, A. P. E. York, A. T. Ashcroft and P. D. Battle, *Catal. Lett.*, **22**, 299 (1993).
19. J. R. Rostrup-Nielsen, *J. Catal.*, **85**, 31 (1984).
20. J. M. Muller and F. G. Gault, *Bull. Soc. Chim. Fran.*, **2**, 416 (1970).
21. R. B. Levy and M. Boudart, *Science*, **181**, 547 (1973).
22. M. J. Ledoux, C. Pham-Huu, J. Guille and H. Dunlop, *J. Catal.*, **134**, 383 (1992).
23. J. S. Lee, S. T. Oyama and M. Boudart, *J. Catal.*, **106**, 125 (1987).
24. L. Leclercq, M. Provost, H. Pastor, J. Grimblot, A. M. Hardy, L. Gengembre and G. Leclercq, *J. Catal.*, **117**, 371 (1989).
25. M. J. Ledoux and C. Pham-Huu, *Catal. Today*, **15**, 263 (1992).
26. "The Chemistry of Transition Metal Carbides and Nitrides" (ed. S. T. Oyama, Blackie Academic and Professional, Glasgow, 1996).
27. J. B. Claridge, A. P. E. York, A. J. Brungs, S. C. Tsang and M. L. H. Green, *J. Catal.*, submitted.
28. E. K. Storms, "The Refractory Carbides", Vol. 2 (Academic Press: New York, 1967).
29. M. Audier, A. Oberlin, M. Oberlin, M. Coulon and L. Bonnetain, *Carbon*, **19**, 217 (1981).
30. London Metal Exchange, 19 Sept., 1996.

TABLES

Table 1. Some characteristics of the metal carbides synthesised by CH_4 TPR.

			CH_4 TPR synthesis	
Precursor	Carbide phase	Structure	Final T / K	S_g / $m^2 g^{-1}$
MoO_3	β-Mo_2C	h.c.p.	1023	91
WO_3	α-WC	h.c.p.	1153	39
Nb_2O_5	NbC_x	f.c.c.	1173	62
Ta_2O_5	TaC_x	f.c.c.	1223	54

x = 0.70-0.99 [NbC_x] and [TaC_x].

Table 2. Results for the dry reforming of methane over the group V and VI transition metal carbides (GHSV = 2.87 x 10^3 h^{-1}, CH_4/CO_2 = 1).

Catalyst	T / K	P / bar	C[CH_4]/ %	C[CO_2]/ %	Y[CO]/ %	H_2/CO
SiC	1223	8.0	13.3	3.4	8.1	-
	1373	8.0	76.3	75.2	75.7	0.90
NbC_x	1223	8.0	67.6	77.3	72.4	0.82
	1373	8.0	83.7	96.3	90.0	1.33
TaC_x	1223*	8.0	54.7	61.5	58.1	0.67
β-Mo_2C	1123	1.0†	92.4	92.5	92.5	0.93
	1223	1.0†	98.8	95.9	95.9	0.92
	1123	8.3	62.5	75.9	69.5	0.78
	1223	8.3	83.3	89.5	86.5	0.88
α-WC	1123	1.0†	92.0	93.1	92.6	0.94
	1123	8.3	62.7	75.4	68.6	0.79

† catalyst deactivates; * initial result could not be obtained.

Table 3. Results for the partial oxidation of methane over molybdenum and tungsten carbide catalysts (T = 1173 K, GHSV = 5.25 x 10^3 h^{-1}, CH_4/air =2/5).

Catalyst	P / bar	C[CH_4]/ %	S[CO]/ %	S[CO_2]/ %	H_2/CO
β-Mo_2C	8.7	88	92	8	2.02
α-WC	8.7	89	90	10	2.05

FIGURES

Figure 1. Stabilities of the transition metal carbides for methane dry reforming (CH_4:CO_2 = 1:1).

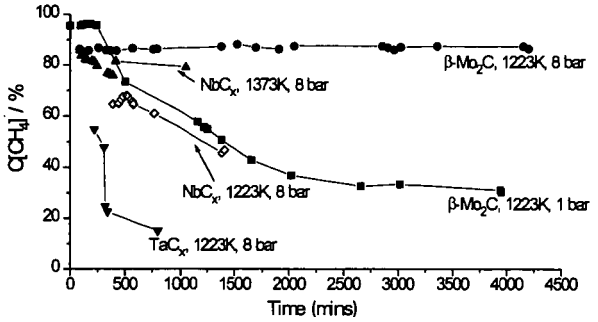

Figure 2. Lifetime study of β-Mo_2C for the methane partial oxidation reaction at 8.7 bar (T = 1173 K, GHSV = 5.25 x 10^3 h^{-1}, CH_4/air =2/5).

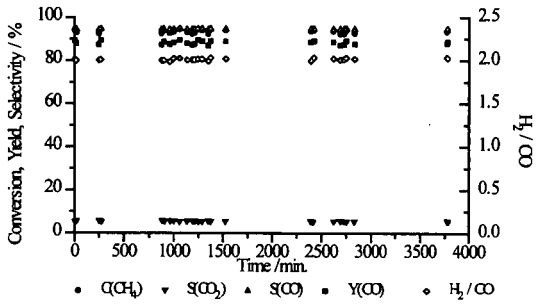

Figure 3a. Effect of temperature on the partial oxidation of methane over β-Mo_2C (8.7 bar, GHSV = 5.25 x 10^3 h^{-1}, CH_4/air =2/5).

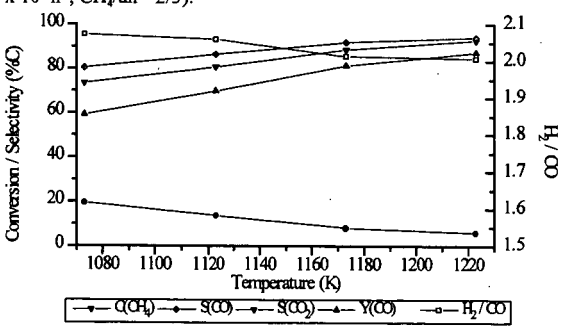

Figure 3b. Effect of pressure on the partial oxidation of methane over β-Mo_2C (1173 K, GHSV = 5.25 x 10^3 h^{-1}, CH_4/air =2/5).

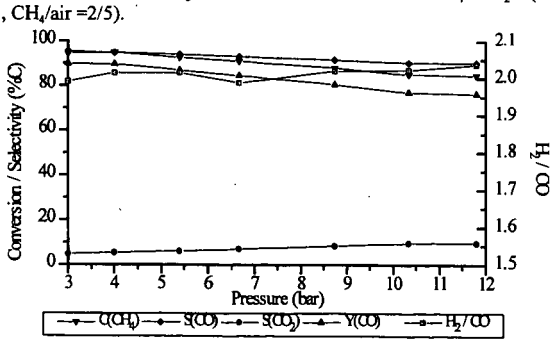

EMERGING APPLICATIONS OF HYDROGEN IN CLEAN TRANSPORTATION

Venki Raman
Air Products and Chemicals Inc.
Allentown, PA 18195

Key Words: Hydrogen, Hythane®, Hydrogen vehicles

Introduction

The present total dependence on oil supplies for our transportation systems is the major cause of air pollution in the growing urban areas of the world, and is clearly unsustainable into the future. The societal will to seek changes in this system is evidenced by the passage of stringent clean air standards that require clean alternative fuels. Emerging trends suggest that we will gradually move from this oil-dependent system to a transportation system that favors cleaner fuels such as natural gas in the near term. For the longer term, our aim will be to use pollution-free fuels derived from renewable resources. At the same time, there will also be a shift from the rather inefficient internal combustion (IC) engine that has dominated our automotive systems to highly efficient, electric motors. The combination of new fuels and new engines to use them, will ultimately produce a new transportation system built entirely on sustainable energy.

Because hydrogen can be produced cleanly from renewable energy resources, and used virtually without any pollution, it may prove to be the ideal energy carrier in the future automobile systems. A plausible strategy for the transition to hydrogen, that is widely subscribed to in the international hydrogen energy community, could involve the initial replacement of present day gasoline and diesel with natural gas, followed by the gradual introduction of hydrogen, which is similar to natural gas in the practical aspects of distribution, transfer and storage.

The key feature of past energy transitions has been the progressive move toward fuels containing less carbon and more hydrogen; witness the shift from dried wood which is mostly carbon (10% hydrogen), to coal (38% hydrogen), oil (64% hydrogen), and natural gas (80% hydrogen). The transition to hydrogen merely continues this pattern. The energy content of the fuels increases as the percentage of hydrogen increases. The shift to fuels containing less carbon has lessened air pollution over the past century (per pound burned). Particulates and carbon dioxide from oil burning are significantly lower than that from burning coal to release the same amount of energy. The shift to natural gas will cut this further and with hydrogen totally eliminated.

International Hydrogen Activities

Driven by concerns about oil dependence, and air quality, and recognizing the benefits of a hydrogen-based transportation energy system, over 30 countries worldwide, have active R&D programs underway in hydrogen energy applications. Major programs are being undertaken in Japan, the U.S. and Germany. Except for space applications which the U.S. leads, the leadership in hydrogen R&D centers in Japan and Germany. Japan has the most ambitious hydrogen energy R&D program called World Energy Network (WE-NET) which is a $2 billion effort over twenty-eight years (1993-2020). Germany has been the leader in hydrogen vehicle applications, and second to Japan in total spending on hydrogen R&D. The U.S. comes in third, followed by Canada, where the province of Quebec has undertaken a major program aimed at looking at harnessing its vast hydroelectric power resources to make liquid hydrogen for export to Europe.

In Germany, the birthplace of the automobile, Daimler-Benz and BMW have pioneered the development of hydrogen-fueled vehicles for over two decades. Daimler-Benz has developed hydrogen IC engines for cars and vans, using metal hydrides for onboard storage of hydrogen, and operated fleets of vehicles in Berlin. More recently their efforts have shifted to buses with liquid hydrogen stored onboard. Several buses are being built in conjunction with bus manufacturer MAN for operation in urban transit, and airport shuttle bus service. A joint German - Russian team including Daimler-Benz Aerospace and Tupolev are in early stages of development of a liquid hydrogen airplane called "Cryoplane". Perhaps the most exciting development at Daimler-Benz has been their unveiling in May 1996 of their second generation hydrogen fuel cell passenger minivan called "NECAR 2" with hydrogen stored onboard as compressed gas. The first prototype NECAR 1 a research vehicle had been unveiled only in 1994. This development program is clearly proceeding at an accelerated pace at Daimler-Benz. The next prototype NECAR 3 is expected to be a new small sedan.

BMW has also been active in hydrogen car developments since about 1979. The focus of BMW's efforts have been centered on liquid hydrogen from the start. BMW has developed 6 generations of cars capable of running on either gasoline or hydrogen. In conjunction with German hydrogen suppliers, they have significantly improved the insulating efficiency, and compactness of onboard liquid hydrogen storage tanks. They have also reduced fueling times from about 1 hour down to about 15 minutes. Now they are developing robotic fueling systems to fully automate the transfer of liquid hydrogen to the car. BMW also participates in a consortium that is conducting a solar-hydrogen demonstration project in Germany.

This facility is an integrated project that produces hydrogen via water electrolysis from solar generated electricity.

In Japan, active hydrogen vehicle projects are underway at Mazda, Toyota, Honda, and Musashi Institute of Technology. Mazda's work has been on hydrogen-fueled IC rotary engines using metal hydrides to store hydrogen onboard the vehicle. Toyota unveiled their first hydrogen fuel cell car in October 1996.

The U.S. Department of Energy has been researching the potential use of hydrogen as an energy carrier and fuel since the early 1970s, following the OPEC oil embargo. Originally, the driving force behind this program was the National need to develop a domestic, sustainable energy base. Basic R&D was conducted at a low level of funding ($0.5-1.0 million) throughout the 1980s. However in 1990 the U.S. Congress enacted into law the Spark Matsunaga Hydrogen Research, Development, and Demonstration Act (P.L. 101-566) which revitalized the then existing Hydrogen Program. The Energy Policy Act of 1992 (P.L.102-486) further supplemented the Matsunaga Act. These actions have resulted in a National Hydrogen R&D program under the management of the DOE which has a current budget of $15 million per year. A new Hydrogen Futures Act of 1996 (P.L. 104-271) was recently enacted authorizing expenditures of $150 million between 1997 and 2001 for hydrogen R&D and demonstration programs. In addition to the Hydrogen Program, DOE supports other hydrogen related programs including work on fuel cell technologies to the tune of $100 million per year.

In addition to the federal program, several state and regional government bodies have also initiated hydrogen vehicle programs of their own including the South Coast Air Quality Management District (SCAQMD) in Southern California, the California Air Resources Board (CARB), Cities of Palm Desert, Palm Springs, and Denver, New York State Energy Research and Development Authority (NYSERDA), Pennsylvania Energy Office (PEO), and others.

Hydrogen Transportation Demonstration Programs

In the area of hydrogen vehicles, active programs are underway in IC engines, IC engine-electric hybrids, and fuel cell engines. These programs represent a progression of increasingly more economically and technically challenging options for the transition of hydrogen into the transportation fuel marketplace.

Hythane®

From the earliest days of combustion science, experiments have established that hydrogen has a strong influence on the combustion of natural gas and other hydrocarbons. More recently, Hydrogen Components Inc., of Colorado has been actively promoting the use of dilute concentrations of hydrogen (10-20 Vol%) blended with natural gas in IC engines. They have registered the trademark Hythane®, and hold a patent on the application of Hythane in IC engines.

It has been shown in laboratory and on-the-road testing that this small level of hydrogen addition to natural gas in IC engines results in reducing levels of carbon monoxide (CO) and oxides of nitrogen (NOx) emissions from these engines an additional 50% over that achieved with "straight" natural gas. The economic rationale for such an approach involving small additions of expensive hydrogen to cheap natural gas relates to the fact that significant leverage in emissions reduction is achieved, i.e., disproportionately greater than the amount of hydrogen added. Such an approach faces a smaller economic hurdle in achieving the benefits of clean air and is more likely to be favorably received by the consumer.

The Hythane application has been developed and tested for gasoline (stoichiometric engines) and diesel type (lean burn) engines[1]. Several test and demonstration programs have been conducted in Denver, Colorado, Erie, Pennsylvania, and Montreal, Canada on small fleets of utility service vehicles and urban transit buses. In these programs optimal hydrogen additions were determined to be between 15-20 vol%. In the case of buses operating on a modified Cummins L-10 engine with natural gas, it was observed that as the hydrogen additive was increased from 0 to about 20 vol% (7% by energy content) the NOx emissions steadily decreased by about 43% due to the ability to operate the engine more fuel lean and also with less spark advance while maintaining the non-methane hydrocarbons emissions constant. Increasing hydrogen content above 20 vol% caused the NOx to increase after adjusting the engine to maintain the same hydrocarbon emissions as the baseline. A 43% NOx reduction with a 7% by energy content hydrogen addition represents a leverage factor of greater than 6. Similarly in tests with gasoline (stoichiometric) engines with three-way catalysts indicated that hydrogen addition to natural gas dramatically reduced CO but increased NOx. However by tuning the engine to operate slightly richer than the baseline operating conditions, it was seen that some of this CO advantage could be sacrificed for significantly lower NOx emissions. Thus tests done in Denver demonstrated that it is possible to operate with Hythane containing 15 vol% hydrogen (5% by energy content) and reduce both CO and NOx to about 50% of the baseline values.

A cost analysis for a 500 vehicle fleet operating on Hythane (5% hydrogen by energy content) based on current liquid hydrogen pricing indicated that Hythane price would be quite competitive with regular unleaded gasoline at about $1.13 per gallon gasoline equivalent[2].

Hydrogen IC Engines

A further enhancement of emissions reduction can be obtained by burning pure hydrogen in IC engines. As stated previously, this has been the subject of detailed investigation by Mercedes-Benz and BMW for quite some time. The approach is to use hydrogen in lean burn engines. Since the lean burn limit of air breathing hydrogen engines is so much greater than hydrocarbon fuels, it is possible to operate at very lean conditions and reduce NOx emissions to extremely low values. This is often accompanied by very low levels of CO emissions emanating from the combustion of traces of lubricating oils used in the engines. In the U.S. a demonstration program lead by Clean Air Now and Xerox Corporation operates a fleet of four service vehicles on hydrogen generated from solar energy at a fuel station in Los Angeles. A similar effort is underway in University of California's Riverside campus.

An improvement on this concept is the hydrogen hybrid electric vehicle which takes advantage of high efficiency electric drive trains and the low emissions of hydrogen IC engines. The concept involves the use of relatively small IC engines operating on hydrogen to power electric generators that charge batteries. The IC engine is sized to match the average power requirement of the vehicle and hence operates continuously at or near its optimum efficiency. The battery is sized to accommodate the peak power surge requirements. This reduces the weight of batteries needed for a given range and gives the vehicle rapid fueling capability. The hybrid electric vehicle is being actively developed for both hydrocarbon fuels and hydrogen. A hydrogen hybrid electric bus is currently undergoing testing in Atlanta by the Westinghouse Savannah River Company. This bus is slated to be put in transit service in Augusta, Georgia following this test program.

Hydrogen Fuel Cell Vehicles

Perhaps the most attractive energy conversion technology that uses hydrogen in a zero-emission vehicle is the fuel cell. Although fuel cells were first invented some 150 years ago, only recently has their pace of development accelerated dramatically. Major automobile manufacturers in the U.S., Europe and Japan all have major development programs underway in an attempt to bring this technology to the market early in the next century. In the U.S. the joint program between the federal government and the "big three" auto manufacturers is actively developing fuel cell cars under the Partnership for a New Generation of Vehicles (PNGV) program.

While fuel cell cars are still under development, hydrogen fuel cell buses are becoming a reality and small fleets (3-4 buses at each location) will begin operation in Chicago, and Vancouver, British Columbia in 1997. The Canadian company Ballard Power Systems has developed the propulsion systems for these buses using their Proton Exchange Membrane (PEM) fuel cell technology. Hydrogen refueling stations at the bus depots are being built to deliver and store hydrogen onboard the buses at 3,600 psi. The hydrogen will be delivered to these sites as liquid and pumped to high pressures using cryogenic liquid pumps. The stations are being designed for fueling a bus in about 15 minutes.

Hydrogen Fuel Supply

In the future, a truly zero emission transportation system could be based on hydrogen produced from renewable energy resources such as solar, wind, geothermal or biomass. However, renewable hydrogen production processes are still in the early stages of development and can not compete with current hydrogen production technologies. As the various hydrogen vehicle technologies rapidly progress towards commercialization, the ready availability of competitively priced hydrogen will be critical to their near term success. The perceived lack of a hydrogen fuel supply infrastructure could be the major barrier to the use of hydrogen in the transportation sector. Some major automobile companies such as Chrysler, Daimler-Benz, General Motors, and Toyota have decided to develop onboard fuel processors to generate the hydrogen required for their fuel cell vehicles from methanol or gasoline. However, it is entirely feasible to ensure an adequate hydrogen fuel supply system, at all stages of the evolution of hydrogen utilization technology, by adapting current industrial hydrogen production and distribution technologies.

About 40 million tons of hydrogen are commercially produced and consumed per year around the world. The energy content of this hydrogen is about 5 quadrillion British Thermal Units (BTU) or slightly more than 1 percent of the world's energy demand. About 95% of the 10 million tons per year of hydrogen produced in the U.S. is consumed "captively" within the producing facility to refine oil, or to produce ammonia and methanol. The rest is produced by a few industrial gas companies, and supplied to customers as a gas in high pressure cylinders and via pipelines, or as a liquid via over-the-road cryogenic tankers. This so called "merchant" hydrogen is used to manufacture specialty chemicals; to hydrogenate fats and oils; for reducing atmospheres in the manufacture of metals, glass and semiconductors; and as a coolant for large electric power generators. The only significant transportation fuel application of hydrogen - about 0.1% of the production - is as a rocket fuel, e.g., to launch NASA's Space Shuttle.

Practically all hydrogen is manufactured today, directly or indirectly, from fossil fuels. The most common commercially practiced technologies include: steam reforming of light hydrocarbons, partial oxidation of heavy oil, recovery from off-gases from the chlor-alkali industry, and refining and petrochemical processes, electrolysis of water, and methanol reformation.

The merchant hydrogen business in the U.S. is supported by well developed transportation and storage systems. Hydrogen is transported and stored as a gas, or liquid depending upon the distance from the user's location to the production plant, and usage rates and patterns, i.e., whether continuous or intermittent. Practically all commercial applications require the hydrogen in gaseous form, thus even when hydrogen is delivered and stored as liquid, it is vaporized at the customer's site prior to use. "Bulk" gaseous hydrogen is usually more expensive to store and ship than an equivalent amount of liquid hydrogen, particularly for distances greater than about 100 miles from the hydrogen production plant.

Among the various options being considered for storing hydrogen on-board the vehicle, perhaps the most challenging, from a fueling system design viewpoint, is high pressure gas at about 3,600 - 5,000 psi. The desired refueling times of about 10-15 minutes can be readily achieved with modifications to current commercial high pressure liquid hydrogen pumping systems. Fleets of up to 100 transit buses or 4,500 personal automobiles can be readily supported with liquid hydrogen deliveries and transferred at high pressure to the on-board tanks using special liquid hydrogen pumps followed by vaporization. Several high pressure hydrogen fueling systems for experimental fleets are currently being developed based on the significant experience gained in the design and operation of compressed natural gas fueling systems. The National Hydrogen Association is leading an effort to develop industry codes and standards for high pressure hydrogen fueling stations and onboard storage systems.

Hydrogen Infrastructure Options To Support Fuel Cell Vehicles

A recently completed study[3], examined how current commercial hydrogen production and supply technologies could be adapted to supply fleets of fuel cell cars at individual fueling stations and the economics of these options. Each car required 12 lbs. hydrogen stored onboard the vehicle as a gas at 5,000 psi. A typical fuel station was designed to dispense 3 tons per day (TPD) of hydrogen, sufficient to refuel 500 cars per day.

The following commercial options for hydrogen supply to the station were considered:

- Hydrogen produced from natural gas in large scale remote steam reformer plants (30-300 TPD), is delivered as liquid up to a distance of 500 miles from the plant.

- Hydrogen produced from natural gas in large regional steam reformer plants (30-300 TPD) is delivered via gas pipelines within a radius of 30 miles of the plant. Fueling stations are spaced 3 miles apart on the pipeline.

- Hydrogen is produced at the fuel station with a dedicated on-site plant (3 TPD) using natural gas steam reformer, heavy oil partial oxidation, or a methanol reformer.

Table 1 summarizes the results of this study and shows the capital investment, and hydrogen price at the pump (without taxes) for these options. Hydrogen fuel can be supplied to the vehicle using current technologies at a cost ranging from $1-2 per lb. depending on the scale of production. Taking into account the projection of a 2 to 3 times superior fuel economy of a fuel cell car over a gasoline car, the last column of Table 1 shows the maximum allowable gasoline price (without taxes) to provide the same cost per mile in an IC engine car as the fuel cell car. To compare this to a typical pump price for gasoline in the U.S., about 40¢ per gal should be added to these prices. With current regular unleaded grade gasoline prices at the pump in the U.S. at around $1.20 per gallon, this analysis indicates that several near term hydrogen production and distribution options are close to being competitive with gasoline on a cost per mile basis.

Development of a hydrogen fuel infrastructure similar to the familiar gasoline supply network, with fuel stations every few miles, in population centers across the U.S. is certainly many years into the future. Large investment in the production and distribution infrastructure are necessary to achieve the lower prices for hydrogen. This certainly dictates that such facilities will not be built until sufficient demand for hydrogen develops as hydrogen-fueled vehicle technology becomes well established and accepted by the public. Thus, the infrastructure to supply fuel cell vehicles with hydrogen will evolve with the start up and growth of this market in several stages:

In regions where merchant hydrogen infrastructure exists, when a local market starts up with a small fleet of fuel cell cars, it would first be supplied by the current commercial distribution system via hauled-in high pressure gaseous hydrogen in tube trailers (to fuel about 20 cars per day) or liquid hydrogen (to fuel 20 - 500 cars per day). As the fleet grows large enough to support the continuous operation of a small reformer, one would be built and liquid hydrogen from a large central plant used as a backup source, and to meet peak demands. As the market grows even larger it could be supplied by a large regional reformer via pipeline, with the excess capacity being liquefied for distribution to areas remote from pipelines.

In areas where merchant hydrogen is not readily available small on-site hydrogen plants would be built to support the fuel station. Recent activity in the area of small reformers for hydrogen production may result in the economic size of on-site plants being reduced from currently accepted sizes. In this connection, methanol reformers appear to offer significant advantage due to their relative simplicity and wide availability of methanol.

Natural gas supplies would probably be sufficient to supply feedstock for hydrogen production for up to several million fuel cell cars, for several decades[4]. In the longer term, other renewable hydrogen production methods such as biomass gasification, or solar energy could be phased in.

References

1. Raman V., Hansel J., Fulton J., Lynch F. and Bruderly D., "Hythane - An Ultraclean Transportation Fuel", Hydrogen Energy Progress X, Proceedings of the 10th World Hydrogen Energy Conference, Cocoa Beach, Florida, Vol. 3, p. 1797 (1994)

2. Hansel J., Kielian D., Lynch F., Ragazzi R., Raman V., and Willson B, "Hythane - A Status Report", 26th International Symposium on Automotive Technology and Automation, Aachen, Germany September 1993.

3. Moore, R. B. and V. Raman "Hydrogen Infrastructure for Fuel Cell Transportation", presented at the 7th Annual U.S. Hydrogen Meeting, National Hydrogen Association, Alexandria, VA, April 1996.

4. Ogden, J.M. et.al. "Hydrogen System Studies", presented at the U.S. DOE Hydrogen Program Review Meeting, April 29 - May 3, 1996.

Table 1. Cost Analysis for Hydrogen Infrastructure to Supply Fuel Cell Automobiles

Hydrogen Production/Delivery Method	Size, TPD	Investment $ Million	Hydrogen Price $/lb	Untaxed Gasoline Equiv. Cost $/gallon[1]
Remote Natural Gas Steam Reformer w/ Liquefier	30	63	1.52	1.12 - 1.61
	300	259	1.07	0.79 - 1.14
Regional Natural Gas Steam Reformer w/30 mile Gas Pipeline	30	82	1.32	0.97 - 1.39
	300	667	1.12	0.83 - 1.19
On-site Natural Gas Steam Reformer	3	9.6	1.62	1.19 - 1.71
On-site Partial Oxidation of Oil	3	12.5	1.80	1.33 - 1.91
On-site Methanol Reformation	3	6.8	1.70	1.25 - 1.80

[1] Untaxed gasoline price to produce same cost per mile in IC engine vehicle as hydrogen in a fuel cell vehicle. The price range indicates different values for fuel economy based on two variants of the Federal Urban Driving cycle.

SLURRY FISCHER - TROPSCH SYNTHESIS IN CHINA

Yu - Long Zhao Liang Bai Bi - Jiang Zhang
Institute of Coal Chemistry State Key Laboratory of Coal Conversion
P. O. Box 165, Taiyuan, Shanxi, 030001, P. R. China

Keywords: Fischer - Tropsch sythesis bubble column slurry reactor(BCSR)
Fe - Cu - K catalyst kinetic parameter solubility

INTRODUCTION

Cina is one of a few countries where coal is used as major energy source. Research and development of clean coal technology is especially important for China to solve the problems of environmental pollution and to increase supply of liquid fuel espceially the unleaded high quality gasoline. It is well known that slurry Fischer - Tropsch synthesis technology (SFTST), which has the advantages on both technology and economics over traditional fixed process as demonstrated by Sasol's Slurry Phase Distillate Process, is an advanced technology of indirect liquefaction of coal. Institute of coal chemistry has developed SFTST on both catalysts and a micro—pilot unit (MPU) as well as chemical engineering since 1986. The present paper will summarized the status and progress in R & D of SFTST.

1 CATALYST

One of the key problems in the development of SFTST is to provide a catalyst with high activity, good selectivity and long catalyst life. Iron catalysts, which are not only hydrogenation catalysts, but also active water gas shift catalysts, are indeed the most promising one as commercial catalyst for SFTST.

The catalysts used in our laboratory were prepared in a continuous multistage stirred precipitation reactor similar to those described by Kölbel[1]. Preparation conditions of catalyst including precipitation temperature, pH value and promoters were examined. Typical catalyst composition was 99.5 Fe; 0.5 Cu; 0.29 K_2O by weight. The pretreatment condition and synthesis results were shown in table 1. From both hydrocarbon yield and time on stream in table 1, it is evident that the synthesis results based on temperature-programmed method are better than those based on non-programmed method. P2 pretreatment was preferred in the lone life test by considering the same ratio of H_2/CO in both pretreatment and synthesis. In order to understand the phase change during catalyst pretreatment, XRD analyses of fresh catalyst and catalyst partially induced at the initial stage and the later stage of pretreatment were compared and shown in Fig. 1. Crystal phase of a fresh catalyst is totally hematite ($\alpha - Fe_2O_3$) as shown in Fig. 1 A, XRD of the catalyst partially induced at the initial stage of pretreatment as shown in Fig. 1 B indicated that magnetic iron oxide and Hägg carbide began to appear, but Hematite still existed. Fig. 1 C is XRD spectrum of the catalyst induced at the later stage of pretreatment. Hematite disappeared totally and magnetic iron oxide and Hägg carbide were the dominant crystal phase. Above results are significant to judge the extent of pretreatment of catalysts. Three long life tests were conducted in a magnetically stirred 1L autoclave. The results are given in table 2. It is found that iron catlaysts prepared had longer life time and thus they were applied in MPU for SFTST.

2 MICRO - PILOT UNIT

Schematic of MPU is shown in Fig. 2. After being purified and preheated to a given temperature, syngas with relatively low H_2/CO ratio (0.5 - 1.5) was bubbled through a slurry of unsupported precipitated iron catalysts suspended in wax medium in BCSR. The gas distributor was a porous sintered metal plate. The catalyst used was the unsupported precipitated iron catalyst promoted by copper and potassium with a particle size less than 44μm. Suspended catalyst was separated from reactor - wax by sedimentation in the settling vessel. The catalyst was recirculated between the enlarged upper section and the bottom of the BCSR through a settling vessel and an 2L autoclave in sequence. Catalyst settling tests on the MPU demonstrated that catalyst concentrations were 0.92wt% at 130℃ and 0.66wt% 200℃ in the wax withdrawn from the section of the settling vessel for the same settling time. It is clear that increasing settling temperature makes it easier to separate catalyst from the reactor - wax. On the other

hand, catalyst concentration in the reactor - wax approaches a constant value as settling time is extended. Therefore, a reasonable settling time can be set up to raise the efficiency of the settling vessel. Operation of separation was conducted every twelve hours. The reactor - wax, in which catalyst concentration was maintained at 0.5 - 0.8wt%, was regularly withdrawn through an overflow outlet. The enlargement of BCSR plays reducing the concentration of catalyst in the slurry entering the settling vessel, and the autoclave is used for the addition and activation of make - up catalyst. Fig. 3 shows variation of catalyst concentration in the reactor - wax with time on stream during the duration test lasted for over 1000h. The ranges of process variables were as follows: 260 - 280℃ (1st - stage)/320 - 340℃ (2nd - stage), 1.4 - 2.4MPa, 2.0NL/gFe • h(1st - stage)/500 - 1000h^{-1}(2nd - stage) and ratio of H_2/CO 0.5 - 1.5. Mean results of the test were as follows: syngas conversion (once - through) 65.1%, yield of C_5^+ 100g/nm^3($CO+H_2$), total hydrocarbon production >350g/gFe. When CO - rich syngas was used, the yield of C_5^+ was 110g/nm^3($CO+H_2$). Examples of matertal balances on a 12 hrs basis are given in table 3. Heat of reaction for FT syhthesis from heat balance at 280℃ for 1st - stage BCSR is 2938.5kJ/m^3($CO+H_2$), which is fairly consistent with 2829.6kJ/m^3($CO+H_2$) reported by farley[2] and 3038.9kJ/m^3($CO+H_2$) calculated by stoichemistry equation. During the duration test, catalyst samples were taken from 1st - stage BCSR at various time on stream for Mossbauer spectroscopic study of iron catalyst and the phase present in the samples were unchanged due to isolation of the sample surrounded with the reactor - wax from ambient. Fig. 5 shows the corresponding phase composition of iron catalyst in BCSR run as a function of time. It is found that the fresh catalyst was 64% of $\alpha - Fe_2O_3$ and 36% of $SP+Fe^{3+}$. The trend with time in the bulk phase composition of catalyst shows that while the extent of reduction and carburization extent of iron catalysts increased with extending time on stream and approached to the steady state with reducing fraction of magnetite. This is in accordance with the results reported by Satterfield et. al. [3] for fused magnetite catlaysts. It is therefore considered that slurry phase operation is favorable of reduction and carburization of iron catalyst to keep catalyst activity and stability constant.

The duration test demonstrated that the performance of operation in the MPU was satisfactory. Its temperature control, flow system and other equipment were reliable. Viscosity of slurry was basically constant throughout the test. The design of the slurry recirculation loop was reasonable with less loss of catalyst and stable operation.

3 Support studies

3.1 Solubilities and Mass transfer coefficients

Equilibrium gas solubilities (C_{eq}) and volumetric liquid - side mass transfer coefficients (k_La) were measured for hydrogen and monoxide in n - paraffin, n - octacosane and FT300 wax at various pressure (1.0 - 4.0MPa) temperatures (100 - 300℃), and a rotate speed of 800rpm in a 1L agitated autoclave. In the range of operating conditions investigated the relationships of gas equilibrium solubilities with temperature and heats of solution were obtained as shown in table 4. The k_La values for hydrogen and carbon monoxide in all liquid used increased with temperature and pressure, but decrease with increasing liquid molecular weight as shown in Fig. 5.

3.2 Kinetic parameter and mathematic simulation

Based on the data obtained from BCSR in MPU, the kinetic parameters of the Fischer - Tropsch synthesis (FTS) on unsupported precipitated Fe - Cu - K catalysts were estimated with a multi - component BCSR model. The main assumptions of the BCSR model under steady state conditions are as follows: 1. Plug flow gas phase and unmixed slurry phase; 2. the main mass transfer resistance to diffusion being at the liquid side of the gas - liquid interface; 3. uniform catalyst concentration throughout the BCSR; 4. FTS reaction rate expression being.

$-R_{H_2+CO} = kC_{H_2}/(1+KC_{CO_2}/C_{CO})$ ($H_2/CO \leqslant 0.8$) where $k = k_0 \exp(-E_a/RT - \beta t)$

The parameter values estimated were $k_0 = 1.36\times10^9$cm^3/gcat.s, $E_a = 100.0$kJ/mol, $K = 0.204$. Table 5 gives comparison of kinetic parameters obtained with those reported by Kuo[4] and Sanders[5]. It is seen from table 5 that kinetic parameters estimated are very close to values reported. The results predicted from FTS rate expression indicated that activity of catalyst used will deactivated by 1% after 35 h on stream, 26% after 1000h and 50% after 2300 h. It is obvious that the stability of the catalyst used should be improved. Also, axial concentration profiles of H_2, CO, CO_2 in both gas phase and liquid phase and the effect of bubble size on syngas conversion were computed by the BCSR model and the kinetic parameters estimated. Axial concentration profiles of each

component in both gas and liquid phases are depicted in Fig. 6.

3. 3 Hydrodynamics

It is known that the FT reaction is a volume reducting reaction. The volume flow rate of gas phase is gradually diminished with increasing conversion. Therefore, phase holdup and axial solids concentration were investigated in a tapered bubble column (0. 1m and 0. 2m id on the top and bottom, respectively, 3m height) with slurry circulation in a system composed of air, water and quartz sand. The axial distribution of solid concentration was measured by the synchronously sampling method and gas holdup by pressure drop method. The effect of solid particle size (142. 5μm, 180μm), solid concentration (0 - 100kg solid/m^3 slurry), slurry velocity (0 - 0. 0157m/s) and gas velocity (0 - 0. 125m/s) on gas holdup and solid axial concentration distribution were determined.

Experimental results were well agreement with the prediction made on the basis of the one dimensional sedimentation - dispersion model. The correlations of particle Peclet Number and gas holdup were obtained as follows:

$$Pe_p = 5.06(Fr_g^6/Re_g)^{0.130}(1+0.019Re_p)$$

where $0.03 \leqslant Pe_p \leqslant 0.4$; $1166 \leqslant Re_g \leqslant 18843$; $5.25 \leqslant Re_p \leqslant 10.45$; $0.0064 \leqslant Fr_g \leqslant 0.104$

$$\frac{\varepsilon_g}{(1-\varepsilon_g)^4} = 0.302(gD^2\rho_L/\sigma_L)^{0.125}\left(\frac{gD^3\rho_L^2}{\mu_L^2}\right)^{0.083}(Fr_g)^{0.958}$$

CONCLUSIONS

Unsupported precipitated Fe - Cu - K catalyst, which was prepared in a continuous precipitator, was applied in MPU. Catalyst activation proceeded well with syngas by the temperature - programmed method. THe 1000h run demonstrated the SFTST at a micro - pilot scale. Operation and performance of the MPU were good. A preliminary measure of separation of catalysts from reactor - wax was realized by a slurry recirculation loop. Under conditions of 260 - 280℃ (1st - stage)/320℃(2nd - stage), 1. 5 - 2. 5MPa, 2. 0Nl/gFe · h(1st - stage), 500 - 1000h^{-1}(2nd - stage), and H_2/CO ratio 0. 6 - 0. 7, a yield of C_5^+ over 100g/nm^3($CO+H_2$) can be achieved. Engineering data and information including kinetic knowleage and solubilities are useful for further development of the process and scale - up and design of the BCSR.

REFERENCES

[1] H. Kölbel. and M. Ralek, Catal. Rev. Sci. Eng., 1980; 21,225

[2] R. Farley and D. J. Ray, The Institute of Petroleum, 1964; 50(482);27

[3] C. M. Satterfield et. al., Ind. Eng. Chem. Prod. Res. Dev., 1986; 25(3);401

[4] J. C. W. Kuo et. al., 1983; "Slurry Fischer - Tropsch/Mobil Two - Stage Process Synthesis to High Octane Gasoline" DOE Report Contract NO. DE - AC22 - 80 PC 30022

[5] E. Sanders and W. D. Deckwer, Can. J. Chem. Eng., 1987; 65(1);119

Table 1 Pretreatment conditions and results of synthesis reaction

Pretreatment						Synthesis reaction						
No.	H_2/CO	T/°C	P	W/S	Note	T/°C	P	W/S	H_2/CO	C_1^+	C_5^+	$R.T$
1	1:0	260	1.5	2	B	260~280	1.5	2.0	2.4	a little liquid		–
2	A	280	0.3	2	C	260~280	1.5	2.0	2.0	92.9	45.9	432
3	2:1	280	1.6	2	C	280	1.5	2.0	2.0	66.7	22.0	126
4	2:1		0.4/0.9	2	P1	260~280	1.5	2.7	2.0	99.5	59.0	640
5	1.5:1		0.3/1.0	2	P1	260~280	1.5/2.5	1.8/3.4	0.85	157.3	105	280
6	1:1		0.3/1.0	2	P2	260~280	1.5/2.5	2.0	1.0	113.1	77.0	1112

Note: $R.T.$–running time, h; A—$N_2/CO=9$; B—isothermal 12 h; C—isothermal 24 h; P1—increasing and decreasing temperature at isorate, then pressuring again, total time 35 h; P2—temperature programmed pretreatment

Table 2 Results of the long life test

Run No.	A-26	A-30	B-6
Temperature / °C	250~280	250~280	260~280
Pressure / MPa	1.5~3.0	1.5~2.5	1.5~2.5
WHSV / $L \cdot g(Fe)^{-1} \cdot h^{-1}$	2.96	2.88	2.96
H_2/CO in feed	1	1	1
Hours on stream / h	1112	1128	1008
X_{CO}	69.5	82.9	78.6
X_{H_2}	40.4	52.7	36.3
X_{H_2+CO}	54.5	67.4	64.4
Hydrocarbon composition /%			
CH_4	6.0	8.1	9.6
C_2H_4	4.8	5.0	4.1
C_2H_6	3.7	2.7	6.2
C_3H_6	7.3	6.2	4.7
C_3H_8	1.9	1.2	3.2
C_4H_8	6.8	4.5	7.4
C_4H_{10}	1.7	1.4	3.9
C_5^+ minus wax trap	45.0	53.5	41.1
wax trap	18.6	14.4	13.1
Hydrocarbons yield			
C_1^+ $g/m^3(CO+H_2)$	113.8	116.9	145.1
C_5^+ $g/m^3(CO+H_2)$	77.0	83.5	91.2

Table 3 Material balance

Temperature/℃	265	265	265	270	275	280
Pressure/MPa	2.0	2.5	2.5	2.0	2.0	2.0
WHSV NL/gFe · h	2.15	2.24	2.26	2.23	2.28	2.31
H_2/CO	0.61	0.62	1.32	0.60	0.60	0.66
X_{n_2+CO} %	69.2	70.4	58.0	75.8	77.7	81.4
Inlet feed syngas NL · h^{-1}	644	671	678	669	684	693
Outlet tail gas NL · h^{-1}	377	385	416	354	355	336
Oil/g · h^{-1}	16.5	17.3	22.8	23.1	23.8	24.8
Wax/g · h^{-1}	50	49.7	30.6	50.2	53.1	54.8
Aqueous/g · h^{-1}	10.4	12.0	26.4	11.3	12.4	16.0
Material recovery %	99.7	98.9	98.5	96.7	94.7	95.1
C_1^+/g[$Nm^3(CO+H_2)$]$^{-1}$	133.6	143.2	132.2	149.2	154.4	163.0
C_2^+/g[$Nm^3(CO+H_2)$]$^{-1}$	113.1	115.2	90.0	123.7	127.1	129.9

Table 4 The correlations of gas equilibrium solubilities with temperature and Heats of solution

medium	H_2		CO	
	Correlation	Heats of solution	Correlation	Heats of solution
paraffin	$0.9892\exp(-4697.9/T)$	4697.9	$0.9889\exp(-2135.9/T)$	2135.9
n-$C_{28}H_{58}$	$0.9892\exp(-5129.4/T)$	5129.4	$0.9889\exp(-2609.9/T)$	2609.9
FT300wax	$0.9897\exp(-8142.3/T)$	8142.3	$1.0108\exp(-5276.6/T)$	5276.6

Solubility ,kmol/kg/atm, Heat of solution ,J/mol

Table 5 Comparison of kinetic parameters

Investigator	catalyst	k_0, $cm^3/gcat.s$	E_A, kJ/mol	K
Kuo (1983)	Fe—Cu—K	6.7×10^9	105.0	0.089
Sanders (1987)	Fe—K	1.42×10^8	88.2	0.316
Authors	Fe—Cu—K	1.36×10^9	100.0	0.204

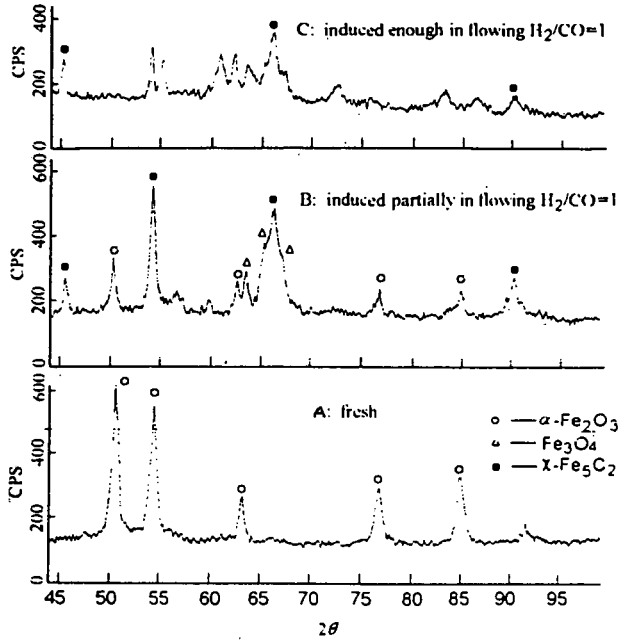

Fig. 1 XRD of the precipitated Fe - Cu - K catalyst

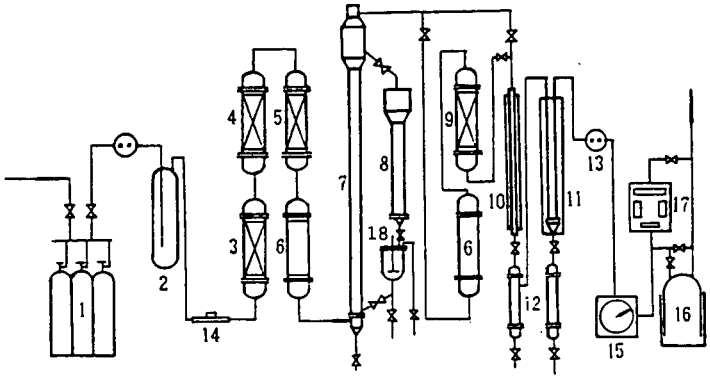

Fig. 2 A simplified flow diagram of the two - stage MPU for the synthsis of hydrocarbons

1. Syngas cylinder 2. Pressure buffer tank 3. Water trap 4. Iron carbonyl removal 5. Sulfide removal 6. preheater 7. 1st - stage BCSR 8. Settling vessel 9. 2nd - stage fixed - bed ZSM - 5 reactor 10. Air condenser 11. Chilled condenser 12. Liquid products receiver 13. Pressure let down valve 14. Mass flow meter 15. Wet - test meter 16. gas holder 16. IR gas analyzer 18. autoclave

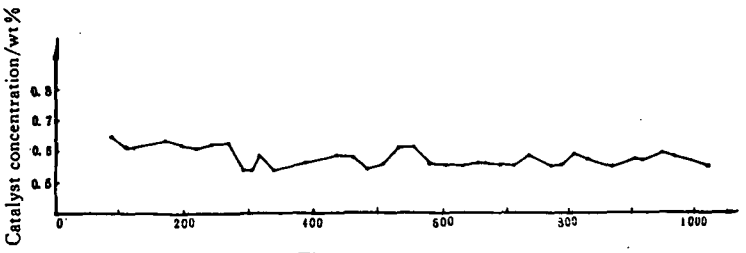

Fig. 3 Variation of catalyst concentration in the reactor - wax with time on stream

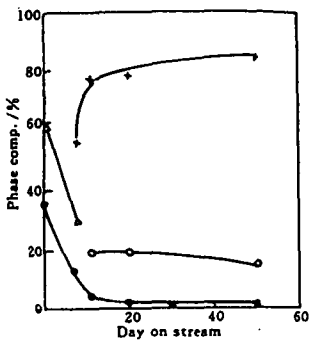

Fig. 4 Variation of bulk catalyst phase composition with time on stream

●—Fe^{3+}; Δ—α-Fe_2O_3;
○—Fe_3O_4; ×—χ-Fe_5C_2

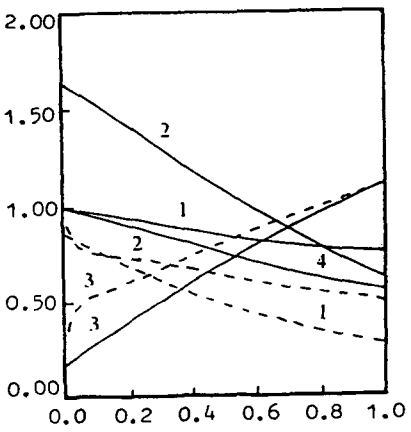

liquid ---- gas ——; 1. H_2, 2. CO, 3. CO_2, 4. U_g

Fig. 6 Dimensionless concentration profiles for each component and gas velocity profile

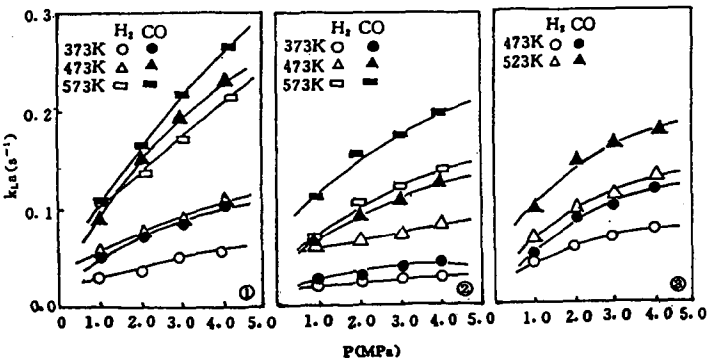

Fig. 5 Volumetric mass transfer coefficient k_La of H_2、CO in various liquids
(① n-paraffin; ② n-octacosane; ③ FT300 wax)

EFFECT OF PRETREATMENT ON CATALYST ACTIVITY AND SELECTIVITY DURING FISCHER-TROPSCH SYNTHESIS IN A SLURRY REACTOR

Dragomir B. Bukur, Xiaosu Lang and Yunjie Ding
Department of Chemical Engineering
Texas A&M University, College Station, Texas 77843

Keywords: Fischer-Tropsch synthesis, iron oxides and carbides.

INTRODUCTION

Promoted iron catalysts, reduced with hydrogen, have been used in commercial fixed bed and entrained fluid bed reactors for synthesis gas conversion to transportation fuels via Fischer-Tropsch synthesis (FTS) at SASOL in South Africa[1]. However, the purpose of pretreatment for iron FT catalysts is not clearly understood. Reduction in H_2 may lead to a zero-valent state, but upon exposure to a synthesis gas the metallic iron is rapidly converted to a carbide phase or a mixture of iron carbides[2,3]. At high syngas conversions, a reaction mixture becomes more oxidizing and magnetite is also formed[1,4,5]. During FTS, the bulk iron may be distributed among several phases: e.g. carbides, oxides and metallic iron, which often results in a lack of correlation between the catalyst bulk composition and its activity and/or selectivity[1,5]. Other pretreatments have been also employed, such as CO activation, synthesis gas pretreatment or induction, and/or H_2 reduction followed by CO treatment or vice versa[4,6].

Also, there has been a large number of related studies on model iron catalysts dealing with an issue of the role of iron phases in FTS. However, this issue still remains to be a controversial one. Briefly, some workers consider the surface carbides, with an underlying iron carbide bulk structure, to be the active phase[2,7]. In the so-called competition model of Niemantsverdriet and van der Kraan[8] iron atoms at the surface are considered as the active sites. In the latter model both bulk carbidation and FTS (hydrocarbon formation) have a common surface carbidic precursor. In addition to these two postulates concerning the nature of the active phase, Teichner and co-workers proposed that Fe_3O_4 (magnetite) is the active phase in FTS[9,10]. Validity of the latter proposal was questioned[11], but some evidence in its support was also presented[12,13].

In this paper we describe new results from our on-going studies[14-17] on the effect of pretreatment procedures on activity and selectivity of precipitated iron catalysts. Results illustrating both the initial and steady state behavior of a catalyst with nominal composition 100 Fe/3 Cu/6 K/16 SiO_2 (on mass basis) during FTS are presented, and activity/selectivity data are correlated with iron phases in the working catalyst under conditions representative of industrial practice.

EXPERIMENTAL

The reactor used in this study was a 1 dm^3 stirred tank reactor (Autoclave Engineers). Detailed description of the reactor system and operating procedures was provided elsewhere[17,18]. The feed gases (H_2>99.5% purity, and CO>99.3% purity) or a premixed gas passed through a series of traps to remove impurities. The feed gas flow rate was controlled using calibrated mass flow controllers, and the feed was introduced into the reactor below a flat blade impeller, used to agitate the slurry. After leaving the reactor, the exit gas passed through a series of product collection traps. All products collected in the steady state traps were analyzed by gas chromatography after physical separation into an aqueous and organic phase. The reactants and noncondensible products leaving ice traps were analyzed on an on-line gas chromatograph (Carle AGC 400). Powder X-ray diffraction (XRD) patterns of the catalyst samples withdrawn from the reactor were obtained on a Scintag XDS2000 system using Cu-Kα radiation (λ= 1.54 Å).

Catalyst preparation involved three steps: preparation of the iron-copper precursor, incorporation of binder/support (silicon oxide), and finally potassium impregnation. The preparation procedure was described in detail previously[19]. In brief, the catalyst precursor was continuously precipitated from a flowing aqueous solution containing iron and copper nitrates at the desired Fe/Cu ratio, using aqueous ammonia. Impregnation with SiO_2 binder/support was accomplished by addition of the appropriate amount of dilute K_2SiO_3 solution to undried, reslurried Fe/Cu co-precipitate. After a vacuum drying step, the potassium promoter was added as aqueous $KHCO_3$ solution via an incipient wetness pore filling technique. Dried catalyst was calcined in air at 300°C for 5 h, and then crushed and sieved to a diameter less than 270 mesh (53 μm). Durasyn - 164 oil (a hydrogenated 1 - decene homopolymer, ~C_{30} obtained from Albemarle Co.) was used as the initial slurry liquid medium.

All pretreatments were conducted in situ at 0.8 MPa. In runs designated SA-0946 and SA-1626 the catalyst was pretreated at 280°C, 750 cm^3/min for 8 h in CO and syngas (H_2/CO = 0.67), respectively. In run SB-2145 the catalyst was reduced with hydrogen at 240°C, 7500 cm^3/min for 2 h, whereas in run SB-2486 the catalyst was exposed to reaction conditions, without any

pretreatment (unreduced catalyst). After the pretreatment, the catalyst was tested initially (baseline conditions) at 260°C, 1.48 MPa, 2.3 Nl/g-cat/h (1.4 Nl/g-cat/h in run SB-2145 only) and syngas feed with $H_2/CO = 0.67$ (molar feed ratio). In addition to baseline conditions, the catalyst was tested at different gas space velocities and reaction pressure, but these results are not reported here.

RESULTS AND DISCUSSION

Catalyst activity

Hydrogen reduced catalyst reached its steady state activity within 4 h from exposure to synthesis gas, and then its activity decreased slowly during the first 150 h of testing (Fig. 1). In the other three tests the time needed to reach a steady state activity was longer, about 20 h for the syngas pretreated and unreduced catalyst, and 80 h for the CO pretreated catalyst. Since the process conditions, including the gas space velocity, were the same in runs SB-2486, SA-1626 and SA-0946, the values of syngas conversion can be used as a measure of relative catalyst FTS activity. Initial activity of the unreduced catalyst (SB-2486) was the lowest, but at approximately 20 h on stream it was the same as that of the CO pretreated catalyst (SA-0946). After 20 h on stream the conversion (activity) of unreduced catalyst started to decline, whereas that of the CO pretreated catalyst continued to increase up to 80 h, and then became stable at about 76%. Initially, the conversion of the syngas pretreated catalyst was higher than that of the unreduced and the CO pretreated catalyst, and it reached its steady state value of ~70% at about 20 h. The steady state activity of the syngas pretreated catalyst was lower than that of the CO pretreated catalyst. Although, the conversion of the hydrogen reduced catalyst (SB-2145) up to 80 h on stream was higher than those obtained in the other three tests, this does not imply the highest catalyst activity, since the gas space velocity in run SB-2145 (1.4 Nl/g-cat/h) was significantly lower than in the other three tests (2.3 Nl/g-cat/h). In order to compare the activity of catalysts in tests under different process conditions, a simple model was used to estimate values of apparent rate constant[20]. The apparent rate constant was calculated assuming that the reaction rate has a first-order dependence on hydrogen pressure, and that the reactor can be modeled as a perfectly mixed flow reactor. At 100 h on stream the estimated values of the apparent rate constant were, in the order of increasing activity, 230 (runs SB-2145 and SB-2486), 330 (SA-1626), and 360 mmol/g-Fe/h/MPa (run SA-0946).

Crystalline phases found in samples withdrawn after the pretreatment (Fig. 4) were as follows: magnetite (hydrogen reduced catalyst); χ-carbide and possibly small amount of magnetite (CO pretreated catalyst); iron carbides (χ-carbide and/or ε'-carbide) and magnetite (syngas pretreatment). Unreduced catalyst had an amorphous structure (iron oxide/oxyhydroxide). Dominant phase in the syngas activated catalyst (SA-1626) after 137 h on stream was ε'-carbide, whereas both ε'-carbide and magnetite were found in the hydrogen reduced catalyst and the unreduced catalyst at 145 h and 147 h on stream, respectively (Fig. 5). Crystalline phases in the CO pretreated catalyst after 113 h on stream were χ-carbide and possibly magnetite.

The FTS on iron catalysts is accompanied by a reversible water-gas-shift (WGS) reaction. Values of carbon dioxide selectivity (% of CO converted to CO_2) provide indication of the WGS catalyst activity. Carbon dioxide selectivity of 50% corresponds to complete conversion of water formed by FTS to carbon dioxide. After 20 h on stream, carbon dioxide selectivities in all four tests were about 48% (Fig. 2). Hydrogen and syngas reduced catalysts reached this value after about 5 h only, the unreduced catalyst at ~8 h, whereas the CO pretreated catalyst achieved its steady state carbon dioxide selectivity at ~20 h on stream. Carbon dioxide selectivity in all tests was never greater than 50%, which would indicate that carbon dioxide is also produced via the reaction between CO and iron oxides in the catalyst.

A very rapid achievement of steady state activity of the hydrogen reduced catalyst (SB-2145) indicates either that magnetite is active for FTS or that is rapidly converted to an active carbide phase. However, the conversion of magnetite to zero-valent iron is a slow step in reduction of iron oxide, and it is unlikely that it can occur to an appreciable extent after 2 h of exposure to syngas at 260°C. For example, the unreduced iron requires about 20 h of exposure to reach its steady state activity (SB-2486). Also, as carburization of iron oxide increases with time, the catalyst activity does not increase with time, but actually decreases slowly. Activity of the unreduced catalyst (largely Fe^{3+} iron) is low initially, and it increases during the first 25 h of synthesis, due to formation of magnetite and/or ε'-carbide, indicating that one or both of these phases are active for FTS. Activity of the CO reduced catalyst is rather low initially (χ-carbide), and increases gradually with time. This behavior is not entirely consistent with hypothesis that iron carbide is the active phase for the FTS. If the latter hypothesis was correct, one would expect the initial activity of the partially carbided catalyst to be markedly greater than that of the catalyst in the form of magnetite. Also, the catalyst in test SA-0946 had a long induction period, and its activity at ~20 h on stream was similar to that of the unreduced catalyst. Initial activity of the syngas activated catalyst (mixture of iron carbide and magnetite) was the highest, but it also

went through an induction period lasting approximately 25 h. Steady state activities, between 113 and 147 h on stream, of catalysts pretreated by CO and syngas were higher than those of the hydrogen and unreduced catalysts. Magnetite was virtually absent in the CO and syngas pretreated catalysts, whereas both hydrogen and unreduced catalyst contained both magnetite and ε'-carbide. All these observations are consistent with hypothesis that both magnetite and iron carbides are active for FTS, and that iron carbides have higher FTS activity than magnetite.

Methane Selectivity

During the first 20 h on stream, methane selectivities (%CO converted to CH_4/%CO converted to products other than CO_2) of the syngas and CO activated catalysts were significantly higher (3.5 - 6%) than those obtained on the hydrogen reduced catalyst and unreduced catalysts (1.5 - 2%). Methane selectivities of the CO and syngas pretreated catalysts decreased with time, whereas those of the hydrogen reduced and unreduced catalysts increased with time (Fig. 3). These data suggest that methane selectivity is low on iron oxides, and is higher on carbided catalysts. A possible reason for markedly higher methane selectivity on carbided catalysts during early periods of synthesis, is that part of methane is produced by reaction between hydrogen and surface carbon formed during the pretreatment.

SUMMARY

After pretreatments in hydrogen, carbon monoxide, syngas (H_2/CO = 0.67), and without pretreatment the precipitated iron catalyst was tested in a stirred tank slurry reactor at 260°C, 1.48 MPa, 1.4 or 2.3 Nl/g-cat/h and H_2/CO = 0.67. Hydrogen reduced catalyst quickly reached steady state activity (within 4 h), whereas the syngas, the CO activated and unreduced catalyst required longer time (up to 100 h for the CO pretreated catalyst). Initially, the CO and syngas activated catalysts, were slightly more active than the hydrogen reduced and unreduced catalyst. Methane selectivities of hydrogen reduced and the unreduced catalyst were initially significantly lower than those on the CO and syngas activated catalyst.

From these results and catalyst characterization by XRD it was concluded that both magnetite and iron carbides are active for FTS, however the activity is higher on partially carbided catalysts. Methane selectivity is lower on the catalyst which contains significant amounts of bulk iron oxides, than on partially carbided catalyst.

ACKNOWLEDGMENT

This work was supported by the U. S. Department of Energy under contract DE-AC22-94PC93069 and Texas Engineering Experiment Station.

REFERENCES

1. Dry, M. E. In *Catalysis - Science and Technology*; Anderson, J. R., Boudart, M. Eds.; Springer - Verlag: New York, 1981; Vol. 1, p. 160.
2. Amelse, J. A.; Butt, J. B.; Schwartz, L. J. *J. Phys. Chem.* 82, 558 (1978).
3. Raupp, G. B.; Delgass, W. N. *J. Catal.* 58, 348 (1979).
4. Anderson, R. B. In *Catalysis* Emmett, P. H. Ed.; Van Nostrand-Reinhold: New York, 1956; Vol. 4, p. 29.
5. Anderson, R. B. *The Fischer-Tropsch Synthesis* Academic Press: Orlando, FL, 1984.
6. Kölbel, H.; Ralek, M. *Catal. Rev - Sci. Eng.* 21, 225 (1980).
7. Raupp, G. B.; Delgass, W. N. *J. Catal.* 58, 361 (1979).
8. Niemantsverdriet, J. W.; van der Kraan, A. M. *J. Catal.* 72, 385 (1981).
9. Blanchard, F.; Reymond, J. P.; Pommier, B.; Teichner, S. J. *J. Mol. Catal.* 17, 171(1982).
10. Reymond, J. P.; Meriadeau, P.; Teichner, S. J. *J. Catal.* 75, 39 (1982).
11. Dictor, R.; Bell, A. T. *J. Catal.* 97, 121 (1986).
12. Soled, S.; Iglesia, E.; Fiato, R. A. *Catal. Letters* 7, 271 (1990).
13. Kuivila, C. S.; Stair, P. C.; Butt, J. B. *J. Catal.* 118, 299 (1989).
14. Bukur, D. B.; Lang, X.; Rossin, J. A.; Zimmerman, W. H.; Rosynek, M. P.; Yeh, E. B.; Li, C, *Ind. Eng. Chem. Res.* 28, 1130 (1989).
15. Bukur, D.B., Koranne, M., Lang, X., Rao, K. R. P. M. and Huffman, G. P., *Appl. Cat.*, 126, 85 (1995).
16. Bukur, D. B., Nowicki, L., Manne, R. K., and Lang, X., *J. Catal.*, 155, 366 (1995).
17. Bukur, D. B., Nowicki, L., and Lang X., *Energy & Fuels*, 9, 620 (1995).
18. Bukur, D. B., Nowicki, L. and Lang, X., Chem. Eng. Sci., 49, 4615 (1994).
19. Bukur, D. B.; Lang, X.; Mukesh, D.; Zimmerman, W. H.; Rosynek, M. P.; Li., C. *Ind. Eng. Chem. Res.* 29, 1588 (1990).
20. Zimmerman, W. H. and Bukur, D. B., *Can. J. Chem. Eng.*, 68, 292 (1990).

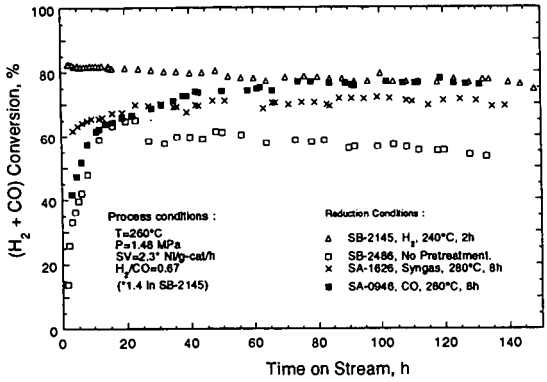

Figure 1. Effect of pretreatment conditions on synthesis gas conversion.

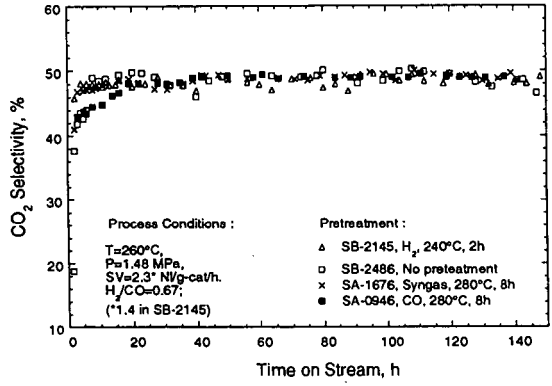

Figure 2. Effect of pretreatment conditions on carbon dioxide selectivity.

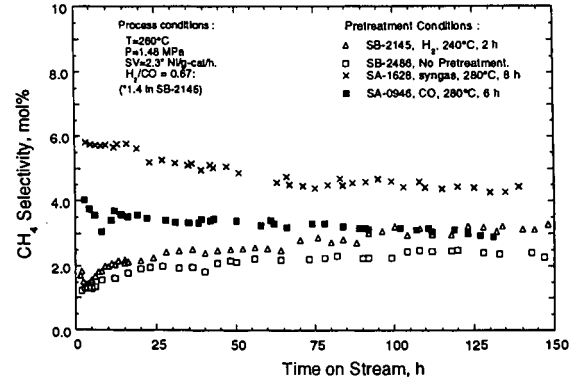

Figure 3. Effect of pretreatment conditions on methane selectivity.

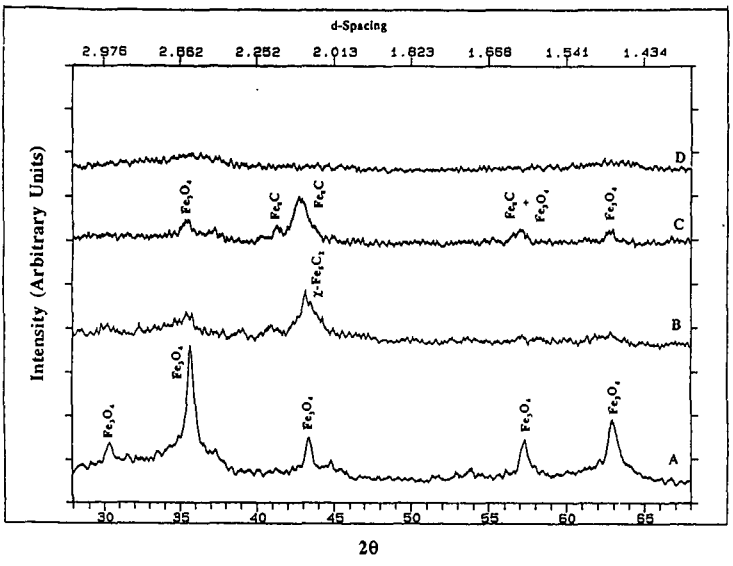

Figure 4. XRD patterns of reduced catalysts (TOS = 0 h) from slurry reactor tests:(A) SB-2145, H_2, 240°C, 2h, (B) SA-0946, CO, 280°C, 8h, (C) SA-1626, syngas, 280°C, 8h, and (D) SB-2486, No reduction.

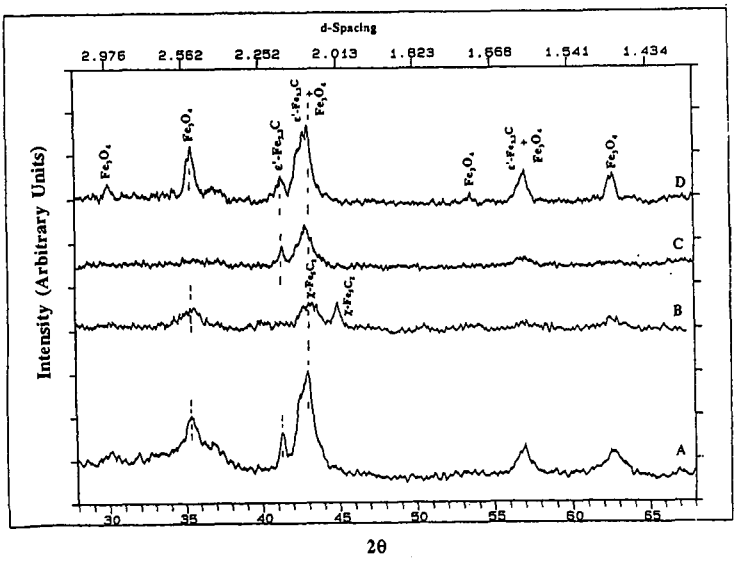

Figure 5. XRD patterns of used catalysts from slurry reactor tests:(A) SB-2145, TOS = 145 h, (B) SA-0946, TOS = 113 h, (C) SA-1626, TOS = 137 h, and (D) SB-2486, TOS = 147 h.

FISCHER-TROPSCH SYNTHESIS FOR CLEAN TRANSPORTATION FUELS

S. Bao, L. Xu, R. O'Brien, A. Raje, D. J. Houpt and B. H. Davis
Center for Applied Energy Research, University of Kentucky
3572 Iron Works Pike, Lexington, KY 40511

Keywords: Fischer-Tropsch Synthesis, Iron Catalyst, Synfuels

INTRODUCTION

The Fischer-Tropsch Synthesis (FTS) is a well established process for the production of synfuels (e.g., 1,2). Today, the process is practiced commercially in South Africa by Sasol and Mossgas and in Malaysia by Shell and partners (3). While FTS was initially envisioned as a means of producing transportation fuels, operators, such as Sasol, have recognized that the recovery of chemicals and/or chemicals feedstock provides a means of improving the profits derived from the commercial operations (e.g., 4). However, while chemicals production may be a very profitable business option for the initial FTS plant operators, as more plants are brought on-stream this will become less profitable as surpluses will drive down the prices of chemical feedstocks. Thus, the ultimate basis for FTS must be the production of transportation fuels.

The FTS process has a decided disadvantage in that the product distribution follows a normal polymerization distribution for a C_1 monomer. Thus, the plot of the log of the moles of each carbon number product versus the carbon number produces a straight line which is defined by alpha, which depends upon the rate of the propagation and termination steps. Furthermore, the value of alpha uniquely determines the product distribution such that illustrated in figure 1 (3). Today, most view the commercialization of FTS as requiring one of two options: (1) the production of heavy wax products which are subsequently hydrocracked to produce transportation fuel range products (e.g., the Shell middle distillate process (SDS); (5) and (2) the conversion of heavy products using a ZSM-5 type of catalyst (e.g., 6).

Because of the highly exothermic nature of the FTS, the ability to utilize a slurry reactor is very desirable (7). However, this operation requires the separation of the catalyst/wax slurry. When operating in a high wax mode in the temperature range of 230°C, more than half of the product must be processed to effect catalyst separation. Iron catalysts are attractive because of the highly olefinic nature of the products and because of the activity for the water-gas-shift (WGS) reaction that permits use of low H_2/CO ratios obtained by gasification of coal. However, unsupported iron catalysts have poor attrition resistance and supported catalysts have not been developed that have sufficient activity for commercial operation. Thus, one of the major operational problems associated with the use of an iron catalyst for FTS in a slurry reactor is catalyst/wax separation.

EXPERIMENTAL

The catalyst was prepared by continuous precipitation from an aqueous solution of iron nitrate containing silica derived from the hydrolysis of tetraethyl silicate using ammonia. Potassium was added to the washed and dried catalyst to provide a composition containing (atomic ratio) 100Fe/4.4Si/1.0K (8). The catalyst was activated in a flow of CO at 270°C and 175 psig during 24 hours. Following activation, synthesis was effected using a H_2/CO = 0.7 feed, 270°C, 175 psig and 3.4 NL/hr.g(Fe). Products were analyzed using a Carle gas analyzer for the gaseous products and g.c. with a DB-5 column for the liquid hydrocarbon products (9).

RESULTS AND DISCUSSION

A high activity iron catalyst has been prepared by precipitation; furthermore, this catalyst has a stable activity such that the decline in CO conversion is less than 1%/week during six months of operation. This catalyst produces a "low alpha" product distribution (figure 2). While this particular run was terminated after 2,000 hours (figure 3), this catalyst has been utilized for runs lasting longer than 4,000 hours with a similar slow decline in activity. When operating in this mode with an alpha value of 0.72 and assuming ideal gas and solution behavior, essentially all of the products would exit the reactor in the vapor phase (10). Thus, while a small contribution of a two-alpha product distribution (e.g., 11) and deviation from nonideality of the gas and/or liquid products may be operable, essentially all of the products should exit the reactor in the gas phase. **Provided this does occur, catalyst-wax separation would not be required.** Even if a small fraction of the product does not exit the reactor in the vapor phase, the ability to activate the catalyst external to the slurry reactor would permit catalyst to be added to make up for the small daily loss of catalyst in any liquid phase products that must be removed from the reactor. This

would permit the catalyst to be utilized in the form of 1-3 micron particle sizes that result from the precipitation and activation procedure rather than having to form the precipitated catalyst into particles in the 50-100 micron range as apparently has been practiced at Sasol (11).

The kinetics of the FTS is such that the productivity of hydrocarbons depends dramatically upon the conversion of CO (12). Thus, at low CO conversion the rate of production of hydrocarbons is much higher than it is at higher CO conversion levels. At the same time, the rate of the WGS reaction is low at low CO conversions but increases as the conversion of CO increases so that at about 50-60% CO conversion the rates of hydrocarbon production and the WGS reaction become about equal and remain so as the CO conversion increases further. This is illustrated in figure 4 showing that the H_2/CO ratio initially decreases with increasing CO conversion, attains a minimum and then increases to the value of the feed gas (defined here as the equivalence point); at CO conversions above the equivalence point the reaction produces hydrogen as well as hydrocarbons and CO_2. In order to take advantage of the higher rate and higher selectivity for hydrocarbons, it has been proposed that the FTS reactor be operated at CO conversion levels that are at or below the equivalence point (12).

The hydrocarbon product distribution obtained at a CO conversion level above the equivalence point is show in Table 1. If the reactor is operated at the equivalence point or even lower CO conversions, the alkene concentrations will be higher than shown in Table 1. Thus, the following should be viewed as the minimum hydrocarbon productivity levels that could be obtained by incorporation of the process consideration described below. The Conversion of Olefins to Diesel and Gasoline (COD) process has been developed by CEF of South Africa and Lurgi of Germany and a proprietary catalyst for this process has been developed by Süd-Chemie and CEF (13). The catalyst has been utilized at the Mossgas plant in South Africa with a through-put of 68 tons/hour. The Mossgas facility is able to utilize a stream that contains oxygenates (1.5-20 wt.%) saturated with water. In this manner, the C_{2-4} olefins shown in table 1 could be converted to transportation fuel. Thus, the gasoline range (C_{4-10}) yield would be about 47% of the product from the low-alpha operation. In addition, the C_{11+} fraction could be hydrotreated as is done in the SDS process to produce even more gasoline as well as high quality diesel.

In summary, the above considerations would provide a means to eliminate the need to effect catalyst-wax separation that would allow catalyst to either be retained within or recycled to the reactor. Whether this proposed option would be a viable one would depend upon the economic impact of the higher amount of methane and ethane that are produced as well as the cost differential between the COD oligomerization and the hydrocracking processes. It appears that the potential advantages would merit an economic evaluation.

ACKNOWLEDGMENT
This work was supported by U.S. DOE contract number DE-AC22-94PC94055 and the Commonwealth of Kentucky.

REFERENCES

1. H. H. Storch, N. Golumbic and R. B. Anderson, "The fishcer-Tropsch and Related Synthesis," John Wiley & Sons, Inc., New YOrk, 1951.
2. R. B. Anderson, "The Fischer-Tropsch Synthesis," Academic Press Inc., New York, NY, 1984.
3. I. Wender, Fuel Proc. Technol., 48 (1996) 189.
4. M. Dry, Catal. & Catal. Proc., Proceedings, S. African Catalysis Society Meeting, October, 1993.
5. J. Eilers, S. A. Posthuma and S. T. Sie, Catal. Lettr., 7 (1990) 253.
6. J. C. W. Kuo, Two stage process for conversion of synthesis gas to high quality transportation fuels, Final Report, DOE Contract DE-AC22-83PC60019, October, 1985.
7. A. Geertsema, Proc. 10th Pitt. Coal Conf., 1993.
8. D. R. Milburn, R. J. O'Brien, K. Chary and B. H. Davis in "Characterization of Porous Solids III," (J. Rouquerol et al., Eds.), Elsevier, Amsterdam, 1994, pp. 753-761.
9. B. H. Davis, "Technology Development for Iron Fischer-Tropsch Catalysts," Final Report, DOE Contract #AC22-91PC90056.
10. A. P. Raje and B. H. Davis, Energy & Fuels, 10 (1996) 522.
11. B. Jager and R. Espinoza, Catal. Today, 23 (1995) 17.

12. A. P. Raje, J. R. Inga and B. H. Davis, Fuel, in press.
13. "The COD Process", published by the Sūd-Chemie Group.

Table 1
Products from the Conversion of Syngas
Using a Low-alpha Iron Catalyst

Carbon Number	Product, wt.%	Olefin, wt.%
1	7,88	---
2	6.45	1.29
3	10.5	7.22
4	8.23	5.72
5	7.46	4.88
6	6.22	3.98
7	5.85	3.58
8	4.50	2.58
9	3.41	1.83
10	3.01	1.53
11+	36.5	---

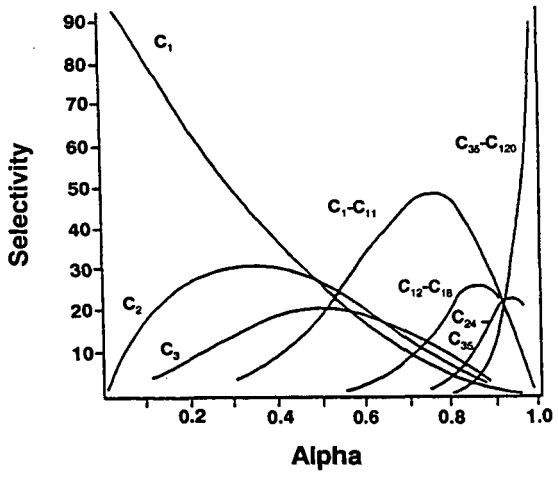

Figure 1. Product distribution dependence upon alpha.

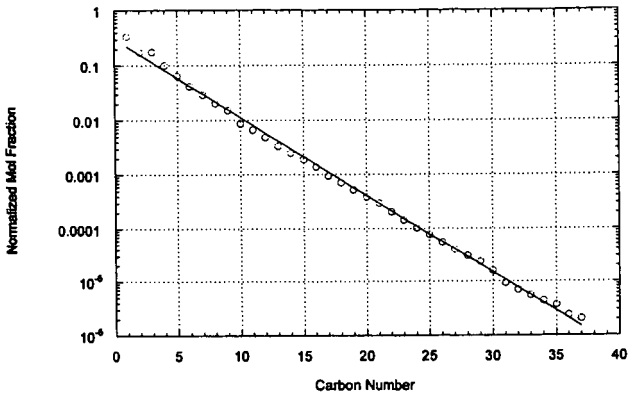

Figure 2. Anderson-Schulz-Flory plot of the products obtained from synthesis with a low-alpha (0.72) iron catalyst.

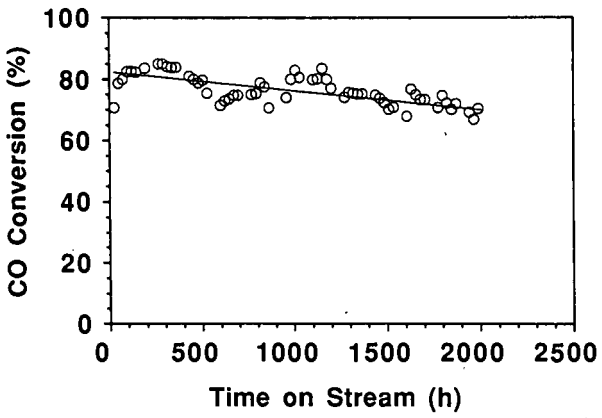

Figure 3. CO conversion with a low-alpha iron catalyst with time-on-stream.

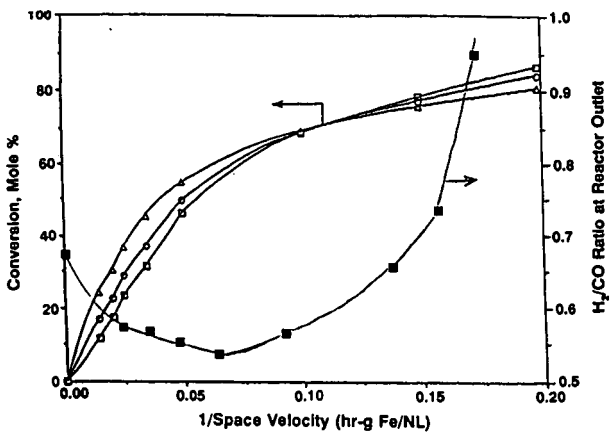

Figure 4. The conversion of CO (□), H_2 (△), (CO + H_2) (○) and the H_2/CO ratio at the reactor exit (■) for a low-alpha iron catalyst.

ALPHA-OLEFIN SELECTIVITY DURING CONVENTIONAL AND SUPERCRITICAL FISCHER-TROPSCH SYNTHESIS.

Dragomir B. Bukur, Xiaosu Lang and Zhentao Feng
Department of Chemical Engineering
Texas A&M University, College Station, Texas 77843

Keywords: Alpha-olefins, Fischer-Tropsch synthesis, supercritical fluids

ABSTRACT

Fischer-Tropsch synthesis was studied on a precipitated iron catalyst (Ruhrchemie LP 33/81) in a fixed bed reactor at several different temperatures (235°C, 250°C and 265°C) and synthesis gas feed compositions (H_2/CO = 0.67, 1 or 2) under both supercritical (propane as a supercritical fluid) and conventional (P = 1.5 MPa) operating conditions. It was found that the supercritical operation results in enhanced selectivity of α-olefins relative to conventional (normal) operation. Both total olefin content and α-olefin selectivity decreased with either increase in conversion or H_2/CO molar feed ratio, whereas olefin selectivities were essentially independent of reaction temperature.

INTRODUCTION

Alpha olefins are used as chemical intermediates for a number of important industrial and consumer products. The even-numbered carbon alpha olefins (C_4 , C_6 and C_8) are used as co-monomers for ethylene and propylene polymerization, whereas the higher molecular weight olefins are used in plasticizers, household detergents and sanitizers [1]. Linear C_{10} olefins and others provide premium value synthetic lubricants. Alpha olefins are produced in significant quantities during conventional Fischer-Tropsch synthesis (FTS) in fixed bed and fluid bed reactors at Sasol in South Africa, and recently Sasol has built a large scale commercial plant for production of 1-pentene and 1-hexene utilizing raw streams from fluid bed FTS reactors [2]. The purification process employed by Sasol entails a series of distillation steps to separate desired alpha olefins from other products. Significant economic benefits can be achieved by increasing the alpha olefin content of FTS products and thus reducing the cost of product separation.

Fischer-Tropsch synthesis in supercritical fluids provides means to accomplish this objective. In recent studies of FTS, on silica supported cobalt-lanthanum and/or alumina supported ruthenium catalysts, in a supercritical n-hexane Fujimoto and co-workers [3-4] have demonstrated certain advantages of this operation, including higher olefin selectivity, relative to gas phase and liquid phase (trickle bed) operation. Lang et al. [5] studied FTS on a precipitated iron catalyst (Ruhrchemie LP 33/81), and found that supercritical operation results in enhanced selectivity of 1-olefins (α-olefins) relative to conventional FTS, but it does not have significant effect on catalyst activity and hydrocarbon product distribution.

Here, we report results from a comprehensive study study with the Ruhrchemie LP 33/81 catalyst, which was used originally in Arge fixed bed reactors at Sasol [6], over a wide range of process conditions. At a given reaction temperature and feed composition, gas space velocity was varied to achieve different levels of syngas conversion. Variations in residence time allow us to distinguish primary and secondary reaction steps that control olefin selectivity.

EXPERIMENTAL

Experimental equipment and procedures have been described previously [5]. Experiments were conducted in a conventional downflow fixed bed reactor (1.3 cm inside diameter, 40 cm^3 effective bed volume for supercritical FTS, and 1 cm inside diameter, 27 cm^3 effective bed volume for conventional FTS) embedded in an aluminum block with a two-zone heater. Carbon monoxide, hydrogen, carbon dioxide, and C_5- hydrocarbons were analyzed by on-line gas chromatography. Condensed C_5+ hydrocarbons, collected for 6-8 h after reaching steady-state at a given set of reaction condition, were analyzed using gas chromatography [5]. Premixed synthesis gas (Iweco, Inc. >99.7% purity) containing approximately 5% of argon as an internal standard, was used as the feed. Propane (Phillips 66 Co., >99% purity) was pumped from a liquid propane dip tube tank using a diaphragm metering pump (American Lewa, Inc.; Model FCMK-1). Olefin selectivities reported here are based on the analysis of gas phase (C_2-C_5 hydrocarbons) and liquid phase products (C_6-C_{15} hydrocarbons).

A precipitated iron catalyst synthesized by Ruhrchemie AG (Oberhausen - Holten, Germany) was used in this test. The nominal catalyst composition is 100 Fe/5 Cu/4.2 K/ 25 SiO_2 (on mass basis), and the preparation procedure is described elsewhere [6]. Catalyst was calcined in air at 300°C for 5 h, and then crushed and sieved to 32/60 mesh size (0.48 mm in diameter). About 3.5 g of catalyst was diluted 1:6 by volume with glass beads of same size prior to loading into the reactor. The catalyst was reduced with hydrogen at 220°C, ambient pressure and a flow rate of 5100 cm^3/min (linear superficial velocity of 150 cm/s) for 1 h.

Following reduction, the catalyst was tested initially at baseline process conditions (1.5 MPa, 250°C, 2 L (NTP)/g-cat·h, H_2/CO = 0.67). After 67 h of conventional FTS at the baseline conditions the total pressure was increased to 5.5 MPa using propane as a balance gas (run FA-1724), while keeping the partial pressure and the flow rate of syngas at the baseline conditions. Since the reaction pressure and temperature (5.5 MPa and 250°C, respectively) are well above the critical pressure and temperature of the propane (4.19 MPa and 96.7°C, respectively), this is

referred to as supercritical FTS. Between 70 and 700 h on stream the catalyst was tested under different sets of process conditions. In another test (run FB-1644) the Ruhrchemie catalyst was evaluated under similar process conditions as those used in run FA-1724, but without supercritical propane (conventional FTS).

RESULTS AND DISCUSSION

Olefin Selectivities - Effect of gas residence time

Effects of gas residence time (i.e. gas hourly space velocity (GHSV) defined as the total volumetric (NTP) feed flow rate of synthesis gas and propane per unit bed volume, ca. 40 cm^3) and carbon number on total olefin selectivity ((1-olefin + 2-olefin)/(1-olefin + 2-olefin + n-paraffin)) and 2-olefin selectivity (2-olefin/ (1-olefin + 2-olefin)) are illustrated in Figures 1a and 1b, respectively. Data shown in Figure 1 were obtained at 250°C with $H_2/CO = 0.67$, GHSV = 330 - 1340 h^{-1} and correspond to syngas conversions of 75 to 34% (periods 2-4 in Table 1). Results obtained at gas hourly space velocities of 680 and 1340 h^{-1} were nearly identical, whereas the residence time effect was clearly observed at the gas space velocity of 330 h^{-1}. Ethylene selectivity was significantly higher at the two higher gas space velocities, whereas the increase of total olefin selectivity at higher carbon numbers was much smaller. Selectivity of 2-olefins decreased (i.e. 1-olefin selectivity increased) with increase in GHSV. The same trends were observed in experiments with different syngas feed compositions ($H_2/CO = 0.93$ and 2.03).

From these observations it is concluded that 1-olefins, and to a smaller extent n-paraffins and 2-olefins, are the primary products of FTS. These conclusions are consistent with those from previous studies with iron FT catalysts [6-8]. At the present time there is no consensus whether some of n-paraffins and 2-olefins are formed by secondary hydrogenation and isomerization reactions, respectively, on sites where chain growth cannot take place, or as primary products following secondary readsorption of 1-olefins on FTS sites [9-11]. Upon readsorption, 1-olefin becomes a reaction intermediate which can either continue to grow and terminate as a longer chain 1-olefin, n-paraffin or 2-olefin, or be terminated to n-paraffin or a 2-olefin of the same carbon number.

Shapes of curves in Figure 1, reflect carbon number (molecular weight) effect on secondary reactions. Ethylene is more reactive than other low molecular weight 1-olefins, and thus its selectivity is low. Decrease in olefin content with increase in carbon number has been attributed to their greater adsorptivity [9], higher solubility in the liquid phase resulting in higher 1-olefin concentrations [8], and/or diffusion enhanced 1-olefin readsorption [10,11]. Madon et al. [10,11] proposed that larger 1-olefins spend longer times in a catalyst pore, due to their lower diffusivities, and this in turn increases probability for their readsorption on FTS active sites before exiting the pore. The increase in 2-olefin selectivity with increase in carbon number (Fig. 1b) or with increase in bed residence time (lower gas space velocity) is due to the same factors mentioned above. Longer residence time of high molecular weight 1-olefins either in the catalyst pores or in the reactor itself, increases probability for secondary 1-olefin readsorption followed by termination as 2-olefin on FTS and/or different type of sites.

Effects of gas space velocity and carbon number on olefin selectivities during conventional FTS (run FB-1644) at 1.5 MPa, 250°C, $H_2/CO = 0.67$ are shown in Figure 2. Qualitative trends are the same as those observed during SFTS (Fig. 1), i.e. the total olefin selectivity increased (Fig. 2a), whereas the 2-olefin selectivity decreased (Fig. 2b), with increase in gas space velocity (decrease in bed residence time). However, the bed residence time effect on selectivity was markedly higher during the conventional FTS, although conversions and nominal gas residence times were similar in both sets of experiments (0.9 - 4.8 min in run FB-1644 vs. 1.3 - 5.1 min in run FA-1792. Residence times were calculated from the ideal gas law, using the arithmetic average of inlet and outlet gas flow rates). Carbon number effect on total olefin and 2-olefin selectivity was also more evident in the case of conventional FTS. Changes in 1-olefin selectivity (1-olefin/(1-olefin + 2-olefin + n-paraffin)) with carbon number, for both modes of operation at syngas conversion of about 80%, are shown in Figure 3. It can be seen that selectivity of C_2 and C_7+ 1-olefins is significantly higher during supercritical FTS, and this is of potential commercial importance.

Results in Figures 1 and 2 show that gas space velocity has a marked effect on olefin selectivity during conventional FTS, and relatively small effect during SFTS. During conventional FTS the reaction mixture inside the reactor is distributed among two phases : gas and liquid. High molecular weight hydrocarbons (C_8+) are leaving the reactor preferentially in the liquid phase, the flow rate of which increases along the reactor length. In a fixed bed reactor the residence time of the liquid phase is much longer than that of the gas phase. This increases probability for readsorption of high molecular weight 1-olefins and leads to increased formation of n-paraffins and 2-olefins via secondary reactions. On the other hand during SFTS operation, there is only one phase in the reactor and the residence time of all products, regardless of their molecular weight, is the same.

Carbon number effects, can be explained in terms of diffusion enhanced 1-olefin readsorption. Larger 1-olefins spend longer time in the catalyst pores than smaller ones, due to their lower diffusivities, and this increases probability for secondary 1-olefin readsorption, double bond isomerization and hydrogenation reactions. Ethylene, which has relatively large diffusivity due to its small molecular size, is significantly more reactive than other 1-olefins [9, 10], and its selectivity is low in comparison to C_3-C_6 olefins. Ethylene selectivity during conventional FTS was smaller than during SFTS at comparable bed residence times, i.e. syngas conversions (Figures 1 and 2). However, the pore residence time of ethylene is greater during conventional FTS, because ethylene diffusivity is smaller in the liquid filled pores (conventional FTS), than in the supercritical propane. Also, at a given gas space velocity, the carbon number effect on either the total olefin or 2-olefin selectivity was much more evident during the conventional FTS. In both modes of operation diffusivity decreases with increase in carbon number (molecular weight), but since diffusivities are significantly smaller in hydrocarbon wax than in the supercritical propane, the intraparticle diffusional resistance during conventional FTS is larger and carbon number effect on olefin selectivity is stronger.

Olefin Selectivities - Effect of reaction temperature
The effect of reaction temperature on olefin selectivities during SFTS and conventional FTS (run FB-1644) at a nearly constant syngas conversion was insignificant for temperatures between 235 and 265°C. Results from previous studies with iron FT catalysts showed different types of behavior, i.e. in some cases the olefin selectivity increased with increase in temperature, but on some catalysts either no effect or the opposite trends were observed [8, 9].

Olefin Selectivities - Effect of reactant composition
Figure 4 illustrates the effect of gas feed composition on olefin selectivity during SFTS at 235°C and syngas conversion of about 30% (data from periods 6, 11 and 15 in Table 1). Total olefin selectivity was lower, and 2-olefin selectivity higher when the synthesis gas with $H_2/CO = 2.03$ was used (representative of syngas obtained from steam reforming or partial oxidation of natural gas). Olefin selectivities were similar in experiments with $H_2/CO = 0.67$ and $H_2/CO = 0.93$.

Concentration of surface hydrogen determines chain termination probabilities and olefin content, and it increases with increase in H_2/CO molar feed ratio. High surface concentrations of hydrogen favor termination reactions, and termination to paraffins rather than olefins, as well as secondary 1-olefin isomerization reactions [8, 11].

SUMMARY

Effects of reaction temperature, gas space velocity and feed composition on olefin selectivity were studied in a fixed bed reactor during conventional FTS, and FTS in supercritical propane. It was found that total olefin content decreased and 2-olefin selectivity increased with either decrease in gas space velocity or increase in H_2/CO molar feed ratio, whereas olefin selectivities were essentially independent of reaction temperature.

Results from bed residence time effect studies in both modes of operation indicate that 1-olefins are the dominant primary products of FTS. Selectivity of n-paraffins and 2-olefins increases, whereas 1-olefin selectivity decreases with increase in carbon number, due to secondary reactions of 1-olefins. At high syngas conversions (~80%), selectivities of high molecular weight 1-olefins during SFTS were significantly higher than those obtained during conventional operation. These results indicate that SFTS is a potentially attractive route for synthesis of high molecular weight alpha olefins from the synthesis gas.

ACKNOWLEDGMENT

This work was supported by the U. S. Department of Energy (University Coal Research Program) under grant DE-FG22-92PC92545 and Texas Engineering Experiment Station.

REFERENCES

1. Lappin, G. R.; Nemec, L. H.; Sauer, J. D.; Wagner, J. D. Kirk-Othmer Encyclopedia of Chemical Technology, 4 th Ed., Vol. 17, Wiley: New York, 1996; pp. 839.
2. Waddacor, M. Chemical Processing SA,. 1 (No.10), (1994).
3. Yokota, K.; Fujimoto, K. *Ind. Engng Chem. Res.* 30, 95 (1991).
4 Fan, L.; Yokota, K.; Fujimoto, K *AIChE J.* 38, 1639 (1992.
5. Lang, X.; Akgerman, A.; Bukur, D. B *Ind. Engng Chem. Res.* 34, 72 (1995).
6. Dry, M. E.*Catalysis-Science and Technology,* Vol. 1, Springer-Verlag: New York, 1981; pp. 160.
7. Schulz, H.; Gokcebay, H.*Catalysis of Organic Reactions*, Marcel Dekker: New York, 1984; pp.153.
8 Dictor, R.; Bell, A. T. *J. Catal.* , 97, 121 (1986).
9. Schulz, H.; Rosch, S.; Gokcebay, H.*Coal: Phoenix of '80s, Proc. 64th CIC. Coal Symp.* Vol. 2, Canadian Society for Chemical Engineering: Ottawa, Canada, 1982; pp. 486.
10. Madon, R. J.; Reyes, S. C.; Iglesia, E. *J. Phys. Chem.* , 95, 7795 (1991).
11. Madon, R. J.; Iglesia, E. *J. Catal.* , 139, 576 (1993).

Table 1. Process conditions and catalyst activity results in test FA-1724

Period, #	1	2	3	4	5	6	7	8	9	10	11	12	13	14	15	16	17	18
Time on stream, h	67	140	164	191	215	239	259	331	352	373	406	428	475	547	571	598	624	691
T, °C	250	250	250	250	235	235	265	265	250	250	250	235	235	250	250	235	235	250
SV, L(NTP)/g-cat·h	2.0	2.0	3.8	1.0	0.5	2.2	7.1	1.4	2.0	5.0	2.0	3.0	1.5	1.4	4.0	2.2	0.5	2.0
GHSV, h^{-1}	175	680	1340	330	288	752	2480	507	680	1750	1234	1047	529	487	1413	772	162	681
H_2/CO feed ratio	0.67	0.67	0.67	0.67	0.67	0.67	0.67	0.67	0.67	2.0	2.0	2.0	2.0	0.93	0.93	0.93	0.93	0.67
CO conv., %	48.5	48.5	32.0	74.7	62.1	26.8	29.2	77.0	43.8	34.2	92.5	48.3	77.3	70.4	26.3	26.0	75.3	33.8
H_2 + CO conv., %	43.1	50.2	34.4	75.5	65.0	29.3	32.5	76.6	46.7	22.1	60.3	30.4	51.7	64.9	27.4	27.7	69.9	35.1
H_2/CO usage ratio	0.82	0.73	0.79	0.69	0.74	0.82	0.85	0.66	0.78	0.95	0.98	0.90	1.03	0.78	1.01	1.06	0.79	0.73
H_2/CO exit ratio	0.60	0.61	0.61	0.61	0.54	0.61	0.57	0.69	0.58	2.59	15.1	3.08	5.45	1.31	0.90	0.89	1.35	0.63

Notes: Conventional FTS during period 1; SFTS during periods 2 - 18 with P_{total} = 5.5 MPa.
Syngas partial pressure P_{H_2+CO} = 0.7 MPa in periods 5 and 11, otherwise P_{H_2+CO} = 1.5 MPa.

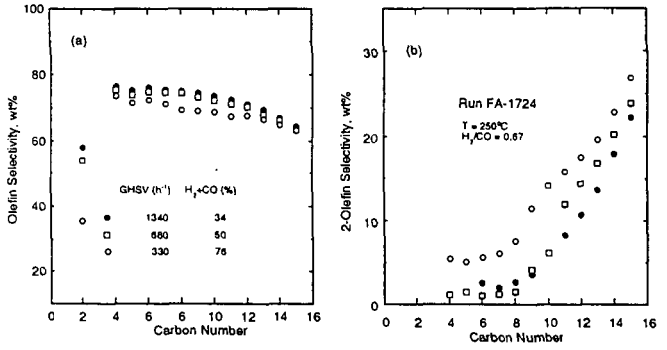

Figure 1. Effect of gas space velocity on: (a) olefin; and (b) 2-olefin selectivity during SFTS at 250°C, H_2/CO = 0.67 and 5.5 MPa (FA-1724).

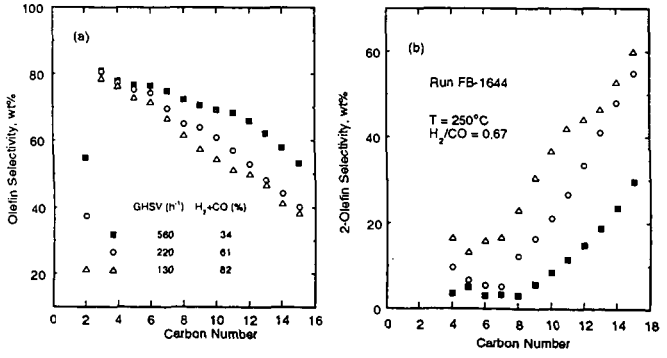

Figure 2. Effect of gas space velocity on: (a) olefin; and (b) 2-olefin selectivity during convencional FTS at 250°C, H_2/CO = 0.67 and 1.5 MPa (FB-1644).

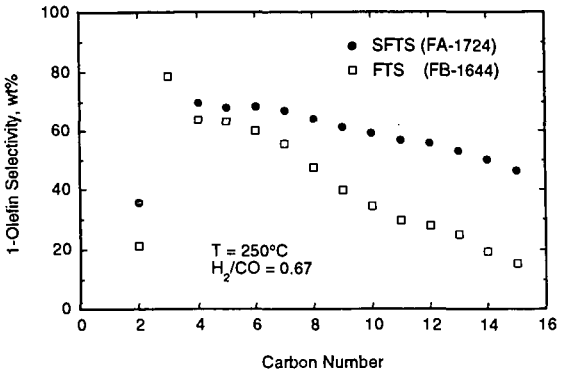

Figure 3. Comparison of α-olefin selectivities during conventional and supercritical FTS at 250°C, $H_2/CO = 0.67$ and syngas conversions of 82% (FB-1644) and 76% (FA-1724).

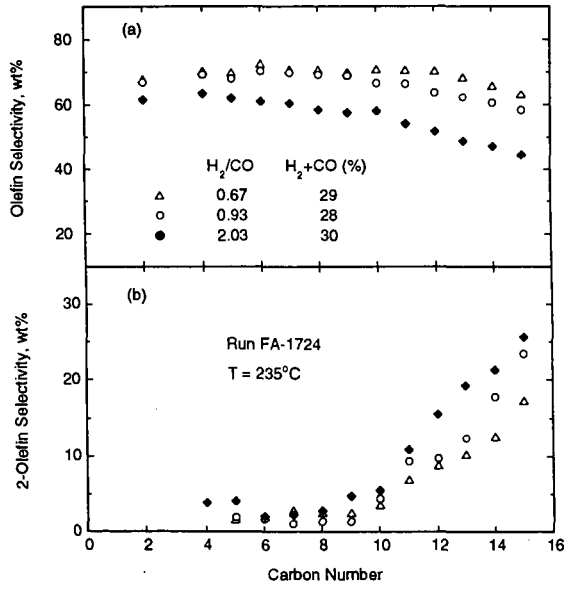

Figure 4. Effect of gas feed composition on: (a) olefin; and (b) 2-olefin selectivity during SFTS at 5.5 MPa and 235°C (FA-1724).

COMPARATIVE STUDIES OF LANTHANUM AND CERIUM AS PROMOTERS OF COBALT BASED FISCHER-TROPSCH CATALYSTS.

B. Ernst[1], A. Kiennemann[1], P. Chaumette[2]
[1]LERCSI-ECPM URA CNRS 1498
1, rue Blaise Pascal 67008 Strasbourg Cedex France
[2]Institut Français du Pétrole
1 et 4, Avenue de Bois Préau
92506 Rueil-Malmaison Cedex France

Keywords : Syngas Chemistry, Co and Co-promoted (La,Ce) catalyst reactivity

INTRODUCTION

These last years, cobalt based catalysts have been widely developed in Fischer-Tropsch synthesis, particularly for the preparation of higher molecular weight fractions (chain growth probability a > 0.9). The most studied catalysts are Co/Al_2O_3 or Co/SiO_2 undoped or doped by a second metal (Ru, Rh, Pt, Re...) and/or oxides (ZrO_2, TiO_2, rare earth oxides...) (1-5). The second metal generally favours the reduction of cobalt by hydrogen spillover phenomena or acts in regeneration of deactivated systems. The oxide operates through its interaction with the metal (TiO_2, ZrO_2), its reducibility (CeO_2), its acidic character (Al_2O_3) or the coverage of the metal particle by different processes including migration to the surface (La_2O_3). In the present work, a comparative study of Co/SiO_2 catalysts and lanthanum oxide or cerium oxide promoted Co/SiO_2 catalysts is reported. Results concerning the preparation, reduction and reactivity with syngas in a slurry type reactor are included.

EXPERIMENTALS

Preparation

A sol-gel type method has been developed (6) instead of a conventional successive impregnation technique, in order to be able to control the cobalt dispersion, even at high cobalt loadings (25 wt%). The overall scheme of preparation is as follows (Scheme 1).

Cobalt, cerium or lanthanum nitrate as well as tetraethoxysilane (TEOS) are dissolved separately in ethanol at 70°C. Once the solutions are mixed, precipitation is performed by adding an excess of oxalic acid dissolved in ethanol at 70°C. The released nitric acid makes the medium acidic, and during ethanol evaporation TEOS is slowly hydrolyzed by the water contained in the precursor salts. The evaporation is performed over a long period (6 hrs) until complete hydrolysis of TEOS. The catalysts are then dried (12 hrs, 100°C) and calcined (550°C, 4 hrs). The different catalysts prepared have the same cobalt weight content, and are described in Table 1.

CharacterizationTechniques

Temperature programmed reduction (TPR) :

TPR experiments were performed by passing pure hydrogen (12 $ml.min^{-1}$) over 0.2 g of calcined sample and a temperature increase rate of 1 $K.min^{-1}$ has been selected. The reduction was monitored by water formation as measured in the exit gas by a catharometer detector.

X-ray diffraction (XRD) :

The monochromatic X-ray beam was produced by a Cu anticathode (λ = 1.5418 Å) in a Siemens D5000 powder diffractometer. The XRD patterns were recorder for 2 values between 10 and 90° with a 0.005° spacing. Identification of the phases were made according to the JCPDS files.

X-ray Photoelectron Spectroscopy (XPS) :

The spectrometer was a Vacuum Generator's ESCA3 fitted with a preparation and an analysis chamber (10^{-10} Torr vacuum) (293 < T < 873 K). The deconvolutions were made both for the $Co2p_{3/2}$ and $Co2p_{1/2}$ peaks. The binding energies were measured by taking the C_{1s} peak of contamination carbon at 284.8 eV as reference.

Transmission Electron Microscopy (TEM) :

The apparatus was a TESCON EM-002B type device (1.8Å resolution, 200kV acceleration potentiel). The analysis for chemical elements was performed by EDS with a KEVEC analyzer (selected area 14 nm). The powdered sample was suspended in ethanol and one drop of the suspension was deposited on a copper grid covered by a carbon membrane.

Reactivity test.

The catalytic tests were performed in a slurry bed reactor (7). Typical conditions were : P = 2MPa, T = 493K, H_2/CO = 2/1, G.S.H.V. = 2000 h^{-1}. The catalysts were reduced ex-situ at temperatures up to 513K under a flow of diluted hydrogen (5% H_2 in N_2) and then under a pure hydrogen flow with an increasing temperature up to 673K with a 1K.min^{-1} slope and a final step at constant temperature (400K) for 14 hrs. The syngas mixture was admitted into the reactor at room temperature. The starting time for the reaction at 493K is taken after stabilization of the catalytic system.

RESULTS AND DISCUSSION

Characterization of the catalysts

Calcined catalysts

By thermogravimetric analysis (TGA), it is shown that cobalt, mixed cobalt-cerium or cobalt-lanthanum oxalates are decomposed between 543 and 603K. At 823K, part of the lanthanum is present as an oxycarbonate. In the XRD diffractogramms and XPS spectra, cobalt is seen to be present as the Co_3O_4 spinel phase, ceria in a fluorite structure and lanthanum as a oxycarbonate but also as a $LaCoCO_3$ perovskite whose proportion increases with the amount of lanthanum added to the preparation.

The XPS analysis of the surface indicates that Co/Si ratio diminishes on the surface after calcination : 0.12 instead of the theoretical bulk 0.403 ratio for the Co/SiO_2 catalysts; 1.1 compared to 1.6 for Co-CeO_2(A)/SiO_2; and 0.3 compared to 1.5 for Co-La(a)/SiO_2).

This clearly shows that after calcination silica is segregated to the surface for the three series of catalysts. It must also be noted that cobalt silicate has not been evidenced. The NMR of silicium (MAS and CP-MAS) has shown that the initial silicagels are transformed to siloxane groups but some isolated silanol groups are also present.

The means size of the cerium oxide crystallites has been evaluated to be about 80-85Å even for the catalysts with the highest cerium contents which indicates a very good dispersion of the promoter. Cerium oxide is present as aggregates and at the edge of these aggregates the CeO_2 and Co_3O_4 crystallites are in close contact with each other.

The size distribution of the cobalt oxide particles has been determined by TEM. The size distribution for Co-Ce(B)/SiO_2 is represented on Figure 1. For Co/SiO_2 the mean size of cobalt oxide crystallites is about 300Å. It is much less (about 135Å) for Co-Ce/SiO_2 and for Co-La/SiO_2 (about 100Å). These results are in good agreement with those obtained by XRD (Figure 1).

The BET surface areas (Table 1) of the catalysts are large. They deacrease upon addition of ceria or lanthanum oxide but remain higher than 100 $m^2.g^{-1}$. It must be noted that the Co/SiO_2 catalyst is microporous and that the mesoporosity increases with the amount of rare earth oxide (porous volume for 0.22 cm^3 g^{-1} to 0.40 $cm^3.g^{-1}$).

Reduced catalysts

The reduction of all these catalytic systems has been followed by TPR and XPS. The TPR curves up to 753K (highest reduction temperature in the reactivity studies) for Co-Ce/SiO_2 and Co-La/SiO_2 are reported on figures 2 and 3.

The TPR curve for Co/SiO_2 shows two reduction peaks (543K, and a broad peak between 603 and 703K) (8). These two peaks are two widely separated to correspond to a two steps reduction of Co_3O_4 to Co° via CoO. It is suggested either that the reduction temperature changes is due to the change in the metal oxide particle size or that the microporosity of the catalyst makes the diffusion of the water produced during the reduction difficult, thus inhibiting the reduction process in the micropores.

For Co-Ce/SiO_2 (Figure 2) two reduction peaks are clearly present especially for the catalysts with the highest cerium contents. The first peak (483-513K) is shifted to lower temperature by increasing the cerium content. It corresponds to the reduction of Co_3O_4 to Co°. It is noteworthy that the presence of ceria lowers the reduction temperature of cobalt. The second peak corresponds to the reduction of ceria (the peak changes with the amount of CeO_2).

The Co-La/SiO_2 catalysts curves have also two maxima except for the highest loaded catalyst for which three maxima are observed (Figure 3). The three maxima are interpreted as the reduction of Co_3O_4 to Co° (~ 553K), the reduction of the perovskite structure activated by the free cobalt (~ 613K) and the decomposition of carbonate species (> 723K). The extent of reduction of all the catalysts obtained by TPR, XPS and oxygen titration are summarized on Table 2.

As can be seen on Table 2, the cerium or lanthanum promoted catalysts are less reduced than the corresponding Co/SiO_2 catalyst (except for Co-La(a)/SiO_2). This point together with the lower initial cobalt oxide particle size (Table 1) will be important in the discussion of the catalytic reactivity results.

The cobalt particle size after reduction has been measured indirectly by reoxidation to Co_3O_4 followed by XRD analysis (Table 2). Compared to the calcined catalysts (Table 1), a decrease of the cobalt oxide particle size (240Å instead of 300Å), as well as a homogeneity for that of Co-Ce/SiO_2 (170, 165, 160 and 135Å for catalysts A, B, C, D respectively) and a slight decrease for Co-La/SiO_2 (120, 105, <100, <100Å) for catalysts a,b,c,d respectively) can be noted.

Catalytic reactivity tests.

All the characterized catalyst have been tested under the conditions described in the experimental part. The results are expressed as: total conversion of CO (CO%), conversion to hydrocarbons (HC%) and CO_2 (CO_2%), and productivity in hydrocarbons (kg.kgcat^{-1}h^{-1}). The specific activity TOF^1 (mole h^{-1}) is defined as the number of CO moles transformed by gram of catalyst and unit time and TOF^2 (mole h-1) as the number of CO moles transformed by cobalt metal site and unit time. The selectivity is expressed in mass per cent on a carbon basis. Table 3 gives the reactivity results for all the catalysts.

It can be noted that the CO conversion and TOF^1 are nearly the same for all the catalysts. For the promoted catalysts, TOF^2 decreases with the promoter content. TOF^2 values are higher for ceria than for lanthana. For some catalyst samples (B and D), they are higher than for Co/SiO_2. Selectivities are reported in Table 4.

The chain growth probability α deduced from the distribution of the hydrocarbons is 0.92 for Co/SiO_2. This value decreased for catalysts doped by ceria [from 0.87 (A) to 0.82 (D,C)] or lanthana [(0.88 (b), 0.82 (a)]. It can be noted the low amounts of promoters (5wt %) are sufficient to induce this decrease. A closer examination of the selectivities obtained shows that as soon as ceria or lanthana are added (Figure 4) :

- The methane selectivity changes drastically. (The mass fraction of CH_4 is increased by a factor of 2 or 3). The formation of methane depends on the amount of ceria or lanthana added.
- The C_5+ mole % fraction decreases strongly upon addition of Ce or La (80.0% for Co/SiO_2 compared to less than 60.0% for Ce and La containing catalysts).
- The mass fraction of C_{22}+ hydrocarbons is divided by 3.
- The C_5-C_{13} fraction is favoured in the presence or cerium or lanthanum The tendency has already been reported for Co-Ce/C tested under atmospheric pressure (9).

From these results it can be seen that the cerium or lanthanum promoted catalysts have about the same activity as the unpromoted ones, however the changes in hydrocarbon distribution are more significant : lower α values, higher methane formation, increase of the C_5-C_{13} fraction and diminution of C_{22}+ yields. The change in hydrocarbon distribution can be attributed to several factors :

- The presence of smaller cobalt crystallites (240, 135-170 and 100-135Å for Co/SiO_2, Co-Ce/SiO_2 and Co-La/SiO_2) respectively.
- A higher extent of reduction for the promoted catalysts.

- The intrinsic properties of ceria or lanthana which can form hydrocarbons by themselves (10). On the catalysts containing cerium or lanthanum, hydrogen chemisorption and desorption experiments (Table 5) show clearly the influence of the promoter on hydrogen desorption. Both promoters act as hydrogen storage agents and thus probably influence the hydrocarbon selectivity of these catalysts (methane formation, decrease of chain growth).
- Modification of the nature of the cobalt site by interaction between cobalt and the rare earth, changing the CO and H_2 chemisorption properties.

CONCLUSION

The present work has evidenced the modifications of the catalytic behaviour of 25 wt%Co/SiO_2 catalysts, when they are promoted by varying amounts of ceria or lanthana. The main changes were found in the cobalt particle size, the reducibility of the metal, and the ability to desorb previously adsorbed hydrogen from the catalyst.

The changes of physical properties of the catalysts have few consequences on the catalytic activity, but strongly influence the hydrocarbons distribution. Addition of CeO_2 or La_2O_3 enhances methane formation, increases the selectivity in the C_5-C_{13} fraction and decreases the chain growth probability α.

LITERATURE CITED

(1) Iglesia, E., Adv. Catal., 39, 221 (1993).

(2) Eri, S., Goodwin, J.G., Marcelin, G., Riis, T., U.S. Patent 4,801,573 (1989).

(3) Iglesia, E., Soled, S.L., Fiato, R.A., U.S. Patent 4,794,099 (1988); 4,960,801 (1990).

(4) Gulf Reasearch Development, US Patent 4,585,798 (1986).

(5) Shell International Research, Europ. Patent 842006 (1984).

(6) Vansant, E.F., van der Voort, P., Vrancken, K.C., Stud. Surf. Sci. Catal., 96, chapter 1 and 2 (1995).

(7) Chaumette, P., Verdon, A., Kiennemann, A., Boujana, S., An Chem. Soc. Div. Petr. chem. Prep., 37, 833 (1992).

(8) Castner, D.G., Watson, P.R., Chan, I.Y., J. Phys. Chem., 94, 819 (1990).

(9) Barsault, J., Biwole, N., Bull. Soc. Chim. Belg., 104, 149 (1995).

(10) Maruya, K., Inaba, T., Maehashi, T., Domen, K., Onishi, T., J. Chem. Soc. Chem. Comm. 487 (1985).

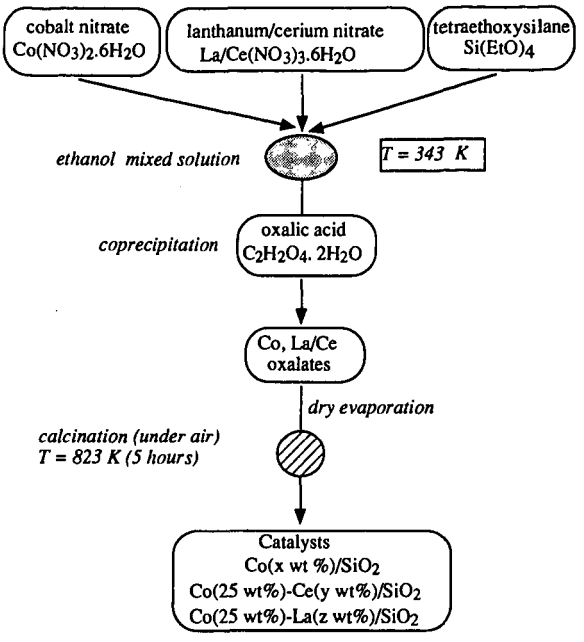

Scheme 1: Catalyst preparation procedure.

Table 1.
Characteristics of catalysts.

Catalysts	Co	Si	Ce or La	O	BET surface area ($m^2.g^{-1}$)	Particle size* cobalt oxide (Å)
Co/SiO_2	25.2	28.4	/	46.1	293	300(300)
$Co-Ce(A)/SiO_2$	25.5	7.4	38.2	26.0	137	185
$Co-Ce(B)/SiO_2$	25.5	16.9	21.5	34.6	103	170(135)
$Co-Ce(C)/SiO_2$	24.6	23.5	8.9	42.7	281	165
$Co-Ce(D)/SiO_2$	23.9	25.0	4.8	43.2	245	185
$Co-La(a)/SiO_2$	24.9	6.9	37.5	28.1	123	125(110)
$Co-La(b)/SiO_2$	24.5	16.0	21.2	34.8	131	125
$Co-La(c)/SiO_2$	24.3	20.8	9.1	43.0	340	100
$Co-La(d)/SiO_2$	24.8	26.4	4.7	43.4	384	110

* oxygen titration (TEM measurement)

Table 2.
Reducibility of catalytic systems

Catalysts	Reduction extent (%) TPR	XPS	Oxygen titration	Co particle size after reoxidation (Å)
Co/SiO_2	73	82	77	240
$Co-Ce(A)/SiO_2$	66	89	89	170
$Co-Ce(B)/SiO_2$	52	-	81	165
$Co-Ce(C)/SiO_2$	51	-	77	160
$Co-Ce(D)/SiO_2$	40	-	52	135
$Co-La(a)/SiO_2$	80	84	81	120
$Co-La(b)/SiO_2$	65	-	76	105
$Co-La(c)/SiO_2$	64	-	65	<100
$Co-La(d)/SiO_2$	39	-	42	<100

Table 3.
Reactivity tests for Co/SiO_2, $Co-Ce/SiO_2$ and $Co-La/SiO_2$ catalysts

	Conversion			HC productivity (a)	TOF[1] (b)	TOF[2] (c)
	CO%	HC%	CO_2%			
Co/SiO_2	10.8	10.7	0.0	68.9	12.7	43.6
$Co-Ce(A)/SiO_2$	11.8	11.4	0.1	50.6	13.7	36.7
$Co-Ce(B)/SiO_2$	13.6	13.1	0.1	53.5	15.8	52.0
$Co-Ce(C)/SiO_2$	9.5	8.6	0.5	37.9	11.4	34.3
$Co-Ce(D)/SiO_2$	12.9	12.6	0.1	54.6	15.9	55.3
$Co-La(a)/SiO_2$	11.6	11.2	0.2	37.2	13.9	21.7
$Co-La(b)/SiO_2$	10.0	9.6	0.1	41.5	11.8	22.6
$Co-La(c)/SiO_2$	14.2	12.9	0.1	56.8	16.3	26.3
$Co-La(d)/SiO_2$	12.3	12.0	0.2	53.9	14.5	38.8

(a) 10^{-3} kg . $kgcat^{-1}.h^{-1}$ (b) 10^{-3} mole h^{-1} (c) 10^{-2} mole h^{-1}

Table 4.
Selectivities obtained with Co/SiO_2, $Co-Ce/SiO_2$ and $Co-La/SiO_2$ catalysts.

Catalysts	Mass selectivity (%)					
	C_1	C_2-C_4	C_5-C_9	C_{10}-C_{13}	C_{14}-C_{21}	C_{22}^+
Co/SiO_2	15.9	2.5	3.1	11.5	24.6	42.4
$Co-Ce(A)/SiO_2$	34.0	9.2	12.3	15.4	15.9	13.2
$Co-Ce(B)/SiO_2$	30.1	9.7	16.6	16.6	15.7	11.3
$Co-Ce(C)/SiO_2$	46.6	8.3	10.0	13.9	14.8	6.4
$Co-Ce(D)/SiO_2$	49.1	5.6	5.8	10.4	17.5	11.6
$Co-La(a)/SiO_2$	48.4	6.5	7.0	16.5	14.7	6.8
$Co-La(b)/SiO_2$	47.7	7.1	3.3	8.9	12.9	20.1
$Co-La(c)/SiO_2$	38.9	5.9	15.2	15.2	14.2	10.6
$Co-La(d)/SiO_2$	43.4	6.6	6.1	14.0	16.7	13.2

Table 5.
Amount of adsorbed and temperature desorbed hydrogen on Co/SiO_2, $Co-Ce/SiO_2$ and $Co-La/SiO_2$ catalysts

Catalysts	Chemisorbed H_2 (μmole.g cat^{-1})	Desorbed H_2 (μmole.g cat^{-1})
Co/SiO_2	11.4	4.5
$Co-Ce(A)SiO_2$	14.5	30.4
$Co-La(a)SiO_2$	14.8	28.3

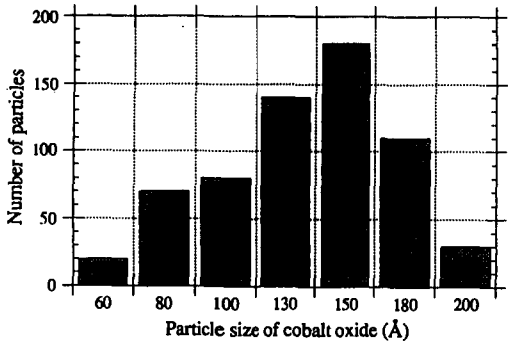

Figure 1. Cobalt oxide particle size distribution for $Co-Ce(B)/SiO_2$ catalyst.

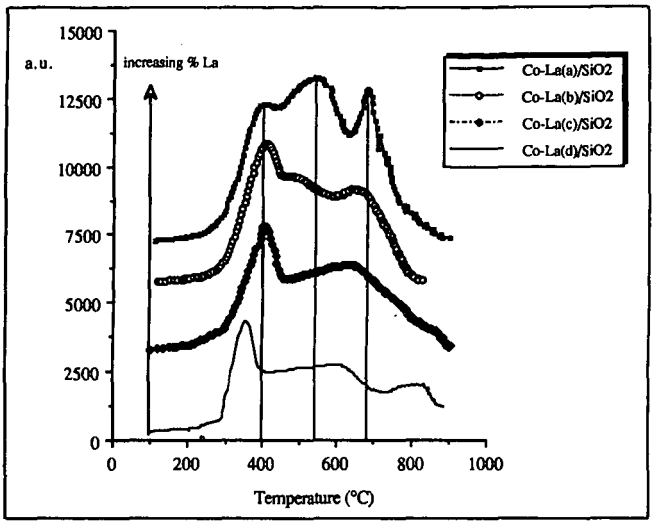

Figure 2. TPR curves for Co-La/SiO_2 catalyst.

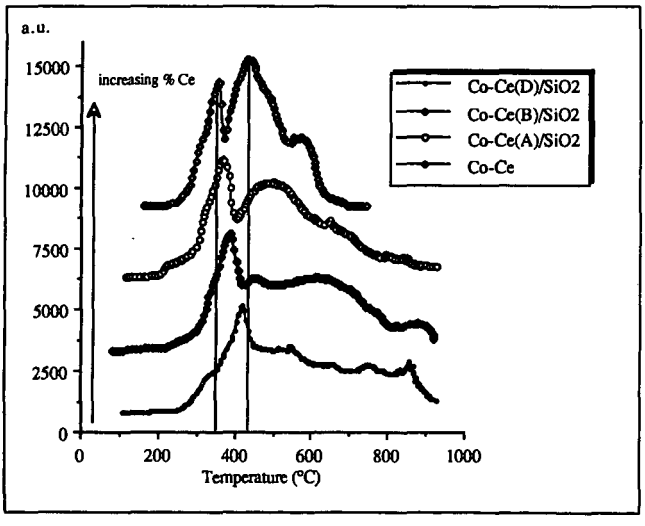

Figure 3. TPR curves for Co-Ce and Co-Ce/SiO_2 catalysts.

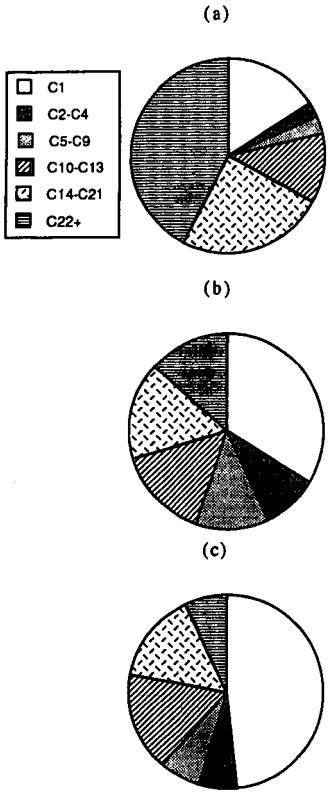

Figure 4. Weight distribution of hydrocarbons on (a) Co/SiO_2 (b) $Co-Ce(A)/SiO_2$ and (c) $Co-La(a)SiO_2$ catalysts.

MANGANESE MODIFIED NANOSCALE COBALT CATALYST TO SYNTHESIZE LONG-CHAIN HYDROCARBONS

Yongqing Zhang,Bing Zhong and Qin Wang
State Key Laboratory of Coal Conversion,Institute of Coal Chemistry,Chinese Academy of Sciences,Taiyuan,030001,PR China

ABSTRACT: Cobalt catalyst supported on ZrO_2 coated SiO_2 aerogel exhibits high FTS activity and C^{5+} selectiity at a moderate pressure in fixed bed reacter. It yields 150g liquid hydrocarbons and FT wax for every cubic meter of syngas. The effect of manganese modification on structure, texture, reduction, H_2 adsorption and FTS performance of Co/ZrO_2-SiO_2 catalyst was examined. The results show that addition of proper amount of manganese lowers the methane selectivity and raises C^{5+} selectivity ,but excessive amount of manganese added leads to opposite results. Carbon number distribution of $Co-Mn/ZrO_2-SiO_2$ no longer follows SF distribution. Distict two peaks (maximium point at C_{11} and C_{17} respectivily) are observed in the profile of carbon number distribution for $Co-Mn/ZrO_2-SiO_2$ indicating the existence of two kinds of active sites.

Keywords: Fischer-Tropsch Synthesis, Nanoscale Catalyst,Manganese Promoter

INTRODUCTION

Fischer-Tropsch synthesis is catalytic reaction of CO hydrogenation for obtaining C^{2+} hydrocarbons.Carbon number distribution of traditional FTS product obey Schulz-Flory distribution which constrains selectivity improvement of toward any product with particular carbon number.Research work of FTS has been concentrated on method and principle to control chain length distribution in last twenty years.Currently, the objective of most FTS research work is to increase the α value to as high as possible(0.95 or above) in order to synthesize long chain hydrocarbons(1).Different conclusions were drawn on the point of weather FTS reaction is structure sensitive (2-3). General result is that specific activity of FTS is affected by properties of support material and active metal crystal size of catalyst. Generally,the enlargement of active metal crystal size will increase the selectivity of long-chain hydrocarbons.It is because that in the process of FTS reaction, growing carbon chain lies on the surface of active metal crystals. So large metal crystal is required to obtain long-chain hydrocarbons. But for catalysts with some extent of metal-support interaction, such as Fe/AC(4) and Co/ZrO_2(5), opposite results were obtained. Selectivity of long-chain hydrocarbons increases with the decreasing of metal crystal size. To this kind of catalyst,minimization of particle size leads to stronger metal-support interaction.Then metal support synergism plays more important role to affect FTS activity and selectivity than metal crystal size of catalyst does. Consequently,preparation of modified ultrafine FTS catalyst with metal support interaction is a promising path to synthesis long chain hydrocarbons with high activity and selectivity.

Sol-gel method is a traditional way to produce ultrafine oxides. Previously,ultrafine SiO_2 aerogel powder was prepared by sol-gel method followed by supercritical fluid drying technique.The SiO_2 aerogel powder obtined was then coated with ZrO_2 to form ZrO_2-SiO_2 complex oxide.Cobalt catalyst supported on this complex oxide is in the category of nano material,its particle size is about 9.0nm.Under moderate pressure and in a fixed bed reactor,this catalyst was proved to be an extremely suitable catalyst for synthesis of long chain hydrocarbons,C^{5+} yield could reach 150g per cubic meter of syngas(6).

Promotion effect of manganese on iron F-T catalyst was studied extensively. The promotion effect was attributed to alkali and structure promotion. One of the characteristics of alkali promotion is to improve the selectivity of long chain hydrocarbons. Consequently, promotion effect of manganese to ultrafine Co/ZrO_2-SiO_2 catalyst on the properties of

structure,texture,reduction and F-T synthesis is investgated in this paper.

EXPERIMENTAL

Catalyst preparation

Ultrafine silica aerogel was prepared by sol-gel method using TEOS as the precusor followed by supercritical fluid drying of the gels in an autoclave.The obtained monoliths were calcinated at 623K for 8hr and crushed. Zirconia coated ultrafine silica support was prepared by coating the ultrafine silica aerogel powder with solution of zirconium nitrate in a rotary evaporator.Dried sample was then calcinated at 673K in air.Preparation of cobalt catalysts was completed using incipient wetness technique with cobalt nitrate as impregnation solutions. Manganese promoted catalysts were prepared using a mixed solution of cobalt nitrate and manganese acetate as the impregnation solutions.Catalysts so obtained were then dried and calcinated before being pellesized and sieved.

Characterization

Cobalt loading of these catalysts were examined by ICP. BET surface areas and the distribution of pore volumes were measured by Micromeritics ASAP 2000 physical adsorption unit. XRD analysis were performed on a Rigaku diffractometer. X-ray photoelectron spectra were recorded with a Perkin-Elmer PHI 1600 ESCA system equiped with Al Kα X-ray excitation source and hemispherical electro analyzer. TPR tests were performed in a U-shape reaction tube with a catalyst loading of 0.2g, Ar purge temperature of 473K,temperature raising rate of 10 K/min, the carrier gas was H_2/Ar(H_2 8.6V%) and the detector was TCD. TPD tests were processed after adsorption of H_2 over catalysts reduced at 673K and cooled in ambient temperature.

Reaction tests

The catalyst precursors (5g) were loaded into fixed bed laboratory reactors and reduced in situ at 673K under hydrogen. Synthesis gas (CO/H_2=1:2) was subsequently fed over the catalysts and the system was kept at steady state before mass balance data were collected. Liquid and solid condensates were collected in two seperate condensers. Product analysis for gas,liquid and solid products were all performed by GC using various columns.

RESULTS AND DISCUSSION

Texture property of Co-Mn/ZrO_2-SiO_2 catalysts

Table 1 illustrates the effect of Mn loading on texture property of Co-Mn/ZrO_2-SiO_2 catalysts. The results indicate that comparing with Co/ZrO_2-SiO_2 catalyst, the addition of manganese decreases the surface area and pore volume of Co-Mn/ZrO_2-SiO_2 catalyst and the change of average pore diameter is slight. The surface area and pore volume of three Co-Mn/ZrO_2-SiO_2 catalysts decrease with an increase of manganese loading.

Structure of Co-Mn/ZrO_2-SiO_2 catalyst

XRD spectras of Co(10.71%)-Mn(1.57%)/ZrO_2-SiO_2 catalyst before and after reaction were both recorded. We concluded that the addition of manganese increases the metal dispertion of cobalt and makes the crystal size of cobalt smaller. Furthermore,$Co_2Mn_2O_{4.5}$ spinel phase was formed after calcination of Co(10.71%)-Mn(1.57%)/ZrO_2-SiO_2 catalyst.

Surface characterization of Co-Mn/ZrO_2-SiO_2 catalysts

Surface property of Co/ZrO_2-SiO_2 and three Co-Mn/ZrO_2-SiO_2 catalysts were studied by XPS. Binding Energy and atomic ratio of the catalysts are listed in Table 2. From comparision of results of surface and bulk atomic ratio, it is evident that beneficiation of manganese at catalysts surface is significant. On the other hand,both $Co2p_{3/2}$ and $Mn2p_{3/2}$ have two BE values which verifies the formation of Co,Mn spinel phase.

TPR results of Co-Mn/ZrO_2-SiO_2 catalysts

Reduction property of Co-Mn/ZrO_2-SiO_2 catalyst was investigated by TPR. The results indicated that manganese promoter reacts with a part of CoO to form Co,Mn solid solution. Therefore the

reduction of CoO is hindered and the reduction degree of catalysts in 673K decreases with the increasing manganese loading.

FTS performance of Co-Mn/ZrO_2-SiO_2 catalysts

The component of a catalyst affects the FTS performace significantly. The change of FTS performance at the same reaction temperature(493K),with the increase of manganese loading, are listed in Table 3. The following conclusions could be drawn:

1) CO conversion rate decreases.
2) Olefin to paraffin ratio increases evidently and then decreases. And olefin to paraffin ratios of all Co-Mn/ZrO_2-SiO_2 catalysts are higher than that of Co/ZrO_2-SiO_2.
3) CH_4 selectivity decreases to a minimum and then increases.
4) C^{5+} selectivity increases to maximium and then decrease.
5) Wax to oil weight ratio increases to maximium and then decreases.

The results indicate that certain amount of manganese addition could increase the selectivity of longer chain hydrocarbons,while excess amount of manganese addition leads to opposite results. FTS performance of Co-Mn/ZrO_2-SiO_2 is explained as the followings:

Decrease of CO conversion rate. (1)Addition of Mn promoter dilutes and covers the Co active sites.(2)The reduction of CoO was hindered by Mn and the degree of reduction of the catalysts at 673K decreases.

Increase of olefin to paraffin ratio. (1) Manganese as a texture promoter. Addition of Mn makes cobalt crystal size get smaller.Small crystal size makes newly produced olefines leave the surface of the catalyst quickly and increase the diffusion of olefin.Therefore, the secondary hydrogenation of olefines is restrained. (2) Group effect caused by beneficial of manganese on catalyst surface.Cobalt active sites are divided into smaller groups and this kind of surface modificaton restrains the hydrogenation of catalysts effectively.(3) Manganese as an electron promoter.Addition of Mn enhances the d-π feedback of CO to Co and therefore weakens Co-H bond.

Decrease of CH_4 selectivity and increase of C^{5+} selectivity. (1) Manganese as an alkali promoter.One of the characteristic of alkali promoter in FTS catalyst is to increase the selectivity of longer-chain hydrocarbons. (2) Group effect of manganese. The formation of methane requires a relatively large distribution of active center groups.

Fig.1 is the products carbon number distribution for Co/ZrO_2-SiO_2 and Co(10.71%)-Mn(1.57%)/ZrO_2-SiO_2 catalysts.It can be seen that carbon number distribution of Co/ZrO_2-SiO_2 catalyst follows Schulz-Flory distribution while that of Co-Mn/ZrO_2-SiO_2 catalyst deviates SF distribution and have two peaks instead.The maximium points are C_{11} and C_{17},respectively. Double-peaks distribution indicates the existence of two kinds of active centers. The author ascribes the active centers to be Co and Co,Mn spinel seperately.The assumption were verified by the results of Hongwei Xiang on Co-Mn/ZrO_2 catalyst and Yongqing Zhang on Co-Cr/ZrO_2-SiO_2 catalyst(7).

References

1.J.J.F.Scholtan,Xu Xiaoding,C.B.Von Der Decken, Intertational Journal of Energy Research,1994,18,P185-P198.
2.Liu Fu and Calvin Bartholomew,Journal of Catalysis,1985,92, P36-P387.
3.Iglesia E.,Reyes S.C.,Madon R.J.,Journal of Catalysis, 1991,129,P238.
4.Shen Jianyi,Zhang Su and Lin Liwu,Journal of Fuel Chemistry (China), 1989,17,P193
5.Xiang Hongwei,PhD Dissertation,Institute of Coal Chemistry, Chinese Academy of Sciences,1995.
6.Zhang Yongqing, Zhong Bing and Wang Qin,Proceedings of Fifth China-Japan Symposium on Coal and C1 Chemistry, Huangshan,China, 1996,P425.
7.Zhang Yongqing,Zhong Bing and Wang Qin,to be published.

Table 1 Texture property of oxidation state $Co-Mn/ZrO_2-SiO_2$ catalysts

Catalysts	Co/Mn Atomic ratio	S_{BET} area (m^2/g)	V_{PN} (cm^3/g)	r_p (nm)
$Co(10.73\%)/ZrO_2-SiO_2$		421.8	0.53	5.0
$Co(10.71\%)-Mn(1.57\%)/ZrO_2-SiO_2$	6.82	378.9	0.51	5.0
$Co(11.58\%)-Mn(3.28\%)/ZrO_2-SiO_2$	3.53	359.9	0.45	5.0
$Co(11.09\%)-Mn(4.36\%)/ZrO_2-SiO_2$	2.54	350.5	0.40	4.6

Table 2 Binding Energy and atomic ratio of $Co-Mn/ZrO_2-SiO_2$ catalysts

Catalysts	Binding Energy (eV)				Co/Mn atomic ratio	
	$Co2p_{3/2}$	percent	$Mn2p_{3/2}$	percent	bulk	surface
$Co(10.73\%)/ZrO_2-SiO_2$	777.91	37.87				
	780.74	62.13				
$Co(11.58\%)-Mn(3.28\%)/ZrO_2-SiO_2$	777.95	41.68	641.58	81.88	3.53	2.30
	780.57	58.32	645.40	18.12		
$Co(10.71\%)-Mn(1.57\%)/ZrO_2-SiO_2$	779.05	72.75	641.09	86.78	6.82	4.17
	781.46	27.25	644.93	13.22		

Table 3. FTS performance of catalysts

Catal.No.	CO conv. (%)	HC.distri.(wt%) C_1	HC.distri.(wt%) C^{5+}	O/P[a]ratio	Yield[g/Nm^3(CO+H_2)] C^{1+}	Yield[g/Nm^3(CO+H_2)] C^{5+}	Wax/Oil (wt)
1	96.38	13.66	81.09	0.092	186.60	151.30	0.81
2	92.31	9.08	87.16	0.15	177.69	154.89	0.91
3	89.80	13.66	79.14	0.41	184.58	146.08	1.57
4	82.81	27.52	57.40	0.21	113.97	65.51	0.21

Reaction conditions: $H_2/CO=2$, P=2.0MPa, T=473K, GHSV=500h^{-1}

a: olefin to paraffin ratio.

No.1: $Co(10.73\%)/ZrO_2-SiO_2$ No.2: $Co(10.71\%)-Mn(1.57\%)/ZrO_2-SiO_2$

No.3: $Co(11.58\%)-Mn(3.28\%)/ZrO_2-SiO_2$ No.4: $Co(11.09\%)-Mn(4.36\%)/ZrO_2-SiO_2$

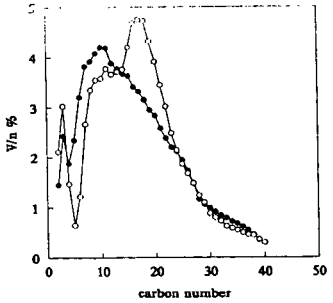

Fig 1. Carbon number distribution of products over (a): Co/ZrO_2-SiO_2 and (b): $Co-Mn/ZrO_2-SiO_2$

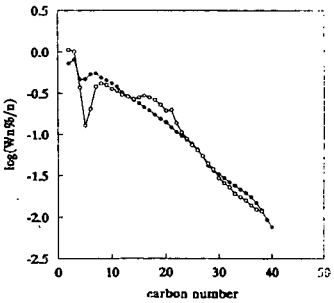

Fig 2. Schulz-Flory distribution of products over (a): Co/ZrO_2-SiO_2 and (b): $Co-Mn/ZrO_2-SiO_2$

FUNDAMENTALS OF CATALYSIS

M.K. Carter
Carter Technologies
P.O. Box 1852
Los Gatos, CA 95031

Keywords: theory of catalysis, transition probability, allowed catalysts

I. Background

Catalysis has been conducted for many years yet no fundamental understanding has emerged which teaches how to design a catalyst at a molecular level. Linus Pauling[1] stated, "It is thought that catalysts speed up reactions by bringing the molecules reacting together and holding them in configurations favorable to reaction." This definition offers a picture of what is to be achieved but does not suggest a mechanism of how catalysis might be accomplished. An alternative definition is proposed: *catalysis is a barrier free transformation from one electronic configuration to another*. This definition is presented as a starting point for a more formal development toward a goal of catalyst design at a molecular level. A true catalyst provides an orbital pathway for reactants to proceed to products such that the thermodynamic change in free energy for the reaction is negative. Thus, the act of catalysis will be treated as a radiationless stimulated emission - a natural transition from one electronic state to another.

II. Geometry

Consider the geometry of a set of atoms which compose a catalyst. Let r be the wave function of the reactant and let p be the wave function of the product. Catalytic conversion of a reactant to a product may be represented by a unitary transformation of r to p as $Ur = p$ so both the length of the vector and the symmetry of the wave function are preserved. This same unitary matrix transforms the wave function of the catalyst c such that $Uc = c$ since a catalyst returns to its original state following conversion of a reactant to a product. The column vectors of the unitary operator U were determined by expansion of the general form of a three by three unitary matrix to find the eigenvalues of $UU^{\dagger} = E$ so the value of the special function, c, could be calculated. The result is presented in figure 1 which shows the only geometric form allowed for a catalyst under such a unitary transformation is a one dimensional or linear geometric configuration. In this case its linear in the x-direction, but this axis is not unique. For example, catalysts represented by Y-M-Y for which M is a transition metal and Y is any appropriate electronegative atom, such as Cl-Mn-Cl or Co-Fe-Co, are described as being in linear geometric configurations. Should the molecule Y-M-Y be inherently non-linear, it may still exhibit catalytic activity during that fraction of time its bending vibration carries it through a linear configuration.

III. Symmetry Requirements

The symmetry of the reactant(s) associated with a catalyst is best described as belonging to a specific symmetry group. For example, carbon monoxide associated with a M_1-M_2-M_1 catalytic backbone, as required for Fischer-Tropsch catalytic conversion of CO/H_2 to hydrocarbons, may be represented as shown in figure 2. The two C-O molecules associated to the catalyst M_1-M_2-M_1 form a group described by the E, C_2, i, S_2', S_2'' and σ_h classes of symmetry operations. These six operations form a special D_{2s} symmetry group as shown in the character table of figure 3. During the instant of catalysis an initial chemical transformation is caused by the shifting of electrons from the catalyst, figure 2A, to form metal-carbon and metal-oxygen sigma bonds, figure 2B. These geometrical configurations represent the individual functions of the degenerate basis E1. One of the two-fold degenerate wave functions represents bonding configuration A while the other describes bonding configuration B. The transformation from one degenerate level to the other may be described as a barrier free electron shift. From the form of the mutually degenerate representations $\Gamma(E_{1A})$ and $\Gamma(E_{1B})$ different cooperative electron bonding may be inferred. Thus, $\Psi_+ = (\Psi_{E1A}+\Psi_{E1B}) = 2\varphi_1-\varphi_2-\varphi_3-2\varphi_4+\varphi_5+\varphi_6$ results from the sum and $\Psi_- = (\Psi_{E1A}-\Psi_{E1B}) = -\varphi_2+\varphi_3+\varphi_5-\varphi_6$ results from the difference of the doubly degenerate functions. The relative sign patterns are shown for both the sum and difference molecular functions in figures 2C and 2D. The sign of the wave function at carbon atoms 2 and 5 remains unchanged from Ψ_+ to Ψ_-. These atoms

represent expectations of the active catalytic sites. Since no change of sign is evident, then catalysis may proceed under the barrier free condition.

The symmetry of a propene-catalyst association also belongs to the special D_{2s} symmetry group. Propene associated with the catalytic site M_2, refer to figure 4, may be represented where only one critical hydrogen atom is shown. Here the sign of the wave function on atoms 1 and 4 remains unchanged from Ψ_+ to Ψ_-. Thus, group symmetry considerations represent these two atoms as the expected catalytically activated sites. Experimental evidence shows the great majority of products formed during Ziegler-Natta catalysis do bond head-to-tail while the mechanism shows a tail-to-tail bond formation. This suggests a methylide and hydride exchange during an intermediate step to affect the apparent final head-to-tail bonded product.

IV. Transition Probability

A measure of the efficiency of catalysis may be determined by its transition probability, just as the intensity of a spectral line may be determined by its transition probability from one state to another allowed state. Such an electronic transition occurring between the product and reactant states Ψ_p and Ψ_r may be expressed by a quantum mechanical probability $|m_\mu|^2$ for which the transition moment m_μ is given by the expression

$$m_\mu = \int \Psi_p^* \mu \Psi_r d\tau$$

where μ is the amplitude of the induced electric moment. Einstein's transition probabilities[5] are seen to be wholly applicable for describing the electronic transition of molecular catalysis. Computation of the transition moment can be conducted specifically by using the set of wave functions which represent a metal-carbon monoxide complex as expressed previously, namely

$$\begin{aligned}\Phi &= \Phi_a + \Phi_b + \Phi_c + \Phi_d \\ &= (1/N_2)[1/6\varphi^{Fe}{}_{4s}+(2)^{1/2}/8\varphi^{Fe}{}_{3dxz}+(2)^{1/2}/8\varphi^{Fe}{}_{3dyz}+1/8\varphi^{Fe}{}_{3dz2}+\varphi^{O1}{}_{2py}+\varphi^{O1}{}_{2pz}]_a \\ &\quad + (1/N_2)[1/6\varphi^{Fe}{}_{4s}-(2)^{1/2}/8\varphi^{Fe}{}_{3dxz}+(2)^{1/2}/8\varphi^{Fe}{}_{3dyz}-1/8\varphi^{Fe}{}_{3dz2}+\varphi^{C1}{}_{2py}+\varphi^{C1}{}_{2pz}]_b \\ &\quad + (1/N_2)[1/6\varphi^{Fe}{}_{4s}-(2)^{1/2}/8\varphi^{Fe}{}_{3dxz}-(2)^{1/2}/8\varphi^{Fe}{}_{3dyz}+1/8\varphi^{Fe}{}_{3dz2}-\varphi^{O2}{}_{2py}+\varphi^{O2}{}_{2pz}]_c \\ &\quad + (1/N_2)[1/6\varphi^{Fe}{}_{4s}+(2)^{1/2}/8\varphi^{Fe}{}_{3dxz}-(2)^{1/2}/8\varphi^{Fe}{}_{3dyz}-1/8\varphi^{Fe}{}_{3dz2}-\varphi^{C2}{}_{2py}+\varphi^{C2}{}_{2pz}]_d\end{aligned}$$

for which the normalization constant is $N_2 = (349)^{1/2}/6$. Here all of the valance orbital functions have been given specifically and each of the four quadrants of the molecular association for the complex have been enclosed in brackets for purposes of organization. The transition moment can be computed, one quadrant at a time, replacing μ by its operator r using the system wave functions Φ as

$$m_\mu{}^a = \int \Phi_a^* r \Phi_a d\tau$$

$$= \int_0^\infty \int_0^\pi \int_0^{2\pi} \Phi_a^* r \Phi_a r^2 \sin\theta \, d\varphi \, d\theta \, dr$$

Orthonormalized hydrogen-like one electron wave functions[2] were used and each of the four quadrant contributions to the transition moment was computed separately. The results by quadrant are

$$m_\mu = m_\mu{}^a + m_\mu{}^b + m_\mu{}^c + m_\mu{}^d = 0.2092110+0.2603221+0.2092110+0.2603221$$

$$\text{or } m_\mu = 0.9390517.$$

The value of the transition moment approaches unity supporting the requirement for a catalyst of linear geometric configuration constrained by a special D_{2s} symmetry group. Such strong transitions are not to be construed as oxidations or reductions since the time of a catalytically stimulated transition is expected to be less than the time of a molecular vibration ($< 10^{-14}$ second) following which the shifted electrons return to the original electronic configuration leaving new products in place of the reactants.

V. Catalyst Stabilization Against Permanent Oxidation

The external atoms M_1- and -M_3 in the linear catalyst cluster M_1-M_2-M_3 are present to stabilize the oxidation state of the catalytic site -M_2-. These groups possess the same or greater electronegativity[3] as -M_2- and represent the only allowed condition for catalysts. This effect is described by positioning local dipoles along the bonds pointing toward the external atoms.

A set of allowed bimetal and centrally symmetric trimetal linear catalysts formed from first row transition metal series elements is presented in figure 5. Similar sets of linear strings of symmetry allowed catalysts can be formed from the second and third row transition metal series. Noncentrally symmetric catalysts, such as Fe-Mn-Cu and interseries catalysts, are also possible provided they conform to the requirements of the theory.

Different oxidation states are required for various types of catalysis. For example, Fischer-Tropsch conversions can be accommodated by strings of zero valent metals such as Fe-Fe and Fe-Fe-Fe while Ziegler-Natta reactions seem to require higher oxidation states such as the Ti^{3+}-Ti^{3+} and Ti^{3+}-Ti^{3+}-Ti^{3+} strings.

VI. Ab Initio Computation of the Energy of a Carbon Monoxide-Catalyst Complex

Strength of the bond between the associated reactant and the active site of the catalyst was considered for the case of a carbon monoxide pi-bonded to the iron atom. A three atom model was developed in which the associated carbon monoxide was positioned symmetrically with the iron atom. Bond distances of 1.830 Angstroms for the iron to carbon and iron to oxygen bonds, and 1.210 Angstroms for the carbon to oxygen bond were assigned. Molecular bond energies were computed using the Hartree-Fock formalism for an eighteen electron spin function for a closed-shell system[4]. The symmetry determined molecular wave function is the best representation for carbon monoxide pi-bonded to the iron atom. It was derived from the same symmetry determined valence electron function employed for the transition moment computation. A single cycle bonding energy of 2.5152 eV (58 kcal/mol) was computed for the complex. The energy level was doubly degenerate as anticipated by the symmetry requirement.

VII. Recent Applications

Generation of a theoretical model based on these ideas forms the basis for identification of specific molecular catalysts for selected chemical reactions through computational methods. Several catalysts have been prepared in the laboratory, based on this work, for use in Fischer-Tropsch conversions, ambient temperature oxidation of gasoline and diesel fuel in water, and other reactions. The Fischer-Tropsch catalyst Co-Fe-Co was responsible for formation of liquid hydrocarbons directly in the C_8 to C_{22} range. GC-MS and FTIR molecular spectra show the products to be linear aliphatic hydrocarbons, refer to figures 6. Approximately half a dozen Cu-Fe and Fe-Fe based oxidation catalysts of the form $Fe(CN)_2L_3$-$FeCl_2L_3$, for L being $K_2Cu(CN)_3$ and related ligands, were prepared for destruction of 20 ppm gasoline and 100 ppm diesel fuel in water in approximately 15 minutes. Refer to figure 7.

VIII. Conclusion

Recognition of a reasonable starting point in the form of a definition of catalysis, namely that *catalysis is a barrier free transformation from one electronic configuration to another*, has became a basis from which the fundamentals of catalysis have been developed. Application of these fundamentals has produced oxidation, Fischer-Tropsch and other catalysts which generated products at good rates at room temperature without prior thermal conditioning. It is hoped that this work will add to the existing body of catalysis knowledge and give industry new opportunities for development, and expanded growth in the future.

References

1. L. Pauling, *General Chemistry*, W.H. Freeman & Company, San Francisco, **1959**, 2nd ed., p115.
2. L. Pauling and E.B. Wilson, *Introduction to Quantum Mechanics*, McGraw-Hill Book Co., New York, **1935**, p 302.
3. L. Pauling, *J.Am.Chem.Soc.* **1932**, 54, 3570.
4. W.J. Hehre, L Radom, P.v.R. Schleyer and J.A. Pople, *Ab Initio Molecular Orbital Theory*, pub. John Wiley & Sons, New York, **1986**, p21.

$$Uc = \begin{vmatrix} 1 & 0 & 0 \\ 0 & 1 & 0 \\ 0 & 0 & -1 \end{vmatrix} \quad \begin{vmatrix} 1 \\ 0 \\ 0 \end{vmatrix}$$

Figure 1. Geometric Vector For A Catalyst

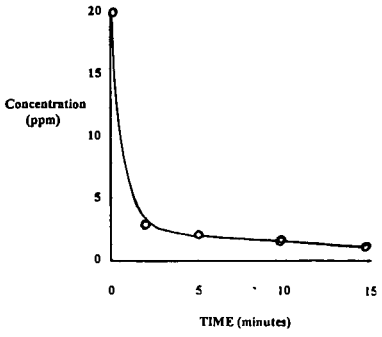

Figure 7. Oxidative Destruction Of Gasoline

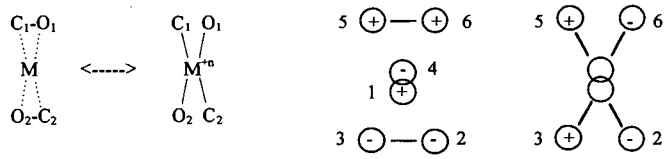

Figure 2. Degenerate Bonding Functions And Signs For Carbon Monoxide On A Catalyst

D_{2s}	E	C_2	i	S_2'	S_2''	σ_h		
A	1	1	1	1	1	1	z, R_z	$\alpha_{x2}+\alpha_{y2}$, α_{z2}
B	1	1	1	-1	-1	-1		
E_1	2	-1	-1	-2	1	1	(x, y) (Rx,Ry)	α_{xz}, α_{yz}
E_2	2	-1	-1	2	-1	-1		$\alpha_{x2}-\alpha_{y2}$, α_{xy}
Γ(sum)	6	0	0	0	0	0		
$\Gamma(\alpha)=\Gamma(A)x\Gamma(E_1)$	2	-1	-1	-2	1	1	$=\Gamma(E_1)$	

The direct product of irreducible representations describing the polarizibility matrix, α, is $\Gamma(A) \times \Gamma(E_1) = \Gamma(E_1)$ which is also irreducible.

Figure 3. Character Table For Special D_{2s} Symmetry Group

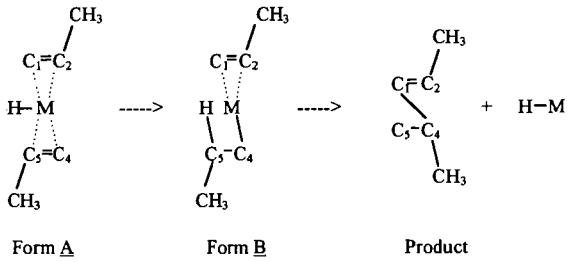

Figure 4. Barrier Free Symmetry Selected Bonding For Ethylene Dimerization

Ti-Ti	Mn-Ti	Co-Cr	Ni-Ti	Ni-Cu-Ni	Ni-Fe-Ni	V-Cr-V	Ni-V-Ni
V-V	Fe-Fe	Co-V	Cu-Cu	Cu-Cu-Cu	Cu-Fe-Cu	Cr-Cr-Cr	Cu-V-Cu
V-Ti	Fe-Mn	Co-Ti	Cu-Ni	Co-Ni-Co	Ti-Mn-Ti	Fe-Cr-Fe	Ti-Ti-Ti
Cr-Cr	Fe-Cr	Ni-Ni	Cu-Co	Ni-Ni-Ni	V-Mn-V	Co-Cr-Co	V-Ti-V
Cr-V	Fe-V	Ni-Co	Cu-Fe	Cu-Ni-Cu	Cr-Mn-Cr	Ni-Cr-Ni	Cr-Ti-Cr
Cr-Ti	Fe-Ti	Ni-Fe	Cu-Mn	Co-Co-Co	Mn-Mn-Mn	Cu-Cr-Cu	Mn-Ti-Mn
Mn-Mn	Co-Co	Ni-Mn	Cu-Cr	Ni-Co-Ni	Fe-Mn-Fe	V-V-V	Fe-Ti-Fe
Mn-Cr	Co-Fe	Ni-Cr	Cu-V	Cu-Co-Cu	Co-Mn-Co	Cr-V-Cr	Co-Ti-Co
Mn-V	Co-Mn	Ni-V	Cu-Ti	Fe-Fe-Fe	Ni-Mn-Ni	Fe-V-Fe	Ni-Ti-Ni
			Co-Cu-Co	Co-Fe-Co	Cu-Mn-Cu	Co-V-Co	Cu-Ti-Cu

Figure 5. Allowed Bi and Symmetric Trimetal First Row Transition Metal Linear Catalysts

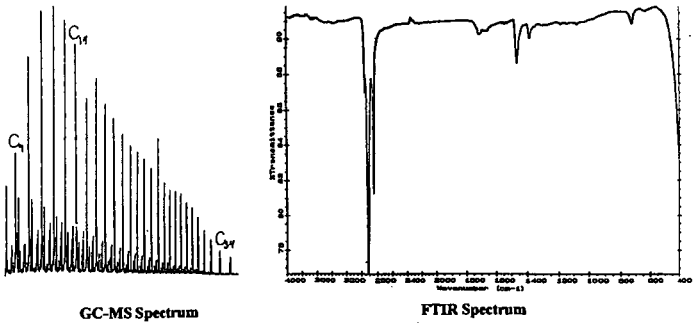

Figure 6. GC-MS And FTIR Molecular Spectra Of Fischer-Tropsch Aliphatic Hydrocarbons

SHELL MIDDLE DISTILLATE SYNTHESIS: FISCHER-TROPSCH CATALYSIS IN NATURAL GAS CONVERSION TO HIGH QUALITY PRODUCTS

J. Ansorge
Shell International Oil Products B.V.
Badhuisweg 3
1031 CM Amsterdam

Keywords : Natural Gas Conversion, Fischer-Tropsch Synthesis, Paraffins

1. INTRODUCTION

The importance of natural gas as a source of energy has increased substantially in recent years and is expected to continue to increase. In the recent past many new gas fields were discovered around the world, leading to a large increase in the proven world gas reserves. Proven world gas reserves are now approaching those of oil and, on the basis of the current reserves situation and relative depletion rates, natural gas seems to be set to outlast oil.

The main drawback of natural gas remains its low energy density, which makes its transportation to the point of use expensive and which may even prohibit its exploration and production. Shell and others have therefore been looking at processes that chemically convert natural gas into liquid hydrocarbons. Critical for the viability of each project is the value of its products. The chemical products like ammonia, urea and methanol have shown a high price volatility in the market with a relatively low entry barrier. Production of top quality middle distillate fuels from gas is favoured by recent developments in fuel quality requirements, the ease of transport and distribution of the products, and the enormous market for the products. The middle distillates from SMDS will therefore be well positioned in the market place of quality transportation fuels.

It has been realised that there are many places in the world where gas is available, without a ready market and where, as a consequence, it would have a much lower intrinsic value compared with transportation fuels. It is this difference in value that would drive a synthetic fuel project and provide opportunities for both government and private enterprises.

The present scene in the field of oil and transportation fuels and the prospects for the near and medium term however, call for a careful and selective approach to any synfuel development. At low fuel oil prices almost no alternative energy technology can compete with existing refining. On the other hand, the crises of the early seventies and early eighties provided important lessons: emergencies come at relatively short notice, and, because of the lead times usually involved in technological development, in a crisis the answers to problems always come too late.

Next to the synthetic hydrocarbon transportation fuels, a similar role could be perceived for methanol. However, use of methanol as a transport fuel has considerable drawbacks. These include the required modifications to fuel distribution systems and to the car / engine fuel system. Synthetic hydrocarbons, on the other hand, have the advantage that they can be readily incorporated into existing fuels which can be used in today equipment. In addition, middle distillates manufactured from natural gas have very environmentally friendly properties, upon which we will elaborate in this paper. The cleanliness of natural gas is, as it were, transferred into its products. The middle distillates from SMDS will therefore be extremely well positioned in a market place with an ever increasing quality demand. Natural gas conversion has become an asset for Shell with the construction and successful operation of the first commercial natural gas to transportation fuels conversion plant , SMDS(M) Bintulu.

2. THE PROCESS

The SMDS process combines conventional and well proven technologies with advanced technology using newly developed heterogeneous catalysts.
The overall process starts with the conversion of natural gas into synthesis gas, for which there are several commercial processes available. For the production of predominantly saturated hydrocarbons, -CH2- , the syngas components H2 and CO, are consumed in a molar ratio of about 2: 1, so a production in about that ratio is desirable. This influences the choice of process, as will be explained below.

The next step of the process, the hydrocarbon synthesis, is, in fact, a modernised version of the classical Fischer-Tropsch (FT) process, with the emphasis on high yields of useful products.

The Fischer-Tropsch process developed by Shell for SMDS favours the production of long chain waxy molecules which, as such, are unsuitable for transportation fuels. The hydrocarbon synthesis step is therefore followed by a combined hydro-isomerisation and hydrocracking step to produce the desired, lighter products. By opting for the production of waxy molecules in the Fischer-Tropsch step, the amount of unwanted smaller hydrocarbons or gaseous products, produced as by-products, is substantially reduced. This means that the process, simply spoken, does not make 'gas' out of gas. Combined with the high selectivity towards middle distillates in the hydrocracking step the overall process shows a high total yield of product in the desired range.

In the final stage of the process, the products, mainly kerosene, gasoil and naphthas, are separated by distillation. By the right operating conditions in the hydrocracking step and the subsequent distillation the product slate can be shifted towards a maximum kerosene mode or towards a maximum gasoil mode depending on market circumstances.

2.1. Synthesis Gas Manufacture

For the production of synthesis gas in principle two technologies are available, viz., steam reforming and partial oxidation.

Steam Reforming (SMR)

Starting from pure methane, SMR is the most commonly used conversion process for natural gas into synthesis gas, and could theoretically produce a synthesis gas with an H2/CO ratio of about 3. This process has the advantage that it doesn't require an air separation unit for the production of pure oxygen.

For the Fischer-Tropsch process SMR turns out to be less suited since the high H2/CO ratio is a disadvantage for a reaction which is highly exothermic and obeys first order kinetics in hydrogen partial pressure. Two other disadvantages are the large size of the reformer furnace which limits the scale-up potential of this synthesis gas technology and the limitation in pressure of about 30 bar, while the Fischer-Tropsch reaction is preferably carried out at somewhat higher pressures.

On the other hand SMR technology might be favourable for small scale Fischer-Tropsch applications and for feed gases having a high content in CO_2.

Partial Oxidation

A synthesis gas with a H2/CO ratio of about 2, can theoretically be produced by partial oxidation of methane with oxygen. Without much correction such gas is suitable for the production of middle distillates. The oxygen source can be air, or pure oxygen or anything in between. The final selection depends on a number of factors and can be different from project to project. However, generally, economics favour the application of pure oxygen.

For this type of partial oxidation several processes exist amongst which Shell's own Shell Gasification Process (SGP) which has been applied for several decades for the gasification of residual oils and has been chosen for the SMDS plant in Malaysia as the most appropriate synthesis gas manufacturing process.

For the catalytic Fischer-Tropsch synthesis, the synthesis gas must be completely free of sulphur. For this requirement all sulphur components are removed upstream of the partial oxidation step. A number of well-known treating processes are available the application of which is mainly guided by the type and concentration of the sulphur components in the natural gas.

2.2. The Hydrocarbon Synthesis Step

In the Heavy Paraffin Synthesis (HPS) step, the synthesis gas is converted into long chain, heavy paraffins. The paraffinic hydrocarbons produced via the FT reaction are highly linear. The formation of the linear paraffinic molecules can be described with the Anderson Flory Schultz [AFS] distribution model. Relation between model, design, product slate, catalyst and plant operation and economics will briefly be discussed.

During the catalysed reaction of synthesis gas to the primary paraffinic product an appreciable amount of heat is released. For the classical catalyst system this requires a considerable control of the temperature in view of the following constraints:

- The temperature window of stable operation is rather small
- A high space-time yield demands a high temperature
- At only moderately higher temperature a side reaction leading to methane formation becomes more dominant, reducing selectivity and, eventually, stability.

Because of these shortcomings, Shell has developed a new and proprietary catalyst system which establishes substantial improvements in all these areas. Its robustness allows the use of a multitubular fixed bed reactor system at a temperature level where heat recovery, via production of medium pressure steam, leads to an efficient energy recovery. The catalyst self can be regenerated in situ whereby the cycle time depends on a number of factors like process conditions, changes in feedgas composition and production planning.

2.3. Heavy Paraffin Conversion (HPC)

One of the prerequisites for obtaining a high selectivity towards n-middle distillates is a sufficiently high average molecular weight of the raw product. This product, which is predominantly waxy but contains small amounts of olefins and oxygenates, has to be hydrogenated to remove the olefins and oxygenates, has to be hydrocracked into the right molecule lengths for kerosene and gasoil and has to be isomerised to improve the cold flow properties. A commercial Shell catalyst is used in a trickle-flow reactor under rather mild conditions of pressure and temperature. The HPC product is subsequently fractionated in a conventional distillation section. The product fraction which is still boiling above the gas oil range is recycled to the HPC section. By varying the process severity or the conversion per pass one can influence the selectivity towards a preferred product. Hence one may opt for a kerosene mode of operation yielding some 50% kerosene on total liquid product or for a gas oil mode of operation producing up to 60% gas oil.

The principle of combining the length-independent chain growth process (in the HPS) with a selective, chainlength dependent conversion process has been applied to selectively produce middle distillates from synthesis gas. The two stage approach creates flexibility for differentiated product slates since the primary Fischer-Tropsch liquid product can be converted into different product distributions by adjusting the cracking severity in the heavy paraffin conversion step.

For the SMDS Bintulu project, the technology was extended to include the production of specially chemicals. This addition was required to support the economy of a relatively small pioneer project. It takes advantage of the high quality of all the products respectively intermediate streams produced. Linear paraffins of varying length are isolated as solvents, detergent feed stocks and waxes. Isomerised molecules boiling below the gasoil range are worked up into lube oils. Their product properties are discussed below in some more detail. Figure 1 depicts a block diagram of the SMDS Bintulu complex.

3. THE PLANT

The first commercial SMDS plant is located in Bintulu, Malaysia. At this place, in the state of Sarawak, sufficient remote natural gas is available for conversion. About 100 MMSCFD are converted into liquid products whereas a much larger amount is liquefied in the Malaysia LNG plant. As an advanced gas conversion technology, SMDS technology is of great interest for Malaysia with its significant gas reserves. A joint venture were formed by Petronas, Sarawak State, Mitsubishi and Shell. The project was developed by Shell Internationale Petroleum Maatschappij (SIPM today SIOP), constructed by Japan Gasoline Corporation (JGC) and is operated by Shell.

A short history of construction, commissioning and start-up including some useful lessons learnt when bringing new technology into life on an industrial scale will be presented during the presentation.

Plant throughput, availability of the complex and reliability of the process units increased over the last three years. It forms a tremendous source of experience and know-how and represents a valuable basis when entering into the next generation SMDS plants.

4. THE PRODUCTS AND THEIR MARKETS

The Fischer-Tropsch synthesis for transportation fuels has the great disadvantage that first the hydrocarbonaceous feedstock has to be gasified and converted into synthesis gas before the route to the transportation fuels can be taken. On the other hand, it turns into an advantage since the target products are built from their molecular building blocks H2 and CO. As described above, after having converted olefins and oxygenates into paraffins separation into valuable products and further conversion / isomerisation into clean transportation fuels can start. Studies and experimental programmes were undertaken to identify and develop the unique SMDS products. The marketing of these products was and is a challenge, but creates simultaneously many opportunities, for example, legislation related to improvement of air quality. To be able to comply with the regulations, components of the purity provided by SMDS products are welcome and very well accepted in the market place.

In fact, SMDS products are extremely clean. They contain no sulphur, no nitrogen and aromatics at the limit of detection. The SMDS products have impurities that are several orders of magnitude lower than highly refined crude oil derived products. Hence, several normal 'oil impurities' are not detectable by the standard methods. Below some typical properties for the product groups as indicated in Figure 1 are briefly discussed.

4.1. Middle Distillates

Naphtha

The naphtha or C5-C8 fraction from SMDS is highly paraffinic. These paraffins are known to have a rather bad combustion behaviour (expressed in a low octane number), When isomerised (predominantly one methyl branch) the front end components can be used in the automotive gasoline pool whereas the heavier molecules (C7, C8) need further upgrading for the gasoline market. This will become important for future SMDS plants since applications as described below can only absorb a limited amount of these products. However, the transportation fuel market is immense, spread all over the world and expanding in some important areas. Actually, the consumption of gasoline is estimated to about 600 million metric tonnes per year and that of gasoil (diesel) to about 370 million metric tonnes per year.

Besides blending SMDS into the gasoline pool it can be used as chemical feed stock for petrochemicals. Its paraffinic nature makes it an ideal cracker feed stock for ethylene manufacture. The paraffinic nature and the purity of the SMDS naphtha results in about 10 percent higher conventional ethylene yields compared to petroleum-derived naphtha feed stock. Expectations have been met when processing SMDS naphtha on large scale in industrial steam crackers, e.g. in Singapore.

The ethylene world market presents about 70 million metric tonnes per annum and is expected to grow with a rate of about 5 % per year in the next 5 to 10 years. The market share of East Asia is estimated to represent about 15 % of the world-wide market by the year 2000. This would represent a doubling of the demand in a relatively short period of time and present opportunities for SMDS naphtha despite the fact that new capacity is planned respectively under construction.

Kerosene

Today, around 90 % of jet-fuel demand is for civil aviation and the remainder for the military sector. In 1992 the world demand for jet fuel was over 125 million tpa. North America accounted for slightly more than half of this, mainly as result of its important domestic aviation market. Outside North America and CIS, civil aviation jet fuel demand has risen between 1982 and 1992 from about 40 million tons to more than 60 million tons. Future growth is predicted at ca 4.5 % per annum. SMDS kerosene can be used to upgrade kerosene fractions having low smoke point and high aromatics, which would otherwise be unsuitable for use in jet fuel.

For the first SMDS plant in Bintulu the produced kerosene is too small to play a significant role in the regional kerosene market. However, a fraction boiling in the kerosene range can be tailored to an iso-paraffinic solvent of high purity. It has a low odour and water-clear appearance and is particularly attractive in applications as printing ink, cosmetics, dry cleaning etc. It is marketed under the tradename SMDS SARASOL 150/200 and some typical properties important for this application are summarised in table 4.

Gasoil/Diesel

Some properties indicating that the SMDS gasoil, too, is of exceptional quality are shown in table 1. Given this quality, the SMDS gasoil is an ideal blending component for upgrading of lower-quality gasoils which don't meet for example the cetane specifications. Alternatively, the SMDS gasoil could enter in a market where premium specifications are valued to meet local requirements. For example, the Californian Air Resources Board (CARB) requires commercial fuels to give lower emissions than a reference fuel, which has a minimum cetane number, low sulphur and aromatics. More details on the environmental impact of SMDS gasoil are described below.

Additionally, SMDS fuels are suitable for special applications, like. high quality lamp oils and e.g. underground truck fuel (in mining), provided that precautions are taken to mitigate the effects of low lubricity and low density. The gasoil has excellent combustion properties, as the typical product data, given in table 3 and compared with important standards, show.

Waxy Raffinate (Base Oils)

The hydrocracker (HPC) in which the linear paraffins are cracked and isomerised to prepare the right boiling range of the middle distillates operates at relatively mild severity. After having distilled the middle distillates a bottom stream remains which is recycled to the hydrocracker. This stream contains a fraction called waxy raffinate which upon solvent dewaxing leads to a stream which combines extremely high viscosity index with very low Noack volatility and forms the main part of a range of wholly synthetic top-tier lubricating oils. These base oils are fit to fulfil ever increasing quality demands like less oil consumption, ability to at higher temperatures and for longer periods, keep modern engines in a better shape.

SMDS Bintulu (Malaysia) presently supplies Shell refineries in France and Japan where SMDS waxy raffinate is processed into finished top-tier motor oils..

4.2 Products on basis of linear paraffins

In Figure 1 it is shown schematically that not all linear paraffins are converted in the HPC into middle distillates. Part of the primary Fischer-Tropsch product which contains a certain percentage of olefins and oxygenates is hydrogenated under such operating conditions that olefins and oxygenates are converted into the corresponding linear paraffins without any isomerisation. The resulting stream of pure, linear paraffins is subsequently separated by distillation to gain access to a range of special products. These products are further characterised below.

Solvents

The C5-C10 SMDS n-paraffins fall into a class of specific solvents. They are completely free of aromatics and sulphur compounds and have a low odour. These solvents fit particularly well into the current environmental requirements since the n-paraffins show the best biodegradability results. The market represents a wide variety of different solvents of which the world-wide demand in aggregate is estimated to be 100,000 tpa. Presently, solvents in this carbon range, particularly hexane and Special Boiling Point (SBP)- types are used in oil-seed extraction, polymerisation and the rubber industry. In view of their application they need to be guaranteed low in aromatics, particularly in benzene. The SMDS solvent cut (and the naphtha fraction too) are suitable for these applications.

Detergent Feedstocks

The next distillation cuts are the C10-C13 and the C14-C18 fractions which are used in further processing steps to obtain industrial detergents and flame retardant materials. The purity of the products satisfies all the performance requirements in the production of linear alkyl benzene, chlorinated paraffins and paraffin sulphonates. The C10-C13 fraction (LDF) is used most widely in laundry applications where its higher than normal C13 content gives the improved detergency. The C14-C18 fraction (HDF) is used in making chloroparaffins of exceptional quality in terms of heat stability and colour. The biodegradability, which is critical in such applications, has been demonstrated to be fully satisfactory since the limited amount of branching present is mostly biodegradable methyl groups (in the alpha position). Some typical properties of the chemicals are shown in table 4.:

Waxes

Linear paraffins above C20 belong to the world of the waxes. Four fractions are separated in Bintulu called SX30, SX50, SX70 and SX100 were SX stands for Sarawax and the figure indicates the typical congealing point of that material. Typical properties of the waxes are given in table 5. Special precautions have been taken to conserve the purity even of the heaviest wax streams. For example, Wiped Film Evaporators (WFEs) are applied to separate the heaviest wax grades. The WFEs operate at a vacuum of about a factor 500-1000 below what is conventional high vacuum technology in standard refinery processing. The low pressure allows a rather mild distillation temperature which together with a very short residence time avoids thermal degradation of the products. Possible ingress of air and formation of unwanted oxygenates can be counteracted by a subsequent final hydrofinishing step. The resulting products (especially SX70 and SX100) are applied in industry segments where extreme purity, high Sayboldt colour quality, thermal stability and specific viscosity behaviour are required. Applications are diverse and vary from candles, paper & packaging, rubber, cosmetics and medicines, electrical use to various outlets, like chewing gum.

The total world paraffin wax consumption is about 3 million tonnes per annum and has over the last 15 years displayed an average annual growth of little over 4 %. Particular growth areas are Asia and Western Europe.

Important markets for waxes are the USA, the central European countries, the Pacific Basin, Japan and Taiwan, India, Brazil and South Africa.

5. ENVIRONMENTAL ASPECTS

The use of the SMDS products as transportation fuels has minimal impact on the environment, based on the excellent product properties. In some countries, notably in the USA, legislation has been proposed, which aims at limiting particulate and sulphur dioxide emissions originating from the combustion of transportation fuels by restricting their aromatics and sulphur levels. From product properties described above it is obvious that SMDS kerosene and gasoil meet such requirements without any problem. In the following section fuel quality aspects of SMDS gasoil will be highlighted, although it should be remembered that engine design and maintenance have an equally important or even greater impact on overall emissions:

Fuel Quality Effects on Vehicle Exhaust Emissions

Extensive work in and outside Shell Laboratories has established the effect of fuel properties on vehicle exhaust emissions.

For example, fuel sulphur has a dominant effect on particulate levels The conversion of fuel sulphur to particulate sulphur is engine dependant but within a relatively narrow range of 1-2%. Thus reduction to 0.05% m from earlier levels of 0.20 %, or higher in some countries, produces a significant emission reduction but further reduction below 0.05%m has only a relatively small influence.

Fuel density has been identified as an important parameter in particulate emissions. Lower density usually gives lower emission. Changes of emission properties in the Federal Test Procedure cycle caused by density changes arise from effects introduced by transient conditions. For example, air/fuel mixture excursions are caused by turbo charger lag during periods of hard acceleration. Reduction in fuel density increases the volumetric fuel consumption at all loads, although the increase in the fuel H2 to C ratio counterbalances the effect to some extent.

Aromatics content has been examined very carefully inside and outside Shell and it has been shown that "total aromatics" have no influence on particulate emissions. In some engines the addition of polyaromatics produces small increases in particulate emissions.

Cetane number is the fuel property having the greatest influence on regulated gaseous emissions (NO., hydrocarbons, and CO) and having a large influences on the cold start performance of an engine. Higher cetane numbers give better performance. However, the benefit in regulated gaseous emissions by increasing the ignition quality through an increase in cetane is limited by the possible steps the markets would and can accept.

In California regulations are quite advanced in controlling exhaust emissions. However, compliance can be achieved in several ways. Application of SMDS gasoil can present an advantage in several of these options depending on the specific market situation and specific conditions in the refineries. Especially where cetane enhancement is required SMDS gasoil can act as cetane improver additives.

6. OUTLOOK

It is not surprising that the conversion of natural gas into middle distillates for the transportation fuel market has by the nature of the process a disadvantage compared to the manufacture of transportation fuels via crude oil distillation : part of the energy content of the feedstock is consumed for the conversion process itself. Moreover, the feedstock (natural gas) itself has alternatives to reach the market, i.e. by pipeline or by liquefaction. On the other hand, the SMDS technology can provide the bridge between vast reserves of natural gas and the large transportation fuel market. This bridge can be built already today if some specific factors come together :

- the investment has to be reasonably low
- the alternative value of the natural gas should be low
- the products fit into the longer market trends.

Above we have shown in detail that every product produced with the SMDS technology provides by the way of its manufacture from the molecular building blocks top quality and fits into increasing efforts of conserving the environment.

If a natural gas reserve cannot be exploited by pipeline or by liquefaction it can be left in the ground or used in a conversion plant. In that case a reasonable natural gas price would be about US$ 0.5 per MMBTU (equivalent to a feedstock cost element in the product of about US$ 5/bbl) to make the products competitive in the transportation fuel market. The total fixed and other variable operating costs are estimated at a further US$ 5/bbl. The total required selling price for the product will depend on numerous factors, including fiscal regimes, local incentives, debt/equity ratio, type of loans and corporate return requirements. The premium that may be realised for the high quality products can be anything between 0 and 8 US$/bbl over and above the normal straight run middle distillate value depending on local circumstances.

An important factor when realising a natural gas to middle distillate conversion complex are the capital costs. These are highly dependent on location. At a location with an industrial infrastructure available specific capital cost would be around US$ 30,000 per daily barrel, whereas for a similar plant in a remote location and on a greenfield site the cost could be substantially higher.

In addition to these factors, the capacity of the plant is of great importance. Especially for remote locations, where self-sufficiency of the plant is essential, larger plants, in the 25,000 to 50,000 bbl/d range, have a much better economy of scale.
Whilst the process is ready for commercialisation, further developments are underway, directed at increasing the efficiency of the process and reducing the capital cost. An important area for these efforts is the synthesis gas manufacturing plant, which constitutes more than 50% of the total process capital cost. Other fields of interest include further catalyst improvement, the design of the synthesis reactors and general process integration within the project. Here the factor 'moving up the learning curve' is of pivotal importance: construction and several years of operation of the SMDS Bintulu complex has provided an extensive know-how which will be applied the next time. It is expected that know-how combined with further improvements for larger size plants, will bring the specific capital costs for remote areas further down.

SMDS technology has been developed to a stage where it can be considered as technically proven and, subject to local circumstances, commercially viable. Installation of SMDS plants can bring significant national benefits to countries with uncommitted gas reserves, either through export from the plant or inland use of the products, thereby reducing the need to import oil and oil products and saving on foreign exchange,
The successful application of the technology in Bintulu presents an important advance in the commercialisation of SMDS conversion technology and an asset in Shell's portfolio of technologies to make natural gas transportable. It provides exciting opportunities in terms of marketing hydrocarbon products of a quality that fits ideally in a business environment, requiring increasingly higher performance standards.

REFERENCES

Eilers, J. Posthuma, S.A, and Sie, S.T., 'The Shell Middle Distillate Process (SMDS)', paper presented at the AICHE Spring National Meeting, Orlando, Florida, USA, March 18-20, 1990.

Post, M.F.M., Van 't Hoog , A., Minderhout, J.IC. and Sie, S.T. (1 989), 'Diffusion limitations in Fischer-Tropsch catalysts' AICHE J. 35 (7),1107-1114

Oerlemans, T.W., Van Wechem, H.M.H., and Zuideveld, P.L., 'Conversion of Natural Gas to Middle Distillates via the SMDS Process', paper presented at the 18th World Gas Conference, Berlin, FRG, July 8- I 1, 1991.

Senden, M.M.G., Sie, S.T., Post, M.F.M., and Ansorge, J. (1 99 1), 'Engineering aspects of the conversion of natural gas into middle distillates', paper presented at NATO Advances Study Institute Conference at the University of Western Ontario, Canada, September 4.

Van der Burgt, M., Van Klinken, J. and Sie, S.T. "The Shell Middle Distillate Synthesis Process", paper presented at the 5th Synfuels Worldwide Symposium, Washington D.C. USA, November 11-13,1985.

Van den Burgt, M.J., Sie, S.T., Zuideveld, P.IL and Van Wechem, H.M.H., 'The Shell Middle Distillate Process, paper presented at the Institution of Chemical Engineers Conference on Natural Gas Conversion, London, UK, January 12, 1988.

Tijm, P.J.A., Van Wechem, H.M.H., and Senden, M.M.G., 'New opportunities for marketing natural gas: The Shell Middle Distillate Synthesis Process', paper presented at the GASTECH 93, 15th International LNG/LPG Conference & Exhibition, Paris, France, February 16-19, 1993.

Booth, M, et al., 'Diesel Fuel Quality in an Environmentally Conscious World', paper presented at 1. Mech. E. International Seminar 'Fuels for Automotive and Industrial Diesel Engines', London, UK, 6-7, April 1993, London

Stradling R.J. et al. (1993) 'The Influence of Fuel Properties and Test Cycle Procedures on the Exhaust Particulate Emissions from Light-Duty Diesel Vehicles' paper presented at I. Mech. E. International Seminar 'Fuels for Automotive and Industrial Diesel Engines', London 6-7, April 1993, London

Cowley T. et al. (1993) 'The Influence of Composition and Properties of Diesel Fuel on Particulate Emissions from Heavy-Duty Engines', paper presented at Fuels and Lubricants Meeting and Exposition, Philadelphia, Pennsylvania October 18-21, 1993

Tijm, P.J.A., Marriott, J.M., Senden, M.M.G and Van Wechem, H.M.H., 'Shell Middle Distillate Synthesis: The Process, The Products, The Plant, paper presented at the Alternate Energy '94, La Quinta, Ca, USA, April 26-29, 1994.

van Herwijnen, Th., 'Shell MDS (Malaysia) Plant On Stream', paper presented at GASTECH 94, in Kuala Lumpur, Malaysia, October 23-25,1994.

Table 1 Typical properties of SMDS Middle Distillates

Property		Unit	Naphtha	Kerosene	Gasoil	method
Density (at 15 oC)		lkg/m3	690	740	780	ASTM D1298
Saybolt colour		-	+30	+30	n/a	ASTM D156
Distillation range	IBP	°C	40	150	200	ASTM D86
	FBP	°C	160	200	360	
Sulphur		PPM	b.d.l.	b.d.l.	b.d.l.	ASTM D1266
Cetane number		-	n/a	60	75	ASTM D976
Smoke point		mm	n/a	>> 50	n/a	ASTM D1322
Flash point		°C	n/a	40	90	ASTM D93
Aromatics		% vol	b.d.l.	b.d.l.	b.d.l.	ASTM D5186

b.d.l. = below detection limits n/a = not applicable

Table 2 Typical properties of Detergent Feedstocks from SMDS

Property	unit	LDF	HDF	Method
Saybolt colour		+30	+30	ASTM D156
Bromine index	mg Br / 100 g	5	6	ASTM D2710
Sulphur		b.d.l.	b.d.l.	ASTM D3120
Carbon distribution				by GC
C9- / C13-	% m	0	1	
C13- / C17-	% m	99.3	99	
C14+ /	% m	0.7		
..... / C18+	% m		0.2	
N-paraffins content	% m	96	95	

b.d.l. = below detection limit

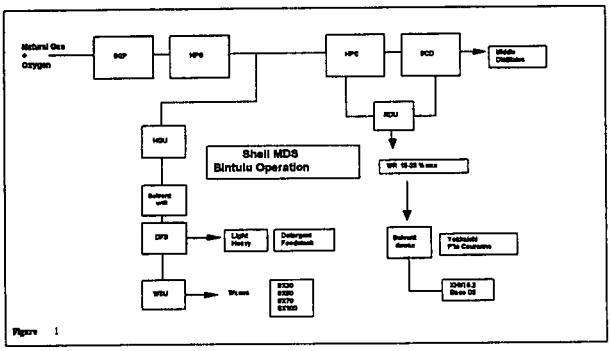

Table 3 **Gasoil Properties compared to CARB specifications**

Gasoil	SMDS product	Californian CARB	CEN Specs
	Commercial Spec.	Reference fuel Spec.	
Cetane number	76	48 min	49 min
Density (kg/m3)	780	N/S	820-860
Sulphur (ppmm)	n/d	500	500 (1996)
Aromatics (% m/m)	n/d	10 max.	N/S
Cloud point oC	1	-5	N/S
CFPP oC	-2	N/S	+5 to -20*
90 % recovery (oC)	340	288-338	
95 % recovery (oC)	350		370 max.

N/S = No Specification * depend on regional application

Table 4 **Typical Properties of SMDS normal paraffin products**

Property	Unit	SARAP AR 059	SARAP AR 103	SARAP AR 147	SARASOL 150/200	Method
Saybolt colour		+30	+30	+30	+30	ASTM DI56
Bromine index	mg Br/ 100g	10	5.0	5.5	20	ASTM D2710
Sulphur	PPM	zero	zero	zero	zero	ASTM 3120
Carbon distr.	% m					GC
n-C5		10				
n-C6		17				
n-C7		19			1	
n-C8		19			3	
n-C9		18			7	
n-C10		8	9		20	
n-C11			30		12	
n-C12			30		8	
n-C13			27	<1	1	
n-C14			<1	26		
n-C15				27		
n-C16				25		
n-C17				17		
n-C18				<1		
N-paraffins tot	% m	91	96	95	50	
Avg. mol. mass		122	167	213	166	
Density	kg/m3	690	750	775	735	ASTM D4052
Distillation	IBP °C	35	190	250	155	
	FBP °C	160	230	280	195	
Flash Point	°C	N/A	75	110	43	ASTM D93
Aniline Point	QC	70	83	93	82	ASTM D611
Pour Point	°C	N/A	-20	5	-35	ASTM D97
Visc. 25 OC	mm/s	0.6	1.7	3.3	1.5	ASTM D445

Table 5 **Typical Wax Properties**

Property	Unit	**SX30**	**SX50**	**SX70**	**SX100**	Method
Congealing point	oC	31	50	70	98	ASTM D938
Saybolt colour	-	+30	+30	+30	+30	ASTM D196
Odour		1.5	1.0	0.5	0.5	ASTM D1833
Oil content (-32 oC)	% m	5	2.5	0.4	0.1	ASTM D721
UV absorptivity		< 0.01	< 0.01	< 0.01	< 0.01	ASTM D2008

ENGINE EVALUATION OF FISCHER-TROPSCH DESEL FUEL, PHASE I

Thomas W. Ryan, III and Daniel A. Montalvo
Southwest Research Institute
San Antonio, Texas

INTRODUCTION

Engine manufacturers and refiners have long recognized the importance of fuel quality on diesel engine performance and emissions. The Coordinating Research Council examined this issue in some detail in a series of projects designed to quantitatively document the relationships between engine performance and emissions and fuel properties and composition[1-5]. This work was performed in what has been called a "prototype" Series 60 Detroit Diesel engine. The results of this work have indicated that cetane number and aromatic content are the primary fuel properties controlling the emissions. Additional work performed at Southwest Research Institute (SwRI) has also indicated that the types of aromatic materials are more important that simply the total mass of aromatic material in the fuel[6]. This same work demonstrated that significant emissions benefits were associated with the use of diesel fuels derived from Fischer-Tropsch processing of coal.

The test protocol used in the Prototype Series 60 testing involved the use of the Federal Heavy Duty Transient Test Procedure (FTP), as specified in the Federal Register. More recently, this same engine and the FTP have been adopted as the basis for the CARB Protocol for certifying reformulated diesel fuels in California.

OBJECTIVE

The main objective of this study was to evaluate Fischer-Tropsch (FT) diesel fuel as a low emissions diesel fuel.

EXPERIMENTAL APPROACH

The work reported in this presentation involves the comparative testing of three Fischer-Tropsch diesel fuels and two different conventional petroleum derived fuels; one representing a national average low sulfur diesel fuel, and one representing a typical low aromatic content California reformulated diesel fuel. The tests were performed in the same Series 60 engine used in the CARB Protocol, following the same basic procedures as used in the protocol.

As indicated, the group of fuels included a low-sulfur emissions 2D reference fuel, identified as Fuel 2D, three FT candidate fuels identified as Fuels B1, B1, and B3, and a "pseudo" California reference fuel, designated Fuel PCR. Transient cycle emissions of HC, CO, NO_X, total particulate (PM), sulfate, soluble organic fraction (SOF) of PM, and volatile organic fraction (VOF) of PM were obtained over repeat hot-start tests.

TEST RESULTS

Figure 1 illustrates that average hot-start transient emission levels of HC, CO, NO_X, PM, and SOF obtained with Fuels B1, B2, and B3, were all lower than those using Fuels PCR and 2D. Compared to Fuel 2D, the FT fuels showing the largest decrease in emissions were Fuel B1 for HC (46%), Fuel B2 for CO (47%), both Fuels B1 and B3 for NO_X (9%), Fuel B2 for PM (32%), and both Fuels B1 and B3 for SOF (47%).

SUMMARY

The main objective of this study was to evaluate the effects Fischer-Tropsch (FT) derived diesel fuels have on emissions from a heavy-duty truck engine. A screening test procedure was used based on transient emissions measurement procedures developed by the EPA for emissions regulatory purposes.

Average emissions of HC, CO, NO_X, PM, and SOF obtained with Fuels B1, B2, B3, and PCR were all less than with reference fuel, Fuel 2D. Furthermore, all these emissions were lower with FT fuels than on Fuel PCR. Fuel B1 had lowest HC, and Fuel B2 had lowest CO. Both Fuels B1 and B3 had low NO_X, but Fuel B2 had lowest PM.

REFERENCES

1. Terry L. Ullman, "Investigation of the Effects of Fuel Composition on Heavy-Duty Diesel Engine Emissions," SAE Paper No. 892072, SAE International Fuels and Lubricants Meeting and Exposition, Baltimore, MA, Sept. 25-28, 1989.

2. Terry L. Ullman, Robert L. Mason, and Daniel A. Montalvo, "Effects of Fuel Aromatics, Cetane Number, and Cetane Improver on Emissions from a 1991 Prototype Heavy-Duty Diesel Engine," SAE Paper No. 902171, SAE International Fuels and Lubricants Meeting and Exposition, Tulsa, OK, Oct. 22-25, 1990.

3. Terry L. Ullman, Kent B. Spreen, and Robert L. Mason, "Effects of Cetane Number, Cetane Improver, Aromatics, and Oxygenates on 1994 Heavy-Duty Diesel Engine Emissions," SAE Paper No. 941020, SAE International Congress & Exposition, Detroit, MI, Feb. 28-March 3, 1994.

4. Kent B. Spreen, Terry L. Ullman, and Robert L. Mason, "Effects of Cetane Number, Aromatics, and Oxygenates on Emissions From a 1994 Heavy-Duty Diesel Engine With Exhaust Catalyst," SAE Paper No. 950250, SAE International Congress & Exposition, Detroit, MI, February 27-March 2, 1995.

5. Terry L. Ullman, Kent B. Spreen, and Robert L. Mason, "Effects of Cetane Number on Emissions From a Prototype 1998 Heavy-Duty Diesel Engine," SAE Paper No. 950251, SAE International Congress & Exposition, Detroit, MI, February 27-March 2, 1995.

6. Thomas W. Ryan III, Jimell Erwin, Robert L. Mason, and David S. Moulton, "Relationships Between Fuel Properties and Composition and Diesel Engine Combustion Performance and Emissions," SAE Paper No. 941018, SAE International Congress & Exposition Detroit, MI, Feb. 28-March 3, 1994.

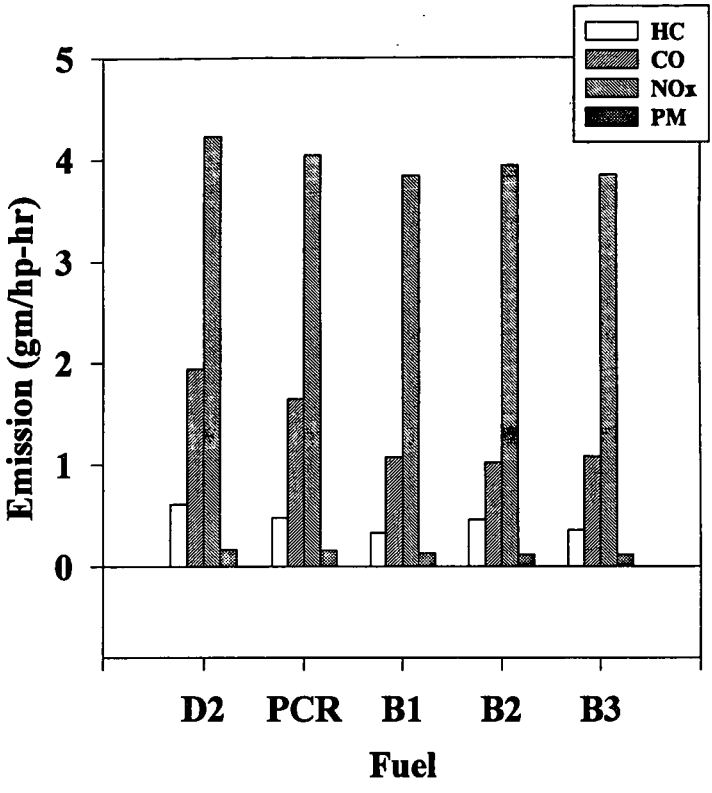

FIGURE 1. HOT-START TRANSIENT EMISSION LEVELS

DESIGN AND ECONOMICS OF A FISCHER-TROPSCH PLANT FOR CONVERTING NATURAL GAS TO LIQUID TRANSPORTATION FUELS

Gerald N. Choi, Sheldon J. Kramer and Samuel S. Tam
(Bechtel Corporation, San Francisco, CA)
Joseph M. Fox III (Consultant)

Keywords: Fischer-Tropsch, natural gas liquefaction, economics

ABSTRACT

There is considerable interest in the development of an economic process for the conversion of natural gas to liquid transportation fuels. Such a process will allow the commercialization of many remote natural gas fields which are not now viable. Under DOE sponsorship, a conceptual plant design, cost and economics were developed for a grass-roots plant using Fischer-Tropsch technology to produce about 45,000 bbls/day of liquid transportation fuels from 410 MMSCF/day of natural gas. The natural gas is converted to synthesis gas via a combination of non-catalytic partial oxidation and steam reforming. This synthesis gas is then converted to liquid hydrocarbons in a two-stage, Fischer-Tropsch slurry-bed reactor system. The Fischer-Tropsch wax and liquid hydrocarbons are upgraded to high quality naphtha and diesel blending stocks by conventional petroleum refinery processes. Economics are dependent on both plant and natural gas costs. At a location where construction costs are equivalent to the US Gulf coast and natural gas costs are low, this plant can be competitive at today's crude oil prices.

INTRODUCTION

Bechtel, along with Amoco as the main subcontractor, has developed a Baseline design (and a computer process simulation model) for indirect coal liquefaction using advanced Fischer-Tropsch (F-T) technology under DOE Contact No. DE-AC22-91PC90027. In 1995, the original study was extended to add four additional tasks; one of which was to develop a case in which natural gas, instead of coal, is used as the feedstock to produce high-quality, liquid transportation fuels. This paper describes the results of this task. It discusses the design of this plant and the economics of liquefying natural gas using F-T technology to produce liquid transportation fuels.

OVERALL PLANT CONFIGURATION

Figure 1 is a simplified block flow diagram showing the overall process configuration of the conceptual design for the natural gas-based F-T liquefaction plant. This design uses proven commercial technology for syngas generation, non-catalytic partial oxidation in combination with steam reforming. A cobalt-based catalyst in slurry-bed reactors is used for the F-T synthesis. The plant is located at a hypothetical southern Illinois mine-mouth location to be consistent with the previous coal based F-T liquefaction study. It produces about 43,200 BPD of high quality gasoline and diesel blending stocks from about 410 MMSCF/day of natural gas. In developing this natural gas case, where applicable, individual plant designs and cost estimates were prorated directly from the coal-based Baseline design.[1]

The overall natural gas-based F-T plant consists of three main processing areas; synthesis gas preparation, F-T synthesis, and product upgrading. In addition, there are eighteen ancillary offsite plants which are similar to those which were developed for the Baseline design with minor modifications as required for this natural gas case.

Synthesis Gas Preparation Area (Area 100)
This area consists of three major plants; air separation, partial oxidation, and steam reforming (sulfur is removed from the natural gas before syngas generation). Most of the syngas is generated by partial oxidation using 99.5% pure oxygen which produces a syngas with a molar H_2/CO ratio of 1.8/1. The steam reforming plant, produces a syngas with a H_2/CO ratio of 5.9/1. This is a relatively small plant. It is used only to supplement the syngas production by the partial oxidation plant by increasing the H_2/CO ratio of the total syngas going to the Fischer-Tropsch synthesis area to a H_2/CO ratio of about 1.9/1.

Fischer-Tropsch Synthesis Loop (Area 200)
This area consists of five plants; F-T synthesis, CO_2 removal, recycle gas compression and dehydration, hydrocarbon recovery, and hydrogen recovery. Hydrogen is recovered from the unconverted syngas. After satisfying the downstream hydroprocessing needs, the excess hydrogen is recycled back to the F-T reactors. The remaining unconverted syngas is used for fuel.

A cobalt-based catalyst was selected for F-T synthesis because it has negligible activity for the water-gas shift reaction compared to an iron-based catalyst, and thus, it requires a syngas with a molar H_2/CO ratio near the stoichiometric value of 2.0/1. Since methane, the principal component in natural gas, has a molar H_2/C ratio of 2.0/1, syngas produced from it has a similar H_2/CO ratio. Also, for iron-based catalyst with a high water-gas shift activity, CO_2 is the primary byproduct from the Fischer-Tropsch synthesis. With cobalt-based catalyst, water is the primary byproduct.

A total of 24 slurry-bed reactors process the syngas from Area 100. These reactors are arranged in eight trains with each train having two first-stage slurry-bed reactors feeding a single second-stage slurry-bed reactor. The unconverted syngas leaving the first-stage reactors is cooled and flashed to condense and remove liquids before being reheated and fed to the second-stage reactors. The CO conversion in each of the parallel first-stage reactors is about 56%, and in the second-stage reactors, the CO conversion is about 59%. This gives an overall CO conversion per pass of about 82%. The first-stage F-T slurry-bed reactors operate at about 428 °F and 335 psig, and the second-stage reactors operate at 428 °F and 290 psig. Excess heat is removed by the generation of 150 psig steam from tubes within the reactors.

Slurry-bed reactor sizing is based on an improved version of the kinetic reactor model which originally was developed by Viking Systems, International.[2] The primary modification to this model was the insertion of the kinetic parameters developed by Satterfield et al for cobalt-based catalyst.[3]

Product Upgrading and Refining Area (Area 300)

This area consists of eight processing plants. Fischer-Tropsch synthesis produces a wide spectrum of hydrocarbon products, similar to crude oil except that naphthenes and aromatics are absent. Upgrading is required to produce high-quality transportation fuels. For consistency with the coal-based Baseline design, Area 300 uses the same conventional petroleum processing technologies to upgrade and refine the F-T products to high quality liquid transportation fuels. This area consists of a wax hydrocracker, distillate hydrotreater, naphtha hydrotreater, catalytic reformer, C5/C6 isomerization unit, C4 isomerization unit, C3/C4/C5 alkylation unit, and a saturated gas plant. Area 300 is designed to produce maximum amounts of high-octane gasoline and high-cetane diesel blending stocks.

PLANT SUMMARY

The conceptual plant consumes about 410 MMSCF/day of natural gas and produces about 45,000 BPD of liquid products. The primary liquid products are C3 LPG, a C5-350 °F fully upgraded gasoline blending stock, and a 350-850 °F distillate. The gasoline product has a clear (R+M)/2 octane of about 88 and is basically a mixture of C3/C4/C5 alkylate, C5/C6 isomerate and catalytic reformate. The distillate product also is high quality and has a high cetane number, on the order of 70. Both products are essentially free of sulfur, nitrogen and oxygen containing compounds.

The plant uses all of the byproduct steam and fuel gas to generate electric power. In addition to supplying its entire power requirement, about 25 MW of excess electric power is sold. The only materials delivered to the plant are natural gas, raw water, catalysts, chemicals and some normal butane which is used as a feed for C4 isomerization and, subsequently, alkylation.

Following the philosophy of the previous indirect coal liquefaction study, the overall plant is designed to comply with all applicable environmental, safety and health regulations. Air cooling is maximized, wherever possible, in order to minimize cooling water requirements. A brief summary of the major feed and product streams entering and leaving this natural gas liquefaction plant is shown in Table 1.

Capital Cost Estimate

Total capital cost for this natural gas F-T plant is about 1.84 billion dollars. This is a mid-1993 cost, consistent with the coal-based F-T study. The estimated plant cost is about 40% less than that for the corresponding coal-based design. A different syngas preparation area and a smaller CO_2 removal plant account for most of the cost reduction. A brief summary of the estimated capital cost breakdown is given in Table 2.

ECONOMIC SENSITIVITY STUDIES

A discounted-cash-flow analysis on the production cost of the F-T products for a 15% internal rate of return on investment was carried out to examine the economics of the natural gas F-T design using similar financial assumptions to those employed for the coal-based F-T study.[4] Inflation projections are based on the 1996 Energy Information Administration forecast.[5] Results are expressed in terms of a crude oil equivalent price (COE) which is defined as the current hypothetical break-even crude oil price where the F-T liquefaction products are competitive with products from crude oil at a typical PADD II refinery.

The primary liquefaction products are gasoline and diesel blending stocks. Their relative values to the crude oil price were determined using a PIMS linear programming model of a typical PADD II refinery using current crude oil prices, processing costs and margins. The methodology of and results from this study are documented in a 1994 ACS paper.[6] For the Baseline coal case, the F-T gasoline blending stock had a value of 10.07 $/bbl more than crude oil, and the F-T diesel blending stock had a value that was 7.19 $/bbl more than crude oil. These same margins are used for this natural gas F-T study since the properties of these F-T gasoline and diesel blending stocks are essentially the same as those from the coal-based Baseline design.

Figure 2 shows the results of the natural gas F-T economic calculations at the southern Illinois siteas a function of the natural gas price using the economic parameters given in Table 3. With natural gas priced at 2.0 $/MMBtu, the calculated COE price is 30.7 $/bbl in current dollars. The economics are strongly

dependent on the natural gas price. If natural gas is available at 0.5 $/MMBtu, the COE drops to only 19.1 $/bbl.

Figure 2 also shows the effects of inereased capital cost (by 25 and 50%) and decreased capital cost (by 10, 25 and 50%). The former are included to show the effect of higher construetion costs at remote sites. The latter are included to show the potential improvement in the economies via advanced technologies and/or location at sites where construction costs are lower. Emerging technologies for synthesis gas generation inelude combined autothermal reforming and ceramie membranes oxidation. These offer a potentially significant reduetion in plant cost. If the syngas generation cost can be eut in half, it would correspond to a 33% decrease in total capital. As shown in Figure 2, the effect on the overall process economies would be substantial.

Figure 3 shows the portion of the calculated COE price attributable to various capital and operating cost items at the hypothetical southern Illinois site with 2.0 $/MMBtu gas. At this gas price, the natural gas cost dominates the process economics. It contributes about 51% of the caleulated COE price. Capital servieing costs account for about 34% of the COE price. Other items contribute the remaining 15% of the COE price with the operating and maintenance labor accounting for about half of this amount.

For a potential remote site where low cost natural gas is available (e.g., 0.5 $/MMBtu), the COE distribution is very different, as shown in Figure 4. Capital servicing costs now predominate and drive the overall project economies. It constitutes about 55% of the calculated COE price. The contribution of advanced technologies to reducing the total capital cost will be greatly enhanced at a remote site.

CONCLUSIONS AND RECOMMENDATIONS

A conceptual plant design with cost estimates has been developed for a Fischer-Tropsch natural gas liquefaction plant producing 43,200 BPD of high-quality, liquid transportation fuels from about 410 MMSCF/day of natural gas. In addition, this plant produces about 1,700 BPD of liquid propane and 25 MW of surplus electric power for sale. The capital cost of this plant is estimated at about 1.84 billion mid-1993 dollars. Since US Gulf coast construction costs are somewhat lower than those in southern Illinois, the above plant at a US Gulf coast location will produce liquid transportation fuels from 2.00 $/MMBtu gas which will be competitive with those produced from erude oil priced below 30 $/bbl. With 0.50 $/MMBtu natural gas, the crude oil equivalent (COE) price will drop still lower, to below 19 $/bbl.

Thus, it is evident that attractive natural gas F-T economics currently only can be attained with low cost gas. There are numerous reserves located at remote areas and/or offshore where the gas has little value because transportation systems are not available to ship it to market. F-T synthesis offers an option to convert these resources into liquid hydrocarbons whieh can be easily transported to existing refineries. Under this scenario, capital servicing costs are the predominant factor driving the overall process economics. However, there are various opportunities to reduce the plant cost. Examples include:

- Simplifying the F-T design at the expense of a minor sacrifice in overall process thermal efficiency. It is also possible (and probably desirable) to eliminate and/or simplify the upgrading area to produce only a F-T syncrude which can be shipped to a conventional petroleum refinery where it would be coprocessed with crude oil.

- Integrating the F-T design with the existing infrastructure. This will be relevant, for example, for a F-T plant at the Alaskan North Slope which converts either the 'gas-cap' or 'associated' gas into a transportable syncrude. The design will utilize the considerable assets/infrastructure at the North Slope and available pipeline capacity as crude production declines to maximize cost savings.

- Investigating and incorporating more advanced processes for syngas generation such as combined autothermal reforming, fluid-bed autothermal reforming, and ceramic membranes oxidation (e.g., DOE Contract No. DE-AC22-92PC92113). Such processes have the potential to significantly reduce the plant cost and improve the economics.

- Developing a practical design for larger diameter slurry-bed reactors. The current plant design has 24 slurry-bed F-T reactors, each about 16 feet in diameter. Larger slurry-bed reactors can significantly reduce the cost of the F-T synthesis plant.

ACKNOWLEDGMENT

Bechtel, along with Amoco who was the main subcontractor for a major portion of this study, expresses our appreciation to the DOE/Pittsburgh Energy Technology Center for both technical guidance and financial funding under Contract No. DE-AC22-91PC90027.

REFERENCES:

1. Topical Report, Volume I, Process Design - Illinois No. 6 Coal Case with Conventional Refining, Baseline Design/Economics for Advanced Fischer-Tropsch Technology, Contract No. DE-AC22-91PC90027, October, 1994.
2. Final Report, Design of Slurry Reactor for Indirect Liquefaction Applications, Contract No. DE-AC22-89PC89870, December, 1991.
3. Final Report, An Innovative Catalyst System for Slurry-Phase Fischer-Tropsch Synthesis: Cobalt Plus a Water-Gas Shift Catalyst, Contract No. DE-AC22-87PC79816, July 1991.
4. Choi, G. N., Kramer, S. J., Tam, S. S. and Fox, J. M. III, "Simulation Models and Designs for Advanced Fischer-Tropsch Technology," Proceedings of the Coal Liquefaction and Gas Conversion Contractors Review Conference, Pittsburgh, PA, Aug. 29-31, 1995.
5. "Annual Energy Outlook 1996 with Projections to 2015," Energy Information Administration, Washington, DC, January 1996.
6. Marano, J. J., Rogers, R., Choi, G. N., and Kramer, S. J., "Product Valuation of Fischer-Tropsch Derived Fuels, Symposium on Alternative Routes for the Production of Fuels," ACS National Meeting, Washington, D.C., August 21-26, 1994.

Table 1

Overall Plant Major Input and Output Flows

Feed			
Natural Gas	412	MMSCF/day	(17,800 MMBtu/hr)
Raw Water Make-up	21	MMGal/day	
N-Butane	3	Mlbs/hr	(340 Bbl/day)
Primary Products			
F-T Gasoline	180	Mlbs/hr	(17,000 Bbl/day)
F-T Diesel	295	Mlbs/hr	(26,200 Bbl/day)
Propane	13	Mlbs/hr	(1,700 Bbl/day)
Electric power	592	MW-hr/day	

Table 2

Cost Breakdown of the Natural Gas Liquefaction Plant

Area	Description	Cost (MM$)	% ISBL
100	Syngas Preparation	707	66
200	F-T Synthesis	226	22
300	Upgrading & Refining	132	12
	Offsites	426	
	HO Service/Fee and Contingency	351	
	Total Cost:	1842	

The above plant costs are estimated to have an accuracy range of +/- 30%.

Table 3

Economic Parameters

N-Butane price, $/bbl	14.5
Electricity, cents/kwh	2.5
Plant life, years	25
Depreciation, years	10
Construction period, years	4
Owner's cost, % of initial capital	5
Owners initial equity, %	75
Bank interest rate, %/year	8
General inflation, %/year	3.2
Escalation above general inflation, %/year	
Natural gas	0.3
Crude oil	2.4
Electricity	-0.1
Federal income tax rate, %	34
State and local tax rates, %	0
Maintenance and insurance, % of capital	1
Labor overhead factor, % of salary	40
On-stream factor, %	90.8

C:\NDAPAPR497B.DOC

Figure 1
Natural Gas Fischer-Tropsch Study
Overall Process Configuration

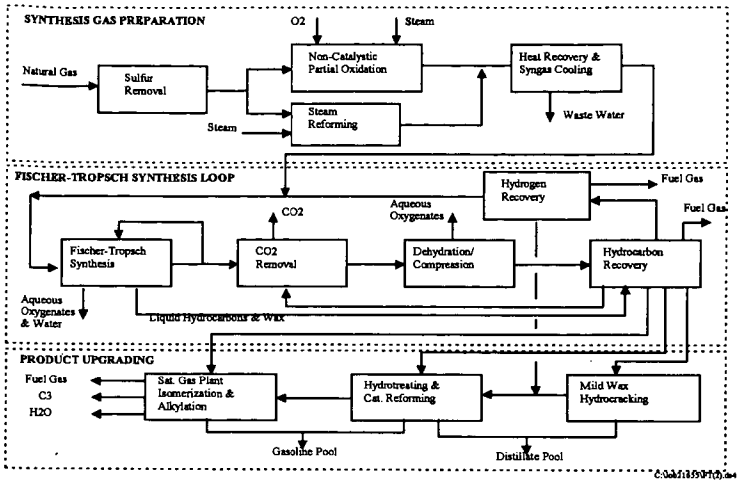

Figure 2
COE Price as a Function of Natural Gas Price and Capital Cost

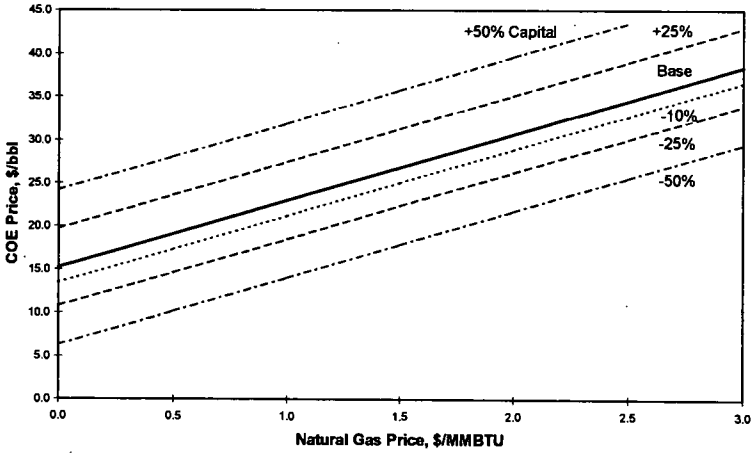

Figure 3
COE Cost Distribution @ 2.00 $/MMBTU Gas
COE = 30.7 $/bbl at Southern Illinois

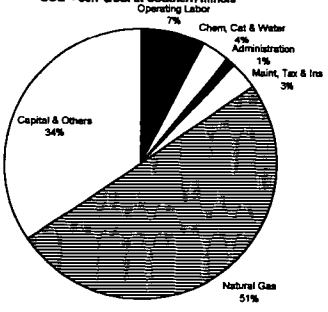

Figure 4
COE Cost Distribution @ 0.50 $/MMBTU Gas
COE = 19.1 $/bbl at Southern Illinois

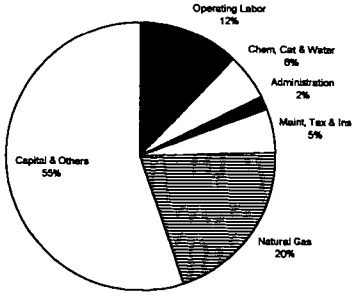

ECONOMIC CONVERSION OF NATURAL GAS TO SYNTHETIC PETROLEUM LIQUIDS

Mark A. Agee
Syntroleum Corporation
400 S. Boston, Ste. 1000
Tulsa, OK 74103

Key Words: Converting Natural Gas into Liquid Fuels Economically

Introduction. Fischer-Tropsch chemistry has been applied for more than 50 years to produce clean synthetic fuels. In recent years, the feedstock focus has shifted away from abundant, available coal to abundant but stranded natural gas. The incentive to do so is huge: Most of the world's proven and discovered, undeveloped reserves of natural gas are unmarketable in their present form. Available technology has offered few options to monetize these remote resources. If they could be economically converted into clean liquid fuels, which could then be economically transported to world commodity markets, the rewards would be enormous: Instead of being locked up, representing an expensive burden of unrecovered costs, a significant percentage of idle reserves would suddenly have the potential to be converted into booked assets of great value. At a conversion rate of 10 to 1--10 MMCF of pipeline quality gas converts to 1 barrel of synthetic product--stranded reserves are equal to several hundred billion barrels of oil.[1]

It is not surprising that a prize of that magnitude would draw a crowd. Some of the world's leading research organizations, galvanized by the prospects, have poured hundreds of millions of dollars into the search. Today, we can state with confidence, these efforts have succeeded. Fischer-Tropsch chemistry can be used in many cases to convert natural gas to synthetic liquid fuels at a cost that is competitive with conventional petroleum products at current prices. In a variety of designs developed by Syntroleum Corporation, economical conversion of gas to synthetic liquids (GTL) can be accomplished in a wide range of sites and circumstances, from small plants in remote locations, onshore and offshore, to very large "natural gas refineries."

The process is competitive at crude oil prices below $20/BBL--roughly $10/BBL less than the level previously considered to be economic for synfuels from natural gas. It has been licensed to one major international oil company for use in projects it has under consideration. Syntroleum is negotiating similar licensing arrangements with several others.

Synfuels Products and Quality. One reason for the ready marketability of synfuels is their superior quality, earning them very high marks in performance tests.[2] Synthetic fuels produced via Fischer-Tropsch chemistry are known for being among the cleanest fuels in the world. The liquid fuels produced by the new process are free of sulfur, metals, and aromatics, and are clear in appearance. They will offer industry a timely option just as refiners are seeking ways to avoid costly "have-to" compliance capital investments that are hard to justify by market conditions.

Characteristics of Syncrude. Synthetic crude made from natural gas is characteristically extremely clean. In the Syntroleum Process, the syncrude produced tends to be mostly saturated, straight chain hydrocarbons, essentially free of sulfur, aromatics and contaminants such as heavy metals commonly found in natural crude. These characteristics make syncrude a valuable blending stock for upgrading natural crude streams.

Because of its purity, high API gravity and highly paraffinic nature, syncrude can be blended with natural crude to gain significant improvements in yields and product quality in many conventional refining applications.

Synthetic Fuels. Synthetic hydrocarbon fuels are superior in many ways to products derived from conventional crude oil (Table 1). The naphtha fraction (C_5-C_8) from syncrude is highly paraffinic. The light end components are more suitable for gasoline production than the heavy end components. However, the heavy ends can be further upgraded via conventional naphtha reforming for the gasoline market.

Synthetic kerosene makes a good linear blending component for upgrading lower-quality stock (Table 1). Because of its outstanding combustion properties, synthetic kerosene can be used to upgrade petroleum kerosene products with low smoke point and high aromatics content which would otherwise be unsuitable for use as jet fuel.

Synthetic diesel, with its high cetane index and absence of sulfur and aromatics, is an ideal blending component for upgrading lower-quality stocks to meet current and future environmental specifications. Because of its superior combustion properties, synthetic diesel is an option for compliance with the most stringent current CARB and CEN standards (Table 2).

The Syntroleum Process. Alternative F-T technologies, as well as LNG, have sought to improve their economics through large plant capacities. They have focused on sizes as large as 50,000 BPD of product as a starting point, requiring 180 BCF of gas per year or approximately 5.4 TCF over a 30-year life. One recently announced proposal for a plant of that size, costing $24,000 per barrel of daily capacity, was a significant development, but limited to a small number of possible fields. Only 2% of the 4,448 identified gas fields outside the U.S. and Canada have the reserves to qualify, and some 30 of these already have significant commitments to large LNG projects.[3]

At plant capacities as small as 5,000 BPD, the Syntroleum Process offers a potential solution for almost 40% of the world's gas fields. In various combinations, the design menu can be adapted to apply to much smaller fields. The plant's relatively small footprint also lends itself to certain offshore, platform-mounted applications. Portable (barge or ship mounted) plants could allow many of the smaller offshore fields to be monetized without the need for long-term reserves.

The Syntroleum Process is a proprietary method for converting natural gas into liquid hydrocarbons (GTL). Research was aimed at developing a process that would achieve two primary objectives: (1) commercial viability with oil prices of $15 to $20/BBL, and (2) design flexibility that would permit a wide range of economic plant sizes suitable for a multitude of site conditions and a significant share of the world's remote gas fields.

The first objective was met by significantly reducing complexity and capital costs in every area of the process. This was vital because of the crucial role of capital efficiency in the economics of synfuels processes. The second was met by creating a menu of design components which, in varying combinations, can be economically applied to plant sizes ranging from as small as 2,000 BPD of liquids production--even smaller in special circumstances--to as large as 100,000 BPD.

Syntroleum uses the same two-step chemistry found in other Fischer-Tropsch processes: Natural gas is converted into synthesis gas, then the synthesis gas is reacted in a Fischer-Tropsch reactor to polymerize hydrocarbon chains of various lengths. But the Syntroleum Process is markedly different in several important ways.

Step One: Synthesis Gas Production. In typical F-T processes, more than 50% of the capital cost relates to the production of synthesis gas, usually generated from natural gas via partial oxidation with oxygen, steam reforming, or a combination of the two. These methods are relatively expensive because the production of oxygen requires an air separation plant. They also have inherent problems that must be solved in various ways to produce an acceptable ratio of hydrogen to CO in the syngas for the F-T reaction. In these approaches, nitrogen is eliminated from the syngas stream as an unwanted inert, but not in the Syntroleum Process.

The Syntroleum syngas step is based on Autothermal Reforming (ATR) with air instead of oxygen in a reactor of proprietary design. The reactor is mechanically simple, easy to start up and shut down, and relatively inexpensive to build (Figure 1). It does not require large scale to be cost effective. Its lower cost is a large contributor to the cost savings realized in the Syntroleum Process.

The ATR consists primarily of a refractory-lined carbon steel reactor vessel and a catalyst. Air and natural gas are fed in at proper ratio and pressure, producing a nitrogen-diluted synthesis gas within the desired H_2/CO ratio of approximately 2.0. The syngas ratio can be adjusted further by the introduction of a small amount of steam or CO_2 into the ATR reactor. Synthesis gas diluted with approximately 50% nitrogen raises an obvious concern that any savings from the much simpler ATR reactor would be lost due to the increased F-T reactor section needed to handle the added inert volumes. However, in the Syntroleum Process, this is not the case.

Step two: Fischer-Tropsch synthesis. Other processes have been careful to avoid the introduction of any inerts such as nitrogen. The Syntroleum Process, on the other hand, incorporates nitrogen into the process. This is possible because its F-T section has no recycle loop. The one-pass design avoids any build-up of nitrogen in the system, thus allowing the use of nitrogen-diluted syngas without impairing performance. The Syntroleum F-T reactor configuration is comparable in size but less expensive than comparable systems with recycle: The

recycle compressor loop, which must handle and be rated for hydrogen service, has been eliminated (Figure 2).

Nitrogen plays a significant role in removing the large amounts of heat generated by the Fischer-Tropsch reaction. Removing the exothermic heat of reaction and controlling reactor temperatures within close tolerances is a critical element of reactor design.

Process Development, Demonstration. After 5 years' research on the process, the company obtained its first patents in 1989. This was followed by construction and operation of a 2 BPD pilot plant in 1990 and 1991. These runs were successful but confirmed the need for a proprietary catalyst system tailored to fit the unique syngas environment created by the process. Syntroleum has since developed several proprietary catalyst systems for use with different variations of the process and continues to focus a significant amount of the company's resources in this area.

The pilot plant continues to be used to evaluate process improvements, including new catalyst systems, reactor designs, and heat integration. It is also used to provide technical information necessary for scale-up and engineering of commercial plants. The company plans to maintain the pilot plant indefinitely to support future development work.

Surplus heat generated from the two reactions combined with combustion of the low-BTU tail-gas stream provides more than enough power for all plant needs. Also, there is a surplus for potential commercial sale, either as steam or electricity, if circumstances permit. The major energy consumer is compression. The energy integration is a key component of a cost effective design and the subject of several patent applications. The only other byproduct of the process is synthesized water, which can be used as boiler feed water or made potable with proper treatment.

Catalyst Technology, Downstream Processing. The process requires a special catalyst system tailored to operate in the unique syngas environment created by the ATR. Syntroleum began development of the Fischer-Tropsch catalysts optimized for such syngas in 1991. The company's high alpha catalyst system is a proprietary, highly active cobalt catalyst. It produces a waxy syncrude that is primarily uniform straight-chain hydrocarbon molecules with relatively low yields of methane (below 10%). Test runs with commercially manufactured batches have demonstrated the viability of the high alpha catalyst system at commercial scale.

Plants designed around the high alpha catalyst produce a waxy syncrude which requires hydrocracking, similar to competing processes, for the production of fuels. With conventional hydrocracking and fractionation, the syncrude can be tailored to optimize diesel yield or kerosene yield.

Work on a "chain-limiting" F-T catalyst began in 1994, with partial funding from three major oil companies. The goal was a catalyst that limits the growth of hydrocarbon chains to eliminate wax production and minimizes the production of light hydrocarbons (C_1-C_4). Recent multiple-week test runs in a fluid bed reactor yielded a product profile that indicates success.

This catalyst promises several additional efficiencies to the process configuration, including a lower operating pressure for the process, use of higher capacity fluidized-bed reactors that cannot be effectively used with the high-alpha, wax-producing catalyst, and elimination of a hydrocracking step.

Multiple Design Combinations. In keeping with initial objectives and the needs expressed by oil and gas companies, Syntroleum focused on a broad approach, one that could be adapted to a wide range of conditions and circumstances. This led to emphasis on commercialization of a menu of components:

- Two ATR (Autothermal Reforming) designs;
- Three heat integration designs which are the subject of several patent applications.
- Four Fischer-Tropsch reactor designs to allow a wide range of flexibility. For example, the "horizontal" reactor lends itself to platform, barge and ship-mounted application.
- Two F-T catalyst systems, the latest of which offers several additional cost saving changes to the process configuration.

Economics, Capital Costs. Syntroleum has collaborated with Bateman Engineering, of Denver, to develop several commercial scale design and capital cost estimates. This was done in parallel with various technical development work over the last several years. These efforts involved refining process models and evaluation of equipment designs. Considerable attention was given to

alternative compression designs, reactor designs and system integration in an effort to minimize capital costs.

A 1995 study was made for a nominal 5,000 BPD first generation plant equipped to produce three fuel feedstocks (diesel/kerosene/naphtha). The estimated installed cost for the facility was $135 million. That translated to $27,000 per barrel of daily capacity, or about $3,000 below the capital cost calculated to be the break-even point for a gas-to-synfuels plant. A more recent study of a second generation design of 5,600 BPD capacity yielded a reduction to $97 million fully installed, or $17,300 per barrel of daily capacity--well within commercial range even at product prices below current levels.

Estimates encompass all process and auxiliary facilities for a complete operating plant located on the U. S. Gulf Coast, including allowance for reasonable infrastructure and utility supply to the site (i.e., gas pipeline, cooling water, rail service, etc.), capital spares, start-up expenses and the like. On-site power generation for plant loads are also included.[4]

Further cost reductions are expected from improvements in the technology which are under development. There will also be normal "learning curve" benefits from commercial experience. Significant economies of scale are achievable with the Syntroleum Process, particularly in the air compression trains. Preliminary review of a "maximum train size" configuration indicates the likelihood of constructing a 20,000 to 25,000 BPD single-train facility for $12,000 to $14,000 per barrel of daily capacity. That is the roughly the same cost as a worldscale conventional refinery--a truly revolutionary development.

Because of the limited opportunities for large plants, Syntroleum's major goal in developing this technology has been to achieve low capital costs at relatively small scales. The company is confident that, with further development, designs will be available for the majority of the world's fields. At one end of the scale is a possible 500 BPD plant for isolated areas, justified by enabling the producer not only to monetize the gas that cannot be flared, but also to produce and sell the oil shut in by the inability to dispose of the associated gas. Syntroleum currently is working with a major company to adapt a design for a 2,000 to 2,500 BPD barge-mounted plant to be installed at a very remote location; the initial estimated cost is $55 million. At the other end of the scale is the possibility of a 100,000 BPD "natural gas refinery" in an industrial area. Between these two extremes there are myriad possibilities for tapping fields now beyond the commercial reach of gas markets.

Implications. For the energy industry, the Syntroleum Process offers a new option with potential application to a wide range of situations where current technology falls short. As the new technology is applied, there will be two immediate effects: (1) supply, with a giant boost in the size and diversity of the world's oil and gas reserves, and (2) financial, as stranded reserves are converted to booked assets on the ledgers of companies and countries that own them. Refiners and power plants will have another option to satisfy their need for cleaner fuels for themselves and their customers. Meanwhile, upstream, industry will completely re-evaluate its strategy--everything from how to retarget exploration to whether to abandon LNG and heavy oil projects or pursue them in conjunction with synfuels.

These are just a few of the possibilities. Oil and gas companies, examining their own project lists and strategies, will see many others. As always happens with any new technology, the users will find applications that the developers never thought of.

REFERENCES

[1] *Oil & Gas Journal, June 19, 1995, p. 37.*

[2] Ryan, Thomas W., III, and Daniel A. Montalvo, "Emissions and Performance of Fischer-Tropsch Diesel Fuels in a Modern Heavy Duty Diesel Engine." Southwest Research Institute paper, 1996.

[3] Ivanhoe, L. F., and George G. Leckie, *Oil & Gas Journal*, Feb. 15, 1993, p. 87.

[4] Manpower requirements, labor costs estimated by Process Technical Services, Houston, specialists in start-ups and contract plant operations.

[5] Compiled from data published by Shell and Syntroleum test data.

Table 1—Typical Properties of Fuel Feedstocks from Syncrude

Property	Test Method	Unit	Naphtha[5]	Kero./JetFuel[5]	Diesel[5]
Density @ 60 °F	ASTM D1298	lb/ft^3	43.6	46.0	48.7
Distillation range	ASTM D86				
IBP		°F	109	311	394
FBP		°F	381	376	676
Sulfur	ASTM D1266	ppm	n.d.	n.d.	n.d.
Cetane number	ASTM D976	—	n/a	58	76
Smoke point	ASTM D1322	mm	n/a	>50	n/a
Flash point	ASTM D93	°F	n/a	108	190
Aromatics	ASTM D5186	%V	n.d.	n.d.	n.d.

n.d. = not detectable/below detection limits; n/a = not applicable.

Table 2—Combustion Properties of Synthetic Diesel

Property	Synthetic Diesel[5]	CARB Specs	CEN Specs
Cetane number	76	48 min.	49 min.
Density (kg/m^3)	771	n/s	820-860
Sulfur (ppm)	n.d.	500	500 (1996)
Aromatics (%m/m)	n.d.	10 max.	n/s
Cloud point (°C)	-48	-5	n/s
CFPP (°C)	-2	n/s	+5 to -20*
Distillation			
90% recovery (°C)	340	288-338	
95% recovery (°C)	350		370 max.

* Depending on climatic band chosen; n/s = no specification; n.d. = not detectable/below detection limits.

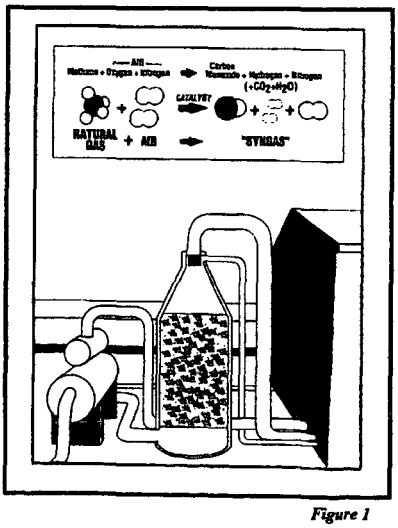

Figure 1

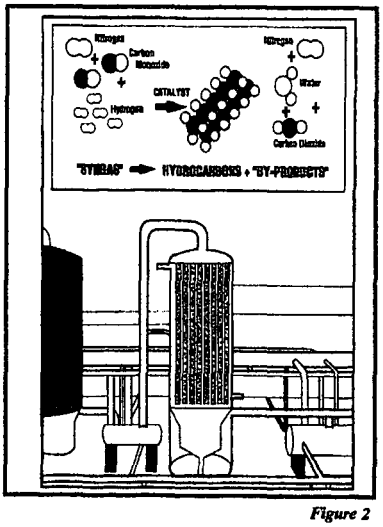

Figure 2

OPPORTUNITIES FOR EARLY COMMERCIAL DEPLOYMENT OF INDIRECT LIQUEFACTION

David Gray and Glen Tomlinson
MITRETEK
7525 Colshire Drive
McLean, Virginia 22102

KEYWORDS: Indirect coal liquefaction, Fischer-Tropsch Synthesis, Pioneer Plants.

Introduction:

Petroleum use worldwide is about 65 million barrels per day (MMBPD) and the Energy Information Administration (EIA) predicts that by 2015, worldwide demand will increase to between 89 and 99 MMBPD[1]. Over 55 percent of world petroleum is used in the transportation sector. Liquid hydrocarbon fuels are ideal for transportation since they are convenient, have high energy density, and a vast infrastructure for production, distribution, and end use is already in place. The estimated ultimate world resource of oil and natural gas liquids (NGL) is 2.5 trillion barrels; the sum of 1.2 trillion barrels for OPEC and 1.3 trillion barrels for non-OPEC[1]. Estimates of proven reserves of oil vary over time because more of the oil *resource* moves into the *reserve* category as a result of variations in the world oil price (WOP) and available technologies. However, the estimated ultimately recoverable world conventional oil resource (EUR) has been remarkably similar for the last 25 years. James MacKenzie of the World Resources Institute[2] cites an analysis of 40 estimates of ultimately recoverable oil, for the years 1975 to 1993, conducted by David Woodward of the Abu Dhabi Oil company. In this analysis, Woodward concluded that " there is a fair degree of consistency among the estimates with the average being 2,000 billion barrels (BBO) and 70 percent falling in the range of 2,000 to 2,400 BBO."

Mitretek has performed analyses of world oil demand and potential supply from the present until the year 2100[3]. The results of these analyses show that when the projected world oil demand is plotted on the ultimate resource curve, it becomes clear that conventional world oil production is likely to peak in a timeframe from about 2015 to 2020 and then irreversibly decline because of resource limitations.

Since oil is the primary fuel for the transportation sector, Mitretek has also examined the potential impact of the above world oil supply scenario on the U.S. transportation sector[3]. This analysis concludes that, even with a rapid penetration schedule for alternatively fueled vehicles, there is likely to be a significant shortfall in petroleum supply in the United States before 2015.

It is, therefore, essential to simultaneously pursue a number of options to mitigate the future domestic petroleum shortfall. These options are: to continue domestic exploration and production using the best technologies available, to continue to develop and deploy alternative fueled vehicles, and to continue to improve efficiencies in all sectors of transportation. Yet, even with all these efforts, this analysis indicates that the domestic demand for liquid fuels will exceed our potential sources of supply. Continuing to increase our reliance on oil imports to alleviate the shortfall is not a long term solution. Rapidly increasing oil demand worldwide will put ever increasing pressure on oil supply and the WOP will rise. The inevitable conclusion is that additional options will be necessary to insure that the U.S. will have the necessary liquid fuels supply to be able to continue its economic growth into the 21 st century. One of these additional options is to produce liquid fuels from our huge domestic coal resources.

Proposed Strategy to Deploy Indirect Coal Liquefaction:

It is estimated that continued R&D in indirect coal liquefaction can reduce the cost of coal-derived fuels from $34 per barrel to about $27 per barrel for a grass-roots stand-alone coal liquefaction facility. However, there is the opportunity to deploy indirect

liquefaction plants at existing facilities, for example petroleum refineries and IGCC facilities, and greatly reduce costs. These plants integrated with existing facilities are called "entrance plants" and preliminary economic analysis has shown that they can be competitive with crude at around $19-23 per barrel. This observation that "entrance plants" have the potential to be competitive with petroleum in the short term presents an opportunity for the early commercialization of coal liquefaction. They also provide a technology bridge to the eventual deployment of stand-alone coal liquefaction facilities. However, private investors and process developers are not likely to design and construct an "entrance plant" until both technical and economic risks are acceptable. Continued bench-scale and proof-of-concept testing of indirect liquefaction technology will result in sufficient data to design and construct pioneer plants. These pioneer plants are small-scale commercial plants that will demonstrate the ability to scale the integrated technologies and thus reduce both the technical and economic risks. Once these risks have been shown to be acceptable by successful operation of pioneer plants, larger "entrance plants" would be constructed and deployed. Eventually, when the most appropriate sites for "entrance plants" have been utilized and the technologies have continued to mature and improve, stand-alone, grass-roots commercial facilities will be deployed.

Pioneer plants will be necessary to reduce technical and economic risks and allow "entrance plants," and eventually stand-alone commercial plants to be deployed. For indirect liquefaction, the pioneer plant is assumed to be located adjacent to an existing petroleum refinery and uses petroleum coke as feed to a gasification/gas cleaning plant to produce clean synthesis gas. In the simplest case, petroleum coke would probably be used as the feed but, if the plant is to be increased in size, coal can be introduced into additional gasifiers. Because the pioneer plant is located adjacent to a refinery, it is assumed that the plant will utilize some of the existing refinery facilities. In this case it is assumed that acid gas from the gas cleaning section can be processed in the existing refinery Claus unit for sulfur recovery. Also the refinery is assumed to process the waste water from the pioneer plant. The clean synthesis gas from petroleum coke gasification is passed once-through a slurry Fischer-Tropsch reactor to produce liquid fuels that are recovered in product separation, and the tail gas is sent to power generation. The pioneer plant sells electric power to the refinery and the liquid fuels are sent over the fence to the refinery for upgrading and blending. In the configuration analyzed here, 3,500 BPD of naphtha, diesel, and wax are produced together with 42 MW of power. Further additions to this pioneer plant could include pressure swing absorbers (PSA) so that hydrogen could be sold to the refinery in addition to power. The F-T unit enhances the refiner's ability and flexibility to make high value products by synthesizing high quality diesel and naphtha. The F-T diesel can be blended with FCC cycle oils to produce high cetane fuel and the naphtha can be blended in the gasoline pool or, since F-T naphtha is an excellent feed, cracked to give ethylene. The wax can be fed to a catalytic cracker to produce more high value diesel and naphtha.

Another example of a pioneer plant configuration for indirect liquefaction is one that could be located at an existing IGCC plant. The additional units required include a polishing reactor for residual sulfur removal, the F-T reactor, product recovery, and a cracker for the wax product. In this case, the IGCC plant would coproduce about 4,200 BPD of fuels in addition to 250 MW of power. Because the synthesis gas from the coal gasifier is now being fed to the F-T unit, natural gas must be imported for combustion in the gas turbines to keep the power output at 250 MW. The synthesis gas is passed once-through the F-T reactors and the tail gas, after product separation is used in the turbines. As the future cost of natural gas increases, it would be less expensive to add additional coal gasifiers and phase out use of the natural gas.

There are both technical and economic risks associated with the design, construction, and operation of the pioneer plant configurations outlined above. The desired strategy is to minimize federal government expenditures in the deployment of these technologies. For this to happen, the private sector must feel confident enough to take the initiative in deployment. If the commercial sector is to take the lead in this deployment, both types of risk must be acceptable. The objective of the pioneer plant concept is to bring the level of risk into an acceptable regime so that commercial entities will continue deployment

through future "entrance" and stand-alone facilities. The government (federal or state) must encourage the private sector to finance the design, construction, and operation of the pioneer plants by providing financial incentives that will allow the products to yield an acceptable return on the investor's capital.

For the indirect pioneer plant located adjacent to the refinery a detailed economic analysis has been performed. It is shown that adequate return on investment can be obtained for these plants if it is assumed that these high quality F-T liquids can command a premium of 20 cents per gallon ($8.40 per barrel) over conventional petroleum. If the average of the nation's state fuel tax (17 cents per gallon) is exempted, effectively making the total incentive 37 cents per gallon, then the ROE rises to over 20 percent. If both state and federal fuel taxes are exempted, then a ROE of over 25 percent would be realized from this investment. Exemption of fuel taxes would appear to result in a net loss in revenue to the government. However, although this is true for the first few years of plant operation, this is generally not so if revenues over the entire 25 year life of the plant are considered. Once the pioneer plant is constructed and operating, the objectives would be for this plant to, not only confirm proof-of-concept integrated operations so that the technical risk is reduced, but also to operate for 25 years as a commercial entity so that the investors would reap the expected ROE. Even if the WOP remains at the low level of projection ($16 per barrel) for the life of the plant, taxes accruing to the government are greater than the cost of incentives to the government. The net result is that in all of these cases the government's net revenue is positive.

Conclusion:

It is concluded that domestic coal is a viable future alternative feedstock to petroleum for the production of high quality transportation fuels that are compatible with the existing liquid fuels infrastructure. These fuels are high quality distillates that in many cases are higher quality than current petroleum fuels. It is recommended that the current program of research and development be continued and extended so that sufficient performance data can be obtained for the design of "pioneer" plants. These plants would be located adjacent to existing facilities, for example, refineries or IGCC plants, and would be operated to demonstrate the integrated technical feasibility of the configurations. These plants would be constructed with private capital and, although incentives may be provided by state or the federal government, net revenues to the government, over the life of the plant, as a result of taxes on net profits would be positive. Once technical risks have been reduced as a result of "pioneer" plant operations, the continued deployment of coal liquefaction technologies would proceed with no further government involvement based on economic feasibility under market conditions.

This project is funded by the United States Department of Energy under contract number DE-AC22-95PC95054.

References:

1) Annual Energy Outlook 1996 With Projections to 2015. Energy Information Administration January 1996. DOE/EIA-0383(96).
2) MacKenzie, James J., *Oil as a Finite Resource: When is Global Production Likely to Peak?* Paper from the World Resources Institute March 1996.
3) Gray, David, and Glen Tomlinson, *Rationale and Proposed Strategy for Commercial Deployment of Coal-Derived Transportation Fuels,* Mitretek Report MP 96W0000209, June 1996.

CAN CARBON DIOXIDE BE REDUCED TO HIGH MOLECULAR WEIGHT FISCHER-TROPSCH PRODUCTS?

Imre Puskas
Research Services, 939 Brighton Drive
Wheaton, IL 60187. Tel.(630) 653-4897

Keywords: clean fuel production, carbon dioxide, Fischer-Tropsch products, methanol, remote natural gas.

INTRODUCTION.

Our interest in the title originates from our efforts to develop an economically viable clean fuel process from natural gas. Natural gas, with its high calorific value (210.8 kcal/g-mol methane) is one of the most preferred fuels from the environmental point of view because of its clean burning characteristics. However, natural gas found in remote areas, far from markets, inaccessible to pipeline transportation, cannot be readily utilized. Currently several alternatives are practiced for remote natural gas utilization (1). Natural gas can be liquified by cooling to its boiling point (-163^{0}C) and shipped in refrigerated containers. Natural gas can also be converted to methanol or hydrocarbon liquids (syncrude) or ammonia at its source, and these products shipped to market.

Both methanol and the Fischer-Tropsch (FT) hydrocarbon liquids are "clean fuels". Their fuel uses have been evaluated (2,3). Currently they cannot compete with the less expensive crude oil-derived fuels. Methanol commands a higher price as a "chemical", but this market is relatively small (estimated 27 MM tons per annum, worldwide) compared to the huge fuel market. Increasing percentage of the methanol production originates from remote gas using giant plants (800-975 M ton/annum capacity), taking advantage of the low gas costs and the economics of large scale production. Historically, the methanol market can be characterized by periods of shortages and periods of overproduction and low capacity utilization. Recently we proposed the development of a methanol-syncrude coproduction technology (4) which could keep the methanol plants running at full capacity even in case of methanol oversupply. The co-production scheme of Figure 1 would provide both economic and technological advances. In the first step, the compressed synthesis gas would be partially converted to methanol. This reaction has equilibrium limitations. The unconverted syngas from the methanol reactor would be converted to hydrocarbons. This latter reaction has no equilibrium limitations. We are currently working on the details of a research and development plan to demonstrate the viability of a co-production technology. The key to success depends on the demonstration that the effluents of the methanol reactor (a mixture of H_2, CO and CO_2) can be efficiently converted to high molecular weight FT products. The percieved difficulty is caused by the presence of carbon dioxide, which is known to yield preferentially methane rather than high molecular weight FT products in reductions (5). This study was undertaken to provide a stimulus for the development of a methanol-syncrude coproduction technology. Reported cases of carbon dioxide reductions to reasonably high molecular weight FT products already exist. The study should be helpful to set the stage for further progress.

HISTORICAL OVERVIEW OF CARBON DIOXIDE REDUCTIONS.

The reactions, utilization and sources of carbon dioxide have recently attracted considerable interest because of the possible ecological effects arising from large scale carbon dioxide emissions into the atmosphere. An information update is provided in very recent reviews by Xiaoding and Moulijn (6) on CO_2 reactions and usage; by Krylov and Mamedov (5) on its heterogeneous catalytic reactions; by Jessop, Ikariya and Noyori (7) on its homogeneous catalytic hydrogenations; by Tanaka on its fixation catalyzed by metal complexes (8); and by Edwards on its potential sources and utilizations (9). One of the most important reactions of carbon dioxide is its reduction to methanol:

$$CO_2 + 3H_2 \xrightarrow{\text{Cu-ZnO, 200-260}^0\text{C, 5-10 MPa}} CH_3\text{-OH} + H_2O \qquad [E\text{-}1]$$

Although carbon dioxide has been reduced to methanol in the past in commercial operations (10,11), current methanol plants use mixtures of carbon dioxide and carbon monoxide. An alternative potential use of carbon dioxide would be its complete reduction to methane or to mixtures of Fischer-Tropsch type hydrocarbons:

$$CO_2 + 4H_2 \xrightarrow{\text{Ni (or Co, Fe, Ru), } 250\text{-}400^0C} CH_4 + 2H_2O \qquad [E\text{-}2]$$

$$nCO_2 + 3nH_2 \xrightarrow{\text{Fe or Co (Ru, Ni), } 200\text{-}300^0C} (CH_2)_n + 2nH_2O \qquad [E\text{-}3]$$

Franz Fischer and coworkers were the first to try to reduce carbon dioxide to hydrocarbon oils, after their development of hydrocarbon synthesis from carbon monoxide. They have found, that carbon dioxide gives preferentially methane, with some gaseous homologues (12). However, liquid and solid hydrocarbons were also obtained in some experiments (13). These early reports have noted, that carbon monoxide was a reaction intermediate (12) and that liquid hydrocarbons were observed in those experiments, when the catalyst was alkalized or it contained a Cu component (13).

In the last decades, many chemists and surface scientists have extensively studied the reduction of carbon dioxide to hydrocarbons and the chemisorption of carbon dioxide on catalytic surfaces. It is out of the scope of this study to review the literature. However, a restricted number of references are cited (14-35) to sample the diversity of worldwide interests. The citations exclude the literature on carbon dioxide reductions to hydrocarbons which proceed via methanol intermediate.

The cited studies unanimously agree with the early conclusions that carbon monoxide is an intermediate formed by the reverse Water Gas Shift (WGS) reaction:

$$CO_2 + H_2 \underset{}{\overset{\text{catalyst}}{\rightleftharpoons}} CO + H_2O \qquad [E\text{-}4]$$

The reduction of carbon monoxide proceeds by the methanation reaction or FT synthesis. Falconer and Zagli have proposed (34) that the preferential formation of methane over higher hydrocarbons is caused by the high H_2:CO ratio on the catalyst surface. While the major product was methane in most of the studies, a few cases of liquid hydrocarbon formation were also reported. Table 1 compiles the best examples of higher hydrocarbon formations. In the Table, we have converted the reported hydrocarbon selectivity data to Anderson-Schulz-Flory (ASF) growth probability values (alphas) to provide a basis for easy comparison of the product molecular weight distributions. ASF alpha values in the 0.6-0.7 range have been achieved, mostly on potassium-promoted Fe catalysts. Kuester (13) has evaluated different variations of unsupported, alkalized Co and Fe catalysts. In their work, reported in 1936, the formation of solid hydrocarbons (waxes) was often observed. Unfortunately, the reported product analyses were qualitative in nature and we were unable to derive chain growth probability values for product characterization. However, the isolation of waxes suggests that the chain growth probability values must have been substantially higher than 0.70, and probably were the highest in Table 1. In the penultimate example of Table 1, the primary olefinic products were converted to aromatic hydrocarbons over the ZSM-5 component of the catalyst. The last example of Table 1 is a case of higher hydrocarbon formation over Rh/Nb_2O_3. This appears to be an interesting case, since Rh is not known for FT catalysis.

In order to understand better how CO_2 reduction can be channeled toward higher hydrocarbon formation, relevant fundamental knowledge on the WGS and FT reactions will be reviewed and discussed below.

THE REVERSE WATER GAS SHIFT REACTION STEP.

The reduction of carbon dioxide to carbon monoxide, known as the reverse WGS reaction [E-4], has been extensively studied (36-39) because of its industrial importance in synthesis gas reactions and hydrogen manufacture. The most efficient heterogeneous catalysts for the WGS reaction are the Cu-based

catalysts, particularly Cu-Zn systems, the iron oxide based catalysts and the alkalized, sulfided Co-Mo catalysts (39). Other metals, oxides also have some catalytic effect, but they have received much less attention. However, alkalization was found to increase substantially the WGS activity of many substances (39). The alkalized FT catalysts have been extensively studied (13,40-43). Their WGS activity has been long known, but most of the cited studies focussed on the effect of alkali promotion on the changes in the rate and the products of the FT reaction. The alkalized FT catalysts seem to be excellent candidates for the reduction of carbon dioxide to FT hydrocarbons as the examples of Table 1 also suggest. Surface scientists have found (44-45) that alkalization of FT catalysts changes the relative chemisorptions of CO and H_2 and that alkalization activates the surfaces for CO_2 chemisorption (24,46).

Carbon dioxide hydrogenation to carbon monoxide [E-4] is a reversible reaction and leads to equilibrium. The equilibrium is independent of the pressure, but is very much influenced by the temperature. In the temperature ranges useful for the FT reaction, the equilibrium is not favorable. Figure 2 illustrates the equilibrium CO_2 conversions as a function of the temperature for 1:1, 3:1 and 4:1 H_2:CO_2 gas compositions. Higher CO_2 conversion can be obtained if the H_2 reagent is used in stoichiometric excess. The equilibrium will be also favorably shifted if the CO is removed from the system. This happens during reductions to the hydrocarbon stage.

THE FISCHER-TROPSCH REACTION STEP.

The FT reaction (E-3) has been very extensively studied because of its commercial significance and because of its scientific complexity and diversity. This brief review will be restricted to certain aspects of FT chemistry which are relevant to our objectives.

In first approximation, the products of the FT synthesis are defined by a single parameter, the chain growth probability (α or alpha) according to the ASF equation:

$$C_n = (1n^2\ \alpha)n\ \alpha^n \qquad \text{(E-5)}$$

where C_n is the carbon selectivity (mass fraction in the ideal case when the products are olefins) of the product with n carbon number and α is the chain growth probability. In practice, a multiplicity of α-s is produced, but an "averaged α" still reasonably defines the products unless the range of the α-s is very broad (47). Deviations from the AFS distribution have been widely reported. Some of the deviations are predictable and well defined (48); others, notably the C1 selectivities, are not well defined.

For the purpose of this treatment, it is proposed, that methanation (E-2) is an extreme case of the FT reaction (E-3) when the chain growth probability value is zero or very low. This understanding seems to be supported by the numerous reports that small amounts of ethane and propane are usually also observed during methanation. The methanation catalysts are very active hydrogenation catalysts, and they hydrogenolize the metal-C1 intermediates on the catalyst surface before they could grow. Furthermore, the methanation catalysts can also hydrogenolize the higher hydrocarbons already formed, which reactions also produce methane. Because of these reactions, the ASF equations may increasingly fail to define the product distributions as the chain growth probability value decreases.

Recently we have proposed for Co/SiO_2 catalysts (47), that the chain growth probability is a function of the catalyst, of the reagent and inert concentrations and of the temperature of the catalyst surface:

$$\alpha = f(C, S_1, \ldots, S_i, T) \qquad \text{(E-6)}$$

Even though the function f cannot be defined, it may be beneficial to review our qualitative knowledge about the factors which together should define α. In E-6, C is the catalyst factor which is composed of numerous elements. The catalytic metal is important. Co, Fe and Ru are known to be able to produce very high α values. There are reports in the literature (49-51)

suggesting that the dispersion of the metal can influence chain growth. Promoters incorporated into the catalysts can also influence chain growth. Alkali metal salts, particularly K salts, were found to greatly increase chain growth (13,40-43). In addition, alkalization had a tremendous influence on the reaction characteristics by changing the relative strengths of H_2, CO and CO_2 chemisorptions. The hydrogenating character of the catalyst was reduced by alkalization, resulting in high olefin yields.

In E-6, $S_1,...S_i$ represent the concentrations of the reagents and inerts (including products). The question is how to define these concentrations in light of the knowledge, that in most FT reactions diffusion controls the rates (47). Due to complex diffusion effects, the concentrations of the components in the immediate vicinity of the catalyst surface might be quite different, than their concentrations in the bulk gas phase. To eliminate the need for considering diffusion effects, $S_1,...S_i$ concentrations represent the concentrations of components A to Z in the immediate vicinity of the catalyst surface. The values of $S_1,...S_i$ are related to their respective bulk gas phase concentrations and are dependent on the prevailing diffusional conditions. Of course, their values can be changed by changing the pressure of the system. Qualitative examples on the influence of component concentration, pressure, diffusion on the chain growth probability are available in the literature. Thus, increasing H_2:CO ratio was shown to give lower alpha values (47). Dilution of the feed with inert gases was also shown to result in lower chain growth probability (47). Diffusional changes were also suggested for observed changes in rate and chain growth probability (52).

The influence of the reaction temperature (T) on the value of the chain growth probability has been long known. Recently we have shown, that over Co catalysts, the alpha value sharply decreases with increasing T (47). Over alkalized Fe catalysts, as reviewed by Dry (43), the effect of T appears to be much more gradual. With these catalysts, chain growth probability of about 0.7 can be obtained even over 300°C. In Table 1, we can see an example of 0.72 chain growth probability from CO_2 reduction at 400°C over a "heavily alkalized" Fe catalyst.

CATALYST AND PROCESS DESIGN REQUIREMENTS.

From the above review it is clear, that a combination of appropriate catalyst design and process design is required for obtaining high molecular weight FT products in CO_2 reductions. The catalyst must contain a WGS component and a FT component. The WGS component must provide fast rates for CO formation and accumulation. Furthermore, the surfaces must be modified for obtaining a proper balance in the chemisorptions of CO_2, CO and H_2. Concerning the process design, the process parameters (T, P, SV, feed composition) need to be optimized for the individual catalyst to provide the most favorable H_2:CO ratios on the catalyst surface for high molecular weight FT products. Conceptually, diffusion control might also serve to regulate the H_2:CO ratio. If gas phase diffusion controls the reagent concentrations on the catalyst surface, the surface is expected to be enriched in hydrogen, because of its high diffusivity arising from its small molecular size [52]. If diffusion through liquids were to control the reagent concentrations on the catalyst surface, the excessive hydrogen concentration on the catalyst surface may be avoided, due to differences in the solubilities of the reagents in hydrocarbon liquids [53]. We are optimistic that utilization of knowledge in catalyst and process design will lead to significant increases in the ASF growth probability values during CO_2 reductions.

REFERENCES.

1 J.M. Fox, Catal.Rev.-Sci.Eng., 35 (1993) 169.
2 M.D. Jackson and C.B. Moyer in Encyclopedia of Chemical Technology, 4th Ed., Vol 1, p.826. Wiley, New York, 1991.
3 P.J.A. Tijm, ACS Fuel Division Preprints, 39 (1994) 1146.
4 I. Puskas, Chemtech, December 1965, p.43.
5 C.V. Krylov, A.Kh. Mamedov, Rus.Chem.Rev., 64 (1995) 877.

6 X. Xiaoding, J.A. Moulijn, Energy&Fuels 10 (1996) 305.
7 P.J. Jessop, T. Ikariya, R. Noyori, Chem.Rev., 95 (1995) 259.
8 K. Tanaka in Advances in Inorganic Chemistry, Ed. A.G. Skyes, Vol. 43, p. 409. Academic Press, San Diego, 1995.
9 J.H. Edwards, Catal.Today, 23, 59 (1995).
10 M.L. Kastens, J.F. Dudley, J. Troeltzsch, Ind.Eng.Chem., 40 (1948) 2230.
11 Anonymous, Chem.Eng., February 11, 1980, p. 49.
12 H. Kuester, Brennst.Chem., 17 (1936) 203.
13 H. Kuester, Brennst.Chem., 17 (1936) 221.
14 P.H. Choi, K-W. Jun, S-J Lee, M-J Choi and K-W Lee, Catal. Lett., 40 (1996) 115.
15 J.A. Fisher and A.T. Bell, J.Catal., 162, (1996) 54.
16 G. Froehlich, U. Kestel, J. Lojewska, T. Lojewski, G. Meyer, M. Voss, D. Borgmann, R. Dziembaj, G. Wedler, Appl.Catal., A134 (1996) 1.
17 S. Mori, W-C. Xu, T. Ishidzuki, N. Ogasawara, J. Imai, K. Kobayashi, Appl.Catal., A137 (1996) 255.
18 K-W Jun, S-J Lee, M-J Choi, K-W Lee, ACS Fuel Division Preprints 41 (1995) 1411.
19 Y. Huang, X. Meng, Z. Dang, S. Weng and C. Zhang, J.Chem.Soc. Chem.Commun., 1995, p. 1025.
20 Y. Kou, Z-h. Suo, J-z. Niu, W-z. Zhang, H-l. Wang, Catal.Lett., 35 (1995) 271.
21 U. Kestel, G. Froehlich, D. Bergmann, G. Wedler, Chem.Eng. Techn. 17 (1994) 390.
22 J-F. Lee, F-S. Chern, M-D. Lee and T-Y Dong, Can.J.Chem.Eng., 70 (1992) 511.
23 T. Kai, T. Matsumura, T. Takahashi, Catal.Lett., 16 (1992) 129.
24 F. Solymosi, J.Mol.Catal., 65 (1991) 337.
25 T. Inui, T. Takeguchi, Catal.Today, 10 (1991) 95.
26 T. Suzuki, K. Saeki, Y. Mayama, T. Hirai, S. Hayashi, React. Kinet.Catal.Lett., 44 (1991) 489.
27 C-K. Kuei, M-D. Lee, Can.J. Chem. Eng., 69 (1991) 347.
28 M-D Lee, J-F Lee, C-S. Chang, Bull.Chem.Soc.Jpn., 62 (1989) 2756.
29 F. Nozaki, T. Sodesawa, S. Satoh, K. Kimura, J.Catal., 104 (1987) 339.
30 K.R. Thampi, J. Kiwi, M. Graetzel, Nature, 327 (1987) 506.
31 A.D. Thomsett, T. Hagiwara, A. Miyamoto, T.Inui, Appl. Catal., 26 (1986) 391.
32 G.D. Weatherbee, C.H. Bartholomew, J.Catal., 87, (1984) 352.
33 J. Barrault, C. Forquy, J.C. Menezo, R. Maurel, React.Kinet. Catal. Lett., 17 (1981) 373.
34 J.L. Falconer, E. Zagli, J.Catal., 62 (1980) 280.
35 D.J. Dwyer, G.A. Somorjai, J.Catal., 7 (1978) 291.
36 C.V. Ovesen, B.S. Clausen, B.S. Hammershoi, G. Steffensen, T. Askgaard, I. Chorkendorff, J.K. Norskov, P.B. Rasmussen, P. Stoltze, P. Taylor, J.Catal., 158 (1996) 170.
37 C. Rhodes, G.J. Hutchings, A.M. Ward, Catal.Today, 23 (1995) 43.
38 S-I. Fujita, M. Usui, N. Takezawa, J.Catal., 134 (1995) 220.
39 D.S. Newsome, Catal.Rev.-Sci.Eng., 21 (1989) 275.
40 D.B. Bukur, D. Mukesh, S.A. Patel, Ind.Eng.Chem.Res., 29 (1990) 194.
41 L. Koenig, J. Gaube, W. Meisel, P. Guetlich, W. Gerhard, C. Plog, Ber.Bunsenges.Phys.Chem., 91 (1987) 116.
42 G. Henrici-Olive, S. Olive, J.Mol.Catal., 16 (1982) 116.
43 M.E. Dry in Catalysis Science and Technology, J.R. Anderson and M. Boudart, Eds., Springer Verlag, Berlin, 1981, Vol 1, p.159.
44 M.E. Dry, T. Shingles, L. Boshoff, G.J. Oosthuizen, J.Catal., 15 (1969) 190.
45 J. Benzinger, R. Madix, Surf.Sci. 94 (1980) 119.
46 G. Meyer, D. Borgmann, G. Wedler, Surf.Sci., 320 (1994) 123.
47 R.S. Hurlbut, I. Puskas, D.J. Schumacher, Energy&Fuels, 10 (1996) 537.
48 I. Puskas, R.S. Hurlbut, R.E. Pauls, J.Catal., 139 (1993) 591
49 A.S. Lisitsyn, A.V. Golovin. V.L. Kuznetsov, Yu.I. Yermakov, Cl Mol.Chem., 1 (1984) 115.
50 K. Fujimoto, T. Nobusawa, T. Fukushima, H. Tominaga, Bull. Chem.Soc.Jpn., 58 (1985) 3164.
51 C.S. Kellner, A.T. Bell, J.Catal., 75 (1982) 251.
52 I. Puskas, B.L. Meyers, J.B. Hall, Catal.Today, 21 (1994) 243
53 J.S. Chou and K-C. Chao, Ind.Eng.Chem. Res., 31 (1992) 621.

Table 1. Reported Examples of Carbon Dioxide Reductions to Higher FT Hydrocarbons.[a]

Catalyst	T (°C)	P (kPa)	% CO_2 conversion[b]	α value[c]	Reference
Fe-K/Al_2O_3	400	2026	69.6; 66.9	0.72	14
Fe-K/Al_2O_3	300	1013	57.7; 50.4	0.66	18
Fe-Mn-K	320	1013	33.8; 29.0	0.56	22
Fe-K	320	1013	34.7; 28.4	0.65	28
Fe-Cu-KCl/ TiO_2-Al_2O_3	270	1520	10.0; 5.3	0.68	33
Co,Fe-Cu,K	150-250	101	?	see text	13
Fused Fe-ZSM-5	350	2100	38.1; 32.6	see text	27
Rh/Nb_2O_5	350	101	11; 10	0.21	29

[a]The H_2/CO_2 feed ratios varied between 4:1 and 1:1.
[b]The first number gives the total conversion (CO + hydrocarbons); the second number the conversion to hydrocarbons.
[c]Our best estimates of the chain growth probabilities from the reported data, unless provided in the publication.

Figure 1. Conceptual Methanol-Syncrude Coproduction Scheme.

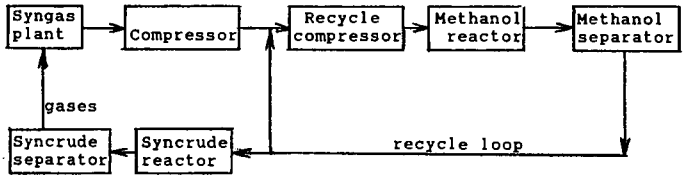

Figure 2. CARBON DIOXIDE CONVERSIONS IN REVERSE WGS EQUILIBRIA

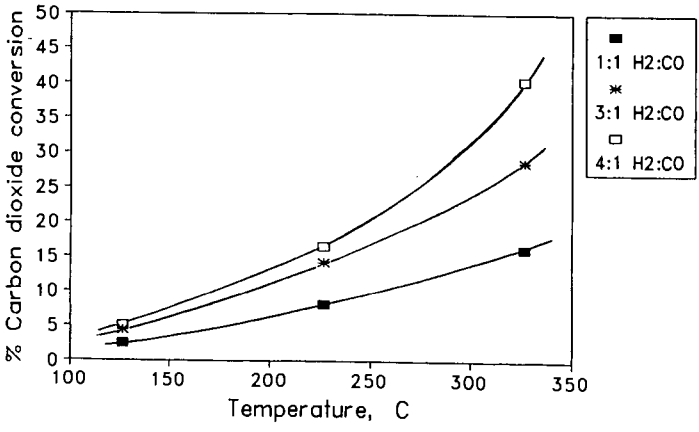

Table 1. Reported Examples of Carbon Dioxide Reductions to Higher FT Hydrocarbons.[a]

Catalyst	T (°C)	P (kPa)	% CO_2 conversion[b]	α value[c]	Reference
Fe-K/Al_2O_3	400	2026	69.6; 66.9	0.72	14
Fe-K/Al_2O_3	300	1013	57.7; 50.4	0.66	18
Fe-Mn-K	320	1013	33.8; 29.0	0.56	22
Fe-K	320	1013	34.7; 28.4	0.65	28
Fe-Cu-KCl/ TiO_2-Al_2O_3	270	1520	10.0; 5.3	0.68	33
Co,Fe-Cu,K	150-250	101	?	see text	13
Fused Fe-ZSM-5	350	2100	38.1; 32.6	see text	27
Rh/Nb_2O_5	350	101	11; 10	0.21	29

[a]The H_2/CO_2 feed ratios varied between 4:1 and 1:1.
[b]The first number gives the total conversion (CO + hydrocarbons); the second number the conversion to hydrocarbons.
[c]Our best estimates of the chain growth probabilities from the reported data, unless provided in the publication.

Figure 1. Conceptual Methanol-Syncrude Coproduction Scheme.

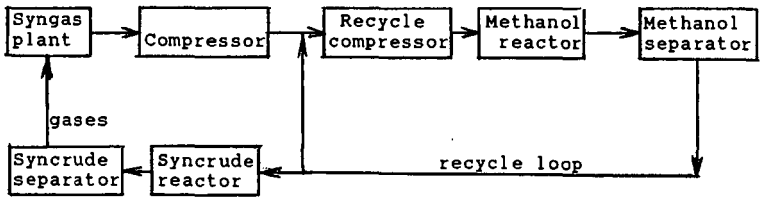

Figure 2. CARBON DIOXIDE CONVERSIONS IN REVERSE WGS EQUILIBRIA

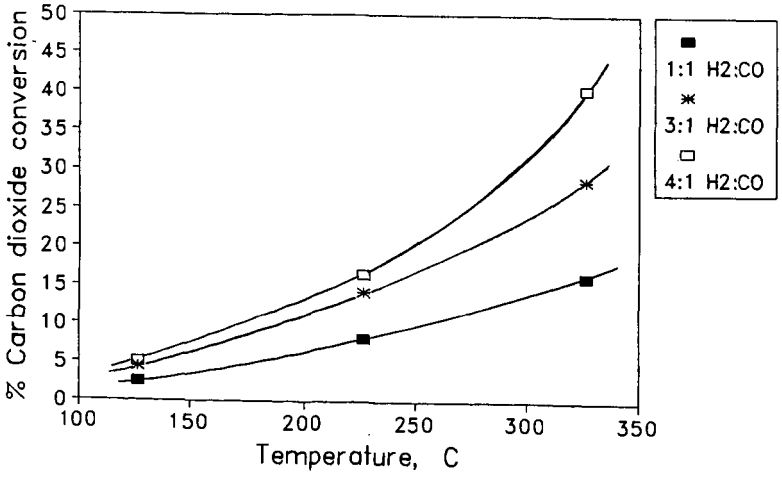

IMPROVED DIMETHYL CARBONATE SYNTHESIS AND PROCESS DESIGN VIA OXIDATIVE CARBONYLATION OF DIMETHYL ETHER METHANOL MIXTURES.

Gary P. Hagen, Arun Basu, Michael J. Spangler, and Michael A. Pacheco
Amoco Corporation
Amoco Research Center
Naperville, Illinois

Keywords: dimethyl carbonate synthesis, dimethyl ether, process design

INTRODUCTION

Enichem has commercialized a continuous solution/slurry-phase process for preparation of dimethyl carbonate (DMC) via the copper (II)-catalyzed oxidative carbonylation of methanol.[1] As of 1993 the capacity of this plant is 22 million pounds/year with worldwide demand approximately half of this amount. Recently in Japan Ube industries has completed construction of a semicommercial plant with a capacity of 11-22 million pounds per year.

DMC has strong growth potential as a phosgene replacement in some applications and as a high-oxygen high-octane fuel additive . As a phosgene replacement, there is a strong environmental incentive to use DMC since it would replace a very toxic compound with a relatively nontoxic one and eliminate environmental concerns resulting from hydrogen chloride production and recycle.

DMC also has strong potential to replace part of the growing worldwide MTBE market, which is expected to reach 66 billion pounds/year by the end of the century. As a gasoline blending agent, DMC has an oxygen content of 53% and a blending octane value of 105 (R+M/2), and these high values dictate a somewhat higher overall value for DMC in comparison to MTBE.

The key to entering this market and the phosgene replacement market lies in the development of an efficient low-cost DMC process based on inexpensive starting materials. Its current cost of $1.40/lb (non-contract) is prohibitively expensive. There are inherent problems in the Enichem process which limit per-pass methanol conversion to about 20% as the result of coproduction of water. This coproduction also results in catalyst degradation/deactivation and hardware corrosion. Production rates of 0.1 LHSV are reported for this system. Similar problems also exist in gas-phase processes such as that developed by Dow Chemical which utilize a copper (II) catalyst supported on carbon. Catalyst modifications have reportedly solved some the deactivation problems but methanol conversion is still limited to about 25%.

BACKGROUND AND OBJECTIVES

Liquid and gas-phase processes for synthesis of DMC via Cu(II)-catalyzed oxidative carbonylation of methanol (MeOH) offer limited reactor performance as the result of the effects of water formed as a coproduct.[2] Reactor water inhibits the catalytic reaction and limits reactant conversion to 30-40%. In halide-containing fixed bed catalyst systems water leaches halide away from the catalyst resulting in long-term deactivation and excessive corrosion of metallic reactor and downstream hardware components. A major goal of this project is to limit water formation and improve gas-phase reactor performance by incorporation of dimethyl ether (DME) as a dehydrated methanol equivalent into the reactor feedstream. DME is less expensive to produce than MeOH on a methanol-equivalent basis and its oxidative carbonylation to DMC would not produce water as a coproduct.

RESULTS AND DISCUSSION

A catalyst consisting of $CuCl_2$/C (Darco-active carbon), known to be active for the oxidative carbonylation of methanol/CO to DMC was found to be inactive for oxidative carbonylation of DME. At all conditions tested, low levels of CO_2 was the only product detected. A catalyst consisting of $CuCl_2$/AMSAC (an acidic molecular sieve) was also inactive and produced significantly more CO_2, suggesting that the sieve-supported Cu(II) species was more of a deep oxidation catalyst than the C-supported material. In the presence of a small amount of water

added to promote initial hydrolysis of DME to methanol, the sieve-based catalyst generated a significant amount of MeOH in addition to the CO_2 but no DMC product. A third catalyst, consisting of an admixture of $CuCl_2$/C and AMSAC was tested with DME/water feed. In this case methanol was formed but with no DMC production. Very little CO_2 was formed with this catalyst so returning the Cu(II) to the carbon support eliminated the deep oxidation activity.

Productive results were obtained with the admixture catalyst and with a DME/MeOH cofeed consisting of DME/MeOH/CO/O_2 (1/1.1/7.2/1.2 mole ratio). Throughout a 1100-minute test, carried out at 126°C, conversion of DME was steady at 30-33%. Methanol conversion was **negative**, at -20% to -30%, thus indicating net production of methanol via hydrolysis of DME. Two principle products, DMC and dimethoxymethane (DMM), were formed, each in about 50% selectivity, and methyl formate and methyl chloride were observed in trace quantities. The net conversion of the total methoxy functionality (CH_3O) in the feed to take into account the negative conversion (or production) of methanol has been calculated. This value ranged from 10-16% over the course of the study. To our knowledge this finding represents the first known net conversion of DME to DMC in an oxidative carbonylation reaction.

The high production of DMM in this study was not anticipated. The formation of this compound, the dimethyl acetal of formaldehyde, suggests that some of the methanol has undergone conversion to formaldehyde and subsequently reacted with methanol to form the acetal. Acidic molecular sieves are well known catalysts for acetal formation, and this reaction would be heavily favored in a low-water reaction environment.

At a more optimum level of $CuCl_2$ (7.6% Cu) and with a new bimodal carbon support, a developmental material obtained from the Mega Carbon Company, significantly higher conversions were obtained with higher selectivities to the desired DMC product. Results are shown in Figure 1. Throughout the course of a 900-minute study, net conversion of CH_3O was maintained at 42-53%. At a typical sample point methanol conversion was 39% and DME conversion was 48%. Selectivity to DMC was 73-81% and selectivity to DMM was 17-25%. These results suggest significantly higher yields than those reported for the commercial liquid-phase process or those obtained in gas-phase studies which utilize only methanol as the oxidative carbonylation substrate.

CONCLUSIONS ON CATALYSIS STUDIES

A traditional catalyst for the oxidative carbonylation of methanol and CO to DMC admixtured with a mildly acidic molecular sieve catalyst allows for the oxidative carbonylation of DME/methanol mixtures to DMC. The results of this study clearly indicate the potential for obtaining high net methoxy conversions via the application of in situ dehydration with DME.

CONCEPTUAL DMC PROCESS TAILORED FOR GASOLINE BLENDING

Based on the initial laboratory data obtained under this DOE-sponsored research and previous Amoco-sponsored work on DMC recovery from a product mixture containing methanol plus water, we have initiated an economic evaluation for the production of DMC as a gasoline oxygenate. In this paper we have briefly summarized some of our initial work on the process integration of syngas production (from natural gas) and DMC synthesis steps, including cost savings ideas on DMC recovery and blending as a gasoline oxygenate. While the initial cost studies will be based on using natural gas as the feedstock, the data can be revised in future to include syngas generation via coal and biomass gasification.

Background on DMC Separation

Separation is a critical aspect of DMC production and is one of the more expensive steps. In a conventional DMC synthesis process via oxidative carbonylation of methanol (e.g., ENIChem technology), DMC is produced at low concentrations (20-40%) and it's recovery involves a separation of the ternary system of methanol/DMC and water. This system comprises at least two binary azeotropes which makes the DMC recovery quite challenging:

Component	Normal Boiling Temperature, (°C)
Methanol	65
DMC	90
Water	100
70% Methanol + 30% DMC	62.7
89% DMC + 11% Water	7.5

Based on the patent literature, there are numerous claims on various separation techniques, including extractive distillation, liquid-liquid extraction, evaporation and selective absorption.[1]

In the past, Amoco had evaluated various engineering options for recovering DMC from a mixture of methanol/DMC and water. In related R&D work, Amoco had obtained three patents on novel liquid/liquid extraction methods using various hydrocarbon solvents.[3-5] In one of these methods, specifically tailored for the use of DMC as a gasoline additive, specific gasoline blendstocks are used to extract DMC from the ternary mixture of DMC, methanol and water. Additional water is used to prevent co-extraction of methanol. In this scheme, distillation of a DMC azeotrope is completely avoided, and a gasoline blendstock with reasonably high oxygen concentration can be produced. The use of gasoline blending components as the extraction solvent eliminates any need for separation and recovery of the extraction solvent. A conceptual flowscheme of the proposed idea is shown in Figure 2.

Various laboratory studies have indicated that with suitable gasoline-range blendstocks, the DMC recovery can approach 90-95% level with (a) very low levels of water (<0.01 wt%) and methanol (<0.5 wt%) in the DMC-rich extract and (b) low levels of DMC (<0.4%) and the extraction solvent (<0.1 wt%).

Conceptual Process Flowscheme

As shown in Figure 2, the key process steps in the production of DMC based on the use of a methanol/DME mixture are: syngas generation from natural gas and oxygen (from air liquefaction), methanol plus DME synthesis from syngas, DMC synthesis from methanol, DME, carbon monoxide and oxygen, carbon dioxide and hydrogen recovery from unreacted gases in the methanol/DME synthesis step and DMC extraction from methanol/DMC/water mixture. For this specific study, DMC is extracted with a refinery hydrocarbon stream (e.g., a reformate stream) that can blended directly with gasoline.

One key consideration for the overall process scheme is that if the hydrogen from the syngas production step is to be used as fuel only, we need to select a suitable syngas generation process that will minimize hydrogen/carbon monoxide ratio (e.g., a partial oxidation process rather than a steam reformer). Regarding methanol/DME synthesis, various publications from Haldor Topsoe and Air Products have indicated that suitable catalysts can be developed to tailor to specific methanol/DME product ratio. In general, the co-production of DME and methanol is favored (namely, needs lower reactor severity) over the production of methanol alone. We are currently evaluating various options for the recovery of unconverted DME, carbon dioxide and hydrogen, and integration of various processing steps to minimize overall capital and operating costs.

References:

1. PERP Report, Chem Systems, Inc., 90S7, "DMC Via Ethylene Carbonate", Dec. 1991

2. Romano, Ugo, et al, "Synthesis of DMC from Methanol, CO, and O_2 Catalyzed by Copper Compounds", IEC Prod. Res. Dev., V-19, 396-403 (1980)

3. US Patent: 5,328,615, July 12, 1994, Amoco Corp., Inventors: M. A. Pacheco and F. D. Darrington

4. US Patent 5,338,878, Aug. 16, 1994, Amoco Corp., Inventors: M. A. Pacheco, F. D. Darrington and A. L. Hensley

5. US Patent 5,489,703, Feb. 6, 1996, Amoco Corp., Inventors: M. A. Pacheco, F. D. Darrington, J. C. Reier, and B.D. Alexander

Figure 1

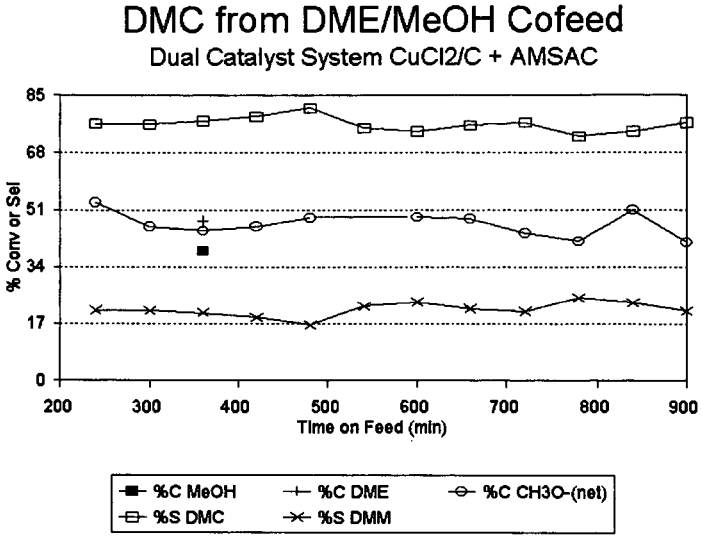

Figure 2

Conceptual Amoco DMC Synthesis Process

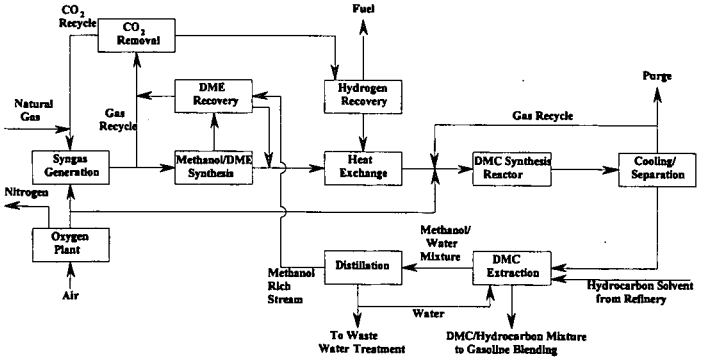

ADVANCES IN LIQUID PHASE TECHNOLOGY

Peter J.A. Tijm*, William R. Brown, Edward C. Heydorn, and Robert B. Moore
Air Products and Chemicals Inc., Allentown, PA

ABSTRACT

The liquid phase methanol (LPMEOH™) process uses a slurry reactor to convert synthesis gas (primarily a mixture of hydrogen and carbon monoxide) to methanol. Through its superior heat management, the process is ultimately suitable to handle synthesis gas generated through gasification of coal, petroleum coke, natural gas, residual oil, wastes, and other environmentally disadvantaged hydrocarbon feedstocks. Apart from production of chemical grade methanol, the process provides economic advantages in the Integrated Gasification Combined Cycle (IGCC) power generation application. Co-production of power and methanol via the IGCC and the LPMEOH™ process provides opportunities for energy storage for peakshaving of electrical demand and/or clean fuel for export. The LPMEOH™ technology has been developed by Air Products and Chemicals, Inc. since the 1980's, extensively proven in a Department of Energy (DOE) - owned process development unit in LaPorte, Texas and selected for demonstration under the DOE Clean Coal Technology Program. The slurry reactor being demonstrated is also suitable for other exothermic synthesis gas conversion reactions, like synthesis of dimethyl ether and other alcohols/oxygenates. This paper presents an overview of LPMEOH™ and other liquid phase technology aspects and highlights the demonstration project at Eastman Chemical Company's coal gasification facility in Kingsport, TN. Commercial aspects of the LPMEOH™ process are also discussed.

INTRODUCTION

With increasing methanol market demand, it was realized by various companies that a breakthrough in technology was required to provide methanol to the market place in a cost competitive way. In the early 1960's an important technology improvement was achieved by Imperial Chemical Industries Ltd. (ICI). They introduced low pressure technology, which was made possible through the development of higher activity catalysts. Since that time, low pressure gas phase methanol process technology has dominated the market. Only in the early 1980's was the potential of liquid phase technology realized by Chem Systems and Air Products and Chemicals, Inc. As result of technology consolidation between both these companies the LPMEOH™ technology was developed, with the financial support of the U. S. Department of Energy (DOE). The concept was proven in over 7,400 hours of test operation in a DOE-owned, 3,200 gallons (U.S.) of methanol per day process development unit located at LaPorte, Texas. (Ref. a). The commercial-scale demonstration plant for the technology has been constructed and is now being commissioned at Eastman Chemical Company's coal gasification facility in Kingsport, Tennessee under the DOE's Clean Coal Technology Program. The LPMEOH™ plant will demonstrate the production of at least 80,000 gallons of methanol per day, and will simulate operation for the IGCC co-production of power and methanol. Construction began in October of 1995 and was, in a record period of 15 months, completed in December of 1996. Commissioning was completed and startup initiated in January of 1997, and will be followed by four years of operation to demonstrate the commercial advantages of the technology.

Air Products and Eastman formed the "Air Products Liquid Phase Conversion Co., L.P." limited partnership to execute the demonstration project. The partnership owns the LPMEOH™ demonstration plant. Air Products manages the demonstration project and provides technology analysis and direction for the demonstration. Air Products also provided the design, procurement, and construction of the LPMEOH™ demonstration plant (i.e., a turnkey plant). Eastman provides the host site, performs the permitting and operation of the LPMEOH™ unit, and supplies the supporting auxiliaries, the synthesis gas, and takes the product methanol.

Most of the product methanol will be refined to chemical-grade quality (99.85 wt % purity via distillation) and used by Eastman as chemical feedstock in their commercial facility. A portion of the product methanol will be withdrawn prior to purification (about 98 wt % purity) and used in the off-site product-use tests.

I. COMMERCIAL APPLICATION

Technology Description

The heart of the liquid phase technology, in this case the LPMEOH™ process, is the slurry bubble column reactor (Figure 1). The liquid medium is the feature that differentiates the LPMEOH™ process from conventional technology. Conventional methanol reactors use fixed beds of catalyst pellets and operate in the gas phase. The LPMEOH™ reactor uses catalyst in powder form,

slurried in an inert mineral oil. The mineral oil acts as a temperature moderator and a heat removal medium, transferring the heat of reaction from the catalyst surface via the liquid slurry to boiling water in an internal tubular heat exchanger. Since the heat transfer coefficient on the slurry side of the heat exchanger is relatively large, the heat exchanger occupies only a small fraction of the cross-sectional area of the reactor. The slurry reactor can thus achieve high syngas conversion per pass, due to its capability to remove heat and maintain a constant, highly uniform temperature through the entire length of the reactor. Thus an essentially exothermic process has been converted to an isothermal process.

Because of the LPMEOH™ reactor's unique temperature control capabilities, it is able to directly process syngas which is rich in carbon oxides (carbon monoxide and carbon dioxide). Gas phase methanol technology would require such a feedstock to undergo stoichiometry adjustment by the water gas shift reaction (to increase the hydrogen content) and carbon dioxide (CO_2) removal (to reduce the excess carbon oxides). In a gas phase reactor, temperature moderation is only achieved by recycling large amounts of hydrogen (H_2)-rich gas, utilizing the higher heat capacity of H_2 gas as compared to carbon monoxide (CO) gas. Typically a gas phase reactor is limited to about 16% CO gas in the inlet to the reactor, in order to limit the conversion per pass to avoid excess heating. Hence recycle ratios of 6 - 10 are typically applied. In contrast, with the LPMEOH™ reactor, CO gas concentrations in excess of 50% have been routinely tested without any adverse effect on the catalyst activity.

A second differentiating feature of the LPMEOH™ reactor is its robust character. The slurry reactor is suitable for rapid ramping, idling, and even extreme stop/start actions. The thermal moderation provided by the liquid inventory in the reactor acts to buffer sharp transient operations that would not normally be tolerable in a gas phase methanol synthesis reactor.

A third differentiating feature of the LPMEOH™ process is that a high quality methanol product is produced directly from syngas which is rich in carbon oxides. Gas phase methanol synthesis, which relies on hydrogen-rich syngas, results in a crude methanol product with up to 20% water by weight. The product from the LPMEOH™ process typically contaitns only 1% water by weight. This methanol product, coproduced with IGCC, is therefore suitable for many applications, and at a substantial savings in purification costs. The steam produced in the LPMEOH™ reactor is suitable for purification of the methanol product (for upgrading to a higher quality) or for use in the IGCC power generation cycle.

Another unique feature of the LPMEOH™ process is the ability to add fresh catalyst online. Methanol catalysts deactivate at a slow rate. With the LPMEOH™ reactor, spent catalyst slurry may be withdrawn and fresh catalyst slurry added on a periodic batch basis. This allows continuous, uninterrupted operation, i.e maximum number of streamdays per year, and also the maintenance of a high productivity level in the reactor. Furthermore, choice of replacement rate permits optimization of productivity versus catalyst replacement cost.

Finally the simplicity of reactor construction is an advantage to the LPMEOH™ process.

Other Liquid Phase Reactions

The technology and process characteristics/advantages as described for the LPMEOH™ process above are also applicable to a variety of other exothermic syngas reactions. In essence it is the combination of technology elements such as the following:
- exothermicity of the chemical reaction of syngas to product
- successful reactor engineering and scale up
- selectivity towards desired reaction products and
- maintenance of catalyst(s) activity

which will determine the competitiveness of the liquid phase technology.

Following the successful development of the LPMEOH™ technology, which hereinafter will be used as an example, Air Products, sponsored by DOE, broadened the scope of its liquid phase technology interest. Air Products, together with various subcontractors, further developed and/or improved the liquid phase technology for the following chemical processes:
- 1. New C_1 - chemistry to Methyl Tertiary Butyl Ether (MTBE)
- 1. a. Liquid Phase Isobutanol/Methanol
- 1.b. Liquid Phase Isobutylene (LPIBE)
- 2. Liquid Phase Di-Methyl Ether (LPDME)
- 3. Liquid Phase Water Gas Shift
- 4. Liquid Phase Fischer-Tropsch

The new C_1-chemistry to MTBE depends on two critical steps. The first is the efficient production of both methanol and isobutanol direct from syngas, and the second is dehydration of isobutanol to isobutylene. Following laboratory autoclave pioneering and suitable catalyst system(s) determination, the LPIBE technology was proven in the LaPorte Alternative Fuels Development Unit (AFDU). Isobutanol conversion as high as 98% with an isobutylene selectivity of 92% was

achieved. High conversion/selectivity is necessary in this, as in many, processes as the product separation of reaction products is difficult and expensive. The Liquid Phase Isobutanol/Methanol production from synthesis gas is presently under further research/demonstration, as previous successful demonstrations are deemed to operate at too high pressures and/or temperatures.

LPDME has been recognized as a possible spring-board molecule for synthesis of fuels and chemicals. Laboratory tests on a dual catalyst system (to perform both methanol synthesis and dehydration in the same reactor vessel) were successful on a laboratory stirred tank reactor scale. Preliminary economics led to high interest in this liquid phase technology and demonstration in the AFDU in LaPorte. LPDME technology is expected to be Air Products' next step in the commercialization of liquid phase technology. Development/cost improvement activities are on-going.

IGCC Coproduction Options

The LPMEOH™ process is a very effective technology for converting a portion of the H_2 and CO in an IGCC electric power plant's coal-derived syngas to methanol. The process is very flexible in being able to process many variations in syngas composition. The LPMEOH™ process can be used with an IGCC electric power plant (Ref. b), to provide the once-through methanol production as depicted in Figure 2. The process can be designed to operate in a continuous, baseload manner, converting syngas from oversized gasifiers or from a spare gasifier. The process can also be designed to operate only during periods of off-peak electric power demand to consume a portion of the excess syngas and allow the electricity output from the combined-cycle power unit to be turned down. In this latter circumstance, the gasification unit continues to operate at full baseload capacity, so the IGCC facility's major capital asset is fully utilized.

In either baseload or cycling operation, partial conversion of between 20% and 33% of the IGCC plant's syngas is optimal, and conversion of up to 50% is feasible. The degree of conversion of syngas (or the quantity of methanol relative to the power plant size) determines the design configuration for the LPMEOH™ process. In its simplest configuration, syngas (feed gas) at its maximum available pressure from the IGCC electric power plant is passed once, without recycle through the LPMEOH™ plant (Figure 3), and partially converted to methanol. The unreacted feed gas is returned to the IGCC power plant's combustion turbines.

If greater amounts of syngas conversion are required, different once-through plant design options (Figure 3) are available. The feed gas pressure to the reactor is a prime determinant of the degree of syngas conversion, as shown in Figure 4. Reaction pressure for methanol synthesis design is usually 750 psia or higher. The higher the pressure at which the syngas is available, the greater is the degree of conversion and the lower the conversion cost. The LPMEOH™ process design options for greater syngas conversion are:

- Once-Through, with Feed Gas Compression:

When the feed gas pressure from the IGCC electric power plant is low (e.g. below 750 psia), feed gas compression may be added to the LPMEOH™ process design, to increase reactor productivity and the overall conversion of syngas to methanol.

- Limited Gas Recycle:

One design technique to increase the degree of syngas conversion is to condense out methanol from the reactor effluent and to recycle part of the unreacted feed gas back to the reactor inlet. With the LPMEOH™ process, this simple recycle refers to recycle of CO-rich gas. The recycle ratio required for the LPMEOH™ is moderate, for example, one part unreacted syngas to one part fresh feed gas. This 1 to 1 recycle ratio is usually quite effective in optimizing the methanol production. At higher recycle ratios, little is gained since most of the available H_2 has already been converted to methanol.

- Once-Through with Water Addition:

Of course, the richer the once-through syngas is in CO, the more the production is limited by the availability of H_2. If additional conversion is desired, the LPMEOH™ process design can be altered to generate additional H_2. The inherent shift activity of the methanol catalyst can be utilized to accommodate a modest amount of shift activity within the reactor. This is done by the addition of water, as steam, to the syngas before it passes through the liquid phase methanol reactor. Within the reactor, the additional steam is converted to H_2 which is, in turn, converted to methanol. In the water addition case, the increase in conversion is accompanied with a modest increase of water in the crude methanol product and of CO_2 in the reactor effluent gas.

Any combination of these LPMEOH™ process design options may be used to achieve the desired degree of syngas conversion. There is still no need for upstream stoichiometric adjustment of the feed gas by the water-gas shift reaction and CO_2 removal; so the simplicity of once-through CO-

rich gas processing is retained.

Baseload Coproduction of Methanol and Power

Process design study work for the LPMEOH™ process has been directed towards converting a portion of coal-derived syngas produced in an IGCC electric power plant to methanol. A feed gas containing 35% H_2, 51% CO, 13% CO_2 and 1% inerts (nitrogen) was used for preparing the baseload methanol coproduction economics.

With a given gasification plant size, the IGCC coproduction plant can be designed to accommodate a range of methanol to power output ratios. For example (Ref. c, d), a gasification plant, with two gasifiers of 1735 million Btu (HHV) per hour output each (equivalent to some 2200 tonnes per day of coal input), could be sized for baseload power output of 426 megawatts of electricity (MWe) and for baseload methanol coproduction of 152,000 US gallons per day (G/D). Other methanol and power plant size options for this gasification plant size are shown in Table 1.

Table 1. Methanol Plant to Power Plant Size Ratio

% of Syngas Converted to Methanol (%)	Baseload Power Plant Size (MWe)	Baseload Methanol Plant Size (G/D)	Methanol Plant to Power Plant Size Ratio (G/D per MWe)
0	500	0	0
13.8	**426**	**152,000**	**357**
20.0	394	210,000	533
30.0	342	330,000	965

The IGCC coproduction plant with 426 MWe of power and 152,000 G/D of methanol is used for the baseload production cost estimate for coproduced methanol, shown in Table 2. If the baseload fuel gas value is $4.00 per million Btu, then 152,000 G/D of methanol can be coproduced from coal for under 50 cents per gallon.

As expected, the methanol production cost is lower at larger methanol plant sizes. Figure 5 shows the effect of plant size for once-through methanol coproduction. Methanol production costs for two of the LPMEOH™ plant design options for higher syngas conversion: 1 to 1 gas recycle, and 1 to 1 gas recycle with water addition, are also shown.

Today, new methanol plants are being built where natural gas is inexpensive (Chile, Saudi Arabia). These new world scale plants range in size from 700,000 to 900,000 G/D (2000 to 2700 metric tons per day) in size. The economy of scale savings; in natural gas gathering, syngas production, and in methanol storage and ocean transport facilities; drive these plants to a large size. Estimates (Ref. e, f) show that an 836,000 G/D remotely located methanol plant (with the same 20% per year capital charge as in Figure 5), with natural gas at $0.50 to $1.00 per million Btu, has a total ex-plant methanol production cost of 46 to 50 cents per gallon. Adding ocean freight, duty and receiving terminal storage typically adds 8 to 10 cents per gallon; giving a total delivered U.S. Gulf Coast methanol cost (Chemical Grade) of 55 to 60 cents per gallon.

Figure 5 is interesting because it provides an unexpected result. Methanol coproduction with IGCC and the once-through LPMEOH™ process does not need large methanol plant sizes to achieve good economics. The gasification plant is already at a large economical scale for power generation; so the syngas production economics are already achieved. Methanol storage and transport economics are also achieved by serving local markets, and achieving freight savings over the competing methanol, which is usually shipped via the U. S. Gulf coast from areas with inexpensive feed gas (like natural gas or associated gas).

The 50 cents per gallon coproduction cost for a 152,000 G/D once-through LPMEOH™ plant size is in local markets competitive with new world scale natural gas based methanol plants. Figure 5 shows an additional 3 to 4 cent per gallon saving for a 365,000 G/D LPMEOH™ plant size. These additional savings might be used to off-set higher freight costs to more distant local customers; while still maintaining a freight and cost advantage over the imported methanol from the Gulf Coast.

The 50 cents per gallon coproduction cost for a 152,000 G/D once-through LPMEOH™ plant size in local markets is competetive with new world scale natural gas-gased methanol plants. Figure 5 shows an additional 3 to 4 cent per gallon savings for a 365,000 G/D LPMEOH™ plant size. These additional savings might be used to offset higher freight costs to more distant local

customers, while still maintaining a freight and cost advantage over the imported methanol from the Gulf Coast.

TABLE 2. Production Cost Estimate for Coproduced Methanol
LPMEOH Plant Capacity: 152,000 gallons per day (500 sT/D)
Capital Investment: $29 million

	Baseload
Methanol Plant Operation:	7884 hr/yr
Methanol Production (million gall./year):	49.9
Methanol Production Cost	**cents/gallon**
Syngas cost:	
Feed Gas @ fuel value ($4.00/mmBtu)	98.7
Unreacted (CO-rich) gas @ fuel value ($4.00/mmBtu)	(68.4)
Sub-total; net cost of syngas converted:	**30.3**
Operating cost:	
Catalyst and chemicals	2.6
Export steam	(2.9)
Utilities	0.9
Other (fixed) costs	4.0
Sub-Total; Operating Costs:	**4.6**
Capital charge @ 20% of investment per year	**11.6**
Total Methanol Production Cost:	**46.5**

Basis:
U. S. Gulf Coast Construction, 4thQ 1996 $
Includes owner costs and 30 days of Product Storage
CO-rich feed gas from IGCC electric power plant at 1000 psia, with 5ppm (max.) sulfur. Once-through LPMEOH process design with 1562 mmBtu/hr in, 1082 mmBtu out tHHV). Excludes License and Royalty fee. Air Products is the LPMEOH process technology licensor. Product methanol with 1 wt % water; Chem. Grade would add 4 to 5 cents per gallon.

II. DEMONSTRATION PLANT - STATUS

Development of the LPMEOH™ technology came to further fruition through cooperation between Air Products, DOE and Eastman Chemical Company under the DOE Clean Coal Technology Program (Ref. g).

Kingsport Site

Eastman has an extensive chemical complex at the Kingsport site, where originally methanol was produced by distillation of wood and later changed to conversion of coal-derived syngas. Coal gasification operations at Kingsport began in 1983. Figure 6 shows an aerial view of Eastman's Kingsport gasification facility. Texaco gasification is used to convert about 1,000 tons-per-day of high-sulfur, Eastern bituminous coal to synthesis gas for the manufacture of methanol, acetic anhydride, and associated products. Air Products provides the oxygen for gasification by a pipeline from an over-the-fence air separation unit. The crude synthesis gas is quenched, partially shifted, treated for acid gas removal (hydrogen sulfide and carbonyl sulfide, and CO_2, via Rectisol), and partially processed in a cryogenic separation unit to produce separate H_2 and CO streams. The H_2 stream is combined with clean synthesis gas to produce stoichiometrically balanced feed to a conventional gas phase methanol synthesis unit. Methanol from this unit is reacted with recovered acetic acid to produce methyl acetate. Finally, the methyl acetate is reacted with the CO stream to produce the prime product, acetic anhydride (and acetic acid for recycle). Figure 7 shows the process block flow diagram for the Kingsport gasification facility including the LPMEOH™ demonstration plant.

LPMEOH™ Demonstration Plant Design

The site available at Kingsport provides a 270 ft. by 180 ft. plot for the demonstration plant and tank truck loading areas. An area next to the site was made available for establishing the

construction trailer, fabrication, and laydown areas. Figure 8 is an aerial view of the site prior to the start of construction. Air Products was responsible for the engineering design and construction of the project. Eastman was responsible for the outside battery limits design and construction, the permitting, and for providing the digital control programming. Eastman reviewed the detailed design of the demonstration plant.

Because the gasification facility produces individual streams of clean synthesis gas, CO, and H_2-rich gas, there is the capability to blend gases and mimic the gas compositions of a range of gasifiers. Hence, the broad applicability of the LPMEOH™ technology could be proven and formed part of an elaborate test program, to be discussed later. Those test objectives also provided a design challenge for the Air Products/Eastman design team. Of primary importance was the integration of the LPMEOH™ demonstration plant within the Kingsport gasification complex. Since the feed composition to the reactor was to be varied from H_2-lean to H_2-rich (25% to 70+%H_2) and the flow to the reactor by at least a factor of two, all of the product and byproduct streams within and outside the battery limits were affected. Control valves and instrumentation for the demonstration plant were required to have functionality over and beyond those for a normal commercial facility. Extreme cases of about twenty different heat and material balances were considered for specification of each piece of equipment, flow measurement device, control valve, and safety relief device.

The DOE approved Eastman's Kingsport, TN facility as the site of the LPMEOH™ Demonstration Plants in October of 1993. Air Products and Eastman worked with the DOE to define the size of the plant and develop a Statement of Work for the LPMEOH™ Demonstration at Kingsport. This Project Definition phase including a cost estimate was completed in October of 1994. Preliminary detailed design work on equipment layouts and development of P&ID's began shortly after this. Full authorization from the DOE for Design and Construction was effective February 1, 1995. The reactor was the first piece of equipment to be placed on order in November of 1994. Equipment deliveries began in November of 1995. The State air permit was received in March of 1996. The DOE completed its National Environmental Policy Act (NEPA) review and issued a Finding of No Significant Impact (FONSI) in June of 1995. Construction at the site began in October of 1995. Construction was essentially completed in December of 1996.

Instrument Loop Checking began in October 1996. Commissioning began in December of 1996, followed by startup in late January of 1997. Thereafter a four-year methanol test operation was started in February of 1997. The operating test program will end in the year 2001. The off-site fuel use tests will be performed over an 18 to 30 month period, beginning in May of 1998.

III. DEMONSTRATION PLANT - TEST PLANS

Methanol Operations - Demonstration Test Plan

Three key results will be used to judge the success of the LPMEOH™ process demonstration during the four years of operational testing:

- Resolution of technical issues involved with scaleup and first time demonstration for various commercial-scale operations
- Acquisition of sufficient engineering data for commercial designs
- Industry acceptance

The demonstration test plan has been established to provide flexibility in order to meet these success criteria. Annual operating plans, with specific targeted test runs, will be prepared and revised as necessary. These plans will be tailored to reflect past performance as well as commercial needs. User involvement will be sought.

The LPMEOH™ operating test plan outline, by year, is summarized in Table 3. The demonstration test plan encompasses the range of conditions and operating circumstances anticipated for methanol coproduction with electric power in an IGCC power plant. Since Kingsport does not have a combined-cycle power generation unit, the tests will simulate the IGCC application. Test duration will be emphasized in the test program. The minimum period for a test condition, short of the rapid ramping tests, is 2 weeks. Numerous tests will have 3-6 week run periods, some 8-12 weeks, and a few key basic tests of 20 to 30 weeks.

Table 3. LPMEOH™ Demonstration Test Plan Outline

Year 1

- Catalyst Aging
  - Catalyst Life Versus LaPorte process development unit and Lab Autoclaves
- Process Optimization / Maximum Reactor Productivity
  - Catalyst Slurry Concentration
  - Reactor Slurry Level
  - Catalyst Slurry Addition Frequency Test
- Establishment of Baseline Condition

Years 2 & 3

- Catalyst Slurry Addition and Withdrawal at Baseline Condition
- Catalyst Attrition/Poisons/Activity/Aging Tests
- Simulation of IGCC Coproduction for:
  1. Synthesis Gas Composition Studies for Commercial Gasifiers
     Texaco, Shell, Destec, British Gas/Lurgi, Other Gasifiers
  2. IGCC Electrical Demand Load Following:
     Rapid Ramping, Stop/Start (Hot and Cold Standby)
  3. Additional Industry User Tests
- Maximum Catalyst Slurry Concentration
- Maximum Throughput/Production Rate

Year 4

- Stable, extended Operation at Optimum Conditions
- 99% Availability
- Potential Alternative Catalyst Test
- Additional Industry User Tests

Applications for the Coproduced Methanol Product

The methanol coproduction process studies show that the LPMEOH™ process can produce a clean high quality methanol product at less than 50 cents per gallon from an abundant, non-inflationary local fuel source (coal). As previously indicated the quality of the methanol produced approaches closely that of chemical grade methanol. This allows in certain applications for limited distilling of the product and, hence, another advantage for the LPMEOH™ process. Serving local markets, the methanol coproduced at central IGCC electric power plants, can be a valuable premium fuel or fuel feedstock for many applications, such as:

1. An economical hydrogen source for small fuel cells being developed for transportation applications. Methanol is a storable, and transportable, liquid fuel which can be reformed under mild conditions to provide an economical source of hydrogen for fuel cells.
2. Reformed under mild conditions, liquid phase methanol may be an economical hydrogen or carbon monoxide source for industrial applications.
3. A substitute for chemical grade methanol being used for MTBE manufacture.
4. An environmentally advantaged fuel for dispersed electric power stations. Small packaged power plants (combustion turbine, internal combustion engine, or fuel cell) provide power and heat locally, at the use point; without any competition like natural gas pipelines and high voltage power lines. Since methanol is an ultra-clean (zero sulfur) fuel which burns with very low (better than natural gas) emissions of nitrogen oxides, the incremental power is very clean.
5. Finally, the coproduced methanol may be used by the utility owning the IGCC facility (see Figure 2). Potential uses are: a) as a backup fuel for the IGCC plant's main gas turbines; b) as a fuel for a separate, dedicated cycling combined-cycle unit at the same site; c) as the fuel exported to the utility's distributed power generation system(s); or d) as the transportation fuel for the utility's bus or van pool. Since the methanol is derived from the coal pile, the IGCC facility can be truly independent and self-sufficient for fuel needs. In addition, should the external prices for methanol command higher value to the IGCC plant's owner, the methanol can be exported for additional revenues.

Many of the applications listed above are embryo developments. Their ultimate market size potential for transportation applications, for industrial applications and for distributed power generation could become large. The methanol product specification for the applications is not adequately known. Therefore, part of the LPMEOH™ demonstration project's program is to confirm the suitability of the methanol product for these (and other) uses. Product-use tests will allow development of final methanol product specifications. During the demonstration, in the 1998 to 2000 time-frame, about 400,000 gallons of the "as-produced from CO-rich syngas" methanol will be available for off-site product-use testing. The final off-site product-use test plan is now under development. More details will be provided to interested parties.

CONCLUSION

The LPMEOH™ process is now being demonstrated at commercial scale under the DOE Clean Coal Technology Program. The demonstration plant, located at Eastman Chemical Company's Kingsport, Tennessee coal gasification facility site, will produce at least 80,000 gallons-per-day of methanol from coal-derived synthesis gas. Startup was effected in January of 1997, followed by a four-year demonstration test period beginning in February of 1997.

Successful demonstration of the LPMEOH™ technology will add significant flexibility and dispatch benefits to IGCC electric power plants, which have traditionally been viewed as strictly a baseload power generation technology. Now, central clean coal technology processing plants, making coproducts of electricity and methanol, can meet the needs of local communities for dispersed power and transportation fuel. The LPMEOH™ process provides competitive methanol economics at small methanol plant sizes, and a freight and cost advantage in local markets vis-a-vis large remote gas methanol. Methanol coproduction studies show that methanol at less than 50 cents per gallon can be provided from an abundant, non-inflationary local fuel source (coal). The coproduced methanol may be an economical hydrogen source for small fuel cells, and an environmentally advantaged fuel for dispersed electric power.

BIBLIOGRAPHY

Ref. a. "An Update on Liquid Phase Methanol (LPMEOH™) Technology and the Kingsport Demonstration Project"; E. S. Schaub, et. al. (Air Products and Chemicals, Inc.), Fourth Annual Clean Coal Technology Conference; September 5-8, 1995.

Ref. b. "Flexible Electric Power Generation - The Integrated Gasification/Liquid Phase Methanol (LPMEOH™) Demonstration Project", W. R. Brown, et. al. (Air Products and Chemicals, Inc.), Third Annual Clean Coal Technology Conference; September 6-8, 1994.

Ref. c. "IGCC Cost Study"; D. M. Todd (GE Company), J. R. Joiner (Fluor Daniel, Inc.), EPRI Conference on Gasification Power Plants, October 19-21, 1994.

Ref. d. "Gasification Systems - Advanced turbines hold the key to economic IGCC"; Modern Power Systems, August 1995.

Ref. e. "Putting the Future of Methanol in Proper Perspective"; J. R. Crocco, (Crocco & Associates, Inc.), World Methanol Conference, December 5-7, 1989.

Ref. £ "Methanol 93-1, Process Evaluation Research Planning (PERP) Report"; Chem Systems Inc., April 1995.

Ref. g. "Fuel and Power Coproduction - The Liquid Phase Methanol (LPMEOH™) Process Demonstration at Kingsport"; D. P. Drown, et. al. (Air Products and Chemicals, Inc./Eastman Chemical Company/U.S. Department of Energy), Fifth Annual DOE Clean Coal Technology Conference; January 7-9, 1997.

DISCLAIMER/ACKNOWLEDGMENT

This report was prepared by Air Products & Chemicals, Inc., pursuant to a Cooperative Agreement partially funded by the U.S. Department of Energy, and neither Air Products & Chemicals, Inc., nor any of its aubcontractors nor the U.S. Department of Energy, nor any person acting on behalf of either:

(A) Makes any warranty or representation, express or implied, with respect to the accuracy, completeness, or usefulness of the information contained in this report, or that the use of any information, apparatus, method, or process disclosed in this report may not infringe privately-owned rights; or

(B) Assumes any liabilities with respect to the use of, or for damages resulting from the use of, any information, apparatus, method, or process disclosed in this report.

Reference herein to any specific commercial product, process, or service by trade name, trademark, manufacturer, or otherwise, does not necessarily constitute its endorsement, recommendation, or favoring by the U.S. Department of Energy. The views and opinions of authors expressed herein does not necessarily state or reflect those of the U.S. Department of Energy.

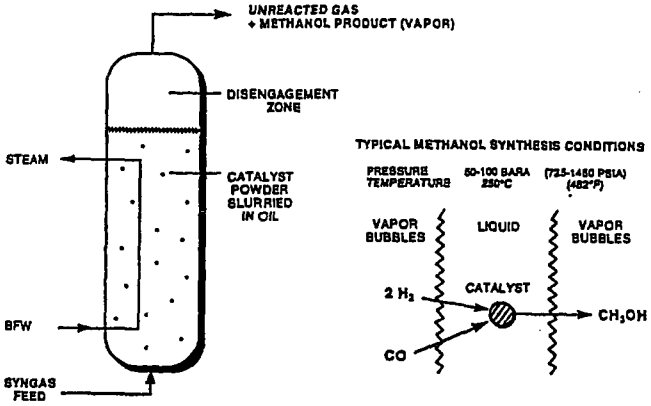

Figure 1. LPMEOH™ Reactor and Reaction Schematics

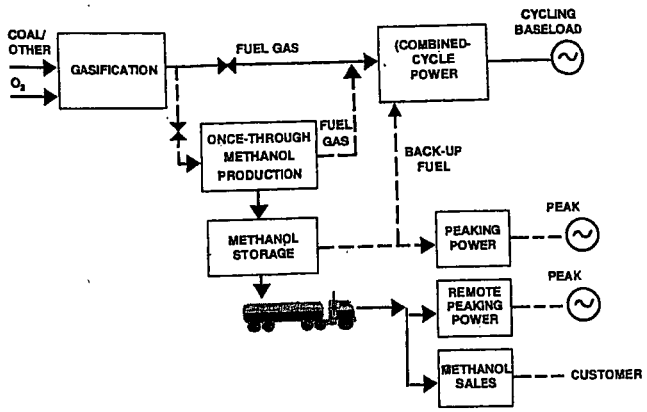

Figure 2. Once-through Methanol Coproduction with IGCC Electric Power

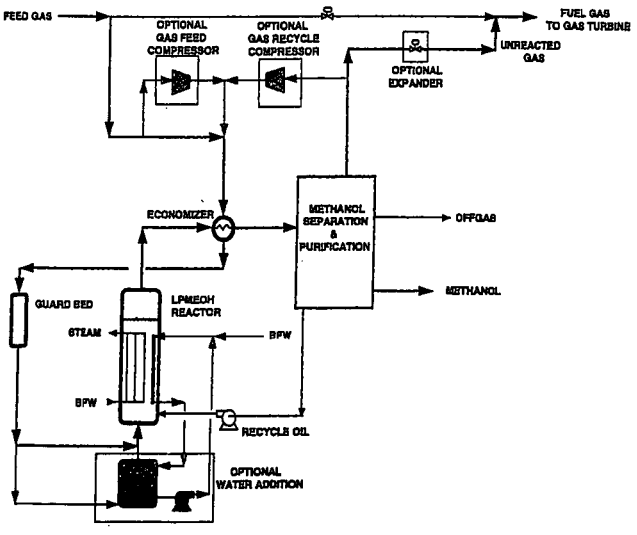

Figure 3. Once-through LPMEOH™ Process Design Options

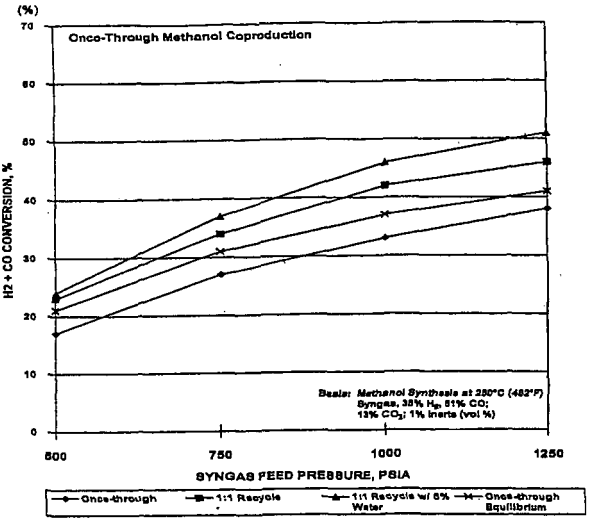

Figure 4. Synthesis Gas Conversion to Methanol

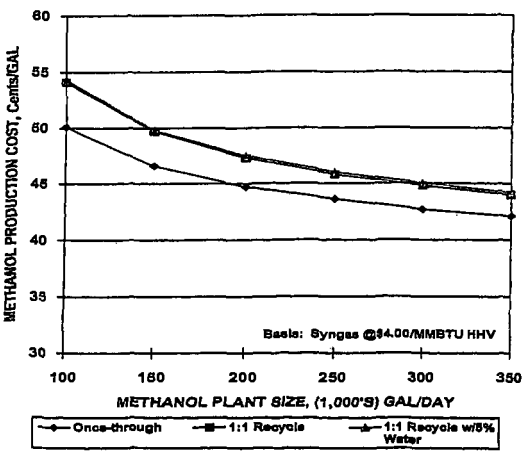

Figure 5. Coproduct Methanol Cost versus Methanol Plant Size.

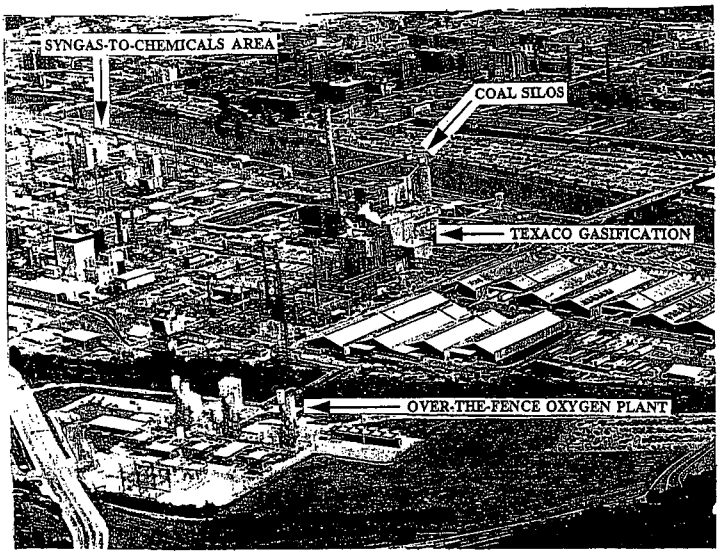

Figure 6. Aerial View of Eastman's Kingsport Complex

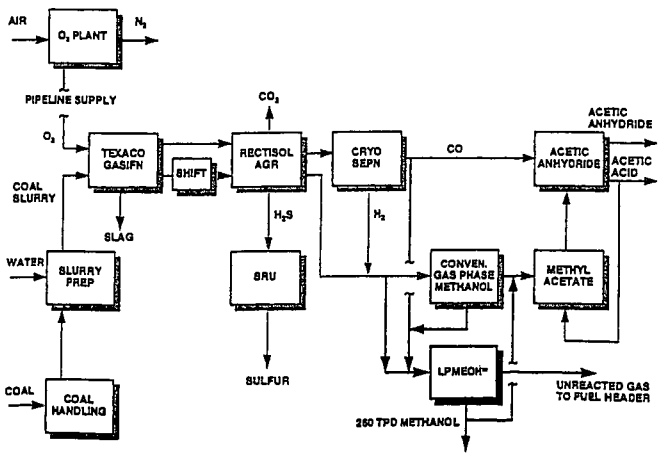

Figure 7. Process Block Flow Diagram of Kingsport Facility Including LPMEOH™ Demonstration Plant.

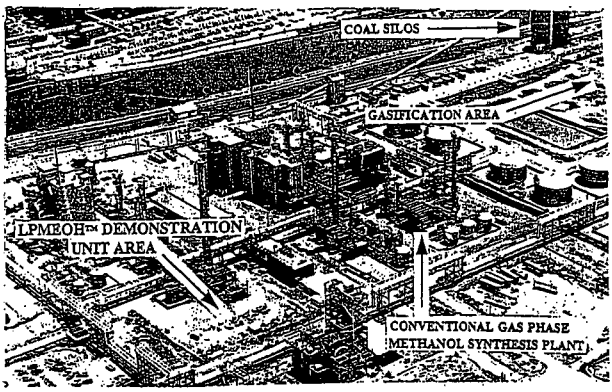

Figure 8. Aerial View of the Site for the LPMEOH™ Demonstration Plant

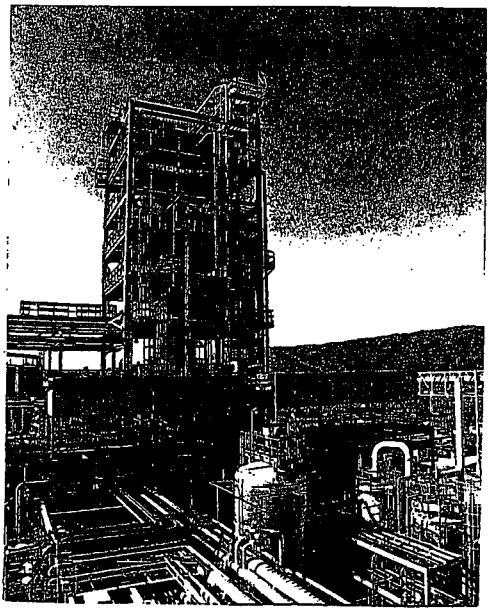

Figure 9. Photograph of the installed LPMEOH™ Demonstration Plant

NEW CLEAN FUEL FROM COAL- DIMETHYL ETHER -

Y. Ohno, T.Shikada, T.Ogawa, M.Ono and M.Mizuguchi ,NKK Corporation,Tokyo 100 and K.Fujimoto ,The University of Tokyo,Tokyo 113,Japan

Keywords: Dimethyl ether , Coal, Clean fuel

1. Introduction

In Asian countries and regions including China, ASEAN and NIES , high speed economic growth is spurring a rapid increase in energy consumption, which means that there is a high probability of this part of the world eventually facing [1] a tight energy supply and demand situation and [2] serious environmental problems (CO2,SOx, NOx, etc.).

On the energy supply side, an increase is forecast in the total volume of crude oil and oil products imported from the middle east and other production regions outside this part of Asia, but it will be necessary to also use unexploited energy resources as lignite, sub-bituminous coal, coal bed methane and unexploited small deposits of natural gas within the region.

Looking at the environmental preservation situation, to deal with existing solid pollutant sources such as relatively large electric power plants and factories ,desulfurization and denitrification plants are effective. For the consumption of fuel in residential and commercial sector and transportation sector, as the sources of pollutants are widely dispersed, measures to clean the fuel itself must be taken.

Forecasts of sharp rises in demand for the clean fuels, natural gas (LNG) and LPG, have aroused fears of a jump in the prices of these products. For this reason, the production of dimethyl ether (DME)--a clean fuel as convenient to transport as LPG--by synthesizing from gas obtained by coal gasification at coal mine for shipment to users in the surrounding countries and regions is extremely significant from the point of view of environmental preservation.

Recently, the DME synthesis from H2/CO has been studied for coproduction with methanol to increase the productivity beyond the methanol equilibrium(3,4).

NKK, which has been studying the synthesis of DME from H2/CO since 1989 (1,2) , is now conducting research on a 50kg/day bench plant.

In this report, we present an overview of the physical properties, uses and synthesis reaction of DME, and an estimation to commercial plant of DME.

2. Physical Properties and Uses of DME

2.1 Physical Properties of DME

Table 1 shows the physical properties and combustion characteristics of DME and various fuels. DME, a colorless gas with a boiling point of -25℃ , is chemically stable and easily liquefied. With properties similar to those of propane and butane, which are principal constituents of LPG, it can be handled and stored using the same technology used to handle and store LPG.

While its net calorific value of 6.903 kcal/kg is lower than that of propane, butane, and methane, it is higher than that of methanol. In gaseous state, its net calorific value is 14,200 kcal/Nm3, which is higher than that of methane. Turning to its combustion properties, its explosion limit is wider than those of propane and butane, but almost identical to that of methane and narrower than that of methanol. Its cetane number is high, ranging from 55 to 60, so that it can be used in diesel engines. Actual engine tests show that its fuel consumption rate is lower than that of diesel oil at the same NOx level and confirm that it is an extremely clean fuel, generating an extremely small quantity of soot(5). Its flame is a visible blue flame similar to that of natural gas, and it can be used just as it is in an LPG cooking stove, and it does not produce aldehyde.

A toxicity study of its use as a propellant for spray cans to replace fluorocarbons has confirmed that its toxicity is extremely low; about the same as that of LPG (6). The study has shown that the toxicity of DME is even lower than that of methanol.

Table 1 Physical Properties and combustion characteristics of DME and other fuels

Properties	DME	Propane	n-Butane	Methane	Methanol
Chemical formula	CH_3OCH_3	C_3H_8	C_4H_{10}	CH_4	CH_3OH
Boiling point (℃)	-25.1	-42.0	-0.5	-161.5	64.6
Liquid density (g/cm³, 20℃)	0.67	0.49	0.57	–	0.79
Specific gravity (vs. air)	1.59	1.52	2.00	0.55	–
Heat of vaporization (kcal/kg)	111.7	101.8	92.1	121.9	262
Saturated vapor pressure (atm, 25℃)	6.1	9.3	2.4	246	–
Burning velocity (cm/s)	50	43	41	37	52
Ignition energy (10^{-4}J)	45	30	76	33	21
Ignition temperature (℃)	350	504	430	632	470
Explosion limit (%)	3.4～17	2.1～9.4	1.9～8.4	5～15	5.5～36
Cetane number	55～60	(5)	(10)	0	5
Net calorific value (kcal/Nm³)	14,200	21,800	28,300	8,600	–
Net calorific value (kcal/kg)	6,903	11,100	10,930	12,000	5,040

( ) : estimated Value

It does not corrode metal but it does corrode rubber type sealant, so these materials must be selected carefully (6).

2.2 Uses of DME

Some is used as solvents, refrigerants, etc., but most is used as a propellant (paint, chemical fertilizers, cosmetics), with 8,000 tons/year produced in Japan and about 100,000 tons/year produced world wide. Its only use as a fuel has been as an intermediate product during the conversion to synthetic gasoline, but to take advantage of its properties similar to those of LPG, China has begun producing DME by dehydration reaction of methanol as a fuel substitute for LPG. Table 2 shows potential uses of DME as a fuel and the energy it will replace. When it is possible to produce it cheaply from coal or natural gas, it will be used widely as a clean fuel which is as convenient to transport as LPG.

Table 2 Potential use of DME as substitute fuel

Transportation	: diesel oil
Domestic use	: coal, coal briquette, fuel gas from coal, natural gas, LPG
Power generation	: coal, natural gas, heavy oil, LPG

3. Synthesis of DME

3.1 DME Synthesis Reaction

Table 3 shows the reactions concerning DME synthesis and the heat of reaction. As shown in Table 3, the DME synthesis reaction (e) from H2/CO consists of three steps: the methanol synthesis reaction (a), the dehydration reaction(b), and the shift reaction (c). Without the shift reaction, the reaction can be carried out following the formula(d) which is given by combining reactions (a) and(b). Because generally the methanol synthesis catalyst encourages the shift reaction(c), the total reaction is likely to proceed between (d) formula and (e) formula.

Because the total reaction is highly exothermic, if the excess reaction heat is not efficiently removed and the reaction temperature is not carefully controlled, there is a risk of the catalyst deactivation by the rising temperature.

Table 3 Reaction concerning DME synthesis and reaction heat

	Reaction			Reaction heat (kcal/mol-DME)
(a)	$2CO + 4H_2$	→	$2CH_3OH$	+ 43.4
(b)	$2CH_3OH$	→	$CH_3OCH_3 + H_2O$	+ 5.6
(c)	$CO + H_2O$	→	$CO_2 + H_2$	+ 9.8
(d)	$2CO + 4H_2$	→	$CH_3OCH_3 + H_2O$	+ 49.0
(e)	$3CO + 3H_2$	→	$CH_3OCH_3 + CO_2$	+ 58.8

Figure 1 shows how the (H2 + CO) equilibrium conversion for these two DME synthesis reaction formulae (d) and (e) and methanol synthesis reaction(a) varies as function of the initial H2/CO ratio and reaction pressure. In each reaction, the equilibrium conversion has its peak where the H2/CO ratio of the reactant gas corresponds to the stoichiometric value, that is, H2/CO = 2 (reaction (d) and reaction(a)) and with H2/CO = 1 (reaction(e)). The equilibrium conversion of DME is higher than that of methanol. For DME synthesis, the maximum value of the equilibrium conversion is higher for the reaction formula (e). This clearly indicates the significance of the fact that the shift reaction (c) proceeds in response to reaction (a) and reaction (b).

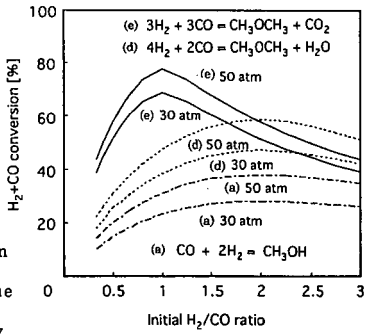

Fig.1 Equiliblium (H_2+CO) conversion to DME or methanol as function of initial H_2/CO ratio and pressure (at 280 ℃)

3.2 Slurry Bed Reactor

The reactor types for catalytic reaction are categorized in fixed bed, fluidized bed and slurry bed. Because DME synthesis reaction is highly exothermic, a fluidized bed and a slurry bed reactor are recommended. Their heat transfer characteristic is so excellent that the temperature distribution in the reactor is flat and that the structure of reactor can be simple.

A slurry bed does not restrict the shape and mechanical strength of the catalyst compared with a fluidized bed. The catalyst in the slurry bed can be easily exchanged by slurry pomp without disturbing the operation when the activity of catalyst decreases. But in the slurry bed, the solubility in the solvent of the water generated on the dehydration catalyst is low, the most of water emerges directly into the gas bubbles and there is a strong tendency for it to emerge from the reactor without reacting with the CO, and overall, the CO conversion becomes low. So adding a shift reaction function to the dehydration catalyst to

convert generated water with the CO immediately to H2 and CO2 has been designed. Because H2 has high solubility and diffusion rate in the solvent, it is consumed by the methanol synthesis reaction, and overall it is possible to obtain a high CO conversion (1,2).

3.3 DME Synthesis Reaction Test

A bench scale experiment was performed based on beaker scale research (1,2). An outline of the test plant is presented in Figure 2. The reactor is a slurry bed bubble tower with an internal diameter of 90 mm and a height of 2 m. The plant capacity is of 50 kg/day of DME. Figure 3 and Figure 4 present, as examples of the results of the experiment, the CO conversion and selectivity of all constituents of the product (CO2 is excluded and the total of DME, methanol, CH4 is considered to 100%) produced in one through operation. There is no other heavy byproduct than methanol and methane.

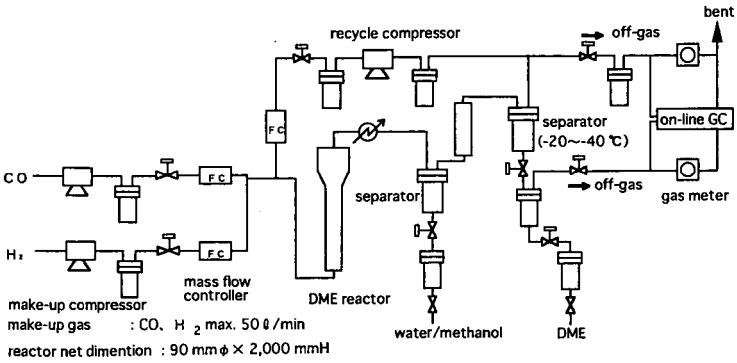

Fig.2 Flow diagram of Bench Plant

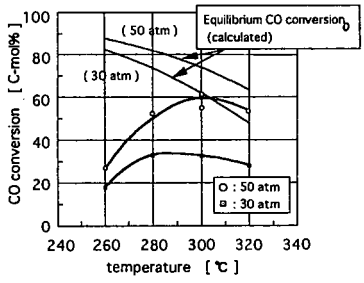

Fig. 3 CO conversion as function of temperature and pressure(one-through,make-up H2/CO=1)

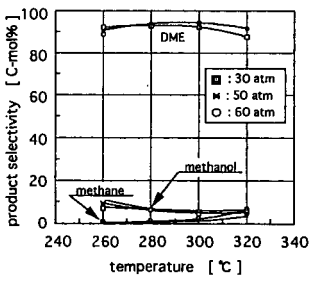

Fig. 4 Product selectivity as function of temperature and pressure

The CO conversion rises as the temperature climbs, and it has the maximum value. This is considered to represent the effect of the equilibrium restrictions caused as the conversion approaches the equilibrium and of the fall in the soluhility of the reaction gas as the temperature rises. A CO conversion greater than 50% and a DME selectivity in excess of 90% were obtained at a pressure of 50 atm and a temperature of 300℃.

As for the catalyst life, as shown in Figure 5 ,during 700 hours of consecutive testing, no deactivation was observed.

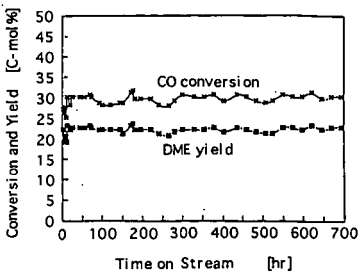

Fig. 5 Catalyst activity as function of time on stream (H2/CO=1,280g,30atm,W/F=12g-cat hr/mol)

4. Synthesis of DME from Coal and Natural Gas and its Uses

4.1 DME Synthesis Process Flow

Figure 6 shows a block diagram to produce DME from coal. Because the H2/CO ratio of synthesis gas obtained by the coal gasification ranges from 0.5 to 1.0, the gas composition is adjusted by the shift reaction so that H2/CO = 1, and it is then supplied for DME synthesis. In this synthesis step where the reaction (e) (H2/CO=1) is achieved, the difference of H2/CO ratio to be adjusted is so narrow in comparison with the reaction(d) (H2/CO=2) that the equipment size and utility consumption for the shift conversion step are smaller.

The effluent from the slurry reactor is cooled and chilled in order to separate the liquid phase (DME , CO2 and small amount of methanol and water) from the gaseous phase containing unreacted H2 and CO. Most of the separated gas is recycled to the reactor. Because the one-through reaction rate is high, the recycle ratio is sufficient at 1:1. After CO2 removal, the product DME is obtained by removing the impure water and methanol to a required level.

In case of natural gas, it can be converted to synthesis gas of H2/CO = 1 by means of CO2 reforming and used to the DME synthesis.

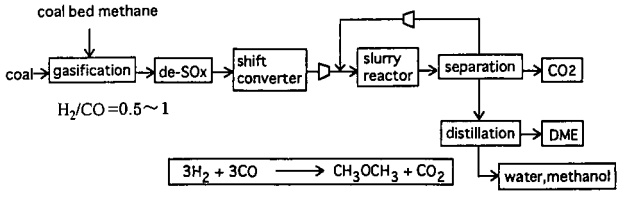

Fig. 6 DME synthesis from coal derived synthesis gas

4.2 Uses of DME

It is expected that DME will be introduced as a LPG-like home use fuel to replace coal and coal briquette and as an engine fuel to replace the light oil used in diesel engines in China, India, Indonesia, and other heavily populated countries with rich coal resources.

In Japan, 25 million tons of non-coking coal is imported to Japan to be consumed in electric power plants. It is forecasted that the future construction of more coal-burning power plants will be accompanied by an increase in the amount of coal consumed for this purpose to 57 million tons/year by 2005; three times as much as that is consumed now.

In Asian region besides Japan, the electricity demand is expected to increase at a rate of 7-8%/year and the coal consumption for power plant will be immense and the environmental pollution will be aggravated.

A concept of a system in which coal is gasified and converted to DME at coal mine, then transported to final consumption area as Japan for use in electric power production has been created as shown in Figure 7 . This system would provide the following potential benefits in comparison with the conventional coal flow.

At coal mine , [1] coal is prepared to reduce transportation costs and provide assurance of sufficient quality, but coal preparation would be unnecessary and all could be used effectively. [2] It would be possible to use low quality coal, for example, lignite coal with high moisture content or inflammable coal which is inadequate to the transportation. [3]Coal bed methane produced as a byproduct of coal mining is generally an unexploited energy resource. As it has a higher greenhouse effect than CO2, its proper treatment will be necessary. Although the coal bed methane generation varies over time, it could be used effectively by injecting it into the coal gasification reactor in which the methane is reformed to synthesis gas.

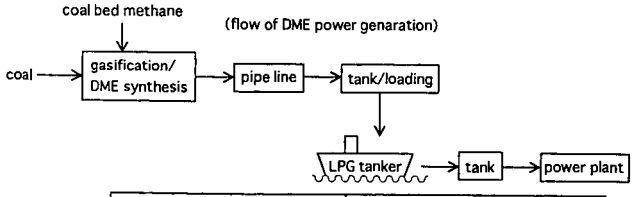

condition		· DME 2,500 t/d (over sea) · 500,000 k W power plant
DME production	plant cost	55 ~ 75 billion yen
	DME cost	2.2 ~ 2.9 yen/10^3 kcal
power genaration cost		8.2 ~ 9.4 yen/kWh

Fig. 7 Power generation through DME flow system and its cost estimation

At the transportation stage, [1] it could be handled in the same way as LPG, so the shipping and receiving base equipment could be simple, and would produce no dust.
In final consumption area , [1] the use of this ash-free clean fuel would eliminate the need for desulfurization and ash disposal treatment, [2] as a gaseous fuel, it would be sure to provide high power generation efficiency with combined cycle power generation, and the problems of providing a coal yard and dealing with ash would be resolved so it could be constructed in the suburbs of cities, thereby reducing transmission power loss.

4.3 Cost estimation of DME production and Electricity from DME burning power generation

Figure 8 shows an example of DME production cost (at coal mine and Japan CIF) in a case where equipment cost varies according to DME plant size with DME production of 910,000 tons/year as a constant condition. As the plant size increases, the cost of producing DME falls to the same level as the price of light oil and of LPG, whose cost is forecast to rise, in regions near coal mine at a production rate of 2,500 tons/day.
In this calculation, the cost of the total plant for DME production from coal is estimated to be 55 billion yen. If the plant costs climb from 55 billion to 75 billion yen, as shown in Figure 7, the DME production cost will be 2.22 yen/10 3 kcal to 2.86 yen/10 3kcal at the production site, while the electric power generation cost rises from 8.2 yen/kwh to 9.4 yen/kwh in Japan. These costs of electricity would be either equal to or lower than the cost of coal burning power generation.

4.4 Comparison of the Environmental Load of Coal burning and DME burning Power generation

The total environmental load produced between the coal production stage in coal mine over sea and the production of power and disposal of waste material in Japan has been compared. Figure 9 shows a result of this study. A switch over to DME flow system is sure to sharply cut the environmental load as follows.
[1] The volume of CO2 emissions would remain almost unchanged. When coal bed methane is emitted in the air, its effective utilization in the coal gasification reactor can cut 20% equivalent to CO2.
[2] No sulfur compounds would be discharged into the atmosphere in the DME flow system.
[3] As DME does not contain nitrogen, there would be no fuel NOx. By incorporating denitrification measures, the amount discharged into the atmosphere could be cut to approximately 1/9 of that discharged from a coal powered plant.
[4] Ash would be discharged as molten slag, it would be easier to use than fly ash, and no heavy metal elution would occur.

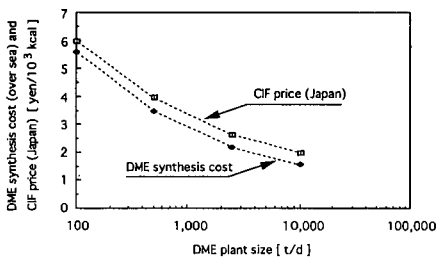

Fig. 8 Cost estimation of DME production

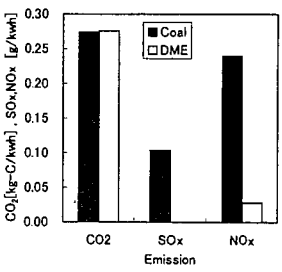

Fig.9 Environmental load of DME flow system and coal flow for power generation

5. Summary

If DME is developed to the stage where it is a practical product and is then distributed as an energy source for home use, transportation, and electric power generation, it will make a significant contribution to the resolution of energy and environmental problems, not only in the country using it for these purposes, but in other Asian countries.
Because DME is not a standard fuel which is already in use, integrated all-encompassing efforts must be made to prepare for its introduction and use from the production through the distribution stage.

References

(1) Y.Z. Han, K. Fujimoto, and T. Shikada: 4th Japan-China symposium on coal and C1 Chemistry proceedings (Osaka 1993), p. 515.
(2) Y.Z. Han, K.. Fujimoto, and T. Shikada: Ind. Eng. Chem. Res (to be published).
(3)Air Products and Chemicals: DOE/PC/90018-T7 (June, 1993).
(4) J.B. Hansen,B.Voss,F.Joensen and I.D.Sigurdardottiv.: SAE950063 (Feb. 1995).
(5)T.Fleisch,C.McCarthy,A.Basu,C.Udovich,P.Charbonneau,W.Slodowske, SE.Mikkelsen and J.McCandless.: SAE950061 (Feb. 1995).
(6) J.Daly and E.Osterman: Chemical Times &Trends,(October,1982),p.38.

LIQUID/CATALYST INTERACTIONS IN A SLURRY REACTOR FOR METHANOL SYNTHESIS USING "ZINC CHROMITE" CATALYST

George W. Roberts, Marco A. Márquez, M. Shawn McCutchen[1] and Carol A. Haney[2]
Department of Chemical Engineering, North Carolina State University, Box 7905, Raleigh, NC 27695-7905
[1] - Current Address: E. I. Du Pont de Nemours and Company, Inc., Jackson Laboratory, Chambers Works, Deepwater, NJ 08023
[2] - Department of Chemistry, Box 8204

Keywords: Methanol, Slurry Liquid, Slurry Reactor, Zinc Chromite

INTRODUCTION

The synthesis of methanol and higher alcohols from mixtures of H_2 and CO (synthesis gas) is a promising approach to producing high-value fuels and chemicals from feedstocks such as natural gas, coal, coke and waste biomass. Slurry bubble column (SBC) reactors have been the focus of considerable attention for alcohol synthesis because the reactions are highly exothermic. Close temperature control is necessary to prevent excessive catalyst deactivation and to achieve high selectivity to oxygenates. The technology for producing methanol in a SBC reactor has been developed on a pilot scale, and is currently being commercialized [1,2,3]. This work has been based on Cu/ZnO, the conventional, low-pressure methanol synthesis catalyst. In addition, laboratory and pilot-plant studies have been conducted using cesium-promoted Cu/ZnO catalyst in a slurry reactor for the synthesis of higher alcohols [4,5]. Alkali-metal-promoted catalysts for higher-alcohol synthesis have evolved from the early work of Anderson and co-workers and Klier and co-workers [e.g., 6-9]. Unpromoted Cu/ZnO catalysts for methanol synthesis typically are operated at about 250°C, and the promoted Cu/ZnO catalysts for higher-alcohol synthesis have been evaluated over a temperature range of roughly 250 to 325°C.

"Zinc chromite", the high-pressure methanol synthesis catalyst, also is a promising starting point for the synthesis of higher (C_2^+) alcohols. However, this catalyst requires a much higher operating temperature, about 400°C, than Cu/ZnO. The liquids that traditionally have been used to slurry the Cu/ZnO catalyst are not thermally stable at this temperature [10-12]. In previous research, a family of liquids was identified that are sufficiently stable, thermally and chemically, to be used in a slurry reactor with the "zinc chromite" catalyst [10-13]. The objective of the present investigation was to explore the performance of an unpromoted "zinc chromite" catalyst in three of the most stable liquids, decahydronaphthalene (DHN or Decalin®, $C_{10}H_{18}$), tetrahydronaphthalene (THN or tetralin, $C_{10}H_{12}$) and tetrahydroquinoline (THQ, $C_9H_{11}N$). Unpromoted "zinc chromite" is essentially a methanol-synthesis catalyst. It is no longer competitive for methanol synthesis with the Cu/ZnO catalyst, which is more active and therefore can operate at lower pressures and temperatures. However, when promoted with alkali metals, "zinc chromite" can produce substantial yields of higher alcohols, particularly 2-methyl-1-alcohols such as isobutanol [14-17]. These alcohols might serve as alternative raw materials for the synthesis of established octane enhancers such as methyl tertiary butyl ether (MTBE). Thus, the present study of interactions between the unpromoted "zinc chromite" catalyst and the three slurry liquids was intended to provide a basis for using of one or more of these liquids as a slurry medium for an alkali-metal-promoted "zinc chromite" catalyst.

EXPERIMENTAL

The equipment used for this research has been described previously in some detail [10-13]. Basically, gases were fed from cylinders through activated carbon traps to remove impurities, including metal carbonyls, and then through mass flow controllers to measure and control the flow rates. The individual gas streams were mixed and compressed to the desired pressure. The compressed gas was passed through another activated carbon trap to remove any iron and/or nickel carbonyls that may have formed during and after compression. The gas was then fed into a 300 cm^3 stirred autoclave reactor. The reactor was charged with 20 grams of catalyst and 80 grams of the slurry liquid. The catalyst was a commercial, high-pressure methanol synthesis catalyst (Zn-0312 T1/8) from Engelhard Corporation, which was obtained in a reduced and stabilized form. The catalyst contained 60 wt% Zn and 15

wt% Cr, with the ZnO and $ZnCr_2O_4$ phases detectable by x-ray diffraction. The as-received BET surface area was 145 m^2/g. The gas leaving the reactor passed into a gas/liquid separator containing a cooling coil to control the temperature of the separator. The gas then passed through a back pressure regulator, through heated lines to prevent condensation and through a wet test meter to measure the gas flow rate. Samples of the reactor feed and effluent were periodically diverted to a dual-column gas chromatograph containing a Carboxen 1000 column followed by a thermal conductivity detector and a Poroplot Q column followed by a flame ionization detector. The former system was used to measure the fixed gases, H_2, N_2, CO, CO_2 and H_2O. The organic species were measured on the second system.

The autoclave reactor was mechanically agitated to ensure complete backmixing, and to ensure that gas/liquid mass transfer did not influence the reaction rate. Because the reactor was backmixed, the rates of formation or disappearance of the various species could be calculated directly from the inlet and outlet compositions and flow rates. The system was operated continuously for periods of one to four weeks. All data was taken at steady state conditions.

A matrix of four experiments was run in each liquid. Two experiments were at a temperature of 375°C, one with a H_2/CO ratio of 0.5 in the feed gas and the other with a feed ratio of 2. The remaining two experiments were at 325°C, at the same two H_2/CO feed ratios. For all experiments, the total pressure was 13.8 MPa and the space velocity was about 5000 sL/kg(cat)-hr.

RESULTS

Figure 1 shows the fractional conversion of carbon monoxide at each of the four operating conditions, in each of the three slurry liquids. The difference in conversion between slurry liquids was substantial. At all four operating conditions, the ratio of the highest conversion to the lowest was between about 2 and 6. The difference in apparent catalyst activity from liquid to liquid was even greater, since the actual partial pressures of CO and H_2 in the reactor were lower in the high-conversion experiments than they were in the low-conversion experiments. The CO conversion was lowest in DHN at all four conditions. At three of the four conditions, the CO conversion was highest in THN. The exception was at 325°C and a H_2/CO ratio of 0.50, where the conversion was higher in THQ than THN.

Figure 1
Effect of Slurry Liquid Composition on CO Conversion

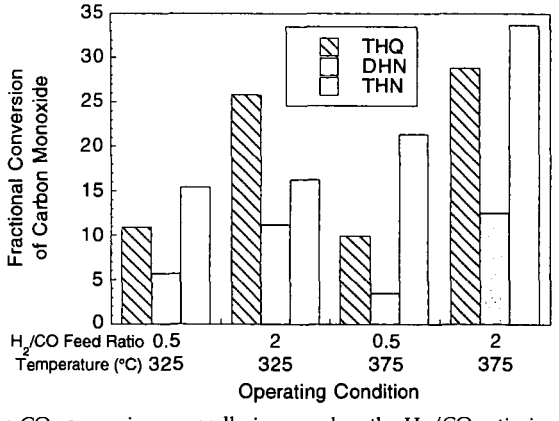

The CO conversion generally increased as the H_2/CO ratio increased from 0.5 to 2. The influence of temperature on conversion depended on the liquid employed. With THN, "normal" behavior was observed, i.e., conversion increased substantially with temperature. However, with DHN and THQ, the effect of temperature on conversion was small. The reason for this difference in behavior is discussed below, in connection with Figure 3.

Figure 2 shows the concentration of methanol in the outlet gas from the reactor at each of the four operating conditions, in each of the three slurry liquids. For comparison, the equilibrium methanol concentration at the specified reactor temperature, with the specified feed gas, also is shown.

Figure 2
Effect of Slurry Liquid Composition on Methanol Production

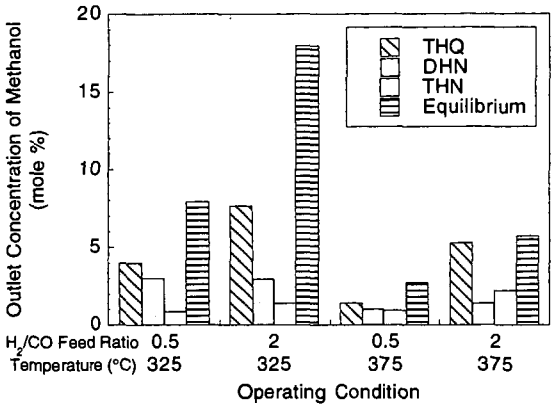

Once again, there was a substantial difference in catalyst performance from liquid to liquid. At all four conditions, the rate of methanol production was higher when THQ was used as the slurry liquid than with either THN or DHN. With the exception of the condition at 375°C and $H_2/CO = 2$, the rate of methanol synthesis was lowest in THN. At the lower temperature, where the reaction is not as close to equilibrium, the effect of liquid composition on the methanol production rate was substantial. For example, at $H_2/CO = 2$ and 325°C, this rate was about a factor of 6 higher in THQ than in THN and about a factor of 2.5 higher in THQ than in DHN.

At both temperatures, the methanol concentration generally increased as the H_2/CO ratio increased, with a given liquid. However, the effect was not as significant with DHN as with the other liquids. In fact, at 325°C with DHN, there was a slight decrease in methanol concentration as H_2/CO increased from 0.5 to 2.

The methanol production rate decreased with temperature at both H_2/CO ratios in THQ and DHN, reflecting the lower equilibrium concentration at the higher temperature. The methanol concentration increased as the temperature increased with THN, probably because the reaction was far from equilibrium in this liquid, at both temperatures.

Figure 3 shows that liquid composition also had a pronounced effect on reaction selectivity. The oxygenates were mostly methanol, plus some dimethyl ether and minor amounts of higher alcohols, primarily ethanol and isobutanol. The hydrocarbons were mostly methane, ethane and ethylene, plus lesser amounts of higher olefins.

Figure 3
Effect of Liquid Composition on Selectivity

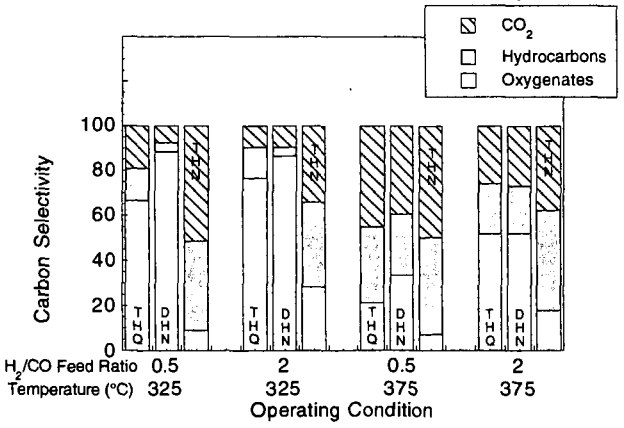

The most significant difference between liquids was the low oxygenate selectivity and high hydrocarbon selectivity in THN, relative to the other two liquids. These effects were especially pronounced at 325°C. The oxygenate selectivity, which never exceeded 30% in THN, was always a factor of about 3 to 10 higher in the other two liquids. Moreover, the high CO_2 selectivity with THN is a direct consequence of the high hydrocarbon selectivity, since "zinc chromite" is an excellent catalyst for the water-gas-shift reaction.

The selectivity to both hydrocarbons and CO_2 increased as the temperature was raised from 325 to 375°C, for all three liquids. The increase was especially pronounced for THQ and DHN since the oxygenate selectivity at 325°C was quite high for both of these liquids. In part, this reflects the fact that the methanol synthesis reaction is close to equilibrium in THQ and THN at 375°C, as shown in Figure 2. This close approach to equilibrium limited the quantity of methanol, the major component of the oxygenates, that could be produced. The oxygenate selectivity generally increased as the H_2/CO ratio was raised from 0.5 to 2 at constant temperature, for all three liquids.

The different product distributions that occur with the three liquids are consistent with the effect of temperature on CO conversion, as noted in connection with Figure 1. The primary products with THN are hydrocarbons and CO_2, and there are no significant equilibrium limitations to the formation of these products at the conditions of these experiments. Therefore, the CO conversion increases with temperature, reflecting the "normal" influence of temperature on reaction kinetics. With THQ and DHN, methanol is the primary product at 325°C. The equilibrium concentration of methanol decreases with temperature, partially offsetting the effect of temperature on reaction kinetics. As a result, the effect of temperature on CO conversion with THQ and DHN is relatively weak.

DISCUSSION

The chemical mechanism(s) that are responsible for the large differences in apparent catalyst activity and selectivity from liquid to liquid are not clear at this time. There has been very little detailed information published on the behavior of the unpromoted "zinc chromite" catalyst in the absence of a liquid, e.g., in a fixed- or fluidized-bed reactor. The problem of comparison is compounded by the fact that the present studies were carried out at a much lower total pressure than typically is used in a methanol synthesis plant employing the "zinc chromite" catalyst. This low pressure probably is characteristic of those that would be used with the promoted "zinc chromite" catalyst for higher-alcohol synthesis. However, the pressure difference makes it difficult to determine which of the liquids most closely approximates "normal" behavior. It is clear that the very low oxygenate selectivity that was observed with THN cannot be typical of conventional, vapor phase operation. The high hydrocarbon and CO_2 selectivities of this liquid, coupled with the high CO conversions, suggest some sort of liquid/catalyst interaction that inhibits methanol synthesis and dramatically increases the rate of hydrocarbon formation.

The methanol-synthesis activity of the "zinc chromite" catalyst in THQ is probably greater than the vapor-phase activity, based on the fact that the methanol synthesis reaction essentially came to equilibrium at 375°C and a H_2/CO ratio of 2 with THQ as the slurry medium. This enhanced rate of reaction may be related to the ability of secondary amines such as THQ to react with oxygenate and/or hydrocarbon fragments on the surface of the catalyst. Analyses of samples of THQ taken during and after reactor operation showed that some alkylation of THQ took place. Moreover, the alkylation of other amines has been reported to occur over various Fischer-Tropsch catalysts during vapor-phase operation, at substantially lower temperatures than those used in this research [18-22]. A mechanistic understanding of the chemistry of the interactions between THQ and the catalyst surface may lead to further improvements in rate and selectivity that can be applied to the synthesis of higher alcohols.

CONCLUSIONS

The composition of the slurry liquid had a major effect on both the apparent activity and selectivity of "zinc chromite" catalyst for the synthesis of methanol in a slurry reactor. Tetrahydronaphthalene (THN) does not appear to be a promising liquid because it causes low rates of oxygenate formation and low oxygenate

selectivities. In contrast, the rate of methanol synthesis was very high in tetrahydroquinoline (THQ), and the oxygenate selectivity was good, especially considering that the rate of the methanol synthesis reaction was retarded by a close approach to equilibrium.

ACKNOWLEDGMENTS

This work was supported in part under a contract with the U. S. Department of Energy, Pittsburgh Energy Technology Center

REFERENCES

1. Studer, D. W., Brown, D. M., Henderson, J. L. and Hsiung, T. H., "Status of the Development of Methanol Synthesis by the LPMEOH* Process", paper presented at U. S. Department of Energy, Pittsburgh Energy Technology Center Indirect Liquefaction Contractor's Review Meeting, Pittsburgh, PA, November 13-15 (1989)

2. Roberts, G. W., Brown, D. M., Hsiung, T. H. and Lewnard, J. J., *Ind. Eng. Chem. Res.*, **32**, 1610 (1993)

3. "Methanol-Producing Clean Coal Technology Project Moves Into Construction In Kingsport, Tennessee", DOE News, October 16, 1995

4. Breman, B. B., Beenackers, A. A. C. M., Schuurman, H. A. and Oesterholt, E., *Catalysis Today*, **24**, 5-14 (1995)

5. Heydorn, E. C., Schaub, E. S., Stein, V. E. E., Underwood, R. P. and Waller, F. J., "Recent Progress on Syngas Conversion to Isobutanol", paper presented at U. S. Department of Energy, Pittsburgh Energy Technology Center Coal Liquefaction and Gas Conversion Contractor's Review Conference, Pittsburgh, PA, September 7-8 (1994)

6. Smith, K. J. and Anderson, R. B., *Preprints, Div. Fuel Chem., ACS*, **29** (5), 269 (1984)

7. Caverley, E. M. and Anderson, R. B., *J. Catal.*, **104**, 434-440 (1987)

8. Klier, K., Herman, R. G. and Young, C. W., *Preprints, Div. Fuel Chem., ACS*, **29** (5), 273 (1984)

9. Vedage, G. A., Himelfarb, P. B., Simmons, G. W. and Klier, K., *ACS Symp. Series*, **279**, 295-312 (1985)

10. McCutchen, M. S., "Synthesis of Alcohols from Carbon Monoxide and Hydrogen in a Slurry Reactor", Ph. D. Thesis, North Carolina State University (1996)

11. McCutchen, M. S., Márquez, M. A. and Roberts, G. W., *Chem. Engng. Sci.*, **51**, 2959 (1996)

12. Roberts, G. W., Màrquez, M. A. and McCutchen, M. S., "Alcohol Synthesis in a High-Temperature Slurry Reactor", *Catalysis Today* (in press)

13. Márquez, M. A., "The Stability of Liquids and the Effect of their Composition on the Production of Methanol in a Slurry Reactor", M. S. Thesis, North Carolina State University (1996)

14. Tronconi, E., Lietti, L., Groppi, G., Forzatti, P. and Pasquon, I., *J. Catal.*, **124**, 376-390 (1992)

15. Tronconi, E., Lietti, L., Forzatti, P. and Pasquon, I., *Applied Catalysis*, **47**, 317-333 (1989)

16. Tronconi, E., Ferlazzo, N., Forzatti, P and Pasquon, I., *Ind. Eng. Chem..Res.*, **26**, 2122-2129 (1987)

17. Tronconi, E., Christiani, C., Ferlazzo, N., Forzatti, P., Villa, P. L. and Pasquon, I., *Appl.Catal..*, **32**, 285 (1987)

18. Wang, C. J. and Ekerdt, J. G., *J. Catal.*, **80**, 172-187 (1983)

19. Wang, C. J. and Ekerdt, J. G., *J. Catal.*, **86**, 239-244 (1984)

20. Kliger, G. A., Glebov, L. S., Popova, T. P., Marchevskaya, E. V., Beryezkin, V. G. and Loktev, S. M., *J. Catal.*, **111**, 418-420 (1988)

21. Glebov, L. S., Kliger, G. A., Popova, T. P., Shiryaeva, V. E., Ryzhikov, V. P., Marchevskaya, E. V., Lesik, O. A., Loktev, S. M. and Beryezkin, V. G., *J. Mol. Catal.*, **35**, 335-348 (1986)

22. Kliger, G. A., Lesik, O. A., Mikaya, A. I., Marchevskaya, E. V., Zaikin, V. G., Glebov, L. S., and Loktev, S. M., *Izv. Akad. Nauk SSSR, Ser. Khim.*, 503 (1991)

SYNTHESIS OF FUEL ALCOHOLS AND MTBE FROM SYNGAS USING SPINEL OXIDE BASED CATALYSTS

David M. Minahan, Walter M. Hart
Technical Center, Union Carbide Corporation, P.O. Box 8361, South Charleston, WV 25303

William S. Epling and Gar B. Hoflund
Department of Chemical Engineering, University of Florida, Gainesville, FL 32611

Keywords: Higher Alcohol Synthesis, Fuel Alcohols, MTBE, Syngas

ABSTRACT

An equal mole mixture of methanol and isobutanol produced from syngas would be an ideal for the production of MTBE for use as a gasoline additive. The best present day syngas to alcohols catalysts and catalyst systems make too much methanol to be economically attractive, with typical methanol/isobutanol mole ratios of 3 or greater. We have investigated a Zn/Cr commercial methanol synthesis catalyst promoted with potassium and find that it is very selective for isobutanol when run under high temperature (> 400 C) and high pressure (>1000 psi) conditions due to both kinetic and thermodynamic considerations. Isobutanol rates >100 g/kg-hr are observed with a methanol/isobutanol mole ratio of 1.9. Surface characterization (via ISS and XPS) shows that the surface of the catalyst changes upon reduction and with use. Movement of potassium and chromium within the surface and near surface region of the catalyst is observed which can be correlated with catalytic performance

INTRODUCTION

Oxygen-containing hydrocarbon compounds can be added to gasoline to both reduce emissions and increase the octane rating of the fuel. Typical additives that have been examined are ethers such as MTBE and TAME and alcohols such as methanol. Methanol can be produced from syngas in high selectivity and can be used as an octane enhancer, but addition to gasoline can cause problems: the presence of water can cause phase separation and the Reid vapor pressure of the mixture is increased, leading to increased emissions from the gas tank. Mixtures of methanol and higher alcohols are a better alternative to methanol alone as ethanol raises the octane rating of the fuel and higher alcohols act as co-solvents, minimizing phase separation and lowering the overall vapor pressure of the additive. For long chain alcohols, branched alcohols are preferred over linear alcohols for enhancing the octane rating, whilst linear alcohols are preferred over branched alcohols for co-solvency characteristics. Ethers such as MTBE and TAME are preferred as additives due to their excellent co-solvent properties, lower volatility as compared with methanol and ethanol and their octane enhancing properties. Nonetheless, branched alcohols such as isobutanol and its higher homologs would still be of interest in their own right or as potential precursors to accepted additives such as MTBE or TAME. Alternatively, an equimolar mixture of methanol and isobutanol could be used as a direct precursor for the manufacture of MTBE.

Higher alcohol synthesis (HAS) catalysts have primarily evolved from modified methanol synthesis catalysts. The original methanol synthesis catalysts were based on a zinc/chromium spinel oxide operated around 400°C, and could tolerate some sulfur impurities in the syngas feed [1]. With the advent of effective desulfurization techniques for the syngas, a second generation methanol synthesis catalyst was developed, based on a more active copper metal based formulation which could operate at substantially lower temperatures (250-300°C) [2]. In both cases, the addition of alkali to the system resulted in the formation of higher alcohols, albeit at a substantially lower overall productivity. Other catalyst systems have been developed based on molybdenum sulfide (Dow/Union Carbide) [3], supported rhodium metal (Union Carbide) [4] and supported Cu/Co clusters (IFP) [5]. Once again, alkali is commonly added to the formulations. An interesting contrast between "modified methanol" catalysts and other systems is in the types of alcohols produced: the "modified methanol" catalysts produce mainly branched alcohols with a non Anderson-Schulz-Flory (ASF) distribution via an aldol condensation mechanism, the major products being methanol and isobutanol. The others produce linear alcohols via classical CO insertion/hydrogenation, producing the characteristic ASF distribution similar to that observed in linear condensation polymerization.

The following major reactions can take place over the catalyst or tube walls:

Alcohol Formation

$$n\,CO + 2n\,H_2 = C_nH_{2n+1}OH + (n\text{-}1)\,H_2O$$

Hydrocarbon Formation

$$nCO + (2n+1)\,H_2 = C_nH_{2n+2} + n\,H_2O$$

Water-Gas-Shift Reaction Equilibrium

$$CO + H_2O = CO_2 + H_2$$

Boudouard Reaction (CO disproportionation)

$$2CO = C + CO_2$$

Catalyst Selection and Testing Protocol

The catalysts examined here are materials consisting of a spinel oxide support (general formula AB_2O_4, where $A = M^{2+}$ and $B = M^{3+}$), promoted with potassium. The spinel itself consists of the traditional zinc/chromium oxide formulation, modified by the inclusion of excess zinc oxide and was obtained from Engelhard Corporation. The catalysts were tested first at low temperatures in stainless steel reactor tubes, then at higher temperatures (> 340 °C) in copper lined tubes to avoid the Boudouard reaction and hydrocarbon formation, known to be catalyzed by stainless steel (Fe, Ni) at these higher temperatures.

Reaction Mechanism

HAS requires at least two complimentary, yet competing reactions: carbon-carbon bond formation and hydrogenation. In the copper metal based, low temperature system, carbon-carbon bond formation is thought to occur via a classical CO insertion mechanism, followed by hydrogenation. In contrast, the high temperature catalysts utilize an aldol condensation mechanism to form the carbon-carbon bonds. The aldol reaction can proceed via acid or base catalysis.

The selection of elements other than copper as hydrogenation catalysts is a crucial feature of the high temperature formulations. Copper cannot be used as it sinters rapidly above 300°C, resulting in catastrophic loss in activity. Thus, temperature cannot be used as a lever in a copper catalyst system in order to improve alcohol activity. Nonetheless, both kinetics and thermodynamics favor HAS at higher temperatures. Methanol synthesis is at equilibrium under reaction conditions and higher alcohols are formed by consecutive reactions from methanol, thus higher temperatures will accelerate the secondary, higher alcohol forming reactions while the equilibrium of the methanol synthesis implies lower methanol concentrations. The net result is a considerable improvement in both the rate and selectivity to higher alcohols at higher temperatures at the expense of methanol. However, higher temperatures also enhance the formation of methane and higher hydrocarbons, so overall catalyst acidity must be carefully controlled. Thus alkali addition (in the form of potassium) helps by both providing basic sites for higher alcohol synthesis via the base-catalyzed aldol condensation and by neutralizing acid sites responsible for hydrocarbon formation.

The thermodynamic equilibrium for methanol formation dictates that methanol concentration grows quadratically with total pressure, while the concentration of higher alcohols exhibits a weaker dependence, resulting from kinetic considerations. Thus, pressure does increase reaction rate, but is not an effective handle for boosting HAS vs. methanol. However, hydrocarbon production is minimized at higher pressures, so total alcohol selectivity should rise.

RESULTS & DISCUSSION

Experiments were run in two different reactors. At lower temperatures (≤340°C) we used a stainless steel tubular microreactor. Low temperature runs were conducted at 12000 GHSV, $H_2/CO=1$ and 1000 psig. Most experiments were run in duplicate.

Low Temperature Operation (up to 340°C): The results are displayed in Table 1 below:

Table 1
K-impregnated Zn/CrO Catalysts - Low Temperature Operation

Temperature (°C)	260			
Potassium Loading	0% K	1% K	3% K	5% K
%CO2-free MeOH Selectivity	92	88	55	59
%CO2-free HC Selectivity	8	12	43	35
%CO2-free ROH Selectivity	92	88	57	65
%CO2-free C2+ ROH Selectivity	0	0	2	6
Isobutanol Rate (g/kg-hr)	0	0	0	0
Total Alcohol Rate (g/kg-hr)	206	104	35	20
Methanol Rate (g/kg-hr)	206	104	34	19
n-Propanol Rate (g/kg-hr)	0	0	0	0
Hydrocarbon Rate (g/kg-hr)	9	7	12	6
% CO Conversion	0.1	0.7	3.5	1.1

Temperature (°C)	300			
Potassium Loading	0% K	1% K	3% K	5% K
%CO2-free MeOH Selectivity	77	57	41	29
%CO2-free HC Selectivity	20	28	44	52
%CO2-free ROH Selectivity	80	72	56	48
%CO2-free C2+ ROH Selectivity	3	15	15	19
Isobutanol Rate (g/kg-hr)	0	0	0	0
Total Alcohol Rate (g/kg-hr)	327	197	99	73
Methanol Rate (g/kg-hr)	318	170	77	50
n-Propanol Rate (g/kg-hr)	4	14	10	9
Hydrocarbon Rate (g/kg-hr)	39	40	40	43
% CO Conversion	3.6	6.7	5.5	3.6

Temperature (°C)	340			
Potassium Loading	0% K	1% K	3% K	5% K
%CO2-free MeOH Selectivity	56	37	23	13
%CO2-free HC Selectivity	39	50	61	64
%CO2-free ROH Selectivity	61	50	39	36
%CO2-free C2+ ROH Selectivity	5	13	16	23
Isobutanol Rate (g/kg-hr)	0	0	0	3.7
Total Alcohol Rate (g/kg-hr)	428	361	197	177
Methanol Rate (g/kg-hr)	405	288	134	84
n-Propanol Rate (g/kg-hr)	7	34	31	45
Hydrocarbon Rate (g/kg-hr)	134	190	172	191
% CO Conversion	11.2	17.4	15.1	20.7

In all cases, higher alcohol production was low. Isobutanol was observed only for the case with the highest potassium loading (5%) at the highest temperature (340 °C). CO conversion increased with temperature as expected. Although higher temperatures increased methanol, total alcohol and total hydrocarbon activities, higher temperatures also promoted hydrocarbon formation at the expense of methanol synthesis. C2+ alcohol selectivity appeared to increase from 260 °C to 300 °C, but a further increase in temperature (to 340 °C) did not result in a corresponding increase in selectivity, probably due to interference from the stainless steel reactor walls. Catalysts impregnated with potassium had higher C2+ alcohol selectivity than the bare support at all three temperatures, and C2+ alcohol selectivity increased with potassium loading. However, total alcohol rates decreased as the loading of potassium on the catalyst increased due mostly to the suppression of methanol synthesis.

These results led us to believe that even higher operating temperatures would be beneficial, provided unwanted side reactions catalyzed by the stainless steel reactor walls could be eliminated. Further tests were performed in copper lined tubes. It should be noted that reaction *rates* are not dramatically increased by increased temperatures, rather the product distribution between methanol/higher alcohols and hydrocarbons is shifted; it seemed prudent,

therefore, to explore the use of higher pressures as a means of boosting reaction rates, so pressures in excess of 1000 psig were also examined.

High Temperature/High Pressure Operation (400°C and above, up to 1500 psig): The results at 12000 GHSV and $H_2/CO = 1$ are displayed in Table 2 below:

Table 2
K-impregnated Zn/CrO Catalysts - High Temperature Operation

Catalyst	Unpromoted Spinel			
Temperature (°C)	400	400	440	440
Pressure (psig)	1000	1500	1500	1000
%CO2-free ROH Selectivity	65	77	43	27
Total Alcohol Rate (g/kg-hr)	111	236	133	59
Methanol Rate (g/kg-hr)	105	223	102	41
n-Propanol Rate (g/kg-hr)	0	0	18	10
Isobutanol Rate (g/kg-hr)	6	13	13	5
MeOH/I-BuOH Mole Ratio	73	68	31	36
Hydrocarbon Rate (g/kg-hr)	30	35	94	86

Catalyst	1% Potassium			
Temperature (°C)	400	400	440	440
Pressure (psig)	1000	1500	1500	1000
%CO2-free ROH Selectivity	61	75	53	53
Total Alcohol Rate (g/kg-hr)	133	251	167	129
Methanol Rate (g/kg-hr)	78	170	49	70
n-Propanol Rate (g/kg-hr)	8	0	9	6
Isobutanol Rate (g/kg-hr)	47	81	103	47
MeOH/I-BuOH Mole Ratio	6.6	8.4	1.9	6.0
Hydrocarbon Rate (g/kg-hr)	48	46	101	6

Catalyst	3% Potassium			
Temperature (°C)	400	400	440	440
Pressure (psig)	1000	1500	1500	1000
%CO2-free ROH Selectivity	80	88	70	70
Total Alcohol Rate (g/kg-hr)	75	159	99	67
Methanol Rate (g/kg-hr)	38	92	26	8
n-Propanol Rate (g/kg-hr)	4	10	0	0
Isobutanol Rate (g/kg-hr)	34	57	67	57
MeOH/I-BuOH Mole Ratio	4.5	6.4	1.5	0.54
Hydrocarbon Rate (g/kg-hr)	11	12	29	21

Catalyst	5% Potassium			
Temperature (°C)	400	400	440	440
Pressure (psig)	1000	1500	1500	1000
%CO2-free ROH Selectivity	96	97	84	83
Total Alcohol Rate (g/kg-hr)	82	159	130	70
Methanol Rate (g/kg-hr)	59	123	47	16
n-Propanol Rate (g/kg-hr)	0	0	23	10
Isobutanol Rate (g/kg-hr)	23	34	51	38
MeOH/I-BuOH Mole Ratio	10	14	3.7	1.7
Hydrocarbon Rate (g/kg-hr)	2	3	15	10

The non-promoted catalyst gives mostly methanol and a small amount of isobutanol. The total alcohol rate more than doubles when the pressure is increased from 1000 to 1500 psig, showing the beneficial effect of pressure on reaction rate. Increasing the temperature to 440°C cuts the totoal alcohol selectivity and the methanol rate in half and almost triples the hydrocarbon rate.

1% potassium promotion does not substantially affect total alcohol selectivity, but the alcohol distribution shifts dramatically in favor of isobutanol. Isobutanol rates >100 g/kg-hr are observed at the highest operating conditions of temperature and presssure (440°C and 1500 psig) with a methanol/isobutanol mole ratio of 1.9. Total alcohol selectivities are above 50%.

Increasing the level of potassium on the catalyst results in an increase in selectivities to total alcohols, but a decrease in total alcohol rate. A methanol/isobutanol mole ratio < 1 (0.54) can be obtained for the 3 wt% potassium catalyst at 440°C and 1000 psi, but the isobutanol rate is reduced to < 60 g/kg-hr. The 5 wt% material is the most selective for alcohols, but the methanol rate has increased and the isobutanol rate has decreased.

Surface Science Characterization

Surface characterization (via ISS and XPS) shows that the surface of the catalyst changes upon reduction and with use. Reduction under hydrogen (250°C for 4.5 hrs in 1 x 10-7 torr hydrogen) induces the migration of potassium to the topmost monolayer resulting in complete surface coverage as observed by ion scattering spectroscopy (ISS). X-ray photoelectron spectroscopy (XPS) data are consistent with these observations and also reveal that the near-surface region of the catalysts consist primarily of zinc oxide. Chromium is observed, and appears to be present as potassium chromate or potassium dichromate.

The used catalysts exhibit a potassium rich surface, but the near surface contains much less potassium and again consists essentially of zinc oxide. The chromium now appears to be present as chromium(III) oxide, hydroxide and some chromium metal. These results suggest that the active phase of the catalyst is potassium supported on zinc oxide, possibly promoted with chromium.

ACKNOWLEDGMENTS

The present work was sponsored by the United States Government Department of Energy (DOE) under DOE Contract No. DE-AC22-91PC90046 through the Pittsburgh Energy Technology Center. Our thanks to Engelhard Corporation for supplying the catalysts and to Paul Ruppert and Dana Jividen for catalyst testing.

REFERNCES

1. Satterfield, C. N., *Heterogeneous Catalysis in Industrial Practice*, 2nd Edition, McGraw-Hill, New York, (1991) p. 454.

2. Forzatti, P., Tronconi, E. and Pasquon, I., Catal. Rev. Sci. Eng. 33(1&2) 109-163 (1991).

3. SRI PEP Review "Dow/Union Carbide Process for Mixed Alcohols from Syngas", March (1986).

4. Bhasin, M. M. ,Bartley, W. J., Ellgen P. C. and Wilson, T. P., *J.Catal.* 54, 120 (1978).

5. Courty, P., Durand, D., Freund, E., and Sugier, A., *J. Mol. Cat.* 17, 241 (1982).

KINETICS OF HIGHER-ALCOHOL FORMATION FROM SYNTHESIS GAS USING STATISTICALLY DESIGNED EXPERIMENTS

Anil Gunturu, Jean B. Cropley, Edwin L. Kugler and Dady B. Dadyburjor
Department of Chemical Engineering, West Virginia University,
P.O. Box 6102, Morgantown WV 26506-6102

Keywords: Statistical design, Synthesis gas, Higher alcohols, Promoted molybdenum sulfide catalyst

Introduction

Alcohols containing upto five carbon atoms can be added to the gasoline pool to improve the octane number without an excessive impact on the environment. The Dow patents [1,2] describe a promoted molybdenum sulfide catalyst for the production of these alcohols from synthesis gas even in the presence of sulfur. Screening studies in our laboratory [3] have indicated that a carbon-supported, potassium-promoted cobalt-molybdenum sulfide catalyst yields exceptionally good results, in terms of the space-time yield (STY) of each higher alcohol.

For the purpose of reactor design, it is necessary to obtain a set of kinetic equations for this catalyst, to represent the formation rates of the alcohols in a range of realistic conditions for a large number of variables. However, the kinetic equations need not necessarily reflect the mechanism(s) of the reactions. The present work describes such a set of equations for methanol, ethanol, propanol and total hydrocarbons. The range of conditions used to obtain the experimental data, and in which the set of equations is valid, was based on the screening study and is characterized by: temperature, 300-350°C; total pressure, 400-1000psi; CO/H_2 ratio, 0.5-2; and methanol, 0-1.2ml/h. A fractional factorial set of experiments was designed to incorporate this large set of parameters. A Berty-type internal-recycle reactor was used, to ensure that the reaction rate corresponded to known (outlet) concentrations of reactants and products.

Experimental

The K-Co-MoS/C catalyst was prepared by incipient-wetness impregnation. The catalyst contained 18wt% Mo with a Co/Mo ratio of 0.34 and a K/Mo ratio of 1.3. The catalyst was reduced to the sulfide form inside the reactor, and thereafter purged in hydrogen. The reactor system is computer controlled and all operating conditions can be set by a PC. The system has four lines for gas feed and one line for the liquid methanol feed. The 16 factorial experiments were performed in random order, so as to make the catalyst age an independent variable as well. An additional, center-point, experiment was repeated after every four runs. Product STYs were obtained every 2h, and each experiment was conducted for at least 12h.

Results

The products were found to be linear alcohols, and follow an Anderson-Schultz-Flory distribution. A detailed examination of the experiments with methanol addition showed (1) that the higher alcohols are generated from secondary reactions involving methanol, (2) that a simple condensation reaction involving only alcohols can be ruled out, and (3) that the most likely process involves CO insertion into a lower-carbon-number alcohol to form a higher alcohol. These observations are consistent with the isotopic-labelling results of Santiesteban [4].

Based on this reaction scheme, a two-step process was used to obtain the kinetic equations. First, simple power-law representations were used to quantify the "gross" rates of formation of each of the alcohols (other than methanol) and the hydrocarbons. By the "gross" rate of formation, we refer to the total rate of formation, regardless of the fact that some of the particular species may react further. Then the rate of formation as actually measured (*i.e.*, after some of the particular species reacts further) would be the "net" rate of formation. Since we assume sequential reactions:

MeOH + CO → EtOH,
EtOH + CO → PrOH,

etc, therefore the "gross" rate of methanol formation is the sum of the "net" rates of methanol, ethanol, *etc.* formation, and so on.) For an alcohol of carbon number n, the power-law rate expression included terms for the partial pressures of CO, H_2, inert, and the alcohol of carbon number n-1, as well as terms for the catalyst age (t), the temperature (T), the pre-exponential

factor (A) and the activation energy (E). The general power-law expression used can be centered around the center-point values of the parameters as:

$$r_n^{gross} = k_n (P/P_{cp})_{CO}^{an} (P/P_{cp})_{H2}^{bn} (P/P_{cp})_I^{cn} (P/P_{cp})_{n-1}^{dn} (t/t_{cp})^{-\lambda n} \quad (1a)$$

where

$$k_n = A_n \exp[-(E_n/R)(1/T - 1/T_{cp})] \quad (1b)$$

Here the subscripts I and cp denote inert and a center-point value respectively. Note that a power-law expression for methanol, for which $n=1$, was not obtained in this first step. Because methanol is used as a reactant in many of the runs in this work, the rate of formation could be positive or negative, and a simple power-law model cannot be used for this purpose. For the other alcohols, the best fit of the power-law models yield values of A_n, E_n, a_n-d_n, and λ_n as shown in Table I. Further, a statistical analysis of the results indicated which parameters were statistically significant for each product.These parameters are identified in Table I.

These parameters were then used in the second step, where a Langmuir-Hinshelwood-type rate expression was used for each product, incorporating only the statistically significant parameters for each product. Now a methanol rate expression can be written, incorporating both forward- and reverse-reaction terms to allow for net rates of formation or net rates of reaction.Kinetic rate constants, equilibrium constants, and activation energy constants representing each statistically significant parameter were obtained by a non-linear best fit of the Langmuir-Hinshelwood-type rate expression. The final expressions can be written as:

$$r_{MeOH}^{gross} = \frac{4.9047\exp[-(117x10^3/R)(1/T-1/T_{cp})]\{\pi_{CO}\pi_{H2}^2 - (0.3359K_{cp}/K_{eq})\pi_{MeOH}\}}{(1 + 0.0696\,\pi_{CO} + 0.64\,\pi_{H2}^2 + 0.694\,\pi_{MeOH})^2} \quad (2)$$

$$r_{EtOH}^{gross} = \frac{1.5259\exp[-(25.0x10^3/R)(1/T-1/T_{cp})]\,\pi_{MeOH}}{1 + 0.7367\,\pi_{MeOH}} \quad (3)$$

$$r_{PrOH}^{gross} = \frac{0.1159\exp[-(86.8x10^3/R)(1/T-1/T_{cp})]\,\pi_{EtOH}}{1 + 0.640\,\pi_{EtOH}} \quad (4)$$

$$r_{HC}^{gross} = \frac{4.6965\exp[-(95.3x10^3/R)(1/T-1/T_{cp})]\,\pi_{MeOH}}{1 + 1.2479\,\pi_{MeOH}} \quad (5)$$

Conclusions

The forms of the final rate expressions obtained imply that, under the present conditions, the rate expressions refer to the intrinsic kinetics and are not strongly governed by internal pore diffusion. Further, it would appear that the chemisorption of alcohol is the rate-limiting step, and that the individual steps of hydrogen cleavage, hydrogenation, dehydration and CO insertion (in the overall CO-insertion mechanism) are not rate limiting.

Acknowledgments

This work was supported by the US Department of Energy under Contract Number DE-AC22-91PC91034.

References

1. M.M. Conway, C.B. Murchison and R.R. Stevens, *US Patent 4,675,344*, (1987).
2. R.R. Stevens, *US Patent 4,752,622* (1988).
3. Z. Liu, X. Li, M.R. Close, E.L. Kugler, J.L. Petersen and D.B. Dadyburjor, *Ind. Eng. Chem. Res.*, submitted (1996).
4. J.G. Santiesteban, Ph.D. Dissertation, Lehigh University (1989).

Table I
Results of Fit to Power-Law Model for Gross Reaction Rates

Species	A_n	E_n	a_n	b_n	c_n	d_n	λ_n
Ethanol	0.959	-38,252	0.1242	-0.3067	-0.0411	0.7307(*)	-0.1511
Propanol	0.0904	-97,852	0.0893	-0.6406	0.0216	0.5642(*)	-0.3226
Hydrocarbons	2.68	-106,478	-0.0273	-0.5212(*)	-0.0123	0.6636(*)	-0.2682(*)

(*) These parameters considered statistically significant

THE PERFORMANCE CHARACTERISTICS OF C_1-C_5 ALCOHOL - GASOLINE BLENDS WITH MATCHED OXYGEN CONTENT IN A SINGLE CYLINDER SI ENGINE

Yasser Yacoub, Reda Bata, Mridul Gautam, Daniel Martin
Department of Mechanical and Aerospace Engineering
West Virginia University
Morgantown, WV 26506

Keywords: alcohol-gasoline blend, engine knock , brake thermal efficiency

ABSTRACT

Alcohols with carbon numbers ranging from C_1 to C_5 were individually blended with unleaded test gasoline (UTG-96). All of the alcohol-gasoline blends had the same oxygen mass content. The performance characteristics of the blends were quantified using a single cylinder spark ignition engine. The knock limiting spark timing was determined by analysis of the third derivative of the measured in-cylinder pressure versus crank angle. The engine operating conditions were optimized for each (C_1-C_5) blend with two different values of matched oxygen content. Adding lower alcohols (C_1,C_2,C_3) to UTG96 improved knock resistance. Further improvement was achieved by increasing the oxygen content of the fuel blend. Blends with higher alcohols (C_4,C_5) showed degraded knock resistance when compared to neat gasoline.

INTRODUCTION

Alcohols are being used as fuel blending components to improve unleaded gasoline octane quality. Normally, methanol and ethanol are the main blending components [1][1]. Addition of small amounts of alcohols, with carbon numbers greater than one, improves fuel blend water tolerance, material compatibility, and volatility characteristics [2-7]. Increasing the alcohol content, which also increases oxygen content, up to a certain concentration (when blended with gasoline) improves the blends' knock resistance. Further increase in alcohol content does not lead to any further improvements in knock resistance [2,8,9].

The global objective of the current study is to examine individual alcohols, when blended with gasoline, with regard to engine knock. The specific objective is to determine whether the improved knock characteristics of an alcohol-gasoline blend is solely dependent on its oxygen content or if other factors are involved.

THE PHYSICAL AND CHEMICAL PROPERTIES

Selected chemical and physical properties of gasoline and alcohols are shown in table 1. When higher alcohols are blended individually with gasoline, larger amounts are needed in the blend in order to match the oxygen content of lower alcohols blends, as shown in figure 1. The changes in properties of blends with oxygen mass contents of 2.5% and 5.0%, relative to neat gasoline, are shown in figures 2 - 5. In general, as the alcohol concentration increases so does the blend's specific gravity, as shown in figure 2. Fuel blends with higher alcohols are slightly denser than those with lower alcohols for given oxygen mass contents of 2.5% and 5.0%. The energy-mass density for each blend is predicted by summing up the mass weighted heating values of the neat components[2]. The higher the oxygen content in the blend, the lower its energy mass-density value, as shown in figure 3. The decrease in the heating value is almost the same for blends with matched oxygen content. The energy-volume density for each blend is computed by multiplying its energy-mass density and its specific gravity. Blends with higher alcohols have larger energy-volume densities, when compared to those with lower alcohols for the given oxygen mass contents of 2.5% and 5.0%, as shown in figure 4. For the same operating conditions, engines burning a stoichiometric mixture need to consume more alcohol-gasoline blend than neat gasoline, as shown in figure 5. It should be noted that other important properties of gasoline-alcohol blends, such as distillation characteristics, reid vapor pressure, and water tolerance, are not discussed.

Table 1. Comparison of selected fuel properties

	Methanol	Ethanol	N-Propanol	N-Butanol	N-Pentanol	Gasoline
Formula	CH_3OH	CH_3CH_2OH	$CH_3CH_2CH_2OH$	$CH_3(CH_2)_2CH_2OH$	$CH_3(CH_2)_3CH_2OH$	—
Oxygen content (mass fraction)	0.50	0.35	0.27	0.22	0.18	0.00
Molecular weight	32.04	46.07	60.10	74.12	88.15	111.21
Specific gravity	0.79	0.79	0.80	0.81	0.81	0.74
Energy-mass density (KJ/gm)	19.93	26.75	30.94	33.22	34.84	42.91
Energy-volume density (KJ/cm^3)	15.78	21.11	24.86	26.90	28.38	31.87
Stoichiometric air/fuel ratio	6.43	8.94	10.28	11.12	11.68	14.51

[1] Numbers in parentheses designate references at end of paper.

EXPERIMENTAL

The engine used is a Waukesha single cylinder spark ignition cooperative fuel research engine with variable compression ratio. The engine bore and stroke are 3.25 and 4.5 in; respectively, giving a displacement of 0.612 L. A DC current General Electric dynamometer is used to motor and load the engine. Unleaded test gasoline (UTG-96) and high purity straight chain (n-) alcohols are used. Table 2 lists the engine conditions which are held constant throughout this investigation.

Table 2. Engine test conditions

Speed (rev./min.)	1000
Equivalence ratio	1.0 ± 0.02
Load	wide open throttle
Coolant temperature (°F)	209
Oil temperature (°F)	153 ± 4
Mixture temperature (°F)	110 ± 3
Air relative humidity (%)	25 ± 4

Alcohols with carbon numbers ranging from C_1 to C_5 are individually blended with unleaded test gasoline (UTG-96). The resulting alcohol-gasoline blends have oxygen mass contents of 2.5% and 5.0%. For each fuel blend, the compression ratio (CR) is changed from a value of 7, to the high knock limiting value in increments of 0.5. The spark timing (ST) is varied from a value of 30 to 5 degrees crank angle (CA) before top dead center (BTDC) in decrements of 5.

ANALYSIS PROCEDURE

For a fixed CR, a polynomial (up to fourth order) in ST is fit to brake thermal efficiency (η) values using the least squares method. The fitted polynomial is used to determine the spark timing for maximum η.

The magnitude of the third derivative of the measured in-cylinder gas pressure is used to quantify the engine knock strength [10]. A value of 50 psia/CA^3 is observed as a maximum threshold to characterize a single pressure trace that does not exhibit any knocking. Figure 6 shows that at low knocking operations, the time-averaged knock strength value is less than the threshold value, over a set of consecutively sampled in-cylinder pressure traces for different operating conditions (CR,ST). It also shows that the percentage of traces that exhibits knocking correlates linearly with the time averaged knock strength over that range. This linear relation is used to calculate values of time averaged knock strength that corresponds to a range of traces that exhibit knock.

For a fixed CR, a polynomial (up to fourth order) in ST is fit to the time-averaged knock strength values using the least squares method. The fitted polynomial is used to determine the spark timing for a range (5-20%) of traces that exhibit knock.

The intersection of the knock limiting spark timing curve ,and that of maximum η, identifies an optimum operating point (ST,CR), as shown in figure 7. The line of maximum BMEP is shown as well. Another operating point of interest is that of the maximum possible CR within the tested range. This is the point of intersection of the 5 CA BTDC spark timing line with the knock limiting spark timing curve.

RESULTS AND DISCUSSION

For the investigated CR range, all blends with 2.5% and 5.0% oxygen content have higher maximum η values as compared to neat gasoline, with the exception of ethanol-gasoline blend with a 2.5% oxygen content, as shown in figures 8 and 9. The increase in brake thermal efficiency with increased alcohol content is attributed to the faster burning rate, and higher cylinder pressure, than those of neat gasoline [2,11]. Detailed thermodynamic analysis of the power cycle is required to explain the improvement in η values for all blends and, specifically, the degradation for the ethanol-gasoline blend with 2.5% oxygen.

Figures 10 and 11 show the knock limiting spark timing at different compression ratios for 5% traces exhibit knocking. The C_1 to C_3 alcohol-gasoline blends show a wider range of operation relative to neat gasoline. On the other hand, higher alcohol (C_4,C_5)-gasoline blends show degraded knock resistance when compared with neat gasoline. These trends are common for the 2.5% and 5.0 % oxygen blends.

In order to quantify each blend's knock resistance characteristics, the areas under the curve in figures 10 and 11 are computed and compared to that of neat gasoline, as shown in figure 12. **Adding lower alcohols (C_1,C_2,C_3) to gasoline has improved knock resistance. Ethanol-gasoline** blends show the highest knock resistance improvement (~ 20%-35 %). On the other hand, blends with higher alcohols (C_4,C_5) show degraded knock resistance, when compared to gasoline. The pentanol-gasoline blend shows the highest knock tendency (~30%-60%). For the 5.0% oxygen

blends, both the improvement and degradation trends of knock resistance are more pronounced when compared with the 2.5% oxygen blends.

For an engine operating at optimum conditions, the improvement in the values for η and CR for different blends, relative to neat gasoline, are shown in figures 13 and 14 respectively. For the 2.5% oxygen blends, the methanol-gasoline blend shows the highest improvement in η (~2%). The ethanol-gasoline blend, however, has the highest improvement (~6.0%) for η when compared with the 5.0% oxygen blends. Blends with higher alcohols (C4,C5) have degraded η values, with the exception of butanol-gasoline blend with 2.5% oxygen. For the 5.0% oxygen blends, both the improvement and the degradation trends for the η values are more pronounced, when compared with the 2.5% oxygen blends with the exception of 2.5% oxygen butanol-gasoline blend. The slight improvement in η value for the butanol-gasoline blend with 2.5% oxygen, is attributed to the blend's higher η value when compared to gasoline at the same CR value. Both 2.5% and 5.0% oxygen ethanol-gasoline blends show the highest improvement (~ 2.5% and 10.0%, respectively) in optimum CR value, when compared with matched oxygen content blends.

For an engine operating at the maximum possible CR and ST of five degrees BTDC, all blends (with the exception of pentanol-gasoline blends) show improvement for the values of η and CR relative to neat gasoline, as shown in figures 15 and 16 respectively. For the 2.5% oxygen blends, methanol-gasoline blends show the highest improvement in η (~4%). On the other hand, the propanol-gasoline blend has the highest improvement in η (~7.5%), when compared with the 5.0% oxygen blends. For the 2.5% oxygen blends, the ethanol-gasoline blend operates at the highest (~15%) CR value and the methanol-gasoline blend operates at the highest (~20%) CR value among the 5.0% oxygen blends.

CONCLUSIONS

Adding lower alcohols (C_1,C_2,C_3) to unleaded test gasoline improves its knock resistance from 8% to 20% for blends with a 2.5% oxygen mass content, when compared to neat gasoline. The knock resistance is further improved (20% - 35% compared to gasoline) by increasing the oxygen content of the blend to 5.0%. Ethanol-gasoline blends show the highest knock resistance improvement (~ 20% - 35 %) among all tested blends.

Blends with higher alcohols (C_4,C_5) show degraded knock resistance when compared to gasoline. Pentanol-gasoline blend exhibits the highest knock tendency, ~ 30% more, than gasoline for 2.5% oxygen blends. The knock tendency is further promoted (~60% more than gasoline) by increasing the oxygen mass content in the blend to 5.0%.

All tested alcohol-gasoline blends have a higher brake thermal efficiency than neat gasoline operating, when compared at the same compression ratio, with the exception of ethanol-gasoline blend with 2.5% oxygen mass content.

For an engine optimized for maximum brake thermal efficiency and knock limiting operating conditions, (C_1,C_2,C_3) alcohol-gasoline blends operate at higher efficiency (~ 2% for C_1-UTG 2.5% O_2 and ~6% C_2-UTG 5.0% O_2) when compared to neat gasoline, due to its higher optimum compression ratio. Ethanol-gasoline blends show the highest improvement in optimum compression ratio (~2.5% for 2.5% O_2 and ~10.0% for 5.0% O_2).

For an engine optimized for knock limiting operating conditions and five degress BTDC spark timing, (C_1,C_2,C_3) alcohol-gasoline blends operate at higher efficiency (~ 4% for C_1-UTG 2.5% O_2 and ~7.5% C_3-UTG 5.0% O_2), when compared to neat gasoline, due to their higher compression ratios (15-20%).

Detailed thermodynamic analysis of the power-gas exchange cycle is required to explain the improved/degraded trend of different blends.

ACKNOWLEDGMENTS

The authors wish to thank the US-DOE Pittsburgh Technology Center, especially Gary Stiegel, Project Manager, for funding this project, Contract No. DE-AC22-91PC91034. Thanks are also due to the National Research Center for Coal and Energy (NRCCE), specifically, Dr. Caulton Irwin, Project Coordinator. Thanks are also due to our project team colleges at WVU Chemical Engineering Department and Union Carbide Company, Charleston, West Virginia.

REFERENCES

1. N. E. Gallopoulos, "Alcohols for Use as Motors Fuels and Motor Fuel Components", Presented at the Coordinating European Council Second International Symposium, Wolfsburg, West Germany, 1985.

2. K. S. Patel , S. Kuma, and O.Y.Kwo, " The Performance Characteristics of Indolene-MPHA Blends in a Spark Ignition Engine", SAE 872069.

3. M. Sposini, R. Pea, et al., Proceedings of the Fifth International Alcohol Fuel Technology Symposium, Vol. II, Auckland, NZ, May 1982.

4. "Alcohols and Ethers A Technical Assessment of Their Application as Fuels and Fuel Components", API Publication 4261, Second Edition, July 1988.

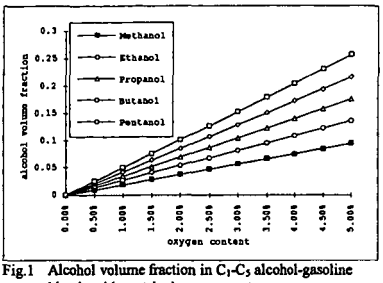

Fig.1 Alcohol volume fraction in C_1-C_5 alcohol-gasoline blends with matched oxygen content.

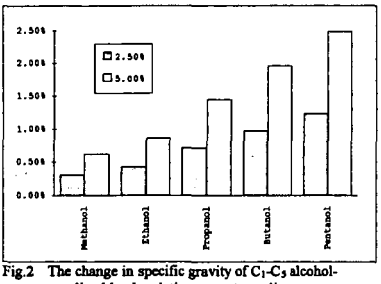

Fig.2 The change in specific gravity of C_1-C_5 alcohol-gasoline blends relative to neat gasoline.

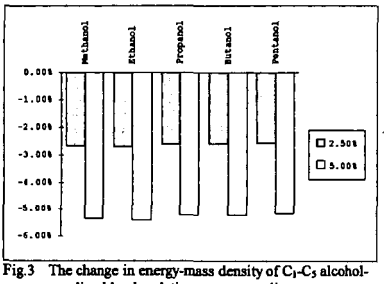

Fig.3 The change in energy-mass density of C_1-C_5 alcohol-gasoline blends relative to neat gasoline.

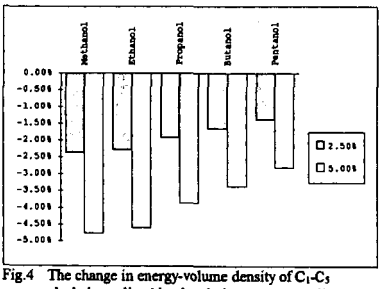

Fig.4 The change in energy-volume density of C_1-C_5 alcohol-gasoline blends relative to neat gasoline.

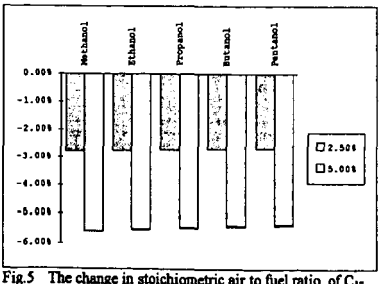

Fig.5 The change in stoichiometric air to fuel ratio of C_1-C_5 alcohol-gasoline blends relative to neat gasoline.

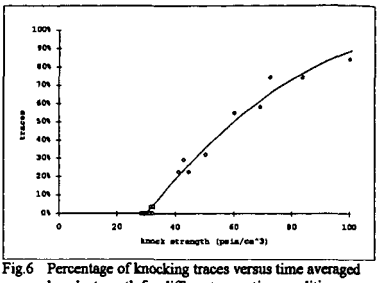

Fig.6 Percentage of knocking traces versus time averaged knock strength for different operating conditions.

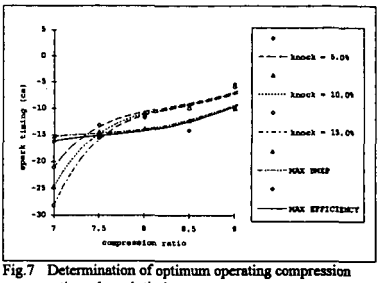

Fig.7 Determination of optimum operating compression ratio and spark timing.

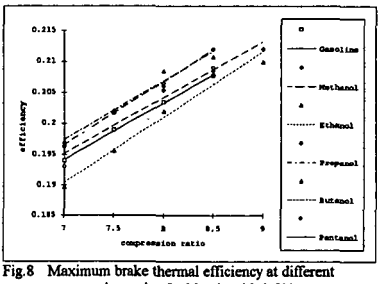

Fig.8 Maximum brake thermal efficiency at different compression ratios for blends with 2.5% oxygen.

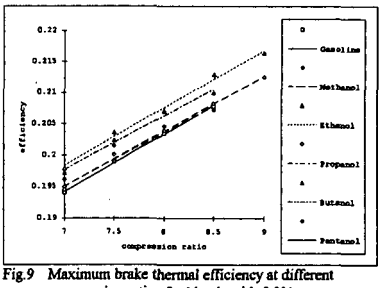

Fig.9 Maximum brake thermal efficiency at different compression ratios for blends with 5.0% oxygen.

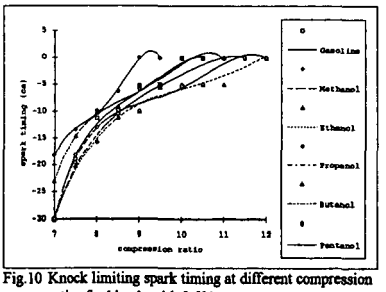

Fig.10 Knock limiting spark timing at different compression ratios for blends with 2.5% oxygen content.

5. E. I. Dupont De Nemours and Company, Inc., "Clean Air Act Waiver Application Section 211(f)", Application to the US. Environmental Protection Agency, Vol. 3, Sect. XIII, 1984.
6. R. L. Furey, "Volatility Characteristics of Gasoline-Alcohol and Gasoline-Ether Fuel Blends", SAE 852116.
7. K. Owen and T.Coley, "Automotive Fuels Reference Book", Second Edition, Society of Automotive Engineers, Inc., 1995
8. K. S. Patel and N.A.Henein, "Burning velocities in Methanol-Indolene Air Mixtures in a CFR Engine", SAE 850111.
9. A. R. Sapre, "Properties, Performance and Emissions of Medium Concentration Methanol-Gasoline Blends in a Single-Cylinder, Spark-Ignition Engine", Paper 881679, Presented at The International Fuels and Lubricants Meeting and Exposition, Portland, Oregon, Oct, 1988.
10. M. D. Checkel and J.D. Dale, "Computerized Knock Detection from Engine Pressure Record", SAE 860028
11. N. D. Brinkman, "Ethanol Fuel - A Single-Cylinder Engine Study of Efficiency and Exhaust Emissions", SAE 810345

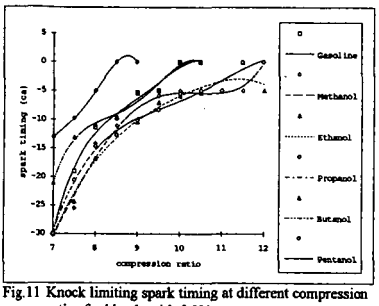

Fig.11 Knock limiting spark timing at different compression ratios for blends with 5.0% oxygen content.

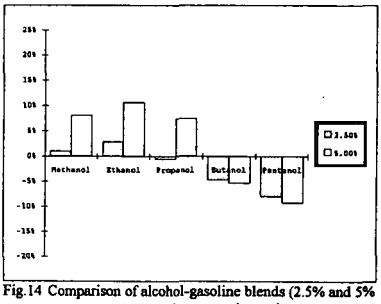

Fig.14 Comparison of alcohol-gasoline blends (2.5% and 5% oxygen mass content)compression ratio to neat gasoline at optimum operation.

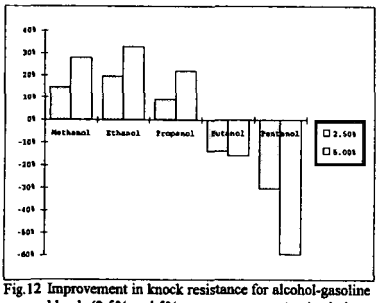

Fig.12 Improvement in knock resistance for alcohol-gasoline blends (2.5% and 5% oxygen mass content) relative to neat gasoline.

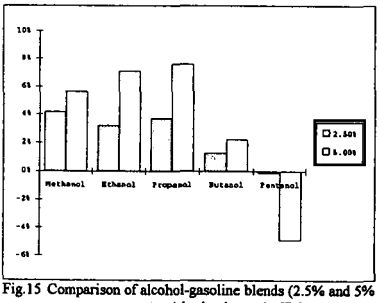

Fig.15 Comparison of alcohol-gasoline blends (2.5% and 5% oxygen mass content) brake thermal efficiency to neat gasoline at maximum compression ratio.

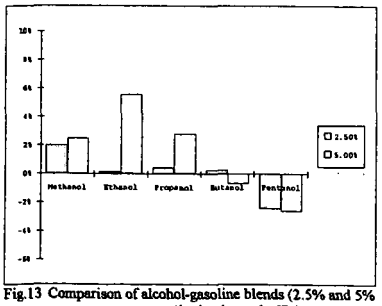

Fig.13 Comparison of alcohol-gasoline blends (2.5% and 5% oxygen mass content)brake thermal efficiency to neat gasoline at optimum operation.

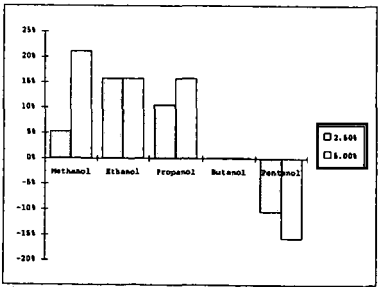

Fig.16 Comparison of alcohol-gasoline blends (2.5% and 5% oxygen mass content) maximum compression ratio to neat gasoline.

ACTIVATION OF LIGHT ALKANES IN THE PRESENCE OF Fe- AND Mn-PROMOTED SULFATED ZIRCONIA

T.-K. Cheung and B. C. Gates
Department of Chemical Engineering and Materials Science, University of California, Davis, CA 95616

ABSTRACT

A strong solid acid prepared by impregnation of sulfated zirconium hydroxide with iron nitrate and manganese nitrate was tested for conversion of *n*-butane, propane, and ethane in a packed bed flow reactor at 40-450°C. At 40°C, the predominant reaction of *n*-butane was catalytic isomerization (with disproportionation). Propane and ethane reacted at 200°C, each of these alkanes being converted predominantly into butanes. The occurrence of *n*-butane isomerization at temperatures <200°C suggests that the catalyst is strongly acidic, and the observations of butane formation from propane and from ethane are consistent with chemistry analogous to superacidic solution chemistry, but not to the exclusion of conventional strong-acid catalysis. The catalyst appears to offer good prospects for low-temperature butane conversion, although it deactivates rapidly. If acid catalysis were to be applied for propane and ethane conversion, more active catalysts would be needed.

INTRODUCTION

Environmental concerns are leading to the replacement of aromatic hydrocarbons in gasoline by branched alkanes and oxygenated compounds such as methyl *tert*-butyl ether. The ether is produced from the reaction of methanol with isobutylene, and the latter can be formed from *n*-butane by isomerization followed by dehydrogenation. Alkane isomerization reactions are catalyzed by very strong acids such as aluminum chloride supported on alumina, which has the disadvantages of being corrosive and expensive to dispose of. Thus, there is a need for improved catalysts and processes for the isomerization of *n*-butane and other straight-chain alkanes. Propane and ethane, which are present in natural gas, could also in prospect be converted by acid catalysis, giving valuable higher-molecular-weight hydrocarbons and liquid fuels (1), but practical catalysts for such conversions are lacking.

Researchers have long been searching for strong solid acids that are noncorrosive and active enough to activate light alkanes at low temperatures. A good candidate is sulfated zirconia, which catalyzes isomerization of *n*-butane at temperatures as low as 25°C (2). The addition of iron and manganese promoters increases the activity of sulfated zirconia for *n*-butane isomerization by three orders of magnitude (3). The discovery of such a highly active acidic catalyst has provided a good opportunity to explore the reactions of light alkanes at low temperatures. Our goals were to investigate the reactivities of ethane, propane, and *n*-butane with iron- and manganese-promoted sulfated zirconia (FMSZ), emphasizing low conversions to allow investigation of the reactivities of these alkanes under conditions of the simplest possible chemistry. Here we summarize new and published results for reactions of these alkanes with FMSZ and, for comparison, with zeolites.

EXPERIMENTAL

FMSZ was prepared by stepwise incipient wetness impregnation from sulfated zirconium hydroxide (Magnesium Elektron, Inc.) that was impregnated with iron and manganese nitrate solutions. The impregnated material was calcined at 650°C. The weight percentages of iron, manganese, and sulfur in the catalyst were determined to be 1, 0.5, and 1.8 %, respectively.

Before each reaction experiment, the FMSZ in flowing N_2 [30 mL(NTP)/min] was heated from 20 to 450°C at a rate of 7.1°C/min, and the temperature was then held at 450°C for 1.5 h. Reactions were carried out in a once-through plug-flow reactor at atmospheric pressure and temperatures in the range of 40-450°C. Some experiments were also conducted to characterize the reactivities of propane and of ethane in the presence of HZSM-5 and USY zeolite.

RESULTS

Conversion of n-Butane. In the presence of FMSZ, *n*-butane was converted catalytically into *i*-butane, propane, *i*-pentane, and *n*-pentane at temperatures <200°C. The selectivity for *i*-butane formation was >95% for *n*-butane conversions <10%. The

overall *n*-butane conversion and the conversions of *n*-butane into products as a function of time on stream in the temperature range of 40-100°C are characterized by a break-in period followed by a period of rapid deactivation. The molar ratio of propane to pentanes approached a value of about 1 at 40°C, after about 25 h on stream. The initial (5 min time on stream) rate of *n*-butane conversion at 75°C and 0.0025 atm *n*-butane partial pressure was 4×10^{-8} mol/(s · g).

Conversion of Propane. The gas-phase products formed from propane in the temperature range of 200-300°C with FMSZ were methane, butanes, and pentanes. The conversion of propane was characterized by an initial break-in period followed by a declining period. The initially formed products were mostly methane and butanes. The selectivity to butanes increased with time on stream initially and then declined slowly, with the selectivity to pentanes increasing. The selectivity to methane simply declined with time on stream. At 250°C, the number of turnovers per sulfate group was greater than 1 after 16 days of operation. At temperatures >300°C, the only gas-phase products observed were methane, ethane, ethene, and propene. The rates of formation of methane and ethene were approximately the same at low conversions. The initial (5 min time on stream) rate of propane conversion with FMSZ at 250°C and 0.01 atm propane partial pressure was 3×10^{-10} mol/(s · g).

USY zeolite was active in converting propane into propene, methane, and ethene only at temperatures >400°C. At a propane conversion of 0.1%, the products observed were methane, ethene, and propene. Because the experiments were not run long enough, the number of turnovers (per Al site) was less than 1.

Conversion of Ethane. In the presence of FMSZ, the products observed for ethane conversion were H_2, methane, ethene, and butanes; at 200°C the products were predominantly butane and ethene. Selectivity to butanes decreased from 30% (at 0.01% conversion) at 200°C to 10% (at 0.1% conversion) at 400°C. In the temperature range of 200-350°C, the conversion to butane, ethene, and methane decreased with time on stream. At temperatures >350°C, the conversion to butanes decreased with increasing time on stream, but the conversion to ethene and to methane decreased and then increased with time on stream, followed by another declining period (Fig. 1). H_2 was observed only at temperatures >400°C; its rate of formation was characterized by an initial increase, followed by a slow decline with time on stream. Because experiments were run for only a few hours, the number of turnovers (per sulfate group) was less than 1. The initial (5 min time on stream) rate of ethane conversion in the presence of FMSZ at 450°C and 0.2 atm ethane partial pressure was 4×10^{-8} mol/(s · g).

With HZSM-5, ethane was converted into ethene in the temperature range of 300-450°C; butane and methane were also formed, but only at temperatures >400°C. In contrast, ethene and H_2 (at nearly the same rates) were formed from ethane in the presence of USY zeolite at temperatures >300°C, and traces of butane were sometimes observed at 450°C. Conversion of ethane with either of the zeolites decreased with time on stream.

The initial (5 min on stream) selectivities observed for FMSZ, HZSM-5, and USY zeolite at low ethane conversions, 450°C, and 0.2 atm ethane partial pressure are summarized in Table 1. At about 0.1% conversion, FMSZ is characterized by the lowest ethene selectivity (94%), whereas USY zeolite is characterized by the highest (99%). Butane formed with a selectivity of 4.1% with FMSZ and 1.8% with HZSM-5; it was not observed for USY zeolite, except for a trace at 0.3% conversion. At 400°C and an ethane conversion of 0.1%, the selectivity to butane with FMSZ was 10%, whereas the selectivity to butane with HZSM-5 was negligible.

DISCUSSION

Alkane Reaction Data. The data allow a rough comparison of reaction rates and product distributions for conversions of relatively unreactive alkanes in the presence of several strong solid acid catalysts, namely, FMSZ, HZSM-5, and USY zeolite. The product distributions obtained at low conversions provide some insight into the reaction mechanisms and how the reactions were initiated.

Because the rates of *n*-butane conversion with FMSZ were high, the butane conversion data demonstrate catalytic reactions. However, the rates of propane and of ethane conversion with FMSZ and with the zeolites were much lower than that of butane conversion, and catalysis was not demonstrated for these reactions.

Carbenium Ion Reactions. Classical acid catalysis of alkane conversion involves reactions of carbenium ions, $C_nH_{2n+1}^+$, which can be formed by protonation of alkenes or hydride abstraction from alkanes. In the presence of FMSZ, the low-temperature (40-100°C) *n*-butane conversion data are consistent with such chemistry, whereby $C_4H_9^+$ reacts with butene (formed by dehydrogenation of butane) to give $C_8H_{17}^+$, which rearranges and undergoes β-scission to give isobutylene, which then undergoes protonation and hydride transfer to yield *i*-butane (4-7). The observation of a nearly 1 to 1 molar ratio of propane and pentanes suggests the occurrence of stoichiometric disproportionation, involving the $C_8H_{17}^+$ intermediate. A question still remains about how the carbenium ion and the butene may be formed at low temperatures with FMSZ.

With FMSZ, the data for propane conversion in the temperature range of 200-300°C are also consistent with classical carbenium ion reactions. Propene formed by dehydrogenation of propane can react with the secondary carbenium ion $C_3H_7^+$ to form $C_6H_{13}^+$, which reacts with propene to form $C_9H_{19}^+$, which then rearranges and undergoes β-scission to give butene and $C_5H_{11}^+$. Butene would undergo protonation and then hydrogen transfer to form butane.

At temperatures >300°C, the observed formation of butane from ethane in the presence of FMSZ, HZSM-5, or USY zeolite could also be explained by carbenium ion chemistry, with butane being formed by reaction of $C_2H_5^+$ and ethene. However, the chemistry now involves a highly unstable primary carbenium ion, and one would expect the reaction to form butane from ethane to be more than the observed two or three orders of magnitude slower than that of propane.

Thus, the results raise the question of whether there is more to the chemistry than carbenium ion reactions. The suggestion of very strong acidity raises the possibility of the involvement of carbonium ions.

Carbonium Ion Reactions. The reactions involving the formation of penta-coordinated carbonium ions, $C_nH_{2n+3}^+$, which can be formed by protonation of alkanes, occur in superacidic solutions (1). This non-classical chemistry has been invoked to explain zeolite-catalyzed cracking of alkanes at low conversions (8). According to a simplified picture of the chemistry, a zeolite catalyst at a temperature of approximately 500°C protonates alkanes to give carbonium ions, which collapse to give alkanes + carbenium ions or H_2 + carbenium ions. Thus, the observations of H_2 in this work suggests the occurrence of such chemistry.

In the temperature range of 40-100°C, the *n*-butane data observed with FMSZ are consistent with carbonium ion and oligocondensation chemistry, whereby *n*-butane is protonated to form $C_4H_{11}^+$, which collapses to give H_2 and $C_4H_9^+$, which reacts (undergoes oligocondensation) with *n*-butane to form $C_8H_{19}^+$; $C_8H_{19}^+$ then rearranges and collapses to yield *i*-butane and $C_4H_9^+$.

At temperatures <300°C, the propane and ethane conversion data observed with FMSZ are also consistent with the hypothesis that oligocondensation occurs. $C_2H_5^+$, formed from protonation of propane, followed by cleavage to give methane, could react with propane to form $C_5H_{13}^+$, which would collapse to give methane and $C_4H_9^+$, which would abstract a hydride to form butane. Similarly, ethane could be protonated to form $C_2H_7^+$, which would decompose to give H_2 and $C_2H_5^+$ or methane and CH_3^+; $C_2H_5^+$ would then combine with ethane to form $C_4H_{11}^+$, which would be deprotonated to give butane.

Thus, the results mentioned in the preceding two paragraphs are consistent with both carbenium ion and carbonium ion chemistry. However, the occurrence of simple stoichiometric dehydrogenation of ethane observed with USY zeolite at low conversions is explained only by a carbonium ion mechanism. Ethane is presumably protonated to form $C_2H_7^+$, which decomposes into H_2 and $C_2H_5^+$, which is deprotonated to form ethene, giving a 1 to 1 molar ratio of H_2 to ethene.

Similarly, propane is protonated to form $C_3H_9^+$, which decomposes into H_2 and $C_3H_7^+$ or methane and $C_2H_5^+$. Propene and ethene are formed after deprotonation of $C_3H_7^+$ and $C_2H_5^+$, respectively. The nearly equal rates of formation of methane and ethene from propane in the presence of FMSZ suggest the occurrence of carbonium ion reactions rather than carbenium ion reactions at low conversions.

Similarly, with HZSM-5 (9), the *n*-butane data at about 500°C are consistent with the hypothesis that $C_4H_{11}^+$ is formed by protonation of *n*-butane. At low *n*-butane conversions, the observation of nearly equal rates of formation of H_2 and of butenes; of methane and of propene; and of ethane and of ethene with HZSM-5 provides further evidence of the occurrence of the carbonium ion mechanism.

However, we emphasize that once alkenes are formed, carbenium ion chemistry takes over because alkenes are readily protonated, and the classical carbenium ion reactions are much faster than those involving protonation of alkanes.

Chemistry of Alkane Conversions. Thus, in summary, the data for light alkane reactions in the presence of solid acids are consistent with chemistry analogous to that occurring in superacidic solutions, provided that conversions are low. As conversions increase, alkenes are increasingly formed via carbonium ion reactions, and classical carbenium ion reactions dominate. The implication is that carbonium ion chemistry appears to play a role in initiation of light alkane conversions with strong solid acids. The lower the temperature at which an alkane is to be activated, the stronger is the acid required; thus, the data suggest that FMSZ may be much more strongly acidic than the zeolites.

However, the chemistry involving FMSZ and alkane conversions is still not fully elucidated, in part because the roles of Fe and Mn are not well understood; the reactions of light alkanes at low temperatures may not be entirely acid-catalyzed. Although there is no evidence in the high-temperature product distribution data of any enhancement in dehydrogenation activity of sulfated zirconia resulting from addition of iron and manganese to sulfated zirconia, these promoters may act as catalysts (10) or redox initiators (11) to produce alkenes, which would then be protonated to form carbenium ions and kick off the conventional catalytic cycles. Alternatively, the promoters may be catalytically involved in alkane conversions as they may somehow increase the acidity of the sulfated zirconia, so that it is capable in protonating alkanes at low temperatures.

CONCLUSIONS

In the presence of FMSZ at 40°C, *n*-butane was catalytically isomerized into *i*-butane and disproportionated into propane and pentanes. Propane and ethane reacted to give butane with FMSZ at 200°C; however, the rate of ethane conversion was about 2 to 3 orders of magnitude less than that of propane conversion, which is 3 to 4 orders of magnitude less than that of *n*-butane conversion. At temperatures >300°C and in the presence of FMSZ, HZSM-5, or USY zeolite, these alkanes are inferred to be protonated to form carbonium ions, which then collapse to give smaller alkanes or H_2 and (after deprotonation) alkenes. The comparison of the product distributions for ethane and for propane conversion suggests that there is no evidence of enhancement in dehydrogenation activity of sulfated zirconia resulting from incorporating Fe and Mn. The chemistry by which these alkanes are converted in the presence of FMSZ is complicated; both classical carbenium ion and non-classical carbonium ion mechanisms seem to contribute to the products observed, and the roles of Fe and Mn promoters are not yet resolved.

ACKNOWLEDGMENTS

We thank Magnesium Elektron, Inc., for providing the sulfated zirconium hydroxide. The research was supported in part by the U.S. Department of Energy, Pittsburgh Energy Technology Center.

REFERENCES

1. Olah, G. A., Halpern, Y., Shen, J., and Mo, Y. K., J. Amer. Chem. Soc., 95, 4960 (1973).
2. Hino, M. and Arata, K., Chem. Commun., 851 (1980).
3. Hsu, C.-Y., Heimbuch, C. R., Armes, C. T., and Gates, B. C., Chem. Commun., 1645 (1992).
4. Bearez, C., Chevalier, F., and Guisnet, M., React. Kinet. Catal. Lett., 22, 405 (1983).
5. Guisnet, M., Avendano, F., Bearez, C. and Chevalier, F., Chem. Commun., 336 (1985).
6. Bearez, C., Avendano, F., Chevalier, F., and Guisnet, F., Bull. Soc. Chim. Fr., 36 (1985).
7. Adeeva, V., Lei, G. D., and Sachtler, W. M. H., Appl. Catal., 118, L11 (1994).
8. Haag, W. O. and Dessau, R. M., in "Proceedings, 8th International Congress on Catalysis, Berlin, 1984," Vol 2, p.305, Dechema, Frankfurt-am-Main, 1984.
9. Krannila, H., Haag, W. O., and Gates, B. C., J. Catal., 135, 115 (1992).
10. Wan, K. T., Khouw, C. B., and Davis M. E., J. Catal., 158, 311 (1996).
11. Lange, F. C., Cheung, T.-K., and Gates, B. C., Catal. Lett., 41, 95 (1996).

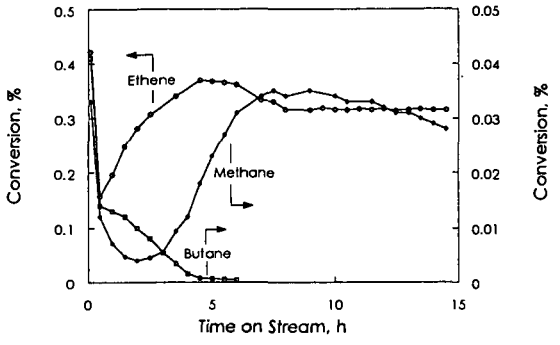

Figure 1. Conversion of ethane into ethene, butane, and methane with FMSZ at 450°C. Feed ethane partial pressure = 0.2 atm, inverse space velocity = 3.7×10^5 (s · g)/mol.

Table 1. Comparison of initial selectivity[a] for ethane conversion in the presence of FMSZ, HZSM-5, and USY zeolite at 0.2 atm ethane partial pressure and 450°C.

Solid acid	$10^{-5}\times$ Inverse space velocity, (s · g)/mol	Ethane Conversion, %	Normalized Selectivity, %		
			Methane	Ethene	Butane
FMSZ	1.83	0.38	3.4	89.7	6.9
FMSZ	1.14	0.29	2.6	91.1	6.3
FMSZ	0.46	0.13	1.7	94.2	4.1
HZSM-5	0.28	0.11	0.9	97.3	1.8
USY zeolite	7.32	0.30	1.7	96.8	1.5
USY zeolite	1.83	0.08	0.7	99.3	0

[a]Data taken at 5 min on stream.

HYDROGEN SPILLOVER CATALYSIS IN PACKED BED REACTORS: KINETICS OF 1-BUTENE HYDROISOMERIZATION OVER DUAL BEDS OF Pt/GRAFOIL AND FeCe/GRAFOIL

John Weigle and Jonathan Phillips*
Penn State University
Department of Chemical Engineering
133 Fenske Lab
University Park PA 16802
PWA@PSU.EDU

Keywords: catalysis, olefins, hydrogen spillover, carbon supports

INTRODUCTION

Recently a new family of very selective and active olefin double bond shift catalysts was discovered (1). These catalysts have potential value for increasing the octane of petroleum components both directly (β-position olefins generally have far higher octane value than α-olefins) and indirectly (improved input to alkylation units leads to higher octane product). This family of catalysts consists of one metal from the first row of the transition metals (typically iron or cobalt), one metal from the lanthanide series (typically cerium or praseodymium) and a relatively small amount of one noble metal (typically palladium). The multimetallic catalysts (e.g. Fe:Ce:Pd, 1:1:0.1) have some catalytic properties of each parent material. For example, FeCePd/Grafoil has selectivity (excellent) similar to FeCe/Grafoil, but high activity similar to that of Pd/Grafoil, a material with poor selectivity.

The following model was proposed to explain the unusual activity and selectivity of the multimetallic catalysts (1). First, the particle surfaces are 'compound'. They consist primarily of 'alloy' transition metal-lanthanide metal zones, but there are also postulated to be small zones of unalloyed noble metal. Second, each zone on the surface performs a different chemical function, and these functions add together to yield highly active and selective catalysts. Specifically, the alloy zone selectively isomerizes the 1-butene, and the noble metal zone provides hydrogen atoms via 'spillover' to allow this process to take place at a high level of activity. This model was shown to be consistent both with the known mechanism of bond shift and with information regarding hydrogen spillover.

Recent results support the above hypothesis. For example, it was shown that a physical mixture of the two components (e.g. FeCe/Grafoil and Pt/Grafoil) is as much as an order of magnitude more active than the sum of each component tested separately for 1-butene isomerization. The synergism also resulted in dramatically improved selectivity (2). It was also found that physical mixtures showed strong synergism for selective conversion of butadiene to butene (3).

These are not the first reports of physical mixtures demonstrating synergistic catalytic properties. Two models exist to explain synergism of physical mixtures. The classic model is the 'polyfunctional catalyst model' (4), and the second is the hydrogen spillover model (5). The earlier results strongly support the hydrogen spillover model. Indeed, it is difficult to identify an intermediate between 1-butene and 2-butene. Such an intermediate is required for the 'polyfunctional catalyst' model. Moreover, as discussed in earlier papers (2,3) the improvement in selectivity found in all cases and the 'limit' on synergism found in the hydroisomerization of butadiene are clearly consistent with the spillover hypothesis, but difficult to explain using any alternative model.

The present study was an attempt to test for spillover leading to synergism in segregated bed reactors. Specifically, the present work was designed to test the hypothesis that hydrogen spillover will lead to synergism in packed bed reactors with two stages, a graphite supported noble metal section and a graphite supported FeCe section. Synergism was found, but surprisingly the bed order was found to significantly impact the results.

EXPERIMENTAL

Catalyst Preparation. Two catalysts, FeCe/Grafoil and Pt/Grafoil, were prepared via the incipient wetness technique (1,6). GTA-grade Grafoil (Union Carbide) is a moderately high surface area (22 m^2/gm), high purity, graphitic material (7). More detail on the catalysts is available elsewhere (1-3).

Kinetics. The bond shift in 1-butene was studied using a differential Pyrex microreactor operated at 1 atmosphere pressure (8). Reaction gas was purchased from Matheson and mixed with rotameters to yield a reaction gas with 2% butene, 18% hydrogen, and helium as balance. Analyses were done using a 6840 Hewlett Packard gas chromatograph equipped with a TC detector, a packed column containing Carbopac C/ 0.19% picric acid obtained from Supelco. In all studies intended for the purpose of comparing levels of activity total conversion was kept to less than 12% in order to justify the 'differential reactor' approximation.

In order to test the impact of physical mixtures on catalytic activity and selectivity physical mixtures containing different absolute amounts and different relative amounts of each material were required. In each case a section of 2 mg of Pt/Grafoil mixed with 18 mg of unloaded Grafoil was placed in the reactor. Variable amounts (zero to seventy mg) of FeCe/Grafoil were also placed in the reactor. Caution was taken to assure that the two beds were firmly in contact, but not mixed. In this configuration the reaction mixture encountered FeCe/Gr first. Beds with the components loaded in the opposite order, so that the reaction gas encountered the Pt/Gr first, were also tested. Next, all the catalyst material was reduced in flowing hydrogen at 400 C for four hours. After cooling the reaction gas mixture was added and the system allowed to stabilize.

RESULTS/DISCUSSION

In previous work (2,3) many relevant control studies were reported, including the impact of Grafoil addition on catalytic behavior (very minor), the activity of FeCe/Grafoil in the absence of any metal (extremely low at temperatures of interest) and the initial activity of noble metal only. This last 'control' was repeated in the present case as well. That is, the activity and selectivity of a bed consisting of 18 mg of Grafoil and 2 mg of Pt/Grafoil at 373 K was determined after 15 minutes or less on stream.

The next studies were designed to determine the activity and selectivity of beds with noble metal on top (first contact with feed mix) and to contrast this with the activity/selectivity of beds in which the alloy fraction is on top and the noble is on the bottom (at reactor exit).

The behavior of systems in which the noble metal is on the bottom are easy to explain. Each addition of FeCe/Grafoil resulted in a significant increase in measured activity (Figure 1). As the FeCe/Grafoil in the absence of noble metal has barely any activity at the temperatures employed, these results indicate synergism. In all likelihood hydrogen atoms generated on the noble metal surface diffuse 'upstream' and activate FeCe in the 'upper bed'.

It should be noted that the data shown in Figure 1a (except for the Pt/Grafoil only case) was collected after the catalysts had been on stream for between two and five hours. In all instances this was found to correspond to a period in which the overall activity of the bed declined relatively little (Figure 2). In most cases the activity dropped by less than 10% during this period.

Selectivity data for the case of the platinum bed on bottom is shown in Figure 1b and it is clear that the selectivity decreases as the activity synergism increases. This is different than that observed previously for well mixed beds with the same net catalyst composition (2). In those studies selectivity was found to improve with each increment of FeCe/Grafoil. A possible explanation for the surprising impact of bed segregation is that all products must pass through a bed of noble metal prior before leaving the reactor. Platinum may be a better catalyst for converting 2-butenes than 1-butene. In contrast, in a well mixed bed much of the 2-butene formed on FeCe may not encounter platinum before leaving the reactor.

Defining synergism in beds in which the noble metal is on top is more difficult. In all cases deactivation was rapid. After one hour on stream the catalysts bed had lost more than 35% of their initial activity in most cases, after two hours activity loss approached 50% and the decline in activity continued rapidly thereafter. Thus, at present no plots of activity or synergism are available.

In sum, it is clear that the present work demonstrates that synergism is found in integral bed reactors, containing segregated beds of platinum and FeCe/Grafoil. The nature of the synergism is a function of several factors, including the relative placement of the beds. In the event that the platinum is on top the overall deactivation rate is rapid. This can be fully explained by the deactivation of platinum. Apparently platinum at the bottom of a bed of FeCe is protected from deactivation and the spillover process continues for a far longer period of time. A second finding is that the overall selectivity of segregated beds is different than that of well mixed beds of the same composition. A third finding is that there appears to be a limit to the 'reach' of spillover. That is, the degree of activity enhancement per gram of FeCe appears to gradually diminish as more FeCe is added.

REFERENCES

1. W.C. Lu, H. Chang and J. Phillips, *J. Catal.* 146, 608 (1994).
2. H. Chang and J. Phillips, *Langmuir* 12, 2756 (1996).
3. H. Chang and J. Phillips, *Langmuir*, in press.
4. P.B. Weisz, *Adv. Catal.* 13, 137 (1962).
5. W.C. Conner, Jr, G.M. Pajonk and S.J. Teichner, *Adv. Catal.* 34, 1 (1986).
6. S.C. Lin and J. Phillips, *J. Appl. Phys.* 58, 1943 (1985).
7. S. Bukshpan, T. Sonnino and J.G. Dash, *Surf. Sci.* 52, 460 (1975).
8. H. Durr and J. Phillips, *J. Catal.* 126, 619 (1990).

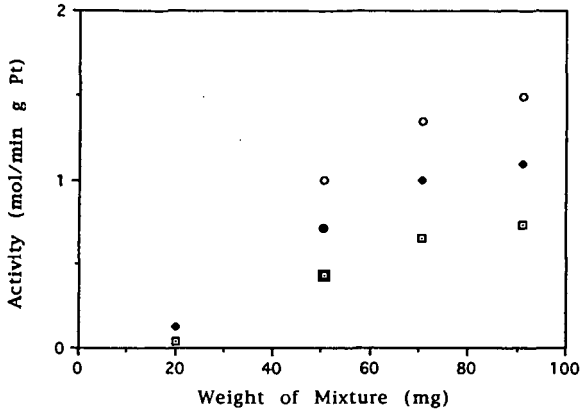

Figure 1a. Activity increase upon addition of FeCe/Grafoil
■ 80C ● 100C ○ 120C

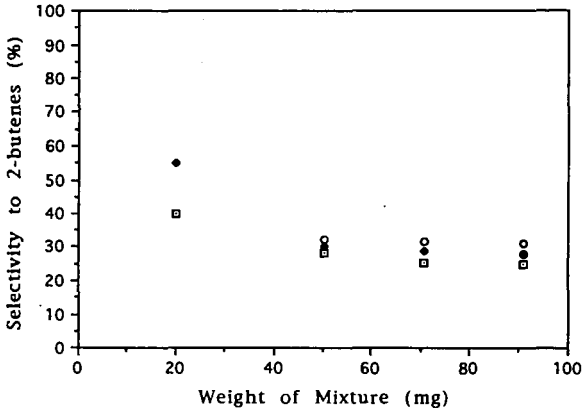

Figure 1b. Selectivity upon addition of FeCe/Grafoil
■ 80C ◆ 100C ○ 120C

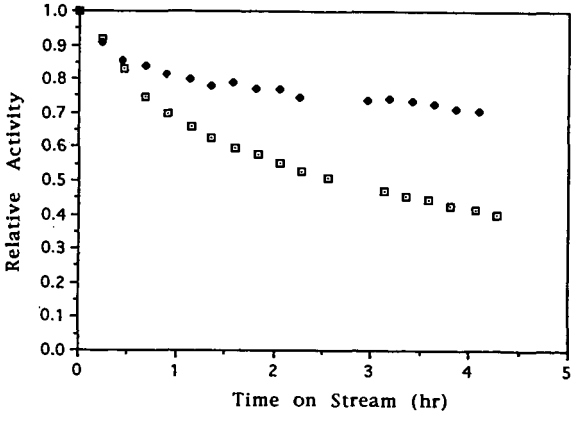

Figure 2. Impact of bed configuration on deactivation rate
▫ Pt/Grafoil on top ● Pt/Grafoil on bottom

ALTERNATE FUELS FROM THE CO-LIQUEFACTION OF COAL, OIL, AND WASTE PLASTICS

A. G. Comolli, L .K. (Theo) Lee, Vivek Pradhan
Hydrocarbon Technologies, Inc.
1501 New York Avenue
Lawrenceville, New Jersey 08648 U.S.A.

INTRODUCTION

The United States generates about 45 million tons of hydrocarbon waste, over 7 million tons of residual oil waste, and 73 million tons of waste paper per year. The approximately 25 million tons of plastic waste generated are discarded after use and end up in sanitary landfills. With existing recycle efforts, only 4% of the waste plastics are re-used. Waste plastics occupy about 21% by volume of U.S. landfills. Currently, the disposal of these wastes represents not only a significant cost ($ 3 billion/year) but also concerns such as loss of a valuable resource, a health hazard, and pollution resulting from conventional disposal methods, such as landfilling and incineration.

Through the efforts of the U.S. Department of Energy at the Pittsburgh Energy Technology Center and Hydrocarbon Technologies, Inc. (HTI), a new and promising application for direct liquefaction has been found. This application involves the combined processing of random waste plastics and waste hydrocarbons with coal and/or petroleum residuum to produce clean transportation fuels and to recover the starting chemicals used for production of new plastics. HTI' CoPro Plus™ process refers to the combined processing of coal with other hydrocarbon feedstocks. Historically this has consisted of various petroleum-derived heavy oil feedstocks; however more recent work has included waste plastics and used rubber tires. The coal feedstocks used are those typically utilized in direct coal liquefaction: bituminous, subbituminous, and lignites. Petroleum-derived oil is typically a petroleum residuum, containing at least 75 W% material boiling above 524°C. The waste plastics and tires are those collected by municipal recycling programs. The feedstocks are combined and processed simultaneously with the dual objective of liquefying the solid feed and upgrading the residuum from either the liquefied solids or petroleum oil to lower boiling (< 524°C) premium products. The new approach of the combined processing of organic wastes with coal and/or heavy petroleum resid strives to:

- Direct organic waste away from landfills.
- Produce valuable products, basic and intermediate chemicals, and fuels
- Solve existing environmental problems created by current disposal methods
- Reduce refinery waste oil pond and land fill inventories
- Enhance domestic resources
  - Supplant oil and fuel supply imports
  - Reduce energy consumption through recycling
  - Improve the trade balance
  - Create a new industry and U.S. jobs

HTI's investigation of the co-processing technology has included work performed in laboratory scale (20 cc microautoclave and a two-stage continuous stirred tank system equipped with one liter reactors), bench scale (25 kg/day throughput) and PDU scale (4 tons/day throughput) operations. In a continuous operation the waste plastics/used tires feedstock and the coal feedstock would be prepared separately and combined with the oil feedstock to form a slurry immediately prior to hydroconversion. The products are then separated downstream and the light oils are sent to an in-line hydrotreater for further upgrading. HTI's approach to coal/oil co-processing has traditionally used a two-stage reaction system with either extrudate catalyst in both reactors or more recently a combination of a dispersed and a supported catalyst in the reactor stages. Current work has been performed with dispersed catalyst in both reactors eliminating the need for handling a supported catalyst. In-line hydrotreating of the light oil products have produced a naphtha fraction with sulfur and nitrogen levels less than 10 ppm, which is below current US requirements for transportation fuels.

PROCESS DESCRIPTION

HTI CoPro Plus™ process (*Figure 1*) entails co-liquefaction of organic wastes with coal and/or oil is a liquid phase hydrogenation process that takes place at temperatures of about 425°C and pressures of 15 MPa. Under these conditions, large molecules are cracked, hydrogen is added and sulfur, nitrogen, and chlorine, etc. are easily separated and recovered after conversion to their basic hydrogenated form. Also, because the process is contained under pressure, all gases and inert components can be captured and reused if desired. Additionally such a coprocessing approach is very energy efficient, with efficiencies of greater than 80%. Co-liquefaction of random waste organic materials with coal provides for the efficient recovery and recycle of problem wastes back into the economy as premium transportation fuels and feedstocks for virgin plastics. Direct liquefaction is also applicable to the conversion and liquefaction of densified solids refuse derived fuels (RDF), formed from municipal and industrial wastes and automobile shredder residue (ASR). On a conversion to transportation fuel basis the recycle and conversion of waste plastics, waste oils, tires and organic wastes with only 50% of the waste being recovered shows that this process can supplement 10% of the United States' daily transportation fuel requirements.

Waste Type	Quantity Per Year	Oil Equivalent Million Barrels/Year
Plastics	3.5 Million Tons	200
Used Waste Oil	1.4 Billion Gallons	33
Rubber Tires	350 Million PTE*	8
Other Organic	34.4 Million Tons	212
Total		453
Total with Coal (1:1)		806
Total at 50% Waste Recovery		453+

* Passenger Tire Equivalents

+ About 10% of daily U.S. Transportation Fuel Use

A techno-economic analysis for a site specific waste/coal direct liquefaction plant at 10,000 bbls/day adjacent to and integrated with an oil refinery with random waste delivered to the plant shows an average required selling price at zero acquisition cost and at 15% ROI of about $16.00 per barrel. If tipping fees are included and if high value plastic feedstocks are recovered, the price could be less than $14/bbl and is cost effective today. This selling price will be in the competitive range by the end of this century, even with a + $20/ton acquisition cost, particularly if the environmental cost benefits of recycling are included. The current national average tipping fee is $28/ton for landfilling and $54/ton for incineration.

EXPERIMENTAL

The results from continuous bench-scale operations at HTI, conducted during 1995-96 as a part of the Proof-of-Concept Bench Option Program, which is co-sponsored by the U.S. Department of Energy, are discussed in this paper. These bench-scale operations, which were conducted at a nominal thrpoughput of about 3 lb/h and spanned over a period of 75 days, studied the coprocessing of waste plastics (from curb-side recycling in Northern NJ) with sub-bituminous coal (Wyoming Black Thunder mine) and petroleum resid (California Hondo-VTB). The bench-scale tests were carried out using HTI's proprietary iron-based dispersed slurry catalyst in hydroconversion reactors. The dispersed slurry catalyst employed was a combination of HTI's proprietary iron catalyst and Molyvan-A. Between 1000-5000 ppm of iron and 50-100 ppm of molybdenum were used for continuous co-liquefaction operations. The highlights of the reactor configuration included a two-stage hydroconversion reactor system, an interstage high pressure separator and an in-line fixed-bed hydrotreater. The overall schematic of the configuration for bench-scale testing was similar to that showed in *Figure 1* for the HTI CoPro Plus™ process.

RESULTS AND DISCUSSION

The reaction operating parameters, in terms of relative severity index for each operating condition, are presented in *Table 1*. The process performance discussed is that actually achieved at these operating conditions. The basis for the economic evaluation is defined by previous work and the assumptions described below and the process performance has been adjusted accordingly for this comparison. These conditions were carried out using a combination of dispersed slurry catalysts, based upon iron and molybdenum.

Typical feed conversions (based on the solubility of pressure filter solids in quinoline), obtained during equilibrium periods are presented in *Table 1*. As can be seen the feed conversions (W% maf feed) varies from 96.1 to 99.9 W% maf. The lowest conversion is for those conditions that contain coal as part of the feed. The conditions without coal are both over 99W% maf feed conversion. This indicates that little or no char (quinoline insoluble material) was formed in the reactors. The 524°C+ residuum conversion varies from 82.7 to 84.0 W% maf feed. Comparing the oil only condition to the oil/plastics condition shows an increase in the residuum conversion. Not surprisingly, the addition of plastic to the coal/oil condition also results in an increase in residuum conversion. The upgrading of the oil only results in a C4-524°C distillate yield of 76.0 W% maf feed. The addition of coal decreases the distillate yield by 6.3%. The addition of plastic to either of these conditions increases the distillate yield; though, more dramatically for the coal/oil condition than for the oil only condition.

Extremely significant to this comparison of process performance is the effect of plastic addition on hydrogen consumption. Not only does the addition of plastic to either oil only operation or coal/oil operation improve performance it also decreases hydrogen consumption. This is due to the plastic feed having a much higher relative concentration of hydrogen than either the coal or oil feedstock, 11.42 W% or 1.70 H/C atomic ratio for the plastic as compared to 10.13 W% or 1.45 H/C atomic ratio for the oil and 4.5 W% dry basis or 0.77 H/C atomic ratio for the coal. The light gas yield, C_1-C_3, also indicates the positive impact of adding plastics to either oil or coal/oil processing. Oil only operation results in a light gas yield of 5.0 W% MAF feed; coal/oil co-processing raises this by 2.4%. The addition of plastics to oil only operation decreases light gas yield by 0.7% and coal/oil co-processing by 2.1%. Plastics not only reduces the total hydrogen consumption but also uses it more efficiently in producing liquid and not gas products.

Figure 2 depicts the significant effect of waste plastics upon reducing the light gas-make and hydrogen consumption in heavy resid conversion or in coal/oil coprocessing. The overall quality of the light distillate products (*Table 2*) has also been excellent. The separator overhead product (SOH) coming out of the in-line hydrotreater are of premium quality with API gravities as high as 50 and H/C atomic ratios close to 2.0. The nitrogen and sulfur contents of the SOH product are very low (below 15 ppm sulfur and 1 ppm nitrogen), as shown in *Table 2*. It is also clear from *Table 2* that the addition of waste plastics either to heavy resid feed alone or to a mixture of coal and heavy petroleum resid, results in a substantial increase in the API gravities of the light distillate product; the lightest boiling naphtha (IBP-177°C) fraction also increases noticeably upon the addition of MSW plastics to the feed. The increase in the percent aromatic character of the SOH distillate during Conditions employing waste plastics in the feed can be attributed to the monomers of styrenic polymers present in the MSW plastic mixture.

The *economic evaluation* studies were based on construction of a fully-integrated grass-roots commercial coal/oil/plastics co-liquefaction complex to manufacture finished gasoline and diesel fuel liquid products. Byproducts from the complex include propane and butane, as well as elemental sulfur and anhydrous ammonia. The co-liquefaction plant in the complex is a multi reactor-train facility, and the total feed processing capacity has been selected assuming the construction of maximum-sized heavy-walled pressure vessels to carry out the co-liquefaction reactions. Coal and waste plastics required in the co-liquefaction plant are prepared on site, and storage is provided for the oil received. Unconverted feed plus residual oil from the co-liquefaction plant are gasified to meet a part of the hydrogen requirements of the complex. Part of the fuel requirement is met by the waste process gases. Natural gas is imported to meet the remaining fuel requirements and to satisfy the remainder of the hydrogen requirements.

The costs and operating requirements of the other process facilities and the off-sites have been estimated from the Bechtel Baseline Design Study, which was developed for the Department of Energy. Total plant costs have been adjusted to a current year time frame with construction at a US Gulf Coast location. The Bechtel Baseline Design Study also provided the economic criteria and financing model used in this evaluation. A four-year construction period was assumed, followed by an operating project life of 25 years. Capital costs including working capital were depreciated over a ten-year period, using straight-line depreciation. A federal tax rate of 34 percent was assumed for the life of the project. Feed costs and product selling prices were inflated at an annual rate of 3 percent. Labor and maintenance staffing requirements and wage rates were developed based on the Baseline Design. Catalyst and chemicals costs were calculated for each plant within the complex, as factored from the Baseline Design. The results of the economic analyses are reported in *Table 3*.

The most significant criterion reported is the equivalent crude oil price. This concept was developed by Bechtel in their Baseline Design Study, and modified slightly for use in this study. From analysis of published data, a correlation was found between crude oil and product prices, depending on the specific product and the price of the product. Relationships were developed for the ratio of the prices of crude oil to the price of the wholesale finished products (gasoline and distillate fuel oil). For a given product slate and product cost, multiplying the product cost by the ratio produces the equivalent crude oil price. This is the price that crude oil on the world market would minimally need to sell at for the proposed facility to have a 15% rate of return on the invested equity. The addition of plastic to either the coal/oil or the oil only feedstock decreases the equivalent crude oil price by 6.07 - 6.71 dollars/barrel. The oil/plastics operation in this grass-roots plant achieves an extremely low value of 20.48 dollars/barrel, putting it nearly in the range of economically commercializing.

The liquid products from these coprocessing operations were clean and good feedstocks for the refining operations, including hydrotreating, reforming, and hydrocracking. For these distillates, heteroatoms could be easily reduced, if needed; also, better FCC gasoline yields require less hydrocracking capacity for coal liquids than petroleum. These distillates made acceptable blendstock for diesel and jet fuel, due to their high cetane number (42-46) and high naphthenes (over 50 v%) content. The superior quality of distillate products from HTI's coprocessing runs (attributable to HTI's in-line hydrotreating operation) was found to fetch a three-dollar premium over the neat petroleum liquids.

CONCLUSIONS

Co-processing of waste plastics with either oil only feedstock or coal/oil feedstock results in a significant improvement in process performance. Total feed conversion is enhanced as are 524°C+ residuum conversion and C_4-524°C distillate yield. The addition of waste plastics to the feed increases hydrogen efficiency as both hydrogen consumption and C_1-C_3 light gas yield decrease. Co-processing of plastics with oil reduced the equivalent crude oil price required to have a 15% rate of return on equity to 20.48 dollars/barrel. This puts the technology in the reach of immediate commercialization with either a small increase in world crude oil prices or minor improvements in the technology to further reduce the product cost.

TABLE 1: Performance Comparison - Yields

	Oil	Coal/Oil	Coal/Oil /Plastics	Oil /Plastics
Feed Composition, W%				
Coal	0	50	33.3	0
Plastic	0	0	33.3	50
Oil	100	50	33.3	50
Relative Severity Index, STTU*				
First Stage	0.78	0.98	1.08	0.90
Second Stage	1.07	1.28	1.47	1.19
Process Performance, W% maf feed				
Feed Conversion	99.9	96.1	96.7	99.7
C_4-524°C Distillate Yield	76.0	69.7	73.9	76.2
524°C+ Conversion	83.3	82.7	83.7	84.0
Hydrogen Consumption	1.72	4.21	3.17	1.35
C_1-C_3 Gas Yield	5.00	7.37	5.31	4.31

*The relative severity index (STTU) is based upon a standard severity index of 1.0 at a space velocity of 800 kg/h/m^3 each reactor and a temperature of 440°C.

TABLE 2: Performance Comparison - Quality

	Oil	Coal/Oil	Coal/Oil /Plastics	Oil /Plastics
Feed Composition, W%				
Coal	0	50	33.3	0
Plastic	0	0	33.3	50
Oil	100	50	33.3	50
SOH Distillate, ASTM D86, W%				
IBP-177°C	39.6	42.1	52.4	53.4
177-343°C	52.1	50.9	40.7	41.7
343°C+	8.3	7.0	6.9	4.9
SOH Quality				
Gravity, °API	49.0	46.1	46.3	51.0
H/C Ratio	1.99	1.96	1.90	1.97
Nitrogen, ppm	32.2	15.5	17.9	5.4
Sulfur, ppm	96.9	52.7	46.2	17.5
%Aromaticity	7.25	17.82	23.49	14.89

TABLE 3: Economic Comparison (12,000 tons/day total feed)

	Oil	Coal/Oil	Coal/Oil /Plastics	Oil /Plastics
Feed Rate				
Coal, tons/day	0	6,000	4,000	0
Oil, barrels/day	66,730	33,365	22,243	33,365
Plastics, tons/day	0	0	4,000	6,000
Liquid Products, barrels/day				
Gasoline	15,148	14,339	15,192	15,328
Diesel Fuel	36,787	34,822	36,896	37,225
Total	51,935	49,161	52,088	52,553
Total Plant Investment, $MM	1,945	2,379	2,078	1,733
Net Operating Cost, $MM/yr	566.8	561.4	486.1	449.7
Net Product Cost, $/barrel	33.22	34.76	28.41	26.05
Equivalent Crude Oil Price,	**27.19**	**28.70**	**22.63**	**20.48**

Figure 1. Simplified Schematic of HTI's CoPro Plus™ Process

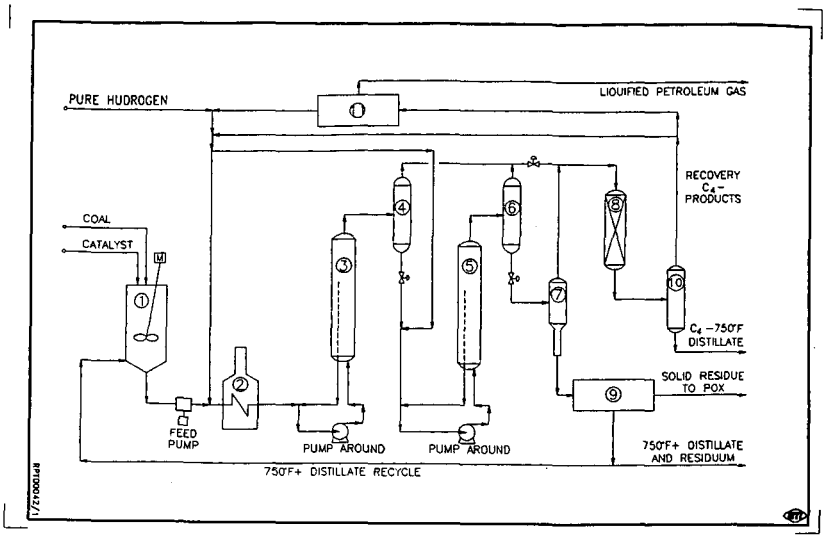

Figure 2. Effect of Waste Plastics on Liquid and Gas Yields, and H_2-Consumption

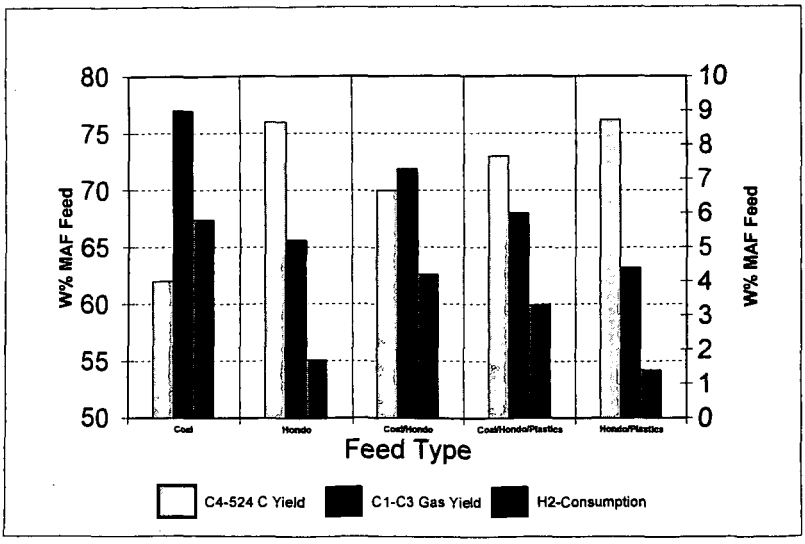

POTENTIAL USES FOR THE TIRE DERIVED PARTICLES PRODUCED BY THE WOMBAT PROCESS.*

David L. Wertz, Rachel Eschette, Ricky Cummings, Jeff Quin,
Mary Martin and Stephen DuBose
Department of Chemistry & Biochemistry
University of Southern Mississippi
Hattiesburg, MS 39406. USA.

Key Phrases: Tire-derived particles, extraction of the inorganics, blended fuels.

Approximately 275 million scrap tires are produced in the United States annually. Most of these tires are not being recycled. At best, they are an expensive nuisance. At worst, they cause significant air, water and soil pollution.

The typical modern tire is composed of a complex inert organic matrix into which several inorganic species have been impregnated to enhance the performance of the tire. Any potential uses of the scrap tires, other than simple (and expensive) reshaping of the physical appearance of the tires, must deal with these inorganic species and the C-C bonding network, both at the molecular level. The Wertz Oxidative Molecular Bombardment at Ambient Temperature (WOMBAT) process attacks the tires at this level. The final product of the WOMBAT process is referred to as tire-derived particles (TDP).

Shown in Figure 1A is the wavelength dispersive x-ray spectrum (WDXRS) of a scrap tire. The peaks in a WDXRS may be related to the presence of an element in the sample by a combination of Bragg's law and Moseley's law, i.e., $Z_J = 1 + \{n/[2 \cdot d_{mono} \cdot Q \cdot \sin\theta]\}$; where Z_J is the atomic number of element J, n is the order of the reflection, d_{mono} is the d-spacing of the crystal monochromator, and 2θ is the angle at which the peak P_J (caused by element J) appears in the x-ray spectrum of the sample. The K_β and K_α peaks for zinc (first, second, and third order reflections), the K_β and K_α peaks for calcium, and the K_α peak for sulfur are clearly discernible in the spectrum, along with the peaks from the exciting radiation -- chromium. Shown in Figure 1B is the WDXRS of TDP which has been produced by the WOMBAT solvent in the closed reactor, indicating that the zinc and sulfur originally contained in the tire have been reduced to < the lower limit of detection for each element in the TDP.

The intensities of the peaks due to different elements (eg. zinc and sulfur in this WDXRS) may not be directly compared to evaluate the relative abundances of these elements without extensive absorption-enhancement corrections being applied to the intensity of the K_α peak characteristic of each element. However, the peak intensity of the K_α and/or K_β peaks in the WDXRS of this sample and in subsequent samples may be used to estimate the change in abundance of that element in a series of samples of similar composition. These WDXRS analyses may be made at least semi-quantitative via comparison to a series of external standard curves containing the element(s) of interest dispersed into a matrix which is similar to that of the TDP. Studies to develop the appropriate absorption-enhancement corrections for zinc and sulfur in a high carbon matrix are on-going.

A two-step process for converting scrap tires to more useful material is being developed in our laboratory. This process involves the use of oxidizing solvent(s) at ambient conditions to separate the scrap tire into (a) steel belts, (b) polymeric cords, and (c) chunks of black solid which have irregular sizes and shapes. These chunks of black solid are the subject of part two of the WOMBAT process, which involves further reaction of the black solid with an oxidizing solvent. The result of process step two is a pulpy material which may be easily washed, dried, and ground into particles.

The partial compositions (measured by gas chromatography) of two samples of TDP and a sample of the rubbery part of an untreated tire are compared in Table I. This comparison shows that the WOMBAT process reduces the carbon, sulfur, and hydrogen abundances, while significantly increasing the oxygen abundance. The results also shown that the largest changes in the carbon and oxygen abundances occur when the process was carried out in an "open" container; i.e., where an infinite supply of atmospheric oxygen and of moisture were present. However, when the black chunks were subjected to the WOMBAT process in a closed system for a much shorter

period of time, the resulting changes in the carbon and oxygen abundances were much reduced. Under these conditions, the resulting TDP is principally carbon (ca. 75%), but it also contains a considerable amount of oxygen (ca. 13%). Studies are currently underway to determine the effect of reaction parameters on the carbon/oxygen ratio produced in the TDP. The sulfur content of the TDP was reduced to 0.8%, while the nitrogen content was increased to 2.6%, when the chunks were reacted in the closed WOMBAT container. Studies are currently being conducted to determine the effect(s) of reaction time and other parameters on the sulfur and nitrogen abundances in the resultant TDP.

All of the results discussed below were obtained from the sample produced in the closed container (TDPA).

^{13}C NMR indicates the absence of aromatic carbons in the WOMBAT TDP.

After minimal grinding, the TDP range in diameter from 1-100 μm and have highly irregular surfaces.

The WOMBAT particles produce a high temperature ash which is 2.4% of the original weight of the TDP. The principal components of the ash are zinc, calcium, iron, and titanium, as shown in Figure 2.

The WOMBAT TDP has been evaluated as a fuel. Shown in Table II is its specific heat compared to that of other, more conventional, fuels as measured in our laboratory using conventional oxygen bomb calorimetry. Our analyses indicate that the specific heat of the WOMBAT TDP is considerably higher than that of bituminous coal. When combusted in our entrained flow thermal reactor at 850°C for an extended period, there is no measurable production of soot from the TDP.

The TDP may be mixed with materials of lesser fuel value to produce synthetic fuel blends. Shown in Figure 3 are the specific heats measured for a series of mixtures containing the TDP mixed with sawdust. The linear relationship between composition and heat content (R^2 = 0.996) indicates that such a mixture may be predesigned to produce a synthetic fuel blend of preselected specific heat. Combustion of such a mixture offers significantly reduced $SO_x(g)$ in the effluent gas and significantly less ash than produced by combustion of typical bituminous coals. Combustion of such a mixture also offers a useful method for utilizing, and thus not landfilling, two nuisance solid wastes -- scrap tires and sawdust.

Experiments with mixtures containing municipal garbage, wood shavings, and other low fuel content solids are on-going.

In addition, preliminary tests indicate that the TDP are capable of extracting some metal ions and some anions from water. Shown in Figure 4 is the WDXRS of a TDP which has been treated with a solution containing $CdCl_2$. New peaks indicating the presence of both Cd(II) and of Cl^- are easily discernible, indicating that the TDP has sequestered each from an aqueous solution. Experiments designed to evaluate and then exploit these capabilities of the TDP are ongoing.

Preliminary evaluation of the TDP as a component for inclusion in specialized polymeric matrices has recently been initiated.

* Financial support by the U.S. DOE, the Mississippi Department of Environmental Quality, and an Aubrey K. Lucas Faculty Excellence Endowment Grant from USM are gratefully acknowledged.

TABLE I. PARTIAL COMPOSITION OF THE TDP COMPARED TO THE COMPOSITION OF THE UNTREATED TIRE.

ELEMENT	SAMPLE		
	TIRE	TDPA	TDPB
C	82.4%	76.3%	48.3%
H	7.8%	2.8%	4.6%
S	2.0%	0.8%	0.4%
N	0.5%	2.6%	3.8%
O	2.4%	13.5%	33.9%

A The process was conducted in the enclosed WOMBAT reactor for 72 hours.

B The process was conducted in a flask which was exposed to atmospheric conditions for 168 hours.

TABLE II. COMPARISON OF THE SPECIFIC HEAT OF THE TDP TO THE SPECIFIC HEAT OF OTHER FUELS USING OXYGEN BOMB CALORIMETRY.

FUEL	SPECIFIC HEAT (kJ/g)	FUEL	SPECIFIC HEAT (kJ/g)
bituminous coal	23	sawdust	18
sub-bituminous coal	21	wood chips	18
lignite	19	garbage	16
WOMBAT TDP	32		

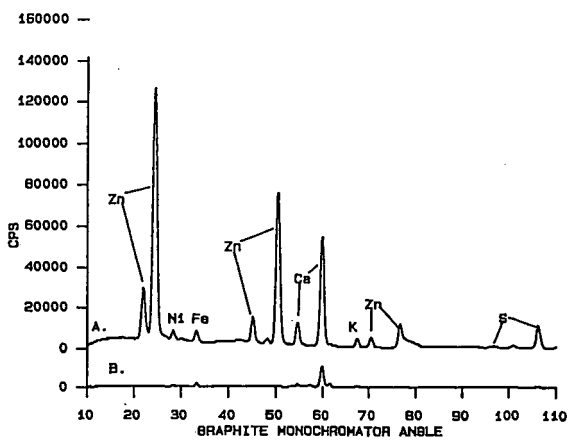

Figure 1. WDXRS of (A) a scrap tire, and (B) TDP produced from the tire.

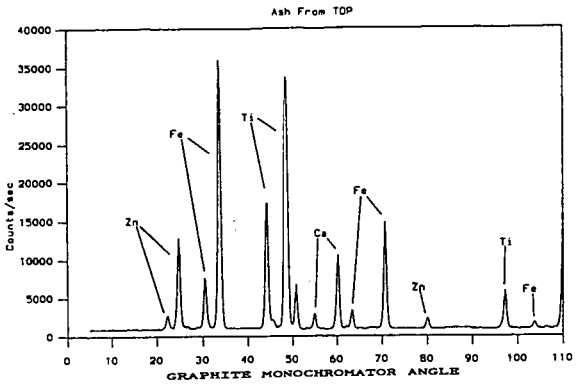

Figure 2. WDXRS of the high temperature ash produced from the TDP.

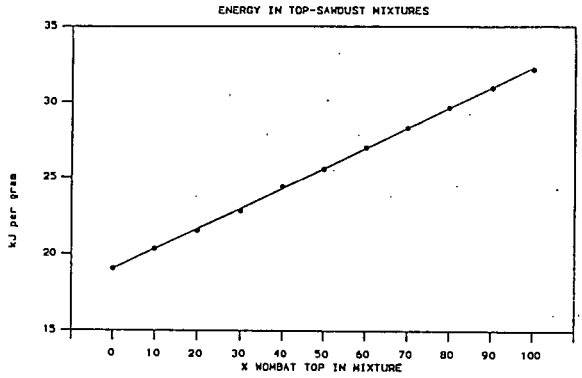

Figure 3. Specific heats of some TDP-sawdust mixtures.

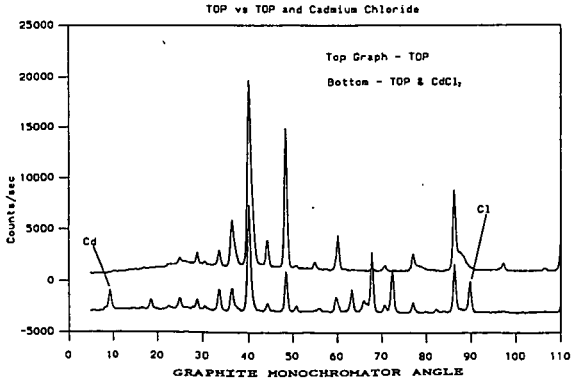

Figure 4. WDXRS of TDP treated with an aqueous solution of $CdCl_2$.

USE OF NET PRESENT VALUE ANALYSIS TO EVALUATE AND SELECT PUBLICLY FUNDED BIOMASS-TO-ETHANOL RESEARCH AND DEVELOPMENT PROGRAMS AND VALUATE EXPECTED PRIVATE SECTOR PARTICIPATION

Norman D. Hinman and Mark A. Yancey
Center for Renewable Fuels and Biotechnology
National Renewable Energy Laboratory
Golden, CO 80401-3393

INTRODUCTION

One of the main functions of government is to invest tax dollars in programs, projects, and properties that will result in greater social benefit than would have resulted from leaving those tax dollars in the private sector or using them to pay off the public debt. One traditional area for investment by government is R&D. According to Battelle, U.S. R&D expenditures reached $164.5 billion in 1994, and federal support represented $69.8 billion (42.4%) of the total (1). If invested wisely, these tax dollars can lead to greater social benefit than would be obtained by leaving them in the private sector or using the money to pay off the federal debt. However, if not invested wisely, this could result in less than optimal social benefit or, even worse, in less social benefit than could be obtained from the other two options. The purpose of this paper is to describe an approach to analyzing and selecting investment opportunities for federal money in public R&D programs and valuating expected private sector participation in the programs and to apply this approach to a specific biomass-to-ethanol R&D opportunity.

BASICS OF INVESTMENT ANALYSIS

For all investment situations there are five basic variables: (1) costs; (2) profits or benefits; (3) time; (4) the discount rate; and (5) risk. In the analysis of investment alternatives for a given situation, the alternatives under consideration may have differences with respect to costs and profits or benefits, project lives, and uncertainties. If the effects of these factors are not quantified systematically, correctly assessing which alternatives have the best potential is very difficult.

Many methods are available to decision makers to systematically evaluate investment options. These methods, described in detail in a variety of books and articles (2), include present, annual, and future value; rate of return; and break-even analysis. The application of each method depends on whether the analysis is for a single opportunity, two mutually exclusive opportunities, or several non-mutually exclusive opportunities. For the single opportunity situation, the decision maker is simply trying to decide if the single investment option meets a minimum expected financial return. For the mutually exclusive situation, the decision maker has two investment options and is trying to decide whether the options meet the minimum expected financial return, and, if both do, which is the best choice. For the non-mutually exclusive situation, the decision maker has several investment options and is trying to decide which of these meets the minimum expected financial return, and, of those that do, which combination of these will provide the maximum return on total investment dollars available.

One must be careful in applying rate of return analysis to mutually exclusive and non-mutually exclusive situations. If one simply calculates the rate of return for each alternative and then chooses the alternative or alternatives with the largest rates of return, this can, and often does, lead to the wrong choice. The correct application of rate of return analysis to either situation is known as incremental rate of return and can be very tedious and time consuming, and one must take extra steps to account for differences in project lives. Net present value (NPV) is the tool of choice for evaluating mutually exclusive or non-mutually exclusive investment options because it is much less time consuming, is straightforward, does not require additional steps or considerations for projects with different lives, allows direct comparison between projects of widely differing objectives and scopes, and allows a rational approach to valuating private sector participation in public programs.

NPV APPROACH TO NON-MUTUALLY EXCLUSIVE INVESTMENTS

A non-mutually exclusive investment situation is one where more than one investment option can be selected, depending on available capital or budget restrictions. The objective is to select those projects that maximize the cumulative profitability or benefit from the available investment dollars. To maximize the cumulative profitability or benefit, the decision maker selects the combination of projects that maximize the cumulative net present value.

To apply NPV to non-mutually exclusive alternatives, the NPV for each alternative is calculated by determining the present value of the profit/benefit stream calculated at the minimum rate of return (hurdle rate) and subtracting the present value of investment dollars and other costs, also calculated at the minimum rate of return.

$$\text{Net Present Value (NPV)} = \text{Present Value Revenues @ } i^* - \text{Present Value Costs @ } i^*$$

i^* = minimum rate of return

If the project NPV is zero, there is enough revenue or benefit to cover the costs at a rate of return that is equal to the minimum rate of return required by the investor. Projects with an NPV less than zero are dropped from further consideration because their rate of return is less than the minimum required return. If the NPV is greater than zero, the NPV represents how many present value dollars will be returned to the investor above and beyond those that will be returned at the minimum rate of return. Once the NPV for each project is calculated, the decision maker looks at all possible combinations of projects to determine which combination (whose total investment does not exceed the amount of money available) has the largest cumulative NPV. This is the best possible investment portfolio. Often, selecting the best portfolio does not involve selecting projects with the largest individual project net present value and does not necessarily involve selecting projects with the highest rates of return.

If one is faced with the daunting task of selecting an investment portfolio when there are dozens of investment options, an alternate method may be used to simplify the process. Growth rate of return or ratio analysis may be used to rank non-mutually exclusive alternatives rather than cumulative NPV analysis (2). Large companies and government programs are often faced with the task of evaluating literally hundreds of potential projects. Many combinations of projects must be analyzed to determine the optimum group of projects that will maximize the cumulative NPV for a given budget. The use of growth rate of return or ratio analysis only requires the calculation of the respective values for each project and then ranking the projects in the order of decreasing values. The illustration of these concepts will not be demonstrated here, but the reader should be aware of these methods to evaluate a complex investment portfolio.

SPECIAL CONSIDERATIONS FOR NON-MUTUALLY EXCLUSIVE GOVERNMENT INVESTMENTS

Converting Intangible Benefits and Costs into Dollar Values

A basic tenant of this paper is that to make rational investments of pubic dollars one must have some approximate, quantitative idea of the value of critical costs and benefits. Moreover, as a practical matter, it is essential that the measure of value be the same for both costs and benefits so that direct comparisons between costs and benefits can be made. The most universal measure of value is the dollar. In the private sector this is the measure of cost and benefit. In the public sector, particularly with respect to R&D programs, it's the established measure of cost. However, on the benefit side, there is no established measure of value. The authors contend that the dollar should be the measure of benefit so that direct comparisons can be made with costs and so that the established and the well recognized investments analysis methodology described above can be employed in the public sector.

In many cases converting benefits and costs to dollars is fairly straightforward. For example, a key benefit that the U.S. Department of Energy (DOE) is interested in is reducing imported petroleum. The dollar value of the yearly benefit can easily be calculated from the present and projected price of petroleum (3). As another example, it is possible to estimate the net annual increase or decrease in jobs that results from introducing new technology. In addition, it is fairly straightforward to place a dollar value on these jobs (4). Other possible costs and benefits are environmental and social, which are more difficult to quantify. Nevertheless, the U.S. Environmental Protection Agency has studied these issues carefully and has given dollar estimates of health costs associated with various types and levels of pollution.

Minimal Rate of Return for Public Projects

Establishing a minimal rate of return for public projects requires some special considerations, which have been reviewed extensively by Terry Heaps (5) for Canadian public projects. He concluded that the correct social discount rate for Canada was 3-7%. In another study performed by Wilson Hill Associates (3) a discount rate of 7% was used for Projects evaluated for the Office of Transportation Programs in DOE.

SELECTING PUBLIC R&D PROGRAMS AND VALUATING EXPECTED PARTICIPATION BY THE IMPLEMENTING INDUSTRY

Commonly, a government R&D program is initiated without the private sector, but the private sector is expected to "come on board" at some point to carry the ball forward into the commercial arena. For these situations, the government and the private sector make investments in R&D and technology commercialization in order to obtain what each desires—social benefit in the case of government, and profit in the case of the private companies.

Analysis of the value of these programs demands answers to three questions: (1) What portion of the R&D cost can the private sector incur and still obtain its minimum return from implementing the technology?; (2) When this private sector cost allowance is subtracted from the total estimated cost to carry out R&D so as to obtain an estimate of the R&D cost that must be borne by government, is the estimated government R&D cost justified given the expected social benefit from implementing the technology?; and (3) If the answer to questions 2 is positive, does the program represent one of government's best opportunities for its limited investment dollars?

The NPV approach to investments provides the answer to all three questions. For example, to answer the first question one calculates the **industry NPV**. To do this, one estimates over time the capital and operating costs the industry at large will incur to implement a new technology and, using the average minimum interest rate for the industry, calculates the present value of these costs to industry at the initial time of commercialization. One also estimates over time the present value at the time of commercialization of the expected increased revenues or savings the industry should experience from implementing the technology. Subtracting the present value costs from the present value revenues gives the industry NPV at the time when commercialization is expected to begin. If the NPV is negative, the industry cannot afford to contribute to the R&D effort and cannot afford the capital and/or operating costs of commercialization. As a result, it will not "come on board" and the government should drop consideration of the program. If the industry NPV is zero, industry cannot afford to contribute to the R&D costs, but can afford the capital and operating costs to implement the technology. In this situation the government will have to incur all the R&D costs in order for industry to adopt the technology. If the industry NPV is positive, the government can expect the industry to participate in the R&D costs at a level equivalent to the NPV. This participation may be provided in the form of cost sharing or through licensing arrangements.

To answer the second question, one calculates the **government NPV**. To do this, the expected social benefits are estimated over time and dollar values are assigned. Then the present value of these benefits is calculated at the time the program was initiated using the social discount factor. Next, the entire R&D costs over time are estimated and discounted to the time the program began using the social discount factor. Next, the expected R&D contribution from industry, calculated above as industry NPV is discounted to the time of initiating the program using the industry discount factor. This industry R&D contribution, discounted to when the program began, is then subtracted from the entire R&D costs, also discounted to when the program began, to obtain the governments expected R&D costs discounted to the time the program began. These discounted government R&D costs are then subtracted from the discounted benefits to obtain the government NPV for the program at the time the program was initiated. If the government NPV is less than zero, the program should not be considered for investment of tax dollars. If the government NPV is zero or greater, it should be thrown in the pot of possible government investments.

To answer the third question, government should list all investment options with a NPV greater than zero and select that combination of projects that will maximize the **governments cumulative net present value.**

VALUATING EXPECTED PARTICIPATION BY INDIVIDUAL COMPANIES

If, from the above analysis, the industry NPV is positive, individual companies that are members of the industry can be expected to cost share in the R&D phase of a program or purchase licensing arrangements. However, the level of cost sharing or license fees will depend on each company's circumstances. The expected level of cost sharing or the licensing fee for a given company can be calculated using **company NPV** derived from projected revenues and costs a company will experience in implementing the technology in commercial use. If the company NPV is negative, the particular company cannot afford to implement the technology even if the technology is provided free. Such a company is not a viable partner to the government program. If the company NPV is zero, the company may be a partner only in the sense that it will implement the government-developed technology if it is free to the company. If the company NPV is positive, the company can afford to cost share the R&D effort or purchase a licensing arrangement at a level equal to the company NPV. Such companies are potentially the most valuable partners to the program.

APPLICATION TO BIOMASS-TO-ETHANOL R&D OPPORTUNITIES

The authors will supply a detailed example of the use of NPV analysis to a biomass-to-ethanol opportunity.

REFERENCES

1. *Manufacturing Engineering*, Vol. 112; No. 2, 1994.
2. Stermole, F.J. (1984), *Economic Evaluation and Investment Decision Methods*, Fifth Edition, Golden, CO.
3. Santone, L.C. (1981), *Methods for Evaluating and Ranking Transportation Energy Conservation Programs Final Report*, Washington, DC, April 30, 1981.
4. Tyson, K.S., Putsche, V., and Bergeron, P. (1996), *Modeling the Penetration of the Biomass-Ethanol Industry and its Future Benefits*, Golden, CO, March 15, 1996.
5. Heaps, T., and Pratt, B. (1989), FRDA Report 071, *The Social Discount Rate for Silvicultural Investments*, Victoria, B.C, March, 1989.

CLEAN GAS TURBINE FUEL FROM PETROLEUM COKE

.Satyan Katta and Gunnar B. Henningsen

The M. W. Kellogg Company
601 Jefferson Ave., Houston, Texas 77210

Keywords: Petrleum coke, partial oxidation and gasification

Introduction

Oil refiners in the United States often rely on coking to reject excess carbon from heavier crudes, resulting in an ever-increasing supply of petroleum coke. Marketing of coke as a fuel is hampered by its high sulfur and metals content which makes it unsuitable for conventional combustors. Several major IGCC projects, based on the low value refinery stocks, are currently progressing through detailed engineering, procurement and construction (1).

In a cost-shared contract with DOE/PETC, Bartlesville, The M. W. Kellogg Company has been investigating the gasification and combustion of high-carbon containing refinery by-products using a laboratory-scale fluidized bed and a sub-pilot scale transport reactor located at Kellogg's Technology Development Center where both fluid bed and transport reactors have been developed for coal gasification (2). The transport reactor process pioneered by The M. W. Kellogg Company, makes use of enriched air to partially oxidize and gasify the petroleum coke. Results of the laboratory and pilot plant program are presented in the paper along with proposed process flow diagram that incorporates some recent advances made in sulfur removal and recovery.

The objective of the study was to develop a process to convert high-carbon refinery byproducts such as petroleum coke and ROSE™ (Residuum Oil Supercritical Extraction) pitch to fuel gases suitable for power generation. Experiments were conducted in the transport reactor (TRTU) to study partial oxidation, gasification and devolatilization of the coke at temperatures up to 1800°F in a continuous mode. In order to extend the data obtained in the TRTU to higher process temperatures (1850 to 2250°F), experiments were conducted in the Bench-scale Reactor Unit (BRU) to study partial oxidation and gasification in a batch mode. The BRU is capable of heating a bed of solids up to 2250°F and above with oxidant injection.

Experimental

Description of Bench-scale Reactor Unit: A simplified flow schematic of the BRU test facility is shown in Fig. 1. It consists of a 2.067-in. inside diameter (i.d.) section of 10-in. height and an expanded section of 3.068-in. i.d. of 12-in. height. It is made of Incoloy 800H alloy and consists of some ancillary equipment including a steam supply system. The reactor is surrounded by two independently-controlled electrical heaters (for top and bottom zones) and contained within a pressure vessel. Only a small pressure differential is used across the hot reactor vessel. The feed gas is electrically preheated. Product gas leaves the reactor, and is sent to a water-cooled condenser and then to a particulate filter. Water collected in the knockout drum is periodically drained from the unit. An on-line GC, that requires 12 min to complete the gas analysis, is connected to the BRU for gas analysis. It is possible to analyze the concentration of hydrocarbons and carbon oxides (CH_4, C_2H_4, C_2H_6, CO, CO_2, H_2, N_2 and the unsaturates) in the effluent gas of the BRU by using gas sample bags. The BRU facility can be operated at temperatures up to 1950°F at pressures up to 450 psig. A particulate filter, maintained at a temperature of 600 to 700°F, was used to capture the fines for analysis of vanadium and nickel which are present in the coke feed.

Petroleum coke was subjected to partial oxidation (POX) in the BRU over a peak temperature range of 1850 to 2250°F. The tests involved heating the bed to a base temperature followed by introducing the oxidant. Within a short period, the bed temperature reached a peak value and then stabilized or decreased gradually. Tests on combined POX and steam gasification and tests with steam gasification only were performed in the BRU.

Description of Transport Reactor Test Unit (TRTU)

A simplified sketch of the reactor system, shown in Fig. 2, consists of a mixing zone, a riser, a cyclone, and a standpipe. The mixing zone of the reactor, which can be operated either as a dense-phase fluid bed or as an entrained reactor, consists of a 10-foot tall section of 1.338 in. i.d. Solids from the standpipe are returned to the bottom of this zone. Fluidization gas, which can be air, O_2, steam, N_2, or any combination of these, is fed to the bottom of the mixing zone through a gas distributor. During standby periods, mixture of steam and N_2 was used. During testing, the steam flow was maintained and N_2 to the mixing zone was replaced with air.

Above the mixing zone is a 32-foot tall riser of 0.815 in. i.d. At the base of the riser is an injection nozzle that is used for feeding petroleum coke. At velocities of 15 to 30 ft/s used during partial oxidation/gasification, the gas residence time was about 1 to 2 sec in the riser. Gas and solids leaving the top of the riser flow to a high-efficiency cyclone, that separates the solids and returns them, via the standpipe, to the mixing zone. Gas leaving the top of the cyclone is cooled, measured, and sampled for analysis.

The standpipe consists of a 33-foot tall section with the same i.d. as the mixing zone. The use of a relatively small diameter standpipe requires a low solids inventory and minimal solids holdup time. Fresh solids are added for make-up, if necessary, to the top of the standpipe to compensate for attrition losses. Solid samples are withdrawn from the bottom of the standpipe. Solids are returned to the bottom of the mixing zone via a lateral leg that is aerated.

The nominal size cuts of coke used in the TRTU and the BRU were 40x140 and 40x80 mesh, respectively. The proximate analysis of the petroleum coke (wt%) was: volatile matter-9.4%, fixed carbon-89.6%, moisture-0.5% and ash-0.5%.

Results and Discussion

Testing in BRU

Tests were conducted in the BRU, in a batch mode, using a bed weight of 200 gm of Lyondell/Citgo petroleum coke with an O_2 concentration range of 15 to 30 vol% in nitrogen over an initial temperature range of 1800 to 1950°F at pressure of 100 psia. The peak bed temperature varied from 1850 to 2250°F. Results from fluidized bed testing show that a sulfur- and metals-free gas, suitable as a gas turbine fuel, can be produced from petroleum coke. The gas residence time in the BRU is about the same as in the TRTU, and hence the BRU results are applicable to the TRTU. The CO/CO_2 ratio was observed to be a function of O_2 partial pressure and temperature. At 30% O_2 concentration and 2000°F, the CO/CO_2 ratio was found to be 3.5. This was the highest ratio that was obtained over the temperature range and O_2 concentrations investigated. The steam gasification rate was determined to be 0.5 lb/lb.hr. The carbon partial oxidation reactions and the carbon gasification reaction in the presence of steam are represented by $C + O_2 \longrightarrow CO_2$; $C + CO_2 \longrightarrow 2CO$; and $C + H_2O \longrightarrow CO + H_2$.

It was also determined that the carbon consumption rate by the combined partial oxidation and gasification by steam is the sum of individual rates obtained in the two processes. The water gas shift reaction was found to be at equilibrium. The devolatilization of coke was studied in the TRTU at a lower temperature, but not in the BRU.

The bed and filter samples obtained at the end of tests were analyzed for vanadium in order to determine if it accumulates in the fines produced during testing. Runs 22 through 25 were done at lower temperatures and the results, presented in Table 1, show that the vanadium present in the feedstock does accumulate in fines. Hence, it should be possible to remove vanadium during coke processing via the fines generated. The nickel content in the bed and filter samples is not meaningful as the thermocouples used in the BRU tests had an Incoloy 800 (high nickel alloy) sheath and were corroded during the tests as a result of high temperatures. In future BRU tests, the thermocouples will be protected by ceramic tubes so that the bed and fines can be analyzed for nickel. Surface areas of fresh and bed samples of petroleum coke from BRU tests were measured by N_2 absorption (BET method). The results are given in Table 2.

The above measurements show up to a ten-fold increase in BET surface area as carbon is converted. After a significant carbon conversion is achieved, the coke partial oxidation rate increases since it becomes more reactive due to the increased surface. Thus, a transport reactor is most efficient in processing coke due to staging which utilizes all the O_2 to react with solid carbon to produce CO and CO_2 without burning volatiles. The recirculating solids have a significantly higher carbon conversion and, so, are more reactive than the fresh feed. Therefore, the coke consumption rate is higher in a transport reactor compared to a fluidized bed.

The temperatures measured in the bed and the gas composition determined using infrared analyzers in test 26 are shown in Fig. 3 and 4. The bed temperature, after reaching a peak value gradually decreased with time showing that the carbon consumption rate increased steadily. The gas composition measured using a GC is also shown in Fig. 4. Additional results, shown in Table 3, indicate that the steam gasification rate is very low as shown by the low conc. of H_2 and that the carbon consumption (cons.) rate increases by a factor of nine as the carbon in the bed is consumed.

The gas composition and temperatures measured in test 22 at a nominal bed temperature of 1900°F are shown in Fig. 5 and 6, respectively. These results show that the CO/CO_2 ratio is very low at this temperature. Results obtained at an O_2 concentration of 30% at initial bed temperature of 1950°F are shown in Table 4. Results for sample 1 correspond to O_2 conc. of 40% which was used for a short period as the peak temperature reached 2300°F.

Testing in TRTU

Petroleum coke was processed with riser and mixing zone densities of 4 and 14 lb/ft^3, respectively at a solid circulation rate of about 600 lb/hr in the TRTU in both partial oxidation and steam gasification modes at temperatures close to 1800°F. These tests confirmed that the inability of operating the TRTU at temperatures exceeding 1800°F prevented complete thermal cracking of volatiles produced, causing coke-like deposits to be formed in the reactor.

Testing in the TRTU showed that the fuel gas produced at temperatures lower than 1800°F has a CO/CO_2 ratio less than or equal to 0.5. This gas has a very low heating value and is not suitable for power generation. The partial oxidation and gasification of petroleum coke could not be studied at higher temperatures in this unit due to equipment limitations. The devolatilization of coke was also studied at temperature of 1800°F and yielded a H_2/CH_4 molar ratio of 4.0.

A product gas heating value of 124 BTU/scf was estimated for a transport gasifier with enriched air-blown (30% oxygen) mode of operation utilizing the results obtained in the BRU and the TRTU.

Flowsheet Development / Process Advantages

Based on the results obtained in the BRU and the TRTU, the process flow diagram, shown in Fig. 7, has been developed to partially oxidize/gasify petroleum coke. This flow diagram incorporates the direct sulfur recovery process, developed by Research Triangle Institute, as this process was deemed best suited for this application. It also incorporates a transport desulfurizer and a transport regenerator for sulfur removal from the product gas. These two units were developed recently by The M.W. Kellogg Co. for the Sierra Pacific project and will be demonstrated shortly. A detailed flowsheet, based on the above flow diagram to generate power from the fuel gas produced from gasification and partial oxidation was developed. Economic analysis of the proposed process is in progress.

The advantages of a transport gasifier over entrained gasifiers, which are being demonstrated to process petroleum coke and other refinery waste streams such as API wastes, acid-soluble oils from alkylation unit, and waste water treatment sludges, are the following:

- It has appreciable carbon inventory while there is none in an entrained gasifier. This factor makes the transport reactor safer and easier to operate.
- Individual refinery waste streams can be injected at different locations where as in an entrained gasifier, these have to be mixed with the main feedstock. The need

for mixing poses significant disadvantages for the latter depending upon the feedstreams.

- There is no short term need for balancing carbon, hydrogen and oxygen in the transport gasifier due to substantial carbon inventory where as it becomes essential to maintain this balance in an entrained gasifier.
- It is thermally more efficient due to a lower operating temperature with less material constraints compared to entrained gasifiers.
- The feeding of petroleum coke can be staged so that the combustion of volatile matter can be prevented in order to increase the heating value of the fuel gas produced. This is not feasible in entrained gasifiers.

Summary

At temperatures close to 2000°F, a CO/CO_2 molar ratio of 3.5 in the product gas was obtained in the BRU. This shows a great improvement in the gas composition over a value of 0.5 obtained in the TRTU at temperatures lower than 1750°F, and that a temperature of 2000°F is required to process petroleum coke to produce a fuel gas of acceptable heating value. A fuel gas heating value of 124 BTU/scf is estimated for a commercial transport gasifier based on these results. These results were used to develop a flowsheet, and a conceptual design for the transport reactor has been completed to perform economic analysis.

References

(1) D. L. Heaven, "Gasification Technologies and World Wide Refining Trends," Presented at NPRA Annual Meeting, San Antonio, March 17-19, 1996.
(2) H. Simons and W. Campbell, "Status of Kellogg's Fluid Bed and Transport Gasification processes," Presented at Institution of Chemical Engineers Conference on Gasification, London, England, November, 1995.

Abbreviations

BRU	bench-scale reactor unit
BET	Brunauer, Emmett, and Teller method based on nitrogen adsorption
DOE	Department of Energy
DSRP	direct sulfur recovery process
FCC	fluid catalytic cracker
GC	gas chromatograph
PG	Product Gas
POX	Partial oxidation
PETC	Pittsburgh Energy Technology Center
ROSE™	Residuum Oil Supercritical Extraction
TRTU	Transport Reactor Test Unit

Table 1 - Analyses of bed and filter samples from BRU tests

Run number	Sample	Vanadium, ppm
Run 26	filter	42,255
	bed	5,760
Run 25	filter	61,710
	bed	4,888
Run 24	filter	14,891
	bed	4,362
Run 23	filter	19,875
	bed	9,838
Run 22	filter	32,873
	bed	5,843
	Fresh	1,752

Table 2 - Surface Areas of Bed Samples

Sample	Surface area (m^2/gm)
24	9.7
25	5.7
26	2.6
Fresh	0.9

Table 3 - Petroleum Coke POX Studies - (Test 26)

	sam. 1	sam. 2	sam. 3	sam. 4	sam. 5
time, min	4	16	29	42	55
bed temp upper, °F	2300	2147	2101	2034	1987
H_2, vol%	0.97	0.21	0.14	0.11	0.12
CO, vol%	30.6	27.1	29.3	29.2	34.4
CO_2, vol%	5.0	13.2	12.9	11.9	9.3
CO/CO_2 ratio	6.14	2.05	2.27	2.46	3.72
C cons.,gm/min	2.18	2.71	2.93	2.80	3.11
C cons. rate, 1/min	0.01	0.02	0.03	0.04	0.09

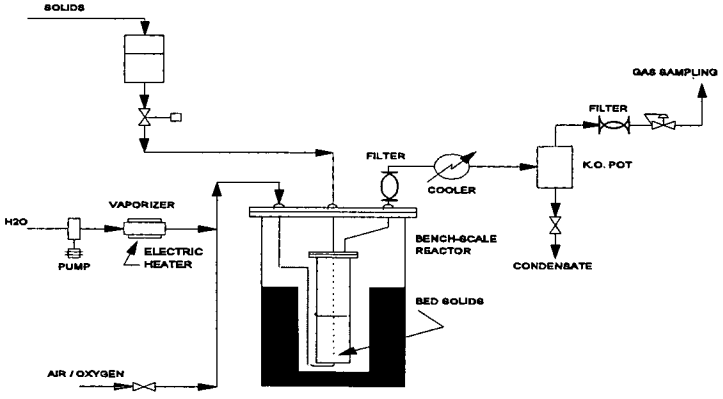

Fig. 1 Bench-scale Reactor Unit for Petroleum coke Processing

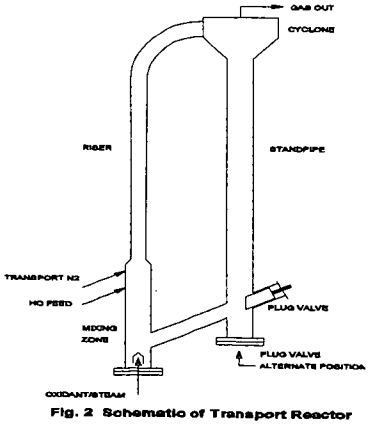

Fig. 2 Schematic of Transport Reactor

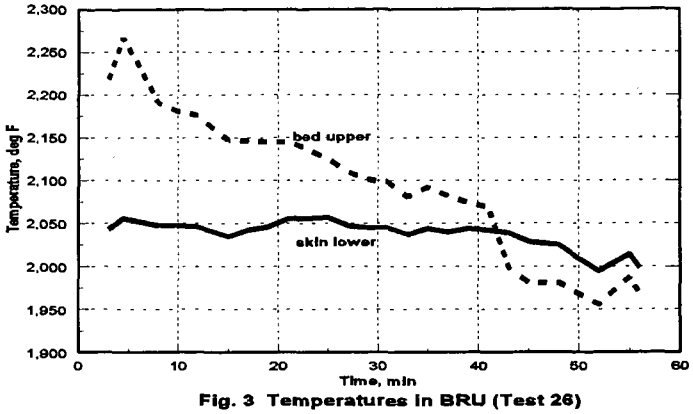

Fig. 3 Temperatures in BRU (Test 26)

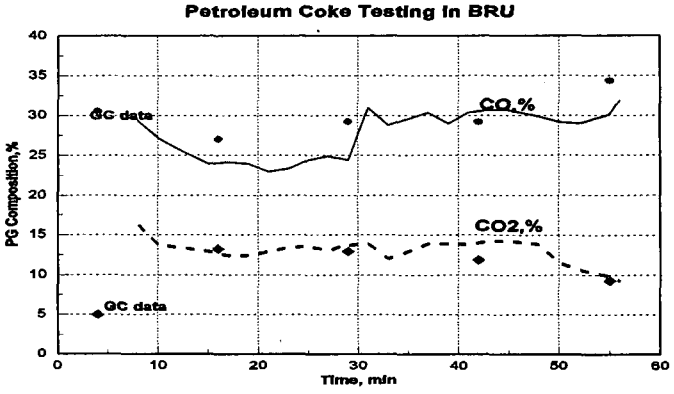

Fig. 4 PG Analysis as per IR analyzers and GC

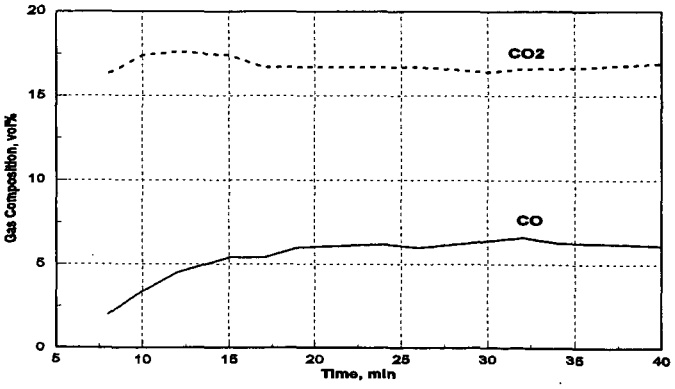

Fig. 5 Product Gas Composition - Test 22A

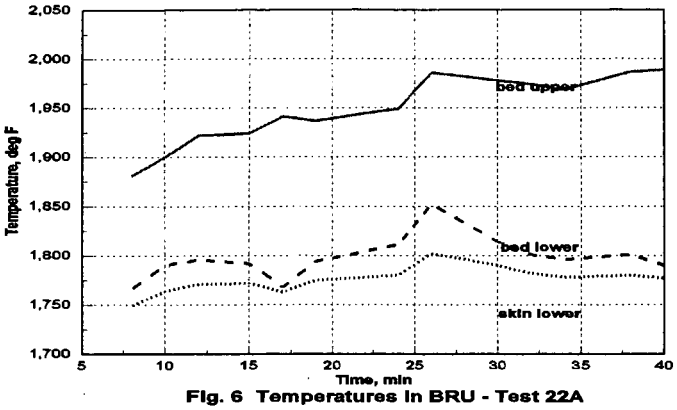

Fig. 6 Temperatures in BRU - Test 22A

Non Adiabatic Gasification of Petroleum Coke

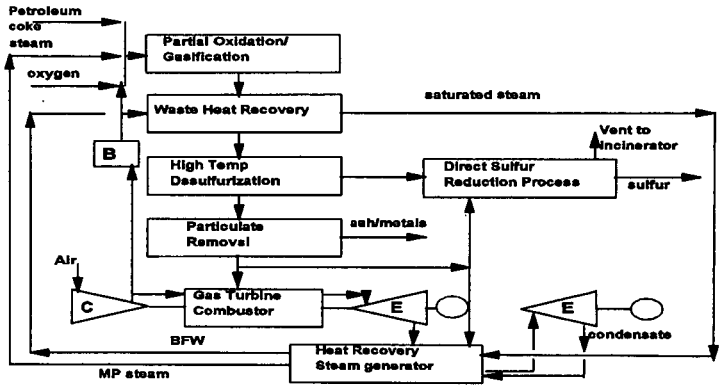

Figure 7. Block Flow Diagram for Petroleum Coke Processing